University of Nottingham
UK | CHINA | MALAYSIA

Development and Evaluation of Sustainable Hydrogel Technologies for Tissue Engineering

By Kayla Danielle Kret, BSc, MSc

Thesis submitted to the University of Nottingham for the degree of Doctor of Philosophy, May 2020.

Acknowledgements

I must thank my PhD supervisors, Dr. Alastair Campbell-Ritchie and Dr. Colin Scotchford, for their expertise and support throughout this journey.

Many thanks go to Julie Thompson for the advice and help on my laboratory work and the many needed chats. I would also like to acknowledge Nikki Weston and Martin Roe (Nanoscale and Microscale Research Centre) and Deborah Surgay (Bio-Support Unit at Sutton Bonington Campus) for their technical guidance.

I cannot thank my friends enough for their emotional and mental support. Special recognition goes to Ana Encerrado, Kathryn Thomas, and Elana Super for making the cell lab more enjoyable.

Finally, and most importantly, I would like to thank my family for supporting me. I could feel all of the encouragement from California and Roxas City, Philippines and I am forever grateful. The most special thanks go to Isaac Griffiths as I could not have gotten through this without his continual support and motivation.

Abstract

With an increasingly active and aging population, injury to ligaments and tendons poses a serious issue to the healthcare system. For ruptures of these ligaments and tendons which cannot be treated conservatively, surgical intervention may be required for an adequate return to health. Current reconstruction options require autologous tissue which can prolong the rehabilitation period and cause inadvertent pain at the donation site. While allografts avoid pain at donation site, they may cause foreign body responses and there is a finite availability of allograft tissue. Therefore, a regenerative therapeutic solution is required that can overcome the known issues of current available grafts for ligament and tendon repair. Recent advances within tissue engineering have led to a deeper understanding of the ligament repair process while circumventing the concerns of autografts and allografts. Challenges arise in creating a scaffold that properly assimilates the ligamentization process while simultaneously offering adequate mechanical strength and tissue formation. Further challenges emerge in recreating the natural graded mineralization of the ligament into fibrocartilage and bone found at the enthesis, or bony insertion region, that is necessary for stress dispersal.

The overall aim of this research was to develop a hydrogel scaffold made from sustainable biomaterials for use in a ligament tissue engineering application that can withstand physiological loading while influencing a fibroblastic response at the midsubstance and an osteoblastic response at the entheses. A cost-effective approach was taken in this research by incorporating materials that are either routinely used in cell culture or readily available at low cost.

The work reported in this thesis describes the development of a chitosan-gelatin hydrogel into a ligament construct, or sinew, consisting of a soft, ligamentous midsubstance and a stiff, bony interface that could be implemented in a tensile loading bioreactor. The thickness of the chitosan-gelatin hydrogel was optimised to promote cell proliferation and production of ligament-like ECM using the NIH-3T3 fibroblast cell line and a primary ovine fibroblast culture. A novel method was developed to fabricate the hydrogel into a detached form that allowed its use in a tensile loading bioreactor system. The method of producing the detached hydrogel scaffolds did not affect the cytocompatibility of the hydrogel but was found to decrease the internal rigidity of the scaffold. The incorporation of calcium phosphate salts into the chitosan-

gelatin hydrogel created a composite hydrogel suitable for enthesis engineering that prompted an osteogenic response from the primary fibroblast culture.

The responses of the two fibroblast cultures were analysed on the chitosan-gelatin hydrogel and composite hydrogel to determine their suitability as a cell source for ligament tissue engineering applications. Both cultures showed a fibroblastic response on the chitosan-gelatin hydrogel, which would maintain the ligament phenotype in the midsubstance of the scaffold. The 3T3 cell line was vital in the early investigation of the chitosan-gelatin hydrogel, however its response was limited on the composite hydrogel. The primary cell culture demonstrated an osteogenic response on the composite hydrogel. Due to this, it was determined that the primary fibroblast culture was a more suitable cell source for a ligament tissue engineering application.

The hydrogel sinews were successfully implemented into a tensile loading bioreactor system capable of applying physiological strain and seeded with the primary fibroblast culture. The effect of the tensile strain on the attached fibroblasts was analysed in comparison with a static culture system. This custom tensile loading bioreactor system was designed as a model for ligament tissue engineering research.

Abbreviations

3T3: NIH-3T3 cell line

ACL: Anterior Cruciate Ligament of Knee

ALP: Alkaline Phosphatase

AM: Anteromedial Bundle of ACL

CA: Composite Hydrogel Coated Acetal Anchor

$CaCO_3$: Calcium Carbonate

$CaHPO_4$: Dibasic Calcium Phosphate

dH_2O: Distilled Water (Not Sterilized)

DMMB: 1,9-dimethylmethylene Blue

DNA: Deoxyribonucleic Acid

ECM: Extracellular Matrix

EDTA: Ethylenediaminetetraacetic acid

ESEM: Environmental Scanning Electron Microscopy

FBS: Foetal Bovine Serum

GAG: Glycosaminoglycan

HBSS: Hank's Balanced Salt Solution

HCl: Hydrochloric Acid

IMS: Industrial Methylated Spirits (diluted with deionized water to 70% v/v)

MA4C: Composite Hydrogel Anchor Dried at 4°C

MAFD: Freeze-dried Composite Hydrogel Anchor

Medium: Cell Culture Medium

MG63: Human Sarcoma Osteoblast Cell Line

MH: Detached Hydrogel Scaffolds Made on Cell Culture Medium

NaOH: Sodium Hydroxide

NAP-XPS: Near Ambient Pressure X-Ray Photoelectron Spectroscopy

NH: Hydrogel Cast without an Intermediate Layer

OPC: Oligomeric Proanthocyanidin

PBS: Phosphate Buffered Saline

PCL: Posterior Cruciate Ligament of Knee

PFib: Primary Ovine Fibroblasts

PH: Detached Hydrogel Scaffolds Made on PBS

PL: Posterolateral Bundle of ACL

PLA: Poly(lactic acid)

PLGA: Poly(lactic-co-glycolic acid)

PLLA: Poly(l-lactic acid); A Derivative of PLA

Poly-HEMA: Poly(2-hydroxyethyl methacrylate)

PTFE: Polytetrafluoroethylene

PU: Polyurethane

SDW: Sterile Distilled Water

TCP: Tissue Culture Polystyrene

THF: Tetrahydrofuran

UV: Ultraviolet

XPS: X-Ray Photoelectron Spectroscopy

MSC: Mesenchymal Stem Cells

Contents

Acknowledgments ..... *i*

Abstract ..... *ii*

Abbreviations ..... *iv*

1. Introduction *1*

1.1. Ligament Injury **1**

1.2. General Project Aims **2**

1.3. Experimental Objectives **2**

2. Literature Review *4*

2.1. Ligament and Tendon Injury **4**

2.2. Anterior Cruciate Ligament Injury **4**

2.2.1. General Structure of the Knee 5

2.2.2. ACL Anatomical Location 6

2.2.3. Role and Function of ACL 7

2.2.4. Biochemical Structure of Ligaments 7

2.2.5. Stages of Ligament Healing 10

2.2.6. Healing Properties of ACL 10

2.3. Current Strategies for ACL Reconstruction **11**

2.3.1. Autografts 11

2.3.2. Allografts 12

2.3.3. Synthetic Grafts 13

2.4. Tissue Engineering **16**

2.4.1. Aims 16

2.4.2. Ligament and Tendon Tissue Engineering 17

2.4.3. Cell Source for Ligament Tissue Engineering 17

2.4.4. Challenges of Ligament and Tendon Tissue Engineering 19

2.5. Scaffolds in Tissue Engineering **23**

2.5.1. Scaffold Composition and Architecture 24

2.5.2. Biodegradability 29

2.6. Hydrogels **31**

2.6.1. Hydrogels in Ligament Regeneration 31

2.7. Bioreactors in Ligament and Tendon Tissue Engineering **33**

2.8. Biological Characterisation of a Tissue Engineered Ligament **38**

2.8.1. Cell Organisation and Morphology 38

2.8.2. ECM Components 38

2.9. Conclusion **39**

2.10. Aims of Research Project **41**

3. General Methodology *42*

3.1. Introduction **42**

3.2. Cell Culture **42**

3.2.1. Cell Culture Maintenance 42

3.2.2. Bringing Cells to Culture from Cryopreservation 42

3.2.3. Passaging Cells 43
3.2.4. Cryopreservation 43
3.2.5. Primary Ovine Fibroblast Culture 43
3.2.6. Cell Seeding 45
3.2.7. PFib Culture 45

3.3. Cell Area Measurement 45

3.4. Cell Culture Assays 45
3.4.1. AlamarBlue 46
3.4.2. Cell Lysing 46
3.4.3. DNA Assay 47
3.4.4. Alkaline Phosphatase Activity 48
3.4.5. Papain Digestion 48
3.4.6. Glycosaminoglycan Assay 48
3.4.7. Environmental Scanning Electron Microscopy 49

3.5. Hydrogel Scaffold 50
3.5.1. Hydrogel Preparation 50
3.5.2. Hydrogel Casting 50
3.5.3. Hydrogel Sterilization 51
3.5.4. Cell Culture and Assays on Hydrogel Scaffolds 51
3.5.5. ESEM 51

3.6. Statistical Significance 51

4. Optimization of Chitosan-Gelatin Hydrogel Thickness to Assess Fibroblast Response 52

4.1. Introduction 52

4.2. Methodology 52
4.2.1. Hydrogel Casting 52
4.2.2. Cell Culture 53
4.2.3. ESEM 53

4.3. Results 54
4.3.1. Morphology of Hydrogel 54
4.3.2. Mean Area of Cells During Culture 54
4.3.3. ESEM Imaging 57
4.3.4. Metabolic Quantification 58
4.3.5. DNA Quantification 61
4.3.6. GAG Content 61
4.3.7. ALP Activity 63

4.4. Discussion 64
4.4.1. Chitosan-Gelatin Hydrogel Cytocompatibility 64
4.4.2. The Effect of Hydrogel Thickness on Cell Proliferation, ECM Production, and Differentiation 65
4.4.3. Modelling with a Cell Line vs. a Primary Culture 67

4.5. Conclusion 69

5. Production of Detached Hydrogel using an Intermediate Layer 70

5.1. Introduction 70

5.2. Methodology 71
5.2.1. Polyurethane Coating 71
5.2.2. Polytetrafluoroethylene Membrane 71
5.2.3. Intermediate Layer 71

5.2.4. Cross-Section Detached Hydrogel Measurement 72
5.2.5. Density Measurement 72
5.2.6. Hydrogel Swelling and Degradation 72
5.2.7. MicroTensile Testing 73
5.2.8. XPS 75
5.2.9. NAP-XPS 75
5.2.10. Cell Culture 75

5.3. Results 76
5.3.1. PU Coating and PTFE Membrane 76
5.3.2. Intermediate Layer 76
5.3.3. Characterisation of the Detached Hydrogel 78
5.3.4. Cytocompatibility 84

5.4. Discussion 86
5.4.1. Physical Properties of the Detached Hydrogel 86
5.4.2. Cell Response to Detached Hydrogels 90

5.5. Conclusion 93

6. Modified Chitosan-Gelatin Hydrogel to Promote an Osteogenic Response ... 95

6.1. Introduction 95

6.2. Methodology 96
6.2.1. Composite Hydrogel Synthesis 96
6.2.2. Cell Culture on Composite Hydrogel 96
6.2.3. Degradation of the Composite Hydrogel 97
6.2.4. Anchor Design 97
6.2.5. Compression Testing of Anchors 99
6.2.6. Degradation of Anchors 100

6.3. Results 100
6.3.1. Composite Hydrogel 100
6.3.1. Adjustment of Calcium Salts to Composite Hydrogel 100
6.3.2. Cell Assays on Composite Hydrogel 100
6.3.3. Degradation of the Detached Composite Hydrogel 109
6.3.4. Anchor Modelling 109
6.3.5. Anchor Compression Testing 111
6.3.6. Degradation of the Composite Hydrogel Anchors 112

6.4. Discussion 112
6.4.1. The Composite Hydrogel as an Enthesis Biomaterial 113
6.4.2. Mechanical Functionality of the Anchors 116

6.5. Conclusion 118

7. Bioreactor Design, Assembly, and Application 120

7.1. Introduction 120

7.2. Methodology 121
7.2.1. Bioreactor Design 121
7.2.2. Experimental Design and Assembly 123
7.2.3. Cell Culture 125
7.2.4. Mechanical Stimulation 125
7.2.5. Cell Culture Assays 126

7.3. Results 127
7.3.1. Bioreactor Design 127
7.3.2. Hydrogel Sinew 129

7.3.3. Metabolic Activity 129
7.3.4. Cell Morphology 130
7.3.5. Cell Lysing and Digestion 132
7.3.6. DNA Content 132
7.3.7. ALP Activity 132
7.3.8. GAG Production 133

7.4. Discussion 134
7.4.1. Bioreactor Design and Application 135
7.4.2. Cell Response on the Hydrogel Sinew 135
7.4.3. Scaffold Modification & Reinforcement 138

7.5. Conclusion 139

8. General Conclusions and Future Work 141

8.1. Chitosan-Gelatin Hydrogel Optimization 141

8.2. Detached Hydrogel Disc Produced by an Intermediate Layer 142

8.3. Composite Hydrogel 143

8.4. Primary Ovine Fibroblast Culture 144

8.5. Bioreactor Design & Application 144

8.6. Future Work 145

9. References 148

10. Appendix 180

10.1. Concentrations for PicoGreen Assay 180

10.2. Concentrations for DMMB Assay 180

10.3. Mean Cell Area Additional Images 180

10.4. Code for Mechanical Stimulation of Bioreactor 186

1. Introduction

1.1. Ligament Injury

Injury to ligaments and tendons that require surgical intervention for repair have become more prominent within the increasingly active and aging population [9]. Each year 32 million musculoskeletal injuries occur in the United States and tendon, ligament, and capsular joint injuries represent 45% of these cases, with numbers for surgical repair of the Achilles tendon and rotator cuff tendons reaching nearly 100,000 [10]. In the US, the occurrence of these injuries costs $1billion to the healthcare system annually [11].

Of the commonly injured ligaments and tendons, damage to the anterior cruciate ligament (ACL) within the knee is often a devastating injury for career athletes and imposes long term health risks, such as osteoarthritis even when repaired surgically. The ACL is a unique ligament within the body that has poor healing capacities, due to its intra-articular yet extra-synovial position which causes a lack of blood and nutrient supply [12]. The ACL is a key component in the stability of the knee during many weight-bearing movements, specifically quick turning motions and sharp changes of direction [13].

Current replacement treatments for ligament and tendon rupture exhibit limitations—primarily the availability of tissue for autografts and allografts and the durability and longevity of synthetic prosthetics. In addition, the repaired tissue fails to replicate the mechanical and structural qualities of the native tissue [14]. The demand for an alternative solution is at an all-time high.

Bioengineering has made advances towards a tissue engineered ligament solution that negates the limited availability of donor tissue and more closely resembles the native tissue structure by combining biological, mechanical, and biomaterial methodologies [15]. Possibilities exist for creating a scaffold out of a biodegradable and cytocompatible biomaterial that promotes cellular ingrowth and is capable of producing a similar mechanical strength of the native tissue. Challenges in ligament tissue engineering arise in optimizing the mechanical strength of the prosthesis and regenerating the graded mineralization of the enthesis, or bony interface [16, 17].

A potential solution would be to manipulate a biomaterial so it consists of two areas, the midsubstance and osseous interface, which allow for the differentiation of a

single cell source into ligamentous and osteoblastic lineages, further increasing the chance of success at the enthesis [18]. The implementation of tensile strain to a biomaterial of this capacity would further strengthen the tissue engineered construct [19]. The characterisation of this ligamentous scaffold would include analysis of the collagen content and organisation, as these are determining factors of tissue strength and function [20, 21]. Additional genetic analysis could also be explored to optimise the ECM production and tissue growth on the scaffold [22, 23]. The development of sustainable biomaterials to create a scaffold that could support the adequate tissue growth and a tensile bioreactor system to optimise the mechanical loading of the tissue could provide an alternative solution to ligament reconstruction grafts and provide a model for further ligament tissue engineering research.

1.2. General Project Aims

This goal of this research is to use a cost-effective approach to develop a hydrogel scaffold that is representative of a ligament, consisting of a midsubstance and two bony interfaces, and can be used in ligament tissue engineering research. The aim of this research is to optimise the use of sustainable biomaterials that can influence the proliferation and growth of fibroblasts to produce an extracellular matrix (ECM) that is similar to the ligamentous midsubstance and osseous interface of a ligament. Further, this project aims to develop a tensile bioreactor system that can transmit physiological strain to the fibroblasts seeded on the hydrogel scaffold and analyse the effect of the tensile strain on both the hydrogel scaffold and attached fibroblasts.

1.3. Experimental Objectives

The experimental objectives of this project were to:

1. Develop and optimise the thickness of a cost-effective chitosan-gelatin hydrogel that is conducive to fibroblast proliferation and production of ECM similar to that of a ligament.
2. Establish an appropriate cell source, either a fibroblast cell line or primary fibroblast culture, for this ligament tissue engineering application.
3. Develop a method of fabricating the chitosan-gelatin hydrogel into a detached form that does not have adverse effects on the cytocompatibility of the hydrogel and determine the effects of this fabrication method on the physical characteristics of the hydrogel.
4. Determine if the creation of a composite hydrogel, through the integration of calcium carbonate ($CaCO_3$) and dibasic calcium phosphate ($CaHPO_4$) into the

chitosan-gelatin hydrogel, stimulates an osteogenic response from the fibroblasts.

5. Develop a design using the composite hydrogel to act as an anchor for the detached hydrogel scaffold within the bioreactor.
6. Manufacture a bioreactor suitable for tissue engineered ligament applications capable of transmitting a physiological strain and simultaneously housing multiple samples with the same tensile loading regime.
7. Examine the effect of tensile strain on both the chitosan-gelatin hydrogel scaffold and attached cells.

2. Literature Review

This literature review will use the anterior cruciate ligament (ACL) as a clinical example to give a background understanding of the nature of ligament and tendon injury and repair. The anatomical structure and variations between ligament and tendons will be discussed, as well as how the anatomy of the ACL contributes to its healing properties. The current available options for ACL reconstruction will be described in detail.

The current reconstruction options cause several areas of concern which have led to advances within tissue engineering to regenerate ligaments and tendons *in vitro*. Ligament tissue engineering is a complex field involving many variables that have an impact on the tissue formation and remodelling. The scaffold, cell source, and mechanical stimulation are discussed within this literature review, including the challenge of engineering the bony attachment. There are several other components such as variation of cell culture medium and the addition of specific growth factors that can influence tissue regeneration but are not discussed within this review.

2.1. Ligament and Tendon Injury

Ligaments and tendons are soft connective tissue that are similar in structure and function within joints [24, 25]. Damage to ligaments and tendons has become an increasingly common injury as the aging population remains active, which can range from a slight sprain to a full rupture. Such injury can occur from repetitive strain lesions or trauma [26]. There may also be a genetic factor that predisposes some individuals to ligament and tendon injury [27].

The healing process of ligaments and tendons is relatively slow due to their low metabolic requirements [25, 28]. Most soft tissue injury will repair without intervention, however there are several instances where surgery is required to repair, or even replace, the damaged tissue, such as rupture of the anterior cruciate ligament (ACL) in the knee, the Achilles tendon in the ankle, or the rotator cuff in the shoulder.

2.2. Anterior Cruciate Ligament Injury

It is estimated that ACL ruptures account for 100,000-400,000 operations per year in the United States [29]. Ruptures can occur from unnatural movements, such as trauma, or instability of the joint caused from lack of strength from surrounding tissues. Ruptures of the ACL are commonly seen in sports that involve a large amount of rapid side-to-side change of direction movements and abrupt deceleration [30]. In

many cases occurring due to sports, contact with an opponent has not occurred and is a result of individual load bearing movements [31].

In addition to operation needed for ACL repair, the progression of osteoarthritis in the joint can be debilitating [32]. Øiestad et al. have reported the occurrence of osteoarthritis after ACL repair at 0-13% while the occurrence increases to 21-48% if there is a combination injury within the joint [33]. Prior to the review by Øiestad et al., it was reported that the incidence of osteoarthritis after ACL rupture was a larger range of 10-90% [34]. The large variation in prevalence of osteoarthritis after ACL injury demonstrates the little understanding there is regarding the healing of the ACL and the associated development of arthritis [29].

2.2.1. General Structure of the Knee

The knee is one of the most complex weight bearing joints in the human body and is comprised of the articulation of the femur on the tibia with the patella articulating with the femur anteriorly [35]. The surrounding muscles, tendons, and ligaments provide the necessary strength and attachment to allow for flexion and extension, the two key movements of the knee, Figure 2.1 [36]. The quadriceps are a group of four muscles that attach the femur to the patella, continuing into the patellar tendon and inserting into the tibia, that produce extension of the knee. The hamstrings, on the dorsal side of the femur, attach from the pelvic bone to the tibia producing flexion of the knee. The associated tendons of these muscles surround the knee providing support to the joint. The ligaments, connecting bone to bone, are important in maintaining stability of the joint and reducing internal rotation [37].

There are several ligaments within the knee attaching from the femur to the tibia that support the joint. The collateral ligaments are on the medial and lateral sides of the joint, aptly named the medial and lateral collateral ligaments [38]. Within the joint, the more complicated cruciate ligaments create a ‘crucifix’ shape as they cross one another. The anterior and posterior cruciate ligaments are essential in keeping the tibia aligned to the femur [37].

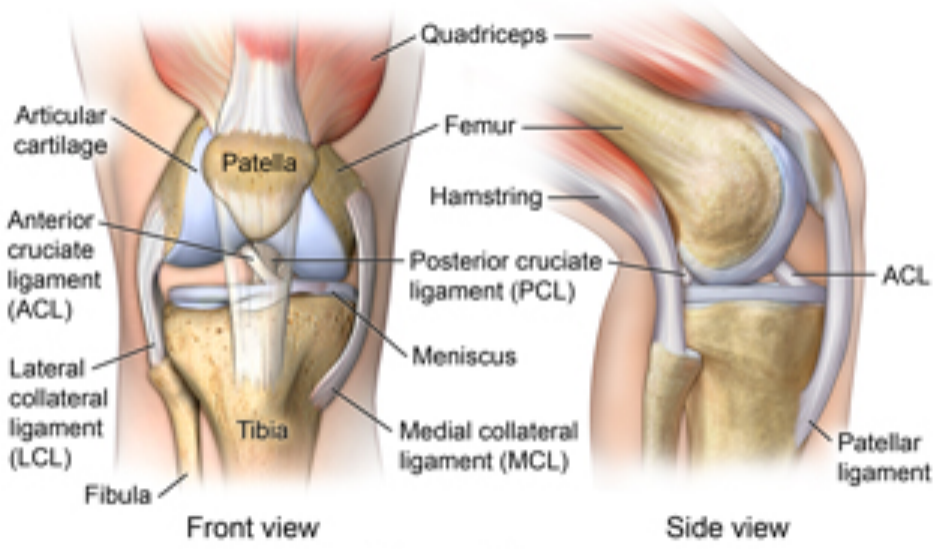

Figure 2.1: Diagram of the knee indicating the ligaments, bones, and some muscles. Image taken from: [https://www.hopkinsmedicine.org/health/conditions-and-diseases/ligament-injuries-to-the-knee].

2.2.2. ACL Anatomical Location

The close proximity of ligaments to joints typically promotes an abundant blood supply [39]. Additionally, the synovial sheath that encloses the joints assists in the nutrient availability to ligaments. The synovial sheath also contributes to the frictionless articulation of the bones within the joint [39].

The anatomical location of the ACL differs in its availability of blood and nutrient supply. The insertion of the ACL on the anterior portion of the articular surface of the tibia and attachment to the posterior region of the articulating surface of the femur create an intra-articular location [40]. This location inhibits the blood and nutrient supply to the ACL [41, 42]. Further, the synovial sheath encloses the joint but excludes the ACL, producing an extrasynovial position and further decreasing nutrient availability [43, 44]. Consequently, the intra-articular and extrasynovial location of the ACL reduces blood supply and nutrient availability, thereby restricting the healing capacity of the tissue should any damage occur.

The attachments sites of the ACL to the femur and tibia are exceptionally important regarding the restored function and mechanical stability after reconstruction [45-50]. The attachment site of ligament to bone is known as the enthesis and encompasses the transition between the soft tissue of the ligament to the mineralized bone tissue known to disperse the great stresses of movement [18, 51, 52]. The enthesis is a complex region due to the differences in micro- and nano-level structure relating to the matrix composition and mechanical integrity [53, 54].

2.2.3. Role and Function of ACL

The primary purpose of the ACL is to prevent anterior tibial displacement and internal rotation [55, 56]. The ACL works in conjunction with the posterior cruciate ligament (PCL), which prevents posterior tibial displacement. These two cruciate ligaments are critical factors in the stability of the knee. The presence of mechanoreceptors in the ACL have a proprioceptive function which aid in stability of the knee [57, 58].

The hamstrings work to protect the ACL as they apply a posterior force on the proximal portion of the tibia, while the quadriceps function as antagonists to the ACL and increase the strain on the ACL when fully flexed [59]. The attachments of the ACL at the femur and tibia cause a rotation producing a 90° lateral spiral which contributes to the ligament having two functional portions, as seen in Figure 2.2 [30, 59-61]. These functional portions are characterized as bundles and named the anteromedial bundle (AM) and the posterolateral (PL) bundle. These bundles function near independently based on the movement of the knee joint; whether the knee is in flexion or extension and if the movement is passive or active [62]. These bundles also cause differing tensile forces to be loaded onto the femoral and tibial entheses sites [63].

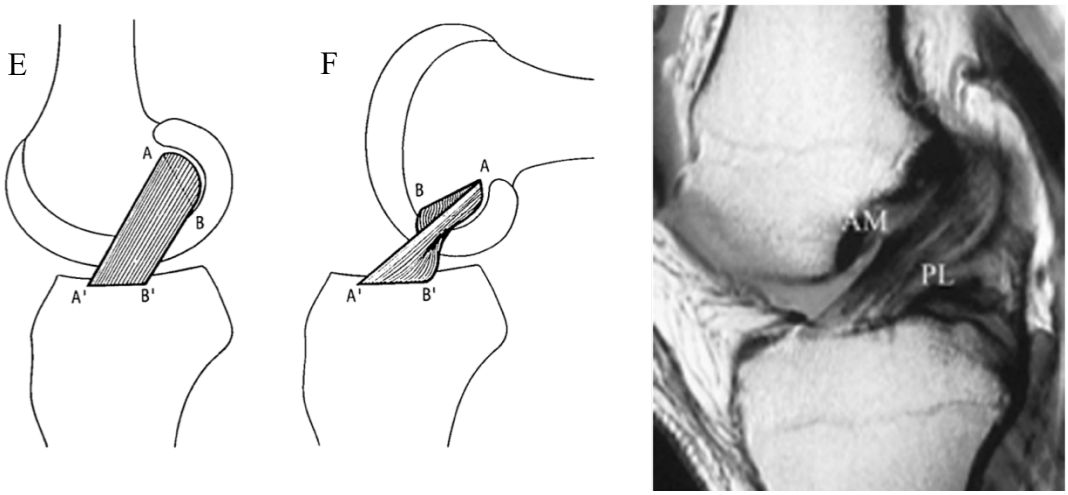

Figure 2.2: Left: A schematic of the ACL showing how the two different bundles interact during extension, E, and flexion, F. During flexion the AM bundle (A-A') becomes taught and thin whereas the PL bundle (B-B') becomes loose and thick. Image adapted from Girgis et al. [30]. Right: An MRI image of the ACL during full extension to highlight the AM and PL bundles. Image adapted from Siebold and Fu [64].

2.2.4. Biochemical Structure of Ligaments

The terms 'ligament' and 'tendon' are often used interchangeably when describing connective tissue in joints, despite distinct anatomical and biochemical

differences between the two [24, 65]. While ligaments attach bone to bone, tendons attach muscle to bone. The biochemistry of ligaments and tendons varies due to the functional nature of each tissue. The structure and function of these tissues are highly linked as the function will dictate the structure and vice versa [65]. That being said, not all ligaments have the same biochemical content [66]. This is also true for tendons.

The extracellular matrix (ECM) of both ligaments and tendons is composed of a high proportion of organised collagen type I and lesser amounts of other proteins, such as elastin, that contribute to its strength and elasticity with a relatively small number of cells in the mature tissue [67]. The difference between the two tissues lies in the collagen type I and type III content in the midsubstance; tendons have nearly 95% collagen type I with 5% other collagen types whereas ligaments can have up to 12-40% collagen type III in the midsubstance [24, 67, 68]. There is also a notable difference in the crosslinking effects of collagen within these tissues [69, 70]. The crosslinking and organisation of the collagen fibrils creates crimp patterns that differ between ligaments and tendons [65].

Ligaments typically have a higher glycosaminoglycan (GAG) content than tendons, which may be due to the more intimate location of ligaments within joints, whereas tendons typically surround joints [24]. Deoxyribonucleic acid (DNA) is also typically found in higher concentrations in ligaments than tendons due to higher cell numbers [71].

The cruciate ligaments of the knee have nearly twice the DNA content and three times the GAG content than the patellar tendon and Achilles tendon, however the total collagen content between these tissues is similar, Table 2.1 [24, 72]. The ACL specifically has been shown to have less mature collagen fibres, with around 10% collagen type III, when compared to the patellar tendon and collateral ligaments, which may explain the higher DNA content [61, 70]. As collagen type III is seen in a higher proportion in the foetus and decreases with age, it can be said that the biochemical structure of the ACL is relatively immature compared to the mature structure of other ligaments and tendons [73].

Proteoglycans are composed of a core protein and one or more covalently attached GAG [74]. Proteoglycans play an important role in mediating fibrillogenesis, resistance of compressive and tensile forces, and cell signalling [75]. The proteoglycan-rich matrix and associated collagen and elastin fibres contribute to the elasticity of these tissues [72, 76]. Aggrecan, decorin, biglycan, and fibromodulin are

the main proteoglycan constituents of ligaments and tendons [77, 78]. Decorin is found in higher percentages in the midsubstance of ligaments than tendons, whereas tendons have a higher aggrecan content [79]. Qu et al. found that the proteoglycan content of the ACL is limited to the ligament and fibrocartilage regions, responsible for the organised collagen fibres [80]. The compressive forces felt near the entheses of ligaments and tendons dictate an increased GAG content and the increased content of aggrecan and decorin, indicating that mechanical loading of these regions is essential in the development of the associated fibrocartilage [81, 82].

The structure-function relationship of ligaments and tendons contributes to the matrix composition of proteoglycan and collagen content [72, 79, 83]. Several studies have reported genetic variability in the genes that encode these proteoglycans can lead to higher susceptibility of ACL ruptures [78, 84]. Additionally, Young et al. found that ruptured ACLs contained less collagen and proteoglycan content than intact ACLs, potentially indicating a difference in ECM prior to rupture reducing the ACLs ability to manage mechanical loading [85]. These studies highlight the important role proteoglycans play in collagen fibre organisation and mechanical strength of tissues.

Table 2.1: Concentrations of total collagen, DNA, and GAG content in selected ligaments and tendons. Adapted from Amiel et. al [24, 66].

	Collagen Content (mg/g dry tissue)	**DNA Content (μg DNA/mg dry tissue)**	**GAG Content (mg/g dry tissue)**
Cruciate Ligaments	802.6±9.8	2.73±0.05	9.89±0.56
Achilles Tendon	868.2±10.2	1.74±0.04	2.75±0.20
Patellar Tendon	867.2±8.9	1.40±0.05	3.92±0.16
Medial Collateral Ligament	797.1±11.1	2.56±0.06	4.56±0.26

2.2.4.1. Crimp Pattern

The complex biochemistry of ligaments and tendons causes a crimp pattern to form throughout the tissue. The crimp pattern is a result of the organisation of collagen fibres and the fibroblast density which aids in transmission of tensile forces [86-89]. The ACL has a fluctuating crimp pattern throughout its midsubstance due to the differing tensile loading in each bundle, as seen in Figure 2.3 [86].

The understanding of the relationship of the microstructure of ligaments and tendons to the biomechanical strain experienced has progressed greatly [87, 88, 90-

92]. Lane et al. have reported that 4 years after implantation of a hamstring graft for ACL reconstruction, the crimp length shortened and the amplitude lessened to resemble a similar crimp pattern as the intact ACL [93]. The assimilation of the hamstring graft further identifies the impact mechanical loading has on the crimp pattern of ligaments and tendons. However, the regeneration of the molecular structure of the tissue after injury is still mostly unknown with research investigating the use of crimped scaffolds and other methods to fully restore the crimp pattern [88, 94].

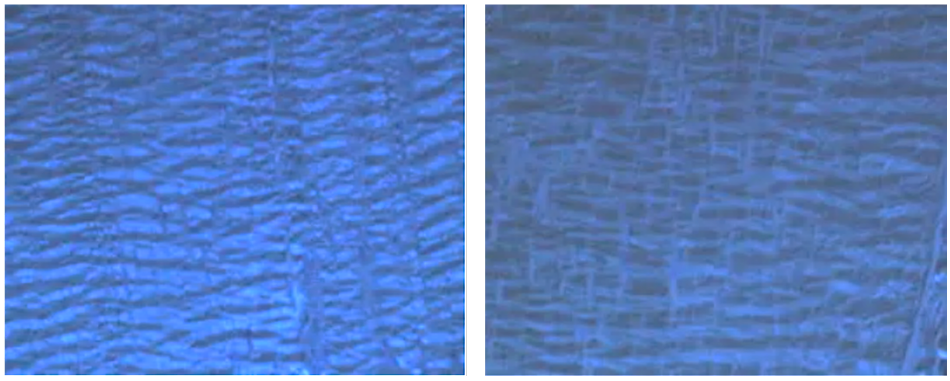

Figure 2.3: The complex crimp pattern of the ACL at the proximal one quarter of the ligament (left) and distal three quarters (right) using a high-resolution microscope and polarized light. Note the tighter crimping pattern found in the proximal portion as compared to the distal portion of the ACL, indicating that the strain may be higher at the proximal portion of the ligament, or PL bundle. Images adapted from Weiss et al. [86].

2.2.5. Stages of Ligament Healing

The typical healing process of ligaments and tendons is complex and regulated by a variety of molecules which may last from several weeks up to several years after injury and often leaves the repaired tissue weaker than the native tissue [95]. The injury site goes through 4 phases: inflammation, proliferation, reparative, and remodelling [95-97]. The understanding of the stages of healing of ligaments and tendons helps to optimise the reconstruction and repair.

2.2.6. Healing Properties of ACL

The inability of the ACL to heal on its own is attributed to the factors previously discussed; the complex anatomy, the extrasynovial location leading to poor vascularization and nutrient supply, the mechanical loading, and intrinsic properties. Therefore, surgery is required to reconstruct the ruptured ligament. The most successful reconstruction options are to completely remove the ruptured ligament and replace it. There are several surgical options to replace the damaged tissue; autografts, allografts, and synthetic grafts.

2.3. Current Strategies for ACL Reconstruction

There are several strategies to replace a ruptured ACL including autografts, allografts, and synthetic grafts. There are considerable benefits and disadvantages to each approach.

2.3.1. Autografts

The ‘gold standard’ of ACL reconstruction remains the implementation of the autograft, due to its relatively high success rate and limited adverse reactions [98, 99]. The bone-patellar tendon-bone graft has been the most commonly used autograft but the hamstring graft has also been increasingly used [50, 100].

The patellar tendon graft takes the middle third of the patellar tendon and a small portion of bone at the attachment to the patella and tibia, creating ‘bony plugs’ on either side of the tendon [98]. The hamstring tendon graft combines portions of the tendons of the semitendinosus, gracilis, and sartorius muscles into a single tendinous graft [101]. A depiction of these grafts can be seen in Figure 2.4.

There are several drawbacks to using an autograft such as donor site morbidity and pain, increased incision size, increased operative time, prolonged rehabilitation time, decreased range of motion, risk of nerve damage, and a finite supply of tissue [102]. The donor site pain and skin incision can be significantly lowered when using the hamstring tendons rather than using the bone-patellar tendon-bone graft [98]. Graft fixation is an important consideration in graft choice as a tendinous graft may require buttons or sutures for fixation while bone-tendon-bone grafts may not require further interference [99]. Further, in both cases the tendon midsubstance of the autografts must undergo ligamentization, a process in which the tendinous graft assimilates to a tissue resembling the native ligament [103]. Janssen and Scheffler have found that during the remodelling of hamstring tendon grafts, the process of ligamentization occurs however the graft does not reach a biological or biomechanical similarity of the intact ACL [104].

An additional concern in using hamstring tendon autografts is the role that hamstring strength plays in protecting the ACL during activity [101]. Pandy et al. found that the co-contraction of the hamstrings can reduce the forces in the ACL by altering the balance of shear forces within the leg, ultimately leading to reduced injury to the ACL [59]. Leiter et al. reports decreased strength during extension and a greater incidence of osteoarthritis after implementation of an autologous hamstring graft compared to the non-reconstructed knee, despite no surgical intervention on the

quadriceps muscle [11]. In using a hamstring graft, there is potential that the strength of the hamstrings may be reduced which could lead to an increased risk of secondary rupture.

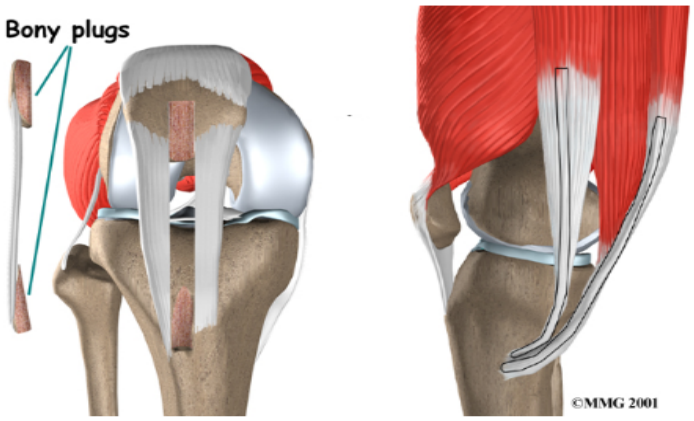

Figure 2.4: Illustrations of the origin of the patellar tendon autograft (left) and the hamstring tendon autograft (right). The black outline in the hamstring tendon autograft indicates the portion of tissue to be removed for the graft. Image taken from: [https://eorthopod.com/hamstring-tendon-graft-reconstruction-of-the-acl/].

The patellar tendon graft produces greater static knee stability and significantly lower graft failure rate when compared to hamstring grafts [105]. However, the harvesting of the patellar tendon results in great pain around the donor site, a loss of extensor strength, and increased risk of future patellar injuries including fracture [106, 107].

In recent years, the practice of using a multiple bundle hamstring tendon graft has been growing in popularity due to the more realistic resemblance to the functional AM and PL bundles, leading to increased graft strength and decreased donor site pain, rehabilitation time, and extension deficit [99, 108-110]. Siebold et al. discovered that the surgical technique for a double bundle graft with four attachment sites improved rotational stability and allowed a more accurate representation of the functional bundles of the native ACL [111]. A clear impediment of creating a double bundle hamstring graft, is the requirement of four attachments to the femur and tibia which significantly increases the chance of poor placement and requires additional sites of osteogenesis.

2.3.2. Allografts

An allograft eliminates the donor site morbidity found with autografts in addition to reducing the incision size and operative time [112]. Allograft tissue for ACL construction can originate from the patellar and Achilles tendons and from the

tendons of the hamstrings and tibialis [11, 102]. There has been increasing research into removing the cellular material from allografts to utilize the optimal architecture of the tissue while removing possible immunogenic factors [113, 114].

The main concerns using allografts are sterilization, disease transmission, graft incorporation, cost, availability of tissue, immunogenic response, and failure rate [100, 112, 115-117]. Allografts may have the distinct benefit of not causing further damage to surrounding tissue however the failure rate of allografts remains significantly higher than autografts [116, 118, 119]. Due to these shortcomings, autografts remain the more common choice for ACL reconstruction.

2.3.3. Synthetic Grafts

Synthetic grafts were heavily researched beginning in the 1980s and continuing into the 1990s, increasing in popularity due to their abundance, mechanical strength, ease of storage, and lack of harvest site morbidity [5, 120, 121]. The aim of synthetic grafts was to eliminate donor site morbidity, deliver a mechanically strong construct, and decrease rehabilitation time ultimately leading to decreased failure and revision rates.

Synthetic grafts have strict requirements in that they need to be cytocompatible, provide adequate mechanical strength, assimilate into the native environment, and provide lasting results [5, 89]. Throughout the years, many prosthetics have entered the commercial market, and several have been withdrawn. Some popular synthetic grafts have been the Ligament Augmentation and Reconstruction System (LARS), the Gore-Tex device—withdrawn from the market in 1993, the Dacron ligament—withdrawn from the market in 1994, the Kennedy Ligament Augmentation Device (LAD), and the Leeds-Keio device [1, 3, 5]. The LARS appears to have the highest rates of success of the synthetic devices, however its sustainability in the long term needs to be evaluated [122, 123]. Table 2.2 summarizes the material composition, failure rate, and commercial availability of a selection of synthetic grafts.

Some synthetic grafts were shown to provide the initial strength to the joint but long-term studies revealed the slow degradation of the mechanical properties over time leading to failure [89, 121]. The mechanical properties of selected synthetic grafts compared to a natural ACL are shown in Table 2.3. An understanding of the long-term mechanical relaxation of the synthetic construct is especially important in the longevity of the prosthetic and the stress protection of the joint [6]. Additionally, these

grafts have been unable to maintain their favourability due to long-term effects such as chronic foreign-body inflammation, pain, synovitis, and osteoarthritis at implant site [5]. Overall, the high failure rates of the majority of the synthetic grafts have deterred their use in clinical practice [2].

Synthetic grafts create ideal prosthetics for ACL reconstruction by avoiding the donor site morbidity and finite tissue availability but the long term function of these devices has yet to be substantiated [120]. Despite the resurgence of interest in synthetic grafts for ACL repair, a prosthetic that accurately replicates the physiological tissue does not currently exist [5].

Table 2.2: Summary of synthetic grafts, adapted from Batty et al., Ghalayini et al., Dheerendra et al., and Petrigliano et al.[1-4]. * indicates data from first generation only.

Name of Graft	Materials	Failure Rate	Market Availability
LARS	Polyethylene terephthalate	2.6%	Currently available
Kennedy LAD	Polypropylene ribbon	13.2 %	Withdrawn 1993
Leeds-Keio I & II	Polyester	16.8%*	Second generation currently available
Dacron	Polyester	29-60%	Withdrawn 1994
Gore-Tex	Polytetrafluoroethylene	33.6%	Withdrawn 1993
Trevira-Hochfest	Polyethylene terephthalate	9.8%	Currently available

Table 2.3: Summary of mechanical properties of several synthetic grafts compared to the ACL. *The tensile strength in young patients is 1730 N and 630 N in older patients. Adapted from Legnani et al., Kdolsky et al., and Ge et al. [5-7].

Properties	Natural ACL	Gore-Tex	Dacron	Kennedy LAD	Trevira-Hochfest	Leeds-Keio
Ultimate tensile strength (N)	1730; 630*	5300	3631	1500	1866	2000
Stiffness (N/mm)	182	322	420	280	68.3	270
Elongation at failure	33%	9%	18.7%	22%	2%	

2.4. Tissue Engineering

To reduce the risks associated with autografts, allografts, and synthetic grafts, there has been a drive towards engineering a hybrid ligament prosthesis combining biological, engineering, and material sciences [4]. This has involved the development of a scaffold that fulfils the mechanical requirements and provides a suitable environment for cellular growth and differentiation. The biochemistry and the anatomical location of the ligament or tendon influence the tissue engineering strategy for scaffold design and construction [15].

This portion of the literature review will discuss ligament and tendon tissue engineering and will give detail regarding advances and studies regarding ligament tissue engineering aimed towards ACL regeneration.

2.4.1. Aims

The aim of tissue engineering is to influence the cellular and biochemical factors of the healing process affecting protein synthesis, leading to enhanced ECM remodelling and tissue repair [15]. Tissue engineering manipulates the repair process on increasing levels of organisation and complexity, as seen in Figure 2.5. The basic components of tissue engineering are the scaffold, the cell source, and the environment providing appropriate nutrients and mechanical stimuli [118, 124]. The combination of these components, in theory, creates a functional tissue if applied within reason. The motivation in tissue engineering research is to find the optimal combination of these factors and then translate the *in vitro* results to *in vivo* use, and further into clinical practice.

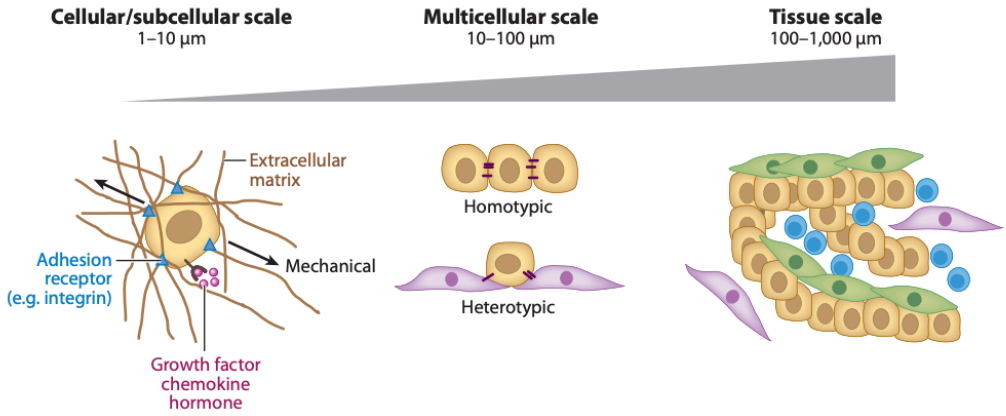

Figure 2.5: A structural scale showing the increasing hierarchy from the cellular to tissue level. At the cellular level, interactions within the ECM, surrounding proteins, and stimuli influence cell response. As the hierarchical structure increases, there are increasingly more components affecting the cellular interactions, such as the cell-cell interaction. At each of the levels, tissue engineering research has developed methods to explore and understand the cellular interactions. Image taken from Underhill et al. [125].

2.4.2. Ligament and Tendon Tissue Engineering

Ligament tissue engineering is a demanding field due to the multiple cell phenotypes within the tissue and great mechanical requirements of the native tissue [126]. There has been extensive research into a variety of biomaterials and synthetic materials to create the optimal scaffold for cell proliferation and ECM organisation [4, 7, 127-131]. The cell source for ligament tissue engineering has been heavily debated due to the complexity of the nature of ligaments [118, 132-134]. Min et al. have reported that the donor cells of allografts are no longer evident beyond 12 weeks while the graft is repopulated by host cells, potentially reducing the importance of the initial cell population [71]. The environment of the seeded scaffold has been manipulated to include a variety of growth factors to promote different aspects of cell maturation and a range of stimuli to compliment the cell growth [124, 135-139]. The evidence of positive fibroblast response to mechanical stimuli has directed ligament tissue engineering research toward the application of tensile strain to the cell construct [8, 136, 140]. In addition to mechanical conditioning, the scaffold architecture has been manipulated through modification of the surface chemistry and the incorporation of growth factors, or their retention during the decellularization process, to promote ligament-like ECM production and direct cell growth [4, 141-143].

2.4.3. Cell Source for Ligament Tissue Engineering

As mentioned previously, the cell source for tissue engineered ligaments is a hotly debated subject and there is no definitive answer to the optimal cell source for a tissue engineered ACL. The abundance, availability, ease of acquirement, and maturity of the cell source are all factors to consider when making a selection for ligament tissue engineering. The most commonly used cells for ACL tissue engineering are mesenchymal stem cells (MSCs) or primary fibroblasts derived from the ACL [126].

2.4.3.1. Mesenchymal Stem Cells

Many researchers use MSCs due to their high capacity for tissue repair and ease of access [132, 134, 144-146]. MSCs are also favourable for their capability of differentiation into fibroblasts and collagen production [15, 147]. The availability of MSCs throughout the body, such as from adipose tissue and bone marrow, is also a factor that positively influences their use. The direct lineage of each of the MSC cell sources is unclear and requires further investigation to understand the differentiation potential for a ligament construct [126]. Further, Sahoo et al. suggests that growth

factors are necessary when culturing with MSCs to facilitate ligament or tendon remodelling [147]. The ideal type of MSCs for ligament repair has not yet been identified.

2.4.3.2. Primary Fibroblasts

There has been interest in using the cells from the ACL itself in the expectation that these cells would have the innate capability of producing the complex ACL biochemical and anatomical structure, leading to a more functional tissue [148-152]. Several studies have reported the successful migration of ACL derived cells into scaffolds and the subsequent matrix proteins synthesized [66, 153-155]. These primary fibroblasts are an interesting alternative cell source to MSCs as the cells already possess the necessary characteristics to produce the desired ECM and tissue of the ACL. Additionally, fibroblasts have the ability to differentiate into several cell lineages, which proves useful for the midsubstance and enthesis requirements of ligament and tendon repair, Figure 2.6 [156]. However, the availability of cells from ACLs remains an issue regarding the adequate storage of explanted cells and pre-transplantation seeding onto the scaffold.

The age of the donor and cell may also be a contributing factor to success of ACL derived cells after seeding onto the graft as several studies suggest that cells sourced from foetal subjects showed better migration, collagen type I secretion, and ECM organisation [150, 157, 158]. However, fibroblasts from ruptured ACLs were found to synthesize and produce collagen up to one year after rupture providing a wider time span to retrieve cells from the donor [150, 153].

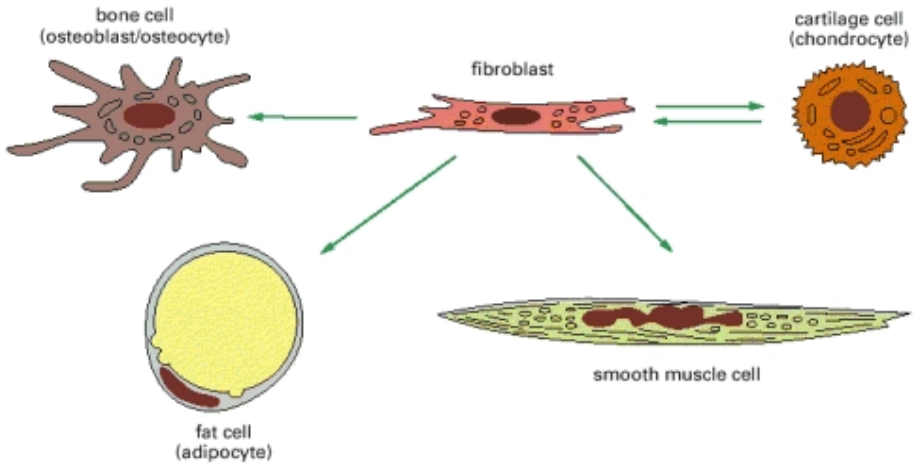

Figure 2.6: Primary fibroblasts have the ability to differentiate into several mature cell types, and de-differentiate back into a fibroblast lineage. Image taken from Alberts et al. [156].

2.4.4. Challenges of Ligament and Tendon Tissue Engineering

Ligament tissue engineering continues to advance with the development of new technology and the increased knowledge of ligament healing and cell response to biomaterials. Aside from the continual research into scaffold construction and optimisation, cell source, and environmental cues there have been challenges within ligament repair surrounding the confluence of the soft ligamentous midsubstance and the stiff mineralized bony region.

2.4.4.1. Enthesis Engineering

A current challenge in ligament and tendon bioengineering is the development of the enthesis, the junction between the soft tissue of the ligament or tendon midsubstance and the osseous end region [137, 139, 159]. The enthesis interface is composed of tissues with varied biomechanical properties that allow for the stress dispersal during movement [160]. The enthesis interface is either classed as a fibrous insertion, where the collagen fibres of the ligament connect into the periosteum of the bone, or a direct insertion, consisting of a fibrocartilaginous region [161]. Direct insertions of ligament into bone are more susceptible to injury and damage from overuse [162].

The entheses of direct insertions, such as found in the ACL, consist of 4 regions of graded mineralized tissue with distinct matrix compositions: a ligament/tendon region, an unmineralized fibrocartilaginous region, a mineralized fibrocartilaginous region, and a bony region, as seen in Figure 2.7 [52]. Each of these regions contains a related cell phenotype; osteoblasts are found within the bony region, fibrochondrocytes within the fibrocartilaginous regions, and fibroblasts in the ligament region [18]. The organisation of the cells within each region also changes, as the cells found in the ligament or tendon region are sparse and elongated towards the axis of tension and the cells in the fibrocartilage are rounded, as seen in Figure 2.8 [163].

Within each of these regions, the collagen type and content differs, as collagen type I is found in an ordered structure within the ligament, collagen types I, II, and III are found within the unmineralized fibrocartilage, collagen types II and X are found within the mineralized fibrocartilage, and mineralized collagen type I is found within the bone matrix [164]. Additionally, an increasing calcium and phosphorus content is seen along the mineralization gradient of these regions [165-167]. A higher content of sulfur has also been detected at the enthesis compared to the ligament midsubstance,

due to the increased sulfated proteoglycan content in this region [165, 168]. The compositional changes, namely the organisation and type of collagen and the mineral content, between these regions create a gradient of mechanical stiffness that helps to disperse the mechanical loading of the joint during movement [169]. Despite the distinct composition of each these regions, they are structurally continuous enabling a strong biomechanical interface.

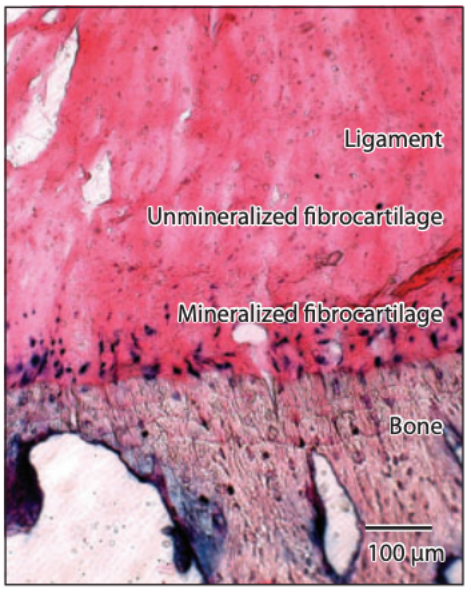

Figure 2.7: The natural ACL enthesis, consisting of a ligament region, unmineralized fibrocartilage region, mineralized fibrocartilage region, and bone. Each of these regions can be seen as compositionally distinct yet structurally fluid. Image taken from Lu et al. [164].

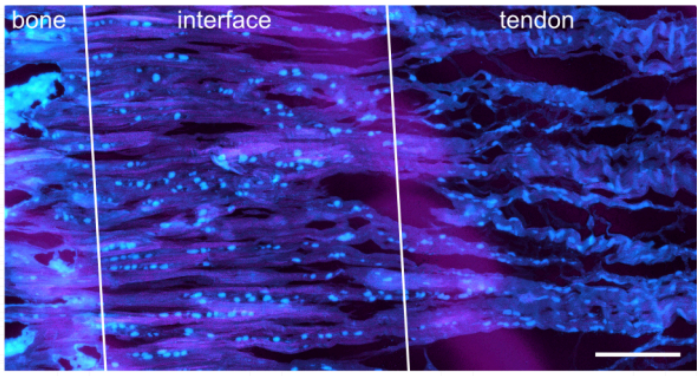

Figure 2.8: The morphology of cells found at the Achilles tendon enthesis. The cells are depicted in cyan. Within the interface region, the cells are rounded and typically found in pairs. In the tendon, the cells are found aligned along the axis of tension between tendon fibres. Scale bar represents 150 µm. Image taken from Kuntz et al. [163].

It has been shown that the entheses of the ACL have deep integrations of the fibrocartilaginous zone into the bone region resulting in a direct insertion of ligament into bone, which is related to the mechanical loading [53, 162, 170]. The ACL enthesis is a strong interface that dissipates the stresses of active and passive movement due to

the alignment of the collagen fibrils into the bone, as seen in Figure 2.9 [161, 169, 171]. The 'surgical juxtaposition' between the soft tissue and bone does not allow the natural re-establishment of the organised fibrocartilaginous zone and mechanical stability, leading to increased occurrence of 'tendon pull-out' [172, 173]. The direct insertion of the ACL enthesis has proven challenging to restore in research, resulting in the engineered enthesis being mechanically weaker than the native junction [52, 63, 174]. The change in viscoelastic properties of the ACL enthesis further complicates the enthesis engineering in *in vitro* and *in vivo* studies [175, 176]. Additionally, the two entheses of a ligament may differ in stress dispersal leading to varied rates of injury and repair, such as the femoral and tibial entheses of the ACL [177].

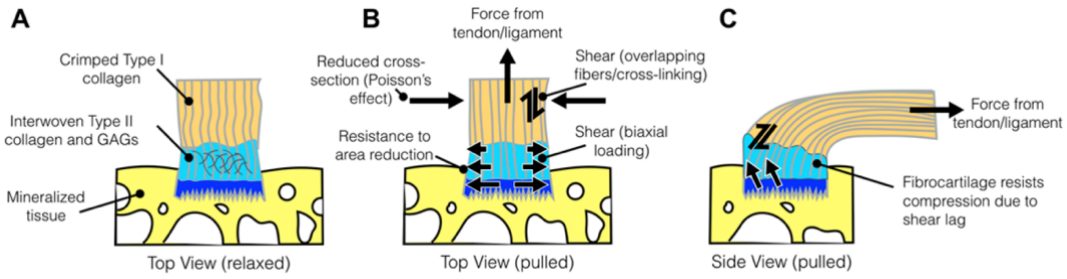

Figure 2.9: The enthesis region shown with the bone in yellow, mineralized fibrocartilage in dark blue, unmineralized fibrocartilage in light blue, and the ligament/tendon in the tan. (A) Shows the relaxed ligament with the crimping pattern intact. (B) The ligament is under tension and the crimping pattern has disappeared due to the collagen fibrils being stretched. (C) The ligament under tension as seen from a side view. In both B and C, the fibrocartilaginous regions are able to dissipate the stress from the applied forces. Schematic taken from Locke et al. [174].

The fibrocartilaginous region has shown to be incapable of natural healing after injury, where fibrous scar tissue is produced that has inferior mechanical properties of the original tissue [167]. Injury to this tissue could cause permanent damage to the enthesis [178]. The decreased healing capacity of enthesis fibrocartilage has prompted the need for intervention. The largely unknown phenotype of fibrochondrocytes and the production of a mineralized gradient have caused difficulties in enthesis engineering [169, 179]. Fibrochondrocytes are phenotypically similar to chondrocytes, however their ability to produce compressive load-bearing ECM is inferior, including the synthesis of proteoglycans such as aggrecan [18, 168]. Spalazzi et al. have found that compression of a tendon graft induced the upregulation of several fibrocartilage markers, such as collagen type II and aggrecan, indicating that fibrochondrocytes can be recruited from the tendon or ligament midsubstance [180]. The role of fibrochondrocytes in the mineralization process is ill known [181]. Several

studies have identified that the mineralization potential of fibrochondrocytes is through the hedgehog signalling pathway, however this originates in prenatal development and would require further investigation to implement the correct signals within a tissue engineered construct [178, 181]. Sun et al. found that the fibrochondrocytes at the ACL entheses had a higher mineralization potential than the fibrochondrocytes found in the articular cartilage or menisci of the knee [179]. The complexity of the ACL fibrochrondrocytes is still widely unknown as research into the derivation and response of these cells continues [169, 182, 183].

To increase the mineralization potential of engineered entheses for ligament or tendon reconstruction, several studies have investigated the incorporation of ceramics as a bone tunnel filler or coating, such as hydroxyapatite, brushite, or calcium phosphate cements [184-190]. Hydroxyapatite is a clear choice for bone grafts due to its crystalline presence in bone matrix, however it is has little resorption potential *in vivo* and its brittle nature can cause implant failure [191]. Brushite has become preferable over hydroxyapatite due to its increased resorption potential, however brushite has shown to be hydrolysed into hydroxyapatite crystals [192]. This has led to the investigation of calcium phosphate salts in the form of ß-tricalcium phosphate and its derivatives [193-196]. The increased availability of calcium and phosphate ions have shown to increase the osteogenic potential of these materials for enthesis engineering [197]. However, these engineered entheses have shown limited potential for biological fixation [184].

Several studies have attempted to build on the success of calcium phosphate salts by creating hybridized tendon grafts from animal models that maintain the biomechanical strength of the native tendon [171, 198-200]. These studies have shown great success in promoting the growth of an interface similar to that of the native ACL enthesis. However, the long-term stability of these hybridized grafts has not yet been reported.

To further increase the biomechanical similarity of the enthesis, recent studies have investigated the use of decellularized tendon-bone grafts to preserve the optimal biomechanical strength of the natural enthesis [173, 201]. The decellularization of tendon-bone constructs is complicated due to the different cell densities of the tissues limiting the access of chemical agents [202]. These decellularized models have shown to preserve the biomechanical properties of the natural enthesis after implantation [173]. Although this research has been limited to animal models, this method has the

potential to be adapted to cadaveric allografts. In fact, Fox et al. have investigated the use of decellularized tendon-bone grafts for reconstruction of hands and found that the mechanical strength of the decellularized graft was not compromised during decellularization and was suitable for post-reconstruction therapy [203].

The enthesis is a key factor to a successful insertion of a ligament. There has been exceptional research into creating mineralized scaffolds for an engineered enthesis but there has been little to report on the functional outcome of the mineralization [204]. There is still much knowledge to be learned from the enthesis complex and the improvement in reconstruction.

2.5. Scaffolds in Tissue Engineering

Tissue engineering aims to create a biomimetic scaffold to simulate the natural environment of the tissue in a structural and mechanical sense. The ideal scaffold for ligament repair should permit the necessary cellular ingrowth and matrix deposition while maintaining the mechanical strength of the native tissue [9, 130, 138, 205-207].

The function and application of the scaffold often dictates the structure, as described in Table 2.4 [141, 208-210]. In this manner, each design parameter can significantly affect the linked function. The choice of material can have a profound impact on several structural aspects of the scaffold, such as the architecture, mechanical strength, and degradation. The study by Dunn et al. highlights the importance of scaffold design for cell maturation, as they found a tenfold increase of collagen synthesis on ligament analogs compared to the tissue culture plastic (TCP) control [211]. In their study, the fibroblasts showed high proliferation on the TCP, however the ligament analog provided a more suitable environment for synthesis of collagen and ligament-like ECM production. The design of a scaffold for tissue engineering must consider the function and application for an ideal material choice and architecture modelling.

Table 2.4: Scaffold function and design parameters. Each function has a linked design parameter. Adapted from Edwards et al. [141].

Function	Design Parameters
Not to provoke an inflammatory or immunogenic response	Must be cytocompatible and non-toxic
Allow significant cell surface interactions	High surface-area to volume ratio
Give way to uniform high cell seeding density	High porosity and pore interconnectivity
Provide appropriate surface for cell attachment, proliferation, and differentiation	Optimum surface chemistry and topography
Promote cell proliferation and migration, leading to tissue growth throughout the scaffold	Optimum pore size to allow for cell penetration
Allow for movement of nutrients and waste	High porosity and pore interconnectivity
Direct orientation of cells and ECM	Correct fibre orientation within the scaffold
Scaffold may degrade to leave only natural tissue	Rate of degradation to match rate of tissue formation (degradation products must not be toxic or promote inflammatory response)
Possess sufficient structural integrity and mechanical strength	Scaffold should equal mechanical properties of developing tissue
Assist in growth of 3D tissue	3D similarity to native tissue

2.5.1. Scaffold Composition and Architecture

The composition of scaffolds is wide ranging and can consist of natural or synthetic polymers, or a combination of these, while the physical architecture of scaffolds can range from fibres, membranes, and hydrogels. Both the composition and architecture of the scaffold can influence cell response and mechanical strength [130]. The choice in biomaterial to create the necessary microstructure for cell response and macrostructure for mechanical strength is highly dependent upon application [141].

One of the most widely used biomaterials for scaffold creation is collagen due to its presence in native tissues. Other prominent biomaterials include gelatin, polylactic acid (PLA) and its derivatives, chitosan, silks, and hyaluronic acid [212-215]. Another increasingly popular natural biomaterial for ligament engineering is fibrin. Fibrin is a protein involved in blood clotting and has been shown to have contractile properties [216-218]. Due to its wound healing capacities, fibrin has seen great success as an injectable glue and as a hydrogel [219]. However, the sustainability

of the mechanical strength of fibrin as a core material for ligamentous scaffolds for tissue engineering requires further investigation [220-222].

Many studies have examined fibres constructed of natural materials, such as silk and collagen, and synthetic polymers as a scaffold for ligament tissue engineering which demonstrate positive cellular ingrowth but have variable mechanical results [213, 223-226]. To improve the strength of fibrous scaffolds, several studies have explored the effect of a braided or woven assembly [227-229]. The increased complexity of the fibrous structure strengthened the scaffold and provided another structural level for cellular attachment [230-232]. These studies have shown the great consideration of the fibre organisation of the scaffold design encompassing the macro-structure for mechanical strength and the micro-structure for a beneficial cell response [233]. The mechanical properties of several scaffold materials are described in Table 2.5.

Table 2.5: Mechanical properties of selected materials for ACL reconstruction. Adapted from Ge et al. [7].

	Ultimate Tensile Load (N)	**Stiffness (N/mm)**	**Elongation at failure (%)**	**Tensile Modulus (MPa)**
Human ACL [234]	2160 ± 157	242 ± 28	~33	110
Patellar-tendon Graft [226]		685 ± 86		
Hamstring Graft [235]	3790-4830	776		
Twisted Silk Cord [226]	2337 ± 72	354 ± 26	38.6 ± 2.4	
Braided PLGA [227]	907 ± 132			100-400
Braided PLLA [228]	21		70	55.0 ± 2.8
Single Collagen Fibres [225]			17.5	359.6 ± 2.9
Chitosan/Hyaluronan Fibre [213]			3.2 ± 0.6	217.6 ± 16.9

2.5.1.1. Collagen

Collagen is the most abundant family of proteins in the human body and is a major structural component in all connective tissues [39, 40]. The ECM of connective tissues, vessels, and bone is composed of strong collagen fibres which are constantly undergoing remodelling [216]. The various types of collagen present in the ECM contribute to the tissue's structural and mechanical properties [236]. The presence and

versatility of collagen in the native tissue makes it a model biomaterial for ligament tissue engineering.

The methods of using collagen as a biomaterial include the decellularization of existing tissues leaving the ECM structure, a xenograft, and the polymerization of collagen to create a functional scaffold [237, 238]. While decellularized ECM constructs have been considered for a ligament prosthesis, the sterilization and availability are factors to consider [114]. The effect the decellularization agent has on the biochemical structure of the scaffold is a key focus of several studies [205, 239-242]. Xenografts are largely available, through the use of animal models, however the risk of disease transmission is increased [205, 243]. Whitlock et. al have shown preliminary success using a xenograft harvested from chicken tendons that did not have an immunological response when implanted *in vivo* and had an optimised porosity for cellular ingrowth without compromised cytocompatibility [113]. Decellularized collagen ECM scaffolds provide an alternative for ligament tissue engineering but more investigation into their sustainability and long-term immunogenic response is needed.

The purification and polymerization of collagen is more commonly used as a material for ligament scaffolds. Collagen has favourable biochemical, biocompatible, and biodegradable characteristics and can be widely used with a number of other biomaterials [130, 244]. Previous studies have used electrospun collagen scaffolds to promote cellular growth and maturity [245-247]. Other studies have produced collagen gels and membranes through lyophilization that aim to mimic the properties of native tissue [212, 248-250].

Collagen fibre constructs, membranes, and gels simply do not have the required strength to be used for ligament or tendon tissue engineering [214, 244]. Therefore, a collagen-based scaffold with the addition of a strengthening or crosslinking agent is commonly found in ligament tissue engineering. These incorporated agents may also help to control the rate of degradation of the collagen scaffold [251]. Physical and chemical crosslinking of the collagen polymers has been shown to improve the mechanical strength but some crosslinking agents, such as glutaraldehyde, result in cytotoxic residue in the scaffold [252-255]. Synthetic polymers have been added to collagen to create a blended scaffold to yield optimal mechanical properties. Some commonly used polymers with collagen are PLA, polyglycolic acid, poly (lactide-*co*-glycolic acid) (PLGA), poly (ε-caprolactone), poly

(ethylene glycol), chitosan, elastin, and hyaluronic acid [131, 138, 256-261]. These collagen-based scaffolds have not yet produced the complete ligament prosthesis suitable for ACL reconstruction but have provided a wealth of information on the cellular response, mechanical properties, and the physical characterisation of the scaffold.

2.5.1.2. Gelatin

Gelatin shares structural similarity with collagen, as it is derived from partially hydrolysed collagens [262, 263]. The availability, biodegradability, and biocompatibility are all factors that have led to the use of gelatin-based scaffolds in a range of biomedical fields [264]. Gelatin has greater similarity to the microenvironment of the native tissue than various other synthetic and non-collagen derived materials [265].

Like collagen, the mechanical strength of gelatin is low, making it a more suitable material for wound dressing or drug delivery. Many studies have investigated the processing of gelatin into nanofibrous scaffolds for increased mechanical strength [262, 266-268]. The biochemical structure of gelatin is compatible for tissue engineering however it requires further reinforcement to create a ligament scaffold.

2.5.1.3. Chitosan

Chitosan is a versatile material that has natural antibacterial properties and is cytocompatible, biodegradable, easily accessible, and cost-effective [269]. Chitosan is derived from the deacetylation of chitin which can be found in the shells of crustaceans, Figure 2.10 [270]. The manufacturing ease of chitosan allows great control over the porosity of the desired scaffold [271, 272]. Additionally, the structural properties of chitosan are similar to GAG which may influence the synthesis of GAG by attached cells [273]. These natural properties of chitosan make it an ideal biomaterial for tissue engineering applications [274, 275].

The cationic nature of chitosan has a beneficial impact on the interactions with GAG and proteoglycans and may also play a role in the adhesivity of fibroblasts to the scaffold [214, 276, 277]. These ionic interactions further accelerate the use of chitosan in cell culture scaffolds.

Chitosan is a versatile biomaterial that can be utilized in a number of different scaffold types. Modifications to the ionic structure of chitosan can allow mechanical and biological variation in the scaffold design [276]. It has been shown that the addition of chitosan to porous collagen scaffolds can improve the biostability of the

scaffold by slowing the rate of biodegradation [251, 256]. An increase in scaffold tensile strength was seen in a study by Tamura et al. who used chitosan-coated alginate filaments [278]. While Surakawa et al. recorded an enhanced fibroblast response on chitosan-coated PLA fibres [279]. Further developments in mechanical strength and fibroblast response were seen by Funakoshi et al. who blended chitosan with hyaluronan to create novel polymer fibres in comparison to chitosan alone [213]. These studies show promising results from the addition of chitosan to scaffolds; however, the mechanical integrity of chitosan is still lacking.

The degradation rate of chitosan decreases with the increasing degree of deacetylation, where highly deacetylated chitosan may remain *in vivo* for several months [280]. Chitosan-based scaffolds with a high deacetylation percentage may provide an adequate time period to allow cellular ingrowth during degradation. The degree of deacetylation also influences the reactivity of the chitosan functional groups and increases water retention [271].

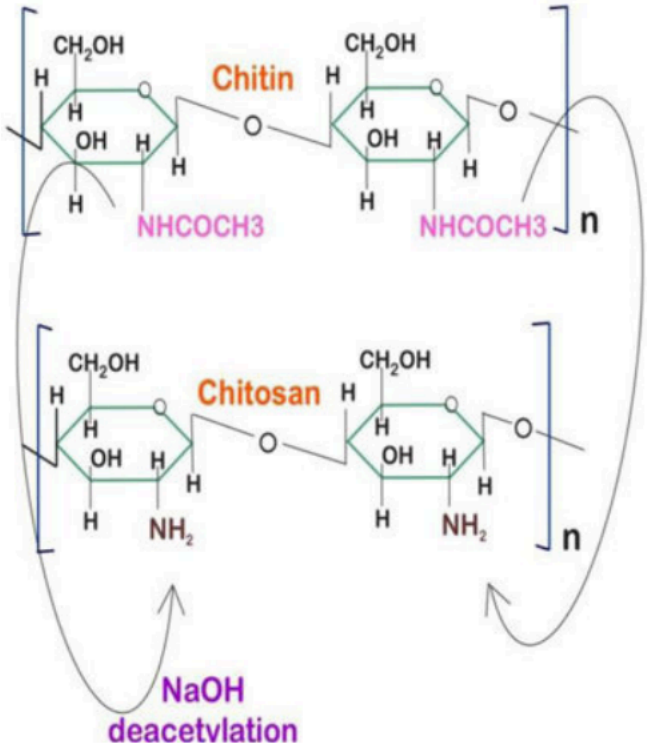

Figure 2.10: The chemical structures of chitin and chitosan indicating the sites of deacetylation [274].

2.5.1.4. Crosslinking of Chitosan Scaffolds

The incorporation of natural crosslinking agents has become increasingly popular to enhance the strength of chitosan scaffolds and to influence the cellular

response [281, 282]. The physical properties of chitosan scaffolds can be controlled through the degree of the crosslinking [283]. Commonly used agents for chitosan crosslinking have included glutaraldehyde, genipin, and oligomeric proanthocyanidin (OPC) [284-286]. Glutaraldehyde has proven to increase the mechanical integrity of chitosan hydrogels, however it has shown to be cytotoxic if not fully consumed during crosslinking [287]. Genipin has widely replaced glutaraldehyde as a crosslinker and has been shown to have anti-inflammatory and anti-bacterial properties [288, 289]. The adhesion and proliferation of fibroblasts has increased on chitosan scaffolds crosslinked with genipin [290, 291]. OPC has been a common addition to chitosan scaffolds for its natural availability and positive cell response [292-294]. The strong hydrogen bonds between chitosan and OPC contribute to the structural integrity of these scaffolds while further enhancing the natural antibacterial properties of chitosan [295-297]. Additionally, Liu et al. has reported that OPC is 120 times less toxic than glutaraldehyde as a crosslinking agent [298]. OPC and genipin are suitable as alternative crosslinking agents for chitosan and collagen-like scaffolds to maintain mechanical properties [299-302].

2.5.2. Biodegradability

The biodegradability of a biomaterial is another area of consideration for scaffold design. The biodegradation of the material must not elicit a foreign body or immunological response from the host [4, 303]. Fibres made of PLA, polyglycolic acid, and PLGA have shown to be biodegradable without producing cytotoxic residues increasing their popularity in tissue engineering research [227]. The products of fibrin biodegradation have been shown to promote cell attachment and proliferation and stimulate angiogenesis [216].

The biodegradability poses a risk to the mechanical strength of the scaffold as the rate of degradation must not exceed the rate of matrix deposition and cellular ingrowth [17, 130]. There is a fine balance in maintaining the required strength of the scaffold while promoting cellular ingrowth and biodegradation. The biodegradation of polyglycolic acid based scaffolds leading to loss of structural integrity has been seen in as little as 2 weeks of immersion in cell culture medium [304, 305]. The biocompatibility and biodegradability of silk scaffolds has increased interest in their use, as Wu et al. have reported an 8% weight loss after incubation for 60 days for a degummed silk fibroin scaffold [306]. The degradation profiles of biomaterials in cell culture environments are important to understand how the material will react as a

scaffold, however cell culture on these biomaterials is required to gain a true understanding of the material's suitability as a scaffold for tissue engineering applications.

An ideal scaffold for ligament repair would allow tissue formation that advances its proportion of mechanical contribution as the scaffold degrades and decreases in mechanical contribution, as depicted in Figure 2.11 [208]. Therefore, understanding of the cellular response and tissue generation during degradation of a scaffold is required. In an *in vivo* study using braided collagen fibres as ACL grafts in goats, researchers found that the distinction between graft and tissue was difficult to interpret with approximately 50% resorption of the scaffold after 6 months [307]. Chen et al. have shown evidence of tissue formation and full degradation of a poly(lactic-co-glycolic acid)-collagen mesh after 12 weeks, however the mechanical integrity of the scaffold was not measured [308]. Surrao et al. found an increase in tensile strength and ECM similar to a natural ACL on crimped poly(lactide) fibrous scaffolds seeded with bovine fibroblasts after 8 weeks of culture and less than 10% mass loss after 4 weeks [309]. A study investigating braided poly(L-lactide) scaffolds with hydroxyapatite enriched bony regions, found sufficient tissue integration across the scaffold after 6 weeks *in vivo* in a rabbit model, however the mechanical integrity was not tested post-operatively [310]. Despite the increased studies of tissue deposition on biodegradable scaffolds for ligament repair, there is little information regarding the combined scaffold resorption, tissue generation, and the subsequent mechanical strength of the scaffold over time.

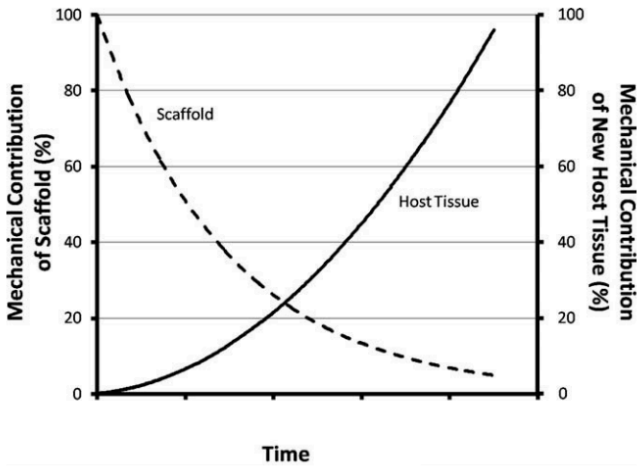

Figure 2.11: Diagram of the mechanical contribution of a scaffold and new host tissue, or tissue generation on a scaffold, over time. The mechanical contribution of the new tissue should overtake the mechanical contribution of the scaffold as it degrades over time. Adapted from Badylak et al. [208].

2.6. Hydrogels

The popularity of hydrogels has surged recently because of their exceptionally tuneable structural, chemical, and mechanical properties and tissue-like water content [217, 311]. Hydrogels are formed of a 3D network of hydrophilic polymers that have the capacity to swell and retain a large volume of water [312]. Hydrogels can provide a more similar environment for cell growth while allowing the diffusion of nutrients and waste [313]. A unique characteristic of hydrogels is their injectability and variable rheology [314].

In order to more accurately replicate the native environment, hydrogels can be synthesized from a variety of materials, from natural to synthetic polymers [315]. The synthesis of hydrogels is highly adaptable and tuneable to the specific application due to the high diversity of available biomaterials and bioadditives, Figure 2.12 [316]. The synthesis of hydrogels is largely based on the desired tissue engineered product.

The mechanical strength of hydrogels is typically low due to its high water content. This is suitable for soft tissues that do not experience high levels of force *in situ*. However, for tissues that require a higher level of structural integrity, studies have explored the addition of PLLA fibres, polycaprolactone and silk fibroin fibres, and titanium springs into hydrogels [317-319]. The flexibility of hydrogel composition has led to the research and implementation of hydrogels in an increasing number of biomedical applications.

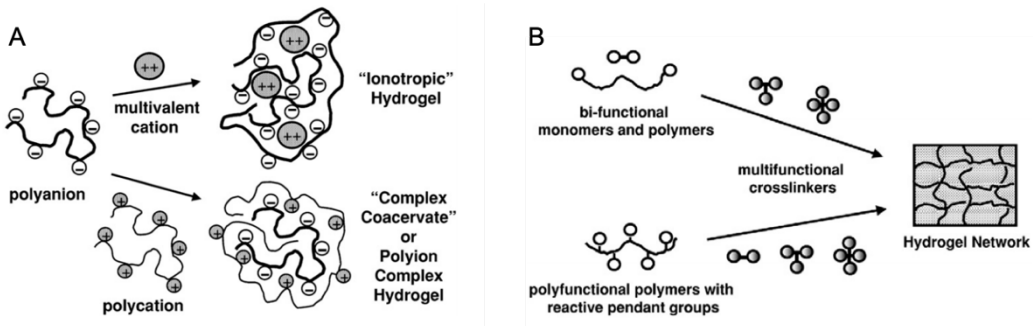

Figure 2.12: Two examples of hydrogel synthesis. A) Formation of ionic hydrogels either through the use of a multivalent cation or a polycation. Examples include alginic acid and polylysine complex and chitosan complexes B) Formation of crosslinked hydrogels using reactant groups. Examples include reactions with collagens, polysaccharides, and poly(ethylene glycol). Image adapted from Hoffman [316].

2.6.1. Hydrogels in Ligament Regeneration

Due to the low mechanical strength of hydrogels, ligament engineering researchers have begun to implement strategies that have shown success in other applications of tissue engineering [320, 321]. For example, building on the success of

electrospun meshes in cartilaginous and vascular studies Thayer et al. incorporated cylindrical electrospun meshes into poly(ethylene glycol) hydrogel networks and found that they provided an adequate mechanical scaffold for ligament engineering but were unable to support cellular growth [322]. Freeman et al. have found that a hydrogel-fibre composite created a scaffold with similar tensile properties to the native ACL and supported fibroblast growth [318]. Paxton et al. have shown that hydrogels can support the addition of hydroxyapatite, or other minerals, for an enhanced enthesis scaffold [184].

Growing numbers of researchers have implemented collagen, gelatin, and chitosan into hydrogels for their natural biocompatible properties, high abundance, low cost, and the increased cellular response leading to an organised ECM. Murray et al. found that collagen-GAG scaffolds supported the migration and complex ECM production of ACL derived cells, however the mechanical integrity was not reported [154, 155]. Several studies have incorporated a collagen-based hydrogel coating onto electrospun fibres of poly(caprolactone), that provide mechanical reinforcement with the collagen hydrogel offering a suitable environment for cellular growth [323, 324]. The hydrogel was found to increase the cytocompatibility, protein adsorption, and fibroblast alignment without alteration of the tensile strength of the fibres. Another study created a novel multi-layered composite hydrogel scaffold of gelatin and poly(caprolactone) fibres that successfully directed human adipose stem cells towards a tenocyte phenotype [265].

Murray et al. have utilized collagen-based hydrogels as a supplement to ACL regeneration that released key proteins and platelets to aid in healing [325]. The hydrogel supplement resulted in improvements in the tensile loading of the porcine ACL. However, this study was performed with a short time point and the longevity of the repair method needs further investigating.

Fibrin has also been a key component of hydrogel scaffolds for ligament tissue engineering based on its function in wound healing [217, 218, 221, 326]. These studies have reported successful contraction and migration of cells within the scaffold. Breidenbach et al. reported the superior mechanical, structural, and biological properties of fibrin hydrogels compared to collagen hydrogels [220]. However, Vavken and colleagues found a negative correlation between the fibrin concentration in hydrogel and the DNA and collagen production from ACL fibroblasts, concluding

that high concentrations of fibrin, such as in medical glue to close wounds, should be used with caution [151].

The water retention of hydrogels has played a large role in their use for tissue engineering applications [323]. Several studies have created hydrogel fibres that maintain the swelling capacity of the hydrogel to better mimic the viscoelasticity of ligaments [318, 327]. However, Bach et al. have shown that the swelling of poly(vinyl alcohol) hydrogel fibres may lead to the release of fibre orientation which can limit the tensile stiffness of the scaffold [328]. The swelling capacity and water retention of hydrogels is a hugely important factor in their use in tissue engineering, however these properties require more investigation as hydrogels become increasingly popular in ligament tissue engineering applications.

These studies highlight the necessity of tailoring hydrogel composition and synthesis to create a scaffold that mimics the natural environment of the ligament or tendon. Hydrogels are becoming an increasingly popular material for ligament tissue engineering. However, the low mechanical strength of hydrogels is a limiting factor to their implementation and translation beyond *in vitro* use.

2.7. Bioreactors in Ligament and Tendon Tissue Engineering

Bioreactors regulate specific environmental factors during cell culture in a reproducible and controllable fashion [140]. In this way, a bioreactor can more accurately simulate the physiological environment of the native tissue and has become an indispensable aspect of ligament tissue engineering. A bioreactor for ligament engineering applications is composed of four key components: the culture chamber, mechanical actuating system, environmental control system, and the medium circulation system, Figure 2.13 [8]. Often, bioreactors will be uniquely created and modified for individual studies. Bioreactors can reduce the manual handling and variation and decrease risk of contamination while increasing scalability and production [329, 330]. The use of bioreactors in combination with engineered scaffolds affords great control over cell behaviour and interactions.

A deeper understanding of the mechanical stimuli requirements for tissue regeneration has made bioreactors an important staple in ligament and tendon tissue engineering. It has been shown that mechanical stimulation is necessary to regulate cell behaviour and simulate the *in vivo* environment leading to the regeneration of load

bearing tissue [331, 332]. Bioreactors for ligament and tendon tissue engineering are predominantly essential for precise application of mechanical stimulation.

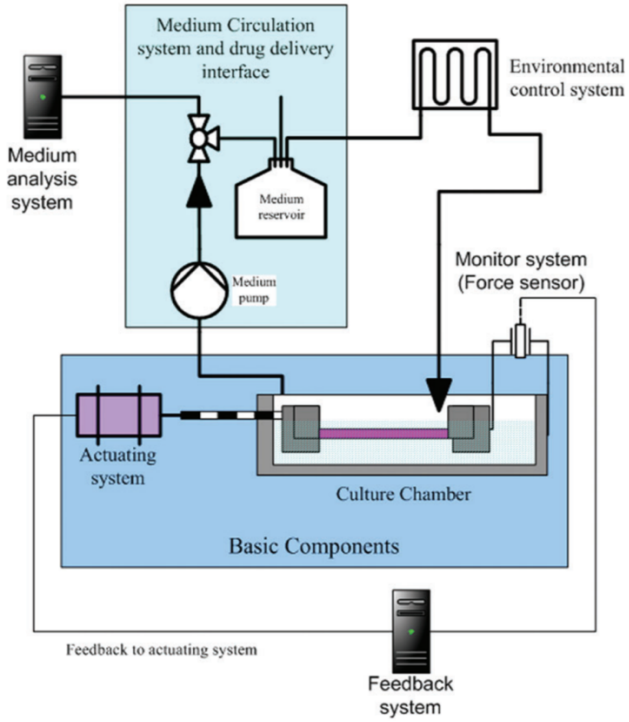

Figure 2.13: The components of a bioreactor for ligament and tendon tissue engineering. The basic components include the actuating system for mechanical stimulus, the culture chamber, the environmental control, and medium circulation. These components can be modified in a number of ways to induce specific cellular responses. Image adapted from Wang et al. [8].

It has been widely reported that fibroblasts require mechanical stimulation during culture to produce an ECM that resembles the native ligament ECM [333-335]. The current drive in ligament and tendon tissue engineering is generating the optimal mechanical stimulation to induce production of a suitable ECM. Bioreactors have become increasingly common within ligament tissue engineering research to replicate the physiological loading of a natural ligament [19, 215, 255, 336, 337]. Due to the necessity of physiological loading during cell culture, the most common bioreactor design for ligament and tendon engineering consists of a cell culture chamber with two points of attachment for the scaffold to the actuating system. One, or both, of these attachments allows the transmission of the physiological loading onto the scaffold and seeded cells. In using this design, the attachments of the scaffold to the actuating system of the bioreactor are an important aspect to consider when developing the scaffold.

Cyclic tensile strain has been shown to increase scaffold strength by increasing total collagen synthesis and cell alignment, Figure 2.14 [65, 149, 338, 339]. However, the application of tensile strain to scaffolds is under debate concerning the rest period, frequency, and strain rate [8, 340, 341]. This has led to a range of strain rates, such as 2% and up to 10%, highlighting the range of physiological strain during movement of the native ACL [62, 149, 215]. The time of applied mechanical strain also ranges from 1hr/day to 8hr/per day [19, 342-344]. Further optimization of the strain regime has concluded that an ample rest period is conducive to cell proliferation and to allow adequate ECM protein synthesis [344, 345]. Several studies utilizing a bioreactor for ligament tissue engineering are outlined in Table 2.6 describing the mechanical parameters, scaffold and cell type, and the overall outcome.

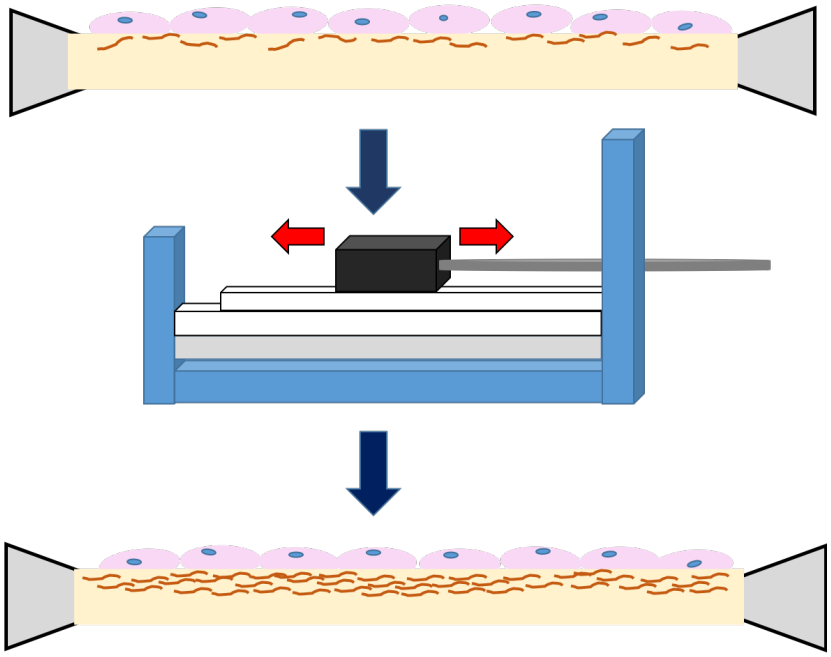

Figure 2.14: A simple schematic of a hydrogel scaffold (yellow) with anchors (grey) at either end seeded with cells (pink) undergoing tensile strain within a bioreactor. The hydrogel scaffold is housed in the bioreactor (middle diagram) in the grey plane below the white planes that control the movement of the anchors. Before the application of strain, the collagen fibres (orange) are unorganised and sparse in number. After the tensile strain, the collagen fibres are more numerous and organised.

Reproducing the natural environment remains a challenge as investigators attempt to create *in vitro* studies that more similarly replicate mechanical behaviours that would occur *in vivo*. This has led to studies creating bioreactors that can apply multi-dimensional strain that more accurately mimics the functional units of the ligament, such as the AM and PL bundles of the ACL [136, 346]. Goodhart et al. investigated a design of bioreactor that applied a spatially-selective strain but did not

find significant differences upon the scaffold, potentially due to the shared medium [347].

Due to the factors described, bioreactors have become an indispensable component of ligament and tendon engineering. Bioreactors offer a controlled and reproducible environment with the potential for upscaling that is not typically seen within cell culture. The mechanical stimulation that bioreactors can provide is an important factor in creating a tissue engineered ligament. However, there are many elements to consider when implementing a bioreactor resulting in numerous custom bioreactors used in research to optimise ligament regeneration.

Table 2.6: A review of several studies that utilized bioreactors for ligament or tendon engineering. Table adapted from Wang et al. [8].

Study	Type of Bioreactor	Parameters of Mechanical stimulation	Scaffold Material	Cell Source	Conclusion
Altman et al. [136]	Biaxial step motor	Cyclic with 90º rotation, 0.0167 Hz, 21 days	Silk fibres and collagen type I gel	Human bone MSC	Elongation of MSCs, increase of cross-section density
Saber et al. [19]	Uniaxial step motor	Cyclic 1.25N, 0.0167 Hz, 1 hour/day for 5 days	Acellular rabbit tendon	Rabbit tenocytes	Increased ultimate tensile stress and elastic modulus
Paxton et al. [341]	Uniaxial step motor	Cyclic, 2.5%strain, 0.5 Hz, 10 min repeated every 6 hrs, 7 days	Fibrin gel	Primary rat Achilles' tendon fibroblasts and Primary chick	Increased collagen and ERK1/2 phosphorylation
Riboh et al. [345]	Flexcell Strain Unit	Intermittent cyclic stretching, 4% strain, 0.1 Hz, 1hr on/2hr off & 1hr on/5hr off, 4 days	Fibronectin-coated silicone UniFlex culture membrane	Epitenon tenocytes, sheath fibroblasts, MSCS from bone marrow and adipose tissue	Increased proliferation and collagen I production, cytoskeletal alignment, nuclear elongation
Kim et al. [149]	Uniaxial	Cyclic stretch, 10% elongation, 10 cycles/min for 24 hrs	Silicon membrane	Human ACL fibroblasts	Increased mRNA expression of collagen I and III and increased TGF-ß1
Kreja et al. [215]	Uniaxial	Intermittent cyclic stretch, 2% or 5% strain, 1 Hz, 1hr/day for 15 days	PLA scaffold	Human MSC and Human ACL fibroblasts	Increased mRNA expression of collagen I and III, tenascin C, fibronectin, and decorin in human ACL samples

2.8. Biological Characterisation of a Tissue Engineered Ligament

Within ligament tissue engineering, there are several biological markers that are used to characterize the scaffold during and after cell growth, including cell morphology, ECM composition, and gene expression. These biological markers are indicative of accurate cell growth, proliferation, migration, and ECM production [348, 349]. Surveying these markers during the process of regeneration in tissue engineering is an important and valuable tool.

2.8.1. Cell Organisation and Morphology

The cell organisation and morphology within a scaffold for ligament tissue engineering are useful measures of cell growth on a scaffold. As discussed previously, the cellular organisation and morphology varies throughout the regions within a ligament, such as the ligamentous region compared to the entheses. Near the middle ligamentous region, the fibroblast morphology is elongated and sparse, whereas near the entheses, the fibrochondrocytes become more rounded and are found in pairs [163]. The cell number also depends on the healing stage of the ligament where mature ligaments have sparse cell numbers and healing ligaments have a dense cell population [96, 350].

Monitoring the cell morphology on a scaffold can help to identify signals of positive regrowth. Additionally, undesirable cell responses can be mitigated early by observing the cell morphology and organisation.

2.8.2. ECM Components

The composition of the ECM determines the structure of the tissue and aids in its function [208]. One of the most important components of the ECM of ligaments is the collagen content and organisation, specifically collagen types I and III [351]. It has been shown that the crosslinking between fibrils and length of collagen fibrils along the longitudinal axis of the ligament increases with maturity of the tissue [20, 352]. The organisation of collagen fibrils is important as they regulate the mechanical forces within the ligament and transmit these forces to the adjacent bone, though the organisation and localisation of collagen fibrils and accompanying proteoglycans in a healing ligament is unknown [352, 353]. The collagen content can be measured through immunoassays while the organisation of the fibrils can be visualised through fluorescent staining.

Decorin, elastin, and tenascin-C are vital proteoglycans within the ECM of ligaments that regulate collagen fibril formation and deposition [348, 354]. These

components are indicative of matrix deposition and remodelling that is essential for ligament repair [350]. Tenascin-C has been used as a ligament-specific biological marker due to its high concentration in ligaments and tendons and its upregulation from mechanical loading [348]. These biomarkers are typically measured with a terminal assay through a range of fluorescent markers and immunoassays to determine concentration and organisation.

Additionally, there are several genetic markers that indicate growth of cells on a scaffold that is similar to a native ligament or tendon [354-356]. These markers include gene expression of collagen I, GAG, and scleraxis [357, 358]. There are also genetic markers that may predispose ligaments and tendons to injury [22]. Genetic analysis has proved to be a useful means to examine cellular growth on a scaffold for a ligament tissue engineering application [354, 357].

2.9. Conclusion

In this literature review, the anatomical and biochemical structure of the ACL was discussed along with its healing capacities and current strategies for reconstruction, as an example of ligament injury and repair. Because of the similarity of ligaments and tendons, tendons have also been discussed in this review. Due to the limited restoration of natural function of the current available grafts for ACL reconstruction, tissue engineering research has begun to develop biomimetic scaffolds as alternative repair options. The selection of scaffold material, cell source, and mechanical stimulation has relied on the underlying knowledge of the ligament healing process and the biomechanical loading of the native intact ligament. Although the ideal tissue engineered ligament has not yet been created, there have been great advancements as new methods and technologies are established.

As ligament tissue engineering progresses, a deeper understanding of the cell phenotypes found in the ligament midsubstance and enthesis region will lead to a more educated cell source choice for grafts. There is no consensus on the most suitable material for ACL scaffolds as there are many factors to consider when developing the scaffold, such as the biodegradability, the architecture, and the response to mechanical stimulation and the cell response to the scaffold. The enthesis has challenged ligament engineering research due to its complex regions of graded mineralization and associated cell phenotypes that create a biomechanically strong interface, resulting in the implementation of calcium phosphate salts to increase the mineralization potential of the graft and to increase the mechanical strength. However, there is a lack of

research incorporating the ligament midsubstance and the enthesis to create a complete bone-ligament-bone scaffold, or sinew, for ligament engineering to examine the tissue formation potential and mechanical strength.

This research aims to add to the understanding of scaffold materials, through the use of cost-effective and sustainable materials (chitosan, gelatin, and OPC) that have not previously been used in the methods described here as a scaffold for ligament tissue engineering. Further, this chitosan-gelatin hydrogel will be developed to contain two bony attachments, representing a sinew structure, that will be implemented within a tensile bioreactor to better understand the effect of cyclic strain on a primary fibroblast culture. The tensile bioreactor used in this study was designed to focus on the effect tensile loading has on the hydrogel scaffold and attached cells. In its design, effects due to other factors seen in previous bioreactors were minimised as far as possible.

2.10. Aims of Research Project

This literature review discussed ligament and tendon injury and repair using ACL injury and its reconstruction as a clinical example. Current tissue engineering approaches to ligament repair were discussed with detail on the demand to develop approaches to better create an engineered prosthesis for ACL repair. While the current autograft and allograft options provide a suitable return of function, there are certain drawbacks such as donor site morbidity, graft failure, and immunogenic responses that have motivated research to find a more suitable alternative. Within tissue engineering there are distinct challenges in creating a scaffold that is biologically and biomechanically similar to the native ligament and produces a successful, permanent enthesis.

This research aims to create a hydrogel scaffold from sustainable biomaterials, chitosan, gelatin and OPC, that can withstand similar mechanical forces to the ACL without permanent deformation through the use of a tensile bioreactor. Modification of the hydrogel to influence an osteogenic response at the enthesis region will be investigated by incorporating calcium phosphate salts into the hydrogel. The cellular response of two different cell cultures will be recorded on the hydrogel midsubstance and enthesis regions.

In the development of the hydrogel scaffold, a novel method of creating a detached hydrogel scaffold will be assessed. The detached hydrogel scaffold will be analysed for its cytocompatibility, surface chemistry, and mechanical properties. This project will conclude with the use of a custom tensile loading bioreactor that incorporates the hydrogel scaffold with calcium phosphate rich enthesis regions to better understand how this scaffold may react *in vivo*.

3. General Methodology

3.1. Introduction

This chapter describes the general methodology that is repeated throughout the workflows. In each workflow, the methodology will be referenced to this chapter and any modification to the protocol will be noted within the chapter.

3.2. Cell Culture

Cell culture protocol was followed as written and adapted by Lesley Cyster, Louise France, Jonathan Ratcliffe, Matthew Moles, and Kayla Kret for the Bioengineering Research Group Cell Culture Laboratory at the University of Nottingham [359].

3.2.1. Cell Culture Maintenance

The cell culture medium consists of Dulbecco's Modified Eagle's Medium (Sigma Aldrich, UK) supplemented with 10% Foetal Bovine Serum (FBS) (Fisher Scientific, UK), 2% antibiotics-antimycotics, 2% HEPES buffer, 1% non-essential amino acids, 1% L-Glutamine (cell culture supplements from Gibco Invitrogen, UK), and 0.25mg/ml of ascorbic acid (Fisher Scientific, UK). Cell culture medium and reagents were warmed to 37ºC in a water bath prior to use.

Live cell cultures were kept in a humidified 37ºC, 5% CO_2 incubator. A deionized water reservoir was kept in the incubator at all times with the addition of copper sulphate (Sigma Aldrich, UK) to eliminate microbial growth.

The NIH-3T3 (3T3) cell line was used for cell culture at passage 7-20 (3T3 Swiss Albino, ECACC, 85022108). A primary cell culture was created from ovine fibroblasts, which is described in further detail in section 3.2.5. Both cell cultures received the same cell culture medium and cell culture treatments.

Cells were kept in cell culture flasks before use on samples. While in flasks, the cell culture medium was changed every two days by aspirating the depleted medium, washing the cells with warm phosphate buffered saline (PBS) (Sigma Aldrich, UK), and then replacing with fresh medium.

3.2.2. Bringing Cells to Culture from Cryopreservation

When cells were not in use, they were stored at -80ºC in a liquid nitrogen tank. Cells were brought up from frozen by leaving the microtubule at room temperature for 1 minute then carefully held in the water bath until 90% defrosted, without letting the water touch the screw top. The contents of the microtubule were then transferred into

a T75 cell culture flask and 10 ml of medium was added. The medium was changed after 24 hours to remove any unattached, dead cells.

3.2.3. Passaging Cells

The cells were passaged after they reached 80% confluence, as observed through phase contrast microscopy, if they were not being used. This was done by aspirating the cell culture medium from the flask, washing with 5 ml of PBS, and adding 1 ml of 0.05% trypsin in disodium ethylenediaminetetraacetic acid (EDTA) (Sigma Aldrich, UK). The flask was then incubated for 3-5 minutes. After incubation, the flask was gently tapped to fully dislodge all of the cells. Cell culture medium was added to the flask in two phases of 6 ml and 3 ml and the cell suspension was added to a Falcon tube. The suspension was centrifuged at 4500 rpm for 4 minutes at 37ºC. The supernatant was removed, and the pellet was then resuspended in *n* ml of medium, with *n* corresponding to the desired number of flasks to be split between, typically 2 or 3. The suspension was then aliquoted between the flasks with 9 ml of warm medium in each to bring the total volume of cell culture medium and cell suspension to 10 ml.

3.2.4. Cryopreservation

When cells reached confluency and were not going to be used, they were frozen down. The cells received the same trypsin treatment as in passaging cells until the resuspension step. After centrifuging and removing the supernatant, the pellet was resuspended in 1 ml of 10% dimethyl sulfoxide (Sigma Aldrich, UK) in FBS. The cell suspension was then transferred into an ampoule and placed into the vapour box of the liquid nitrogen tank. After 24 hours in the vapour box, the ampoule was moved into a storage box.

3.2.5. Primary Ovine Fibroblast Culture

In order to evaluate the scaffolds further, a primary cell culture was utilized. The ovine cranial cruciate ligament and caudal cruciate ligament of the stifle joint were chosen because they are comparable to the human anterior cruciate ligament and posterior cruciate ligament, respectively, Figure 3.1 [360].

3.2.5.1. Specimen Harvesting

Female English Mule Sheep, of biological age 2-4 years old, were culled by trained technicians at the University of Nottingham Sutton Bonington campus. The sheep were killed by either an overdose of phenobarbital or by electric shock and exsanguination. The ovine ligaments of the stifle joint were exposed by creating a large surgical opening medial to the median anterior line at the stifle joint. The muscles

and fascia were cut away to reveal the femur, the menisci, and patella. The patellar tendon was cut distally to allow the free movement of the joint revealing the cruciate ligaments. The joint was then put into full flexion and the cruciate ligaments cut as close to the bone as possible. The tissue was collected and stored in Hanks Buffered Saline Solution (HBSS) (Sigma Aldrich, UK) on ice until digestion could take place, roughly 1.5 hours.

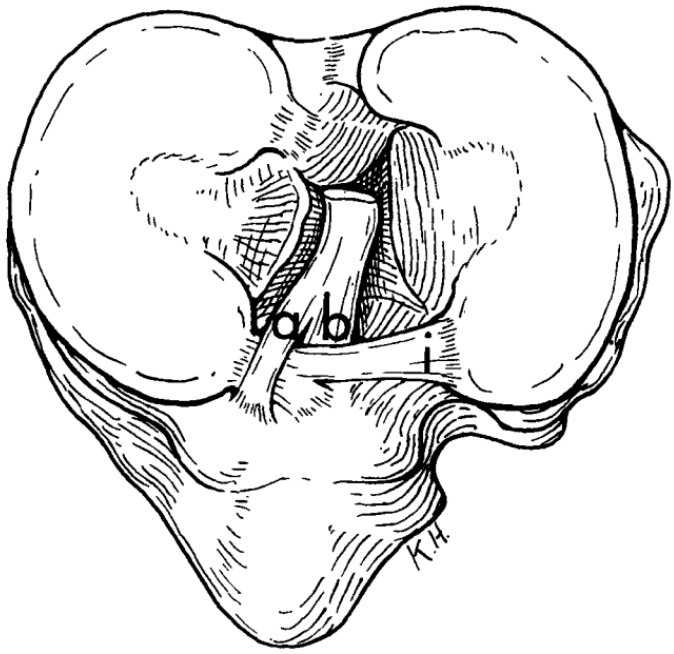

Figure 3.1: Anatomical drawing of the proximal region of the tibia of the stifle joint to show the cranial and caudal cruciate ligaments, a and b respectively. Image taken from Allen et. al [361].

3.2.5.2. Tissue Digestion

Prior to digestion, all tissue was thoroughly washed with PBS and any remaining synovial membrane tissue and bony tissue was removed. After washing, the tissue was finely minced into portions approximately 2mm^2. The minced tissue was then digested using collagenase [150, 345].

The tissue was immersed in a collagenase type I (Sigma Aldrich, UK) solution containing 0.05% collagenase in cell culture medium in 6-well plates. There were three concentrations of collagenase in cell culture medium in the well plates; 2:1, 1:2, and 1:1 with a total volume of 6 ml. The collagenase concentrations completely covered the tissue. The well plates were left to incubate for 24 hours. After incubation, each digestion was added to 9 ml of medium, centrifuged to form a pellet, the supernatant removed, and the pellet resuspended in 1 ml of medium and cultured into a T75 cell culture flask containing 9 ml of fresh medium.

All three concentrations produced viable cells, as judged by phase contrast microscopy, and all flasks were considered available for future experiments. From this point, the ovine ACL and PCL cells from the concentrations were collectively called PFib due to the limited numbers of cells and their morphological similarities [24].

3.2.6. Cell Seeding

When cells reached 80% confluency and ready for use, the cells were seeded onto samples. The same trypsin treatment as passaging was used until the resuspension step where the pellet was resuspended in 1 ml of cell culture medium. The cells were counted using Trypan Blue dye (Sigma Aldrich, UK) and a haemocytometer. To count the cells, 50 µl of cell suspension was mixed with 50 µl Trypan Blue dye and left for 60 seconds to allow the dye to fully incorporate into the cells. The dyed cell solution was then inserted into the haemocytometer and the live cells counted under a phase contrast microscope. The required cell density was calculated, and additional cell culture medium added to the cell suspension as necessary. The cells were then pipetted onto the samples, with an ample amount of cell culture medium added to each well after attachment.

3.2.7. PFib Culture

The PFib cells received the same cell culture medium and treatment that the 3T3 cells received, with the modification that the cells were first cultured in T25 flasks after cryopreservation and then transferred to T75 flasks upon confluency to aid growth. The PFib cells were kept at ultra-low passages, between passages 0-2, before use [362]. The volume of liquids in all processes were scaled down for the T25 flasks.

3.3. Cell Area Measurement

The area of the cells was calculated using Fiji software from photographs taken under a phase contrast microscope throughout culture periods. Photographs from the phase contrast microscope were scaled using a graticule.

A minimum of 45 cells were measured in each photograph, avoiding areas were the cell-cell contact made it difficult to differentiate between cells when possible.

3.4. Cell Culture Assays

Assays were used at different time points throughout cell culture to measure the cell growth, differentiation, and ECM productions of the cells. The metabolic activity assay is an indicator of the viability of the cells and was used at several timepoints throughout the culture as it is not a terminal assay. The deoxyribonucleic

acid (DNA), alkaline phosphatase (ALP), and glycosaminoglycan (GAG) assays are all terminal assays and could only be used at the final time point.

3.4.1. AlamarBlue

The alamarBlue assay (Bio-Rad, UK) is a colorimetric reading of the metabolism by viable cells of non-fluorescent resazurin reduced to fluorescent resorufin, as seen in Figure 3.2.

Figure 3.2: Resazurin reduced to fluorescent resorufin by the metabolic activity of viable cells. Image taken from the Bioengineering Research Group Cell Culture Protocol [359].

At the selected time point, alamarBlue solution was made up in a 1:10 ratio of alamarBlue to HBSS and kept warm in the water bath protected from light. The medium was removed from the samples and the cells were washed with warm PBS. The cells were washed with warm PBS twice more, with the PBS left in the wells for 5 minutes. After the PBS washes, a sufficient amount of the alamarBlue solution was aliquoted into the wells. For example, in a 24-well plate, 1 ml of alamarBlue solution was used and for a 12 well plate, 1.5 ml of alamarBlue solution was used.

The well plate was replaced in the incubator for 80 minutes. After incubation, the plates were wrapped with aluminium foil and placed on the plate shaker at 250 rpm for 5 minutes to thoroughly mix the reacted dye within the solution. Aliquots of 100 µl of each sample and 3 blanks were read in triplicate in a 96-well plate using a fluorescence plate reader (FLX-800, Bio-Tek Instruments, Inc, USA) at excitation 560 nm and emission 590 nm wavelengths.

Because alamarBlue is not a terminal treatment to the cells, the samples were able to continue culture after the assay. If further culture took place, the remaining alamarBlue solution was aspirated from the wells and each sample was washed twice with warmed PBS for 5 minutes. After the PBS washes, additional cell culture medium was added, and the well plates replaced into the incubator.

3.4.2. Cell Lysing

Prior to further assays, the cells were lysed by undergoing a freeze thaw cycle. This was carried out by washing the samples twice with PBS and then adding 1 ml of sterile distilled water (SDW) into each well. The well plates were secured using sterile

tape and subjected to snap freezing using liquid nitrogen. The plates were placed in a Styrofoam box and liquid nitrogen was added to create a shallow layer. The lid was replaced and left for 5 minutes. Once frozen, the plates were transferred into the incubator and allowed to thaw. The well plates were frozen and thawed twice more. The cell lysate was then transferred to microtubules.

3.4.3. DNA Assay

To quantify the DNA content in each sample, the PicoGreen DNA kit (ThermoFisher Scientific, UK) was used following the manufacturer's suggested protocol. A TE buffer was created by adding the concentrated TE stock supplied to room temperature SDW. The reagent was made using the supplied concentrated reagent in TE buffer and protected from light using aluminium foil. The buffer and reagent were made on the day of the assay, as close to the reading as possible.

A standard reference curve, such as the one below in Figure 3.3, was created using the Lambda DNA standard that was supplied with the kit. The DNA standards were created in increasing concentrations from 0-1 µg/ml in the TE buffer. The DNA standards were read by aliquoting 100 µl of each in triplicate into a 96-well plate and then adding 100 µl of the reagent. The plates were covered in foil and placed on a plate shaker at 250 rpm for 3 minutes at room temperature. The plates were then read on a fluorescence plate reader (FLX-800, Bio-Tek Instruments, Inc, USA) at excitation 480 nm and emission 520 nm wavelength. A trendline was created ensuring R^2>0.95. A standard curve was created each time the PicoGreen assay was carried out.

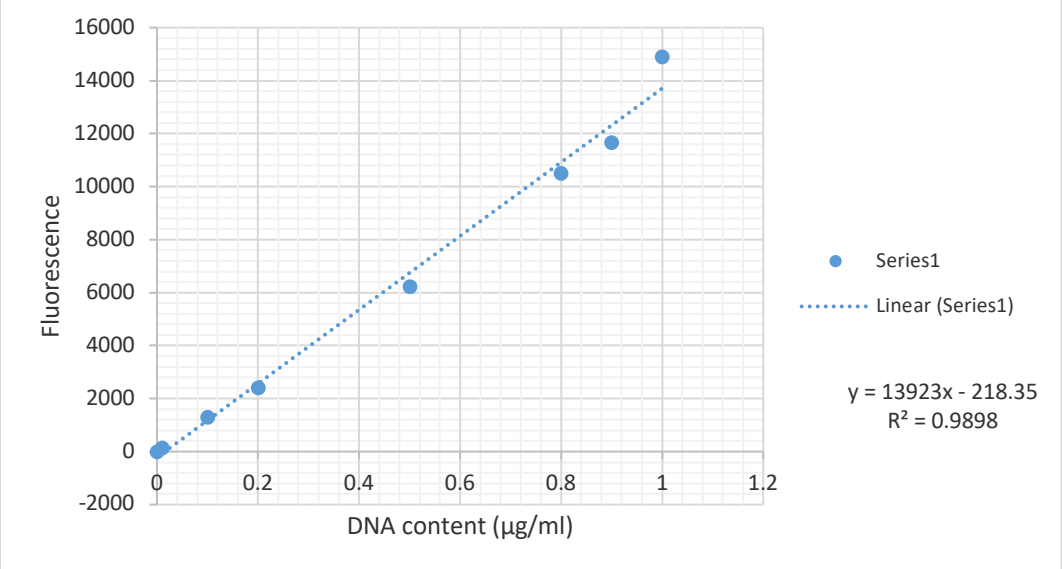

Figure 3.3: A typical standard curve used for DNA quantification with the PicoGreen kit.

Each sample was thawed, vortexed, and then aliquoted in triplicate 100 µl into 96-well plates. Then 100 µl of the reagent was added and the plates covered with foil and left on the plate shaker for 3 minutes at room temperature. The plates were then read using the fluorescent plate reader. The DNA content of each sample was then calculated using the standard curve.

3.4.4. Alkaline Phosphatase Activity

Alkaline phosphatase (ALP) is an early marker for osteogenesis of osteoblast-like cells [363]. ALP is a colorimetric absorbance assay to quantify the amount of ALP present in a sample. A slight colour change to yellow occurs if ALP is present.

ALP activity was measured using the ALP kit (Randox Laboratories, UK) following the manufacturer's protocol. Reagent AB was created by adding 10 ml of Reagent B to Reagent A and mixing thoroughly. The cell lysate was thawed to room temperature and vortexed prior to use. 50 µl of the lysate was aliquoted in triplicate into a 96-well plate followed by 50 µl of Reagent AB. The plate was loosely covered with aluminium foil and left on the plate shaker at 250 rpm for 30 minutes at room temperature. The plate was read using an absorbance plate reader (ELX-800, Bio-Tek Instruments, Inc, USA) at 405 nm wavelength. The ALP activity was normalized against the DNA content of each sample.

3.4.5. Papain Digestion

After lysing, a papain digestion was used to solubilize the ECM to allow for evaluation of sulphated glycosaminoglycans (GAG).

Papain is a proteolytic enzyme that dissociates the ECM once activated [364]. The papain solution consisted of papain buffer (sodium phosphate 0.1M, cysteine hydrochloride 0.005M, EDTA 0.005M, and dH_2O) and 0.1% w/v papain (Sigma Aldrich, UK). The pH of the papain solution was adjusted to 6.5 with 1M hydrochloric acid (HCl) or 1M sodium hydroxide (NaOH), as appropriate. The papain was added to the papain buffer on the same day that the digestion was to take place. The papain solution was added to the lysate samples in a well plate at a 1:1 ratio and left overnight, 18 hours, in a 60ºC oven. The papain digestion was then allowed to come to room temperature prior to use. If the samples were not immediately used after papain digestion, they were stored at 4ºC until use.

3.4.6. Glycosaminoglycan Assay

The 1,9-dimethylmethylene blue (DMMB) assay is commonly used for quantification of sulphated GAG content in tissues, Figure 3.4. The DMMB binds to

sulphated groups of the GAG causing a concentration dependent chromatic change from blue to violet [364-366]. The potential for interference from DNA and the serum in the cell culture medium was accepted [365, 366].

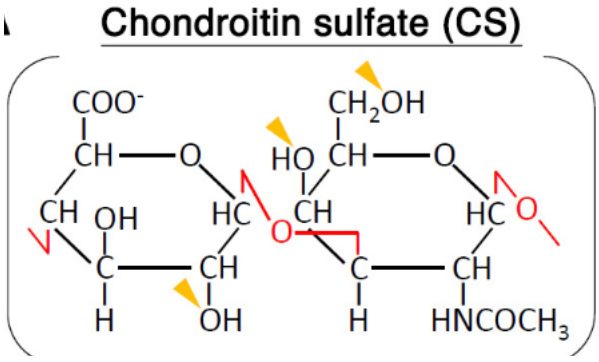

Figure 3.4: The chemical structure of chondroitin sulfate, where the yellow arrows indicate sulfation sites [367].

The DMMB dye was made according to the protocol from Coulson-Thomas and Gesteira [366]. The dye contained 8mg DMMB, 1.52g glycine, 0.8g NaCl, 10% acetic acid made up to 500 ml and pH adjusted to 3.0 with HCl or NaOH, as appropriate. The prepared dye was stored for up to 3 months at room temperature, protected from light.

A standard reference curve was created using chondroitin-4-sulfate (Sigma Aldrich, UK) stock in concentrations ranging from 0 to 100 µg/ml. 20 µl of each of the standards was aliquoted into the 96-well plate in triplicate followed by 200 µl of the DMMB dye and the absorbance read using an absorbance plate reader (ELX-800, Bio-Tek Instruments, UK) at 540nm wavelength. The solution is not stable after adding DMMB and, therefore, was read immediately. The standard curve was calculated ensuring that R^2>0.95.

Following papain digestion, 20 µl of the sample digestion was aliquoted into a 96-well plate in triplicate. Then 200 µl of dye was added to the wells. The plates were read immediately using the absorbance plate reader. The GAG content was calculated using the standard curve.

3.4.7. Environmental Scanning Electron Microscopy

3.4.7.1. Fixation

Prior to environmental scanning election microscope (ESEM) imaging, the cells need to be fixed to reduce any time-dependant damage. A 4% glutaraldehyde solution was added to each sample to completely cover the surface for 45 minutes. After fixation, the samples were gently washed with room temperature PBS three

times. If the samples were going to be imaged immediately, they were additionally washed three times with SDW. If the samples were imaged at a later date, the samples were stored in the 4ºC refrigerator with an excess of PBS. Before imaging, the PBS was removed from the samples and washed three times with SDW. On the day of imaging, the samples were kept with a thin layer of SDW and in a chilled box to reduce any dehydration prior to image capture.

3.4.7.2. ESEM Imaging

The samples were imaged with a FEI Quanta 650 ESEM. The samples were imaged at a decreasing temperature range of 3-0ºC, a decreasing humidity range of 100-85%, and decreasing pressure at 5.5-2.5 torr with a Peltier stage to control the temperature of the sample. At these parameters, the samples were able to be imaged for approximately 30 minutes before damage to the sample occurred.

3.5. Hydrogel Scaffold

3.5.1. Hydrogel Preparation

A solution of 3% w/v chitosan, (85% deacetylated, Sigma Aldrich, UK) and 2% v/v acetic acid (Sigma Aldrich, UK) in dH_2O was left on a heated stirring plate at 37ºC overnight. Concurrently, a solution of 3% w/v gelatin from porcine skin (Fluka Biochemika, Germany) in PBS was left on a heated stirring plate at 50ºC for a minimum of 2 hours, or until fully dissolved. The chitosan and gelatin solutions were then mixed fully at 37ºC with the addition of NaOH to raise the pH to 5.0. Finally, a 2% w/w proanthocyanidin (OPC) (Mushroom Supplies, UK) solution, based on the chitosan-gelatin content, in distilled water was gradually added to the chitosan-gelatin mixture and left to fully mix at 37ºC. The OPC solution was made immediately prior to adding to the chitosan-gelatin mix.

3.5.2. Hydrogel Casting

Prior to casting, the hydrogel was ensured to be at 37 ºC and pH 5.0. The hydrogel was cast into the well and allowed to gel at room temperature, where the volume cast was dependent on application and is specified in each results chapter. Once fully gelled, a 10% NaOH solution was added into the wells to completely cover the hydrogel surface and left at room temperature for 2 hours. The NaOH solution neutralizes the excess acetic acid on the surface and raises the surface pH of the hydrogel and allows for further crosslinking to occur [368]. After 2 hours, the NaOH solution was removed and the hydrogel washed with excess dH_2O.

3.5.3. Hydrogel Sterilization

To sterilize the hydrogels, the well plates were transferred to a cell culture hood to maintain the sterility. The hydrogels were washed three times with SDW. The surface of the hydrogel was then sprayed with IMS and left to evaporate. Any remaining IMS was then washed off with excess SDW. The hydrogels were then subjected to ultraviolet (UV) radiation for 2 hours. After UV radiation, cell culture medium was added to each well covering the hydrogels and allowed to incubate overnight to condition the hydrogel surface. The conditioning medium was removed before any further cell culture took place.

3.5.4. Cell Culture and Assays on Hydrogel Scaffolds

Cell seeding and culture on the hydrogels followed the same protocol as stated above in section 3.2 (page 42). The cell culture assays on the hydrogels followed the same protocols as stated in section 3.4 (page 45), adding a blank of hydrogel without cells as appropriate. The cell culture assays did not have a negative effect on the hydrogel integrity. The hydrogel remained intact within the wells throughout cell culture and the following assays.

3.5.5. ESEM

The hydrogel samples were imaged using ESEM as described previously. The hydrogel samples were prepared with the addition of a glass coverslip in the well plate before casting to allow removal. Samples for ESEM were not used for the DNA, ALP, or GAG assays.

3.6. Statistical Significance

The statistical significance at the 95% confidence interval was determined using mixed effects analysis or one-way/two-way ANOVA analysis with Tukey post hoc comparison using GraphPad Prism™ 8 software (version 8.0.1, GraphPad Software, San Diego, CA, USA, www.graphpad.com). The differences between means were considered to be significant when $p < 0.05$. The mean values with standard error of mean were calculated using GraphPad Prism.

The biological and technical replicates, with repeats, are stated within each experiment, section 4.2.2 (page 53), section 5.2.10 (page 75), section 6.2.2 (page 96), and section 7.2.3 (page 125).

4. Optimization of Chitosan-Gelatin Hydrogel Thickness to Assess Fibroblast Response

4.1. Introduction

Chitosan and gelatin have become popular biomaterials within tissue engineering for their biocompatibility, availability, and tuneable mechanical properties [369-371]. The structural properties of chitosan and gelatin create a more similar microenvironment of native tissues than other synthetic and non-collagen derived materials [265, 273]. The versatility of both chitosan and gelatin have allowed a wide range of scaffolds to be produced, such as fibres and hydrogels, as well as the incorporation of additional materials to modify scaffold properties [278, 279, 293, 372]. Previous studies using chitosan-gelatin hydrogel have shown the optimization of crosslinking of these biomaterials has produced favourable cell adhesion and spreading for tissue engineering applications [370, 373].

This chapter discusses a sustainable hydrogel created from chitosan and gelatin and crosslinked with OPC as a scaffold for tissue engineering. The 3T3 cell line and primary ovine fibroblast culture will be used to determine cytocompatibility and suitability of the hydrogel thickness. The cellular response on each thickness of hydrogel will be measured through metabolic activity, DNA content, GAG content, and ALP activity. The metabolic activity assay and DNA assay will give an indication of cell proliferation and density. The DMMB assay will determine the GAG production within the ECM. Although there is not expected to be high levels of ALP activity, the ALP assay will illustrate the differentiation capability of the fibroblasts. The cell morphology and mean cell area will also be analysed. These results will determine the optimal hydrogel thickness and most suitable cell source for future works.

4.2. Methodology

4.2.1. Hydrogel Casting

The chitosan-gelatin hydrogel was created using the same protocol as stated in section 3.5 (page 50). To assess cytocompatibility and optimise the cell response, the hydrogel was cast in thickness from 0.5mm to 2.5mm increasing in increments of 0.5mm in a 24 well plate. TCP was used as a positive control. The volume of hydrogel

to be cast was calculated using the diameter of the well and the desired thickness. Once cast, the hydrogels underwent the same sterilization protocol as outlined previously.

4.2.2. Cell Culture

The 3T3 cell line and the PFib culture were individually seeded onto the hydrogel of increasing thickness. Both cell types underwent the same protocol for cell seeding as outlined in section 3.2.6 (page 45) with a seeding density of 10,000 cells/cm^2 at a volume of 500 µl. The wells were topped up with 1 ml of cell culture medium after 1 hour allowing the cells to adhere to the hydrogel. The cell culture medium was replaced after 48 hours and then every 2-3 days. There was one biological replicate and 12 technical replicates, repeated twice.

The cell culture was carried out to 28 days. Images using phase contrast microscopy were taken throughout the culture period to monitor the growth and morphology of the cells. The mean area of the cells was measured at each time point.

At Day 3, 7, 14, 21, and 28 an alamarBlue assay was carried out following the protocol in section 3.4 (page 45). The PBS washes were done with extreme care to prevent disrupting the cells. Samples were read in triplicate and blanked against alamarBlue dye. The cell culture medium from each sample was collected at Day 28 and stored at -20°C for further analysis. The collected cell culture medium included the final 3 days of culture.

After the final alamarBlue assay, all samples underwent the freeze/thaw process. The cell lysate was used for the DNA and ALP assays and was then digested in papain for the DMMB assay. The collected cell culture medium was similarly prepared and assayed following the DMMB protocol. These assays were carried out according to the protocol outlined previously.

The mean ALP activity results from the MG63 cell line (human osteosarcoma, ECACC, 86051601) and a primary osteoblast culture from neonatal mouse calvaria were used as a reference for osteoblastic levels of ALP activity. The MG63 and primary osteoblasts were cultured on TCP at a similar initial cell density to the same timepoint. These osteoblast cultures were not used for any other assays.

4.2.3. ESEM

The hydrogel was cast into the well plates with an added glass coverslip allowing the removal of the hydrogel after cell culture. The hydrogel was similarly cast in increasing thickness, sterilized, and seeded with 3T3 or PFib cells. After 28

days of culture, the hydrogel samples were fixed as described previously and removed from the well plate for imaging.

4.3. Results

4.3.1. Morphology of Hydrogel

The hydrogels were homogenous within the cell culture plate across all thicknesses. It was observed that the edges of the hydrogel formed a meniscus against the wall of the well due to the surface tension of the hydrogel. This did not appear to affect the bulk thickness of the hydrogel near the centre of the well. However, this could not be experimentally quantified as the hydrogel could not be removed from the well.

4.3.2. Mean Area of Cells During Culture

The measured mean area of the 3T3 cells remained under 2.0 μm^2 at all time points across all sample thicknesses, as seen in Figure 4.1. The 0.5mm sample had the largest mean cell area of 1.9348 μm^2 at Day 3 and then decreased to below 0.7 μm^2 beyond Day 7. The smallest mean area of 3T3 was seen at Day 7 on the 0.5mm sample at 0.12909 μm^2. The mean area of the 3T3 cells on the 2.5mm sample could not be recorded beyond Day 21 due to the opacity of the hydrogel.

The 3T3 mean cell area on the 0.5mm sample experienced a significant decrease at Day 7 followed by a significant increase at Day 21. The 1.0mm exhibited a similar trend with a significant decrease at Day 7 followed by significant increases at the subsequent timepoints until Day 24. The 1.5mm sample showed a more variable trend with significant decreases in the mean cell area at each timepoint until Day 14, followed by a brief increase at Day 21, a decrease at Day 24, and a further increase at Day 28. The 2.0mm sample demonstrated a significant decrease in mean area at each timepoint until Day 21. The 2.5mm sample displayed a significant decrease in mean area at Day 21. The TCP sample had a significant decrease of mean area at Day 7, a significant increase at Day 14, and another significant increase at Day 24.

The PFib cells are a larger cell type than the 3T3s, visibly seen through phase contrast microscopy. The mean area of the PFib cells experienced a more variable change throughout the culture period, as seen in Figure 4.1. Images were unable to be taken after Day 21 for the 2.0mm sample and beyond Day 7 for the 2.5mm sample. The largest mean cell area was seen on the TCP sample at Day 24 with 2.307 μm^2. The smallest mean area was seen on the 2.0mm and 2.5mm samples at Day 3 with areas of 0.319 μm^2 and 0.310 μm^2, respectively.

The PFib cell area on the 0.5mm sample displayed a significant decrease in mean area at Day 7, a significant increase at Day 24, followed by a significant decrease at Day 28. The 1.0mm sample experienced a significant decrease in mean area at Day 7 followed by a significant increase at Day 17. The 1.5mm sample experienced a significant increase in mean area between Day 7 to Day 14, a significant decrease to Day 21, a significant increase at Day 24, followed by a significant decrease at Day 28. The TCP sample showed significant increases in mean cell area at Day 7 and Day 24. There were significant declines in cell area on the TCP sample at Day 14 and Day 28.

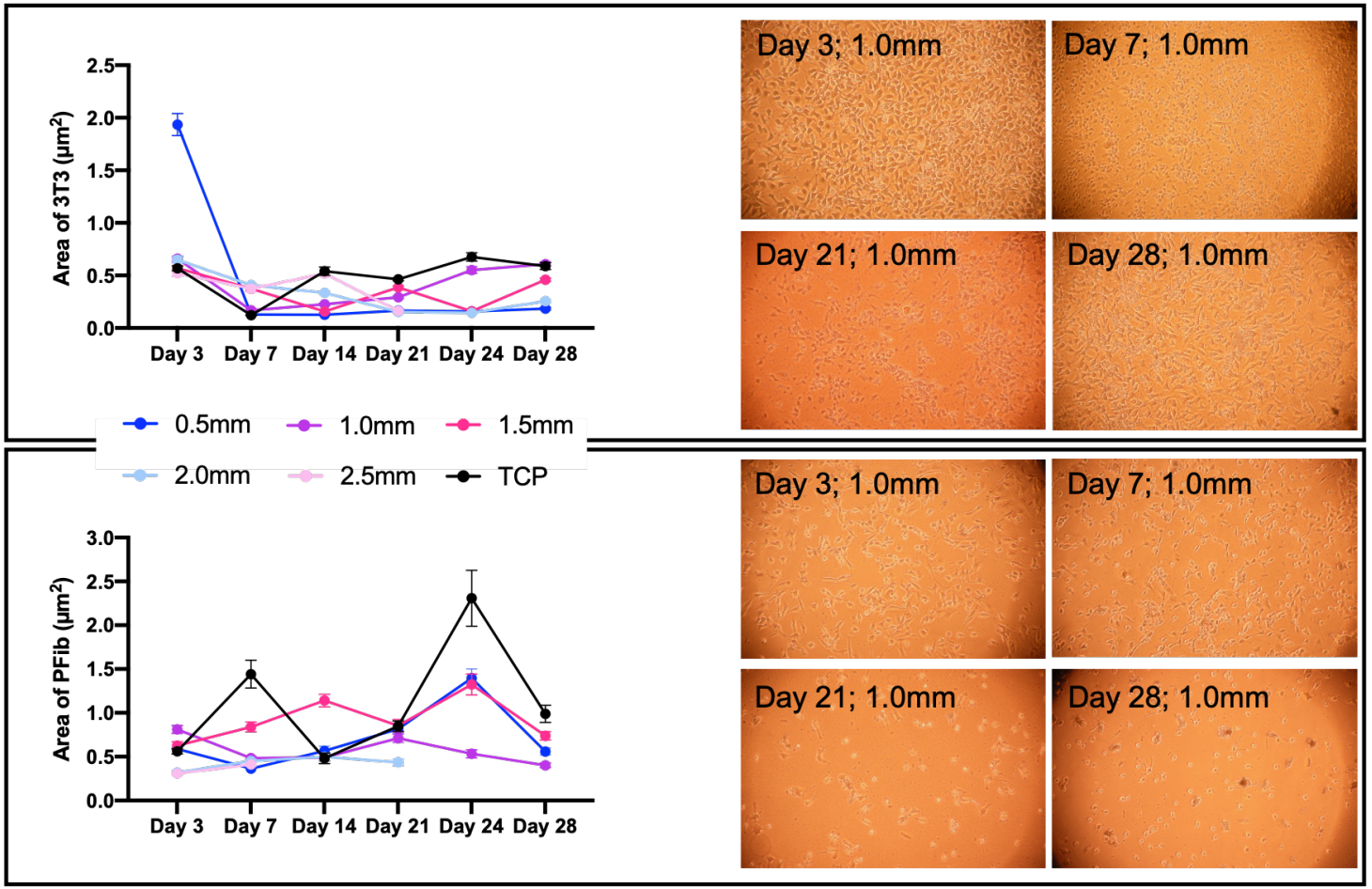

Figure 4.1: The mean cell area of 3T3 and PFib cells measured using a phase contrast microscope and calculated using Fiji software over a period of 28 days with images used for mean cell measurement for both cell types from the 1.0mm samples located on the right. Note the 2.0mm and 2.5mm hydrogel samples were opaque and measurements were unable to be taken at several time points for both cell types. The error bars represent standard error of mean. Where n>45. Additional images found in section 10.3.

4.3.3. ESEM Imaging

The 3T3 cells were found to be numerous and created a confluent cell layer, or monolayer, on all sample thicknesses as observed through phase contrast microscopy. The monolayer was visible on several samples using ESEM imaging, as seen in Figure 4.2. However, a layer of water obscured the visibility of cells on several samples. Where a water layer obscured visibility, such as on the 2.0mm sample, some features of the cells could be seen above the water layer but the morphology could not be identified. While in a monolayer, the morphology of individual 3T3 cells was difficult to identify using ESEM.

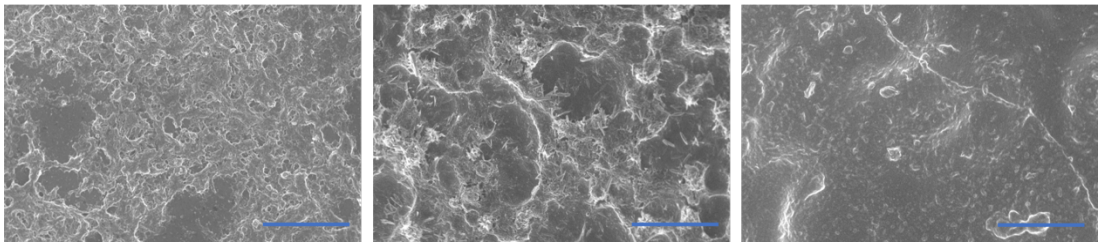

Figure 4.2: ESEM images of 3T3 cells grown on 1.0mm (left), 1.5mm (middle), 2.0mm (right) thickness chitosan-gelatin hydrogel after 28 days of culture. A complete monolayer can be seen on the 1.0mm and 1.5mm sample. There appears to be some damage to the monolayer of the 1.5mm sample, potentially from fixation or the imaging process. A water layer restricts the visibility of the cells on the 2.0mm sample, however some features of the cells can be seen above the water layer. The blue line indicates 50 µm.

The PFib cells did not create a monolayer on any of the hydrogel thicknesses, as seen through phase contrast microscopy and ESEM. As a result, individual cells with a spread morphology could be identified on the samples, as seen in Figure 4.3. A water layer was visible on all samples during ESEM imaging, restricting the visibility of cells. On the thinner hydrogel samples, the PFib cells showed a spread morphology with many extensions. The PFib cells displayed a more elongated morphology on the thicker hydrogel samples rather than a spread morphology as seen on the thinner hydrogel samples. A water layer can be seen on the 2.0mm sample, however the morphology of the PFib cells was still visible.

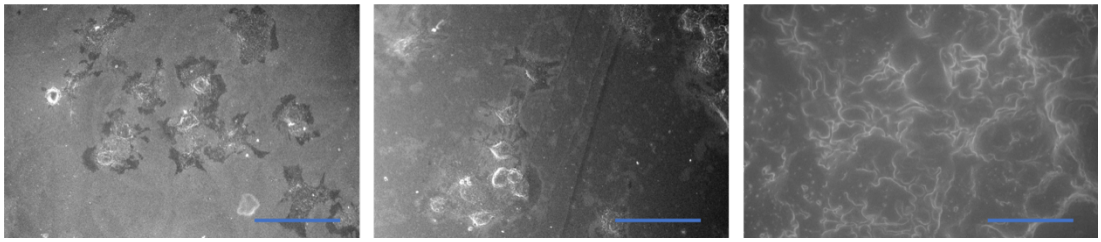

Figure 4.3: ESEM images of PFib cells grown on 1.0mm (left), 1.5mm (middle), and 2.0mm (right) thickness chitosan-gelatin hydrogel after 28 days of culture. The 2.0mm image was taken immediately prior to the freezing of the sample and the water layer seems to be semi-frozen around the cells. The blue line indicates 100 µm.

4.3.4. Metabolic Quantification

The metabolic activity of cells is a reliable indicator of proliferation of the cells and cytocompatibility of the substrate. In combination with the cell area and morphology, the metabolic activity can illustrate the cycle of proliferation and growth of the cell.

4.3.4.1. Metabolic Analysis of 3T3 Cells

The 3T3 cells on the 0.5mm sample showed a significant decrease in metabolic activity at Day 7, as seen in Figure 4.4. There was a similar decline in metabolic activity at the subsequent timepoints beyond Day 7. The metabolic activity on the 0.5mm sample did not significantly recover from the decline. The 3T3 cells on the TCP control exhibited a similar trend, however there was a significant increase in metabolic activity at Day 28 when compared to Day 14, the lowest metabolic activity.

The 1.0mm sample showed a significant decrease in metabolic activity at Day 14 when compared to Day 3 however, this sample showed a significant resurgence of proliferation and metabolic activity at Day 28 when compared to Day 14. The 1.5mm sample experienced a similar trend, with a significant decline in metabolic activity at Day 14 and a significant increase at Day 21. The metabolic activity on the 2.0mm and 2.5mm samples did not display significant declines at any timepoint. There was a significant increase in metabolic activity on these thicknesses at Day 28.

4.3.4.2. Metabolic Analysis of PFib Cells

The metabolic activity of the PFib cells did not experience significant declines in activity at any point across all sample types, as seen in Figure 4.5. There was a steady positive trend in metabolic activity across all samples from Day 3 to Day 28. There was a significant increase in the metabolic activity on all hydrogel samples at Day 14, TCP excluded. Overall, the metabolic activity of the PFib cells at Day 28 was significantly higher than the activity recorded at Day 3 and 7 for all hydrogel samples.

There were significant differences in metabolic activity between the 3T3 and PFib cells across sample thicknesses and timepoints. The 3T3 metabolic activity was significantly higher than the PFib metabolic activity at Day 3 on the 0.5mm, 1.0mm, and 1.5mm samples. Between Day 7 and Day 21, the PFib metabolic activity was significantly higher than the 3T3 metabolic activity across the samples. However, at Day 28 the only significant difference between the two cell types was found on the 0.5mm and TCP samples where the PFib cells showed higher metabolic activity.

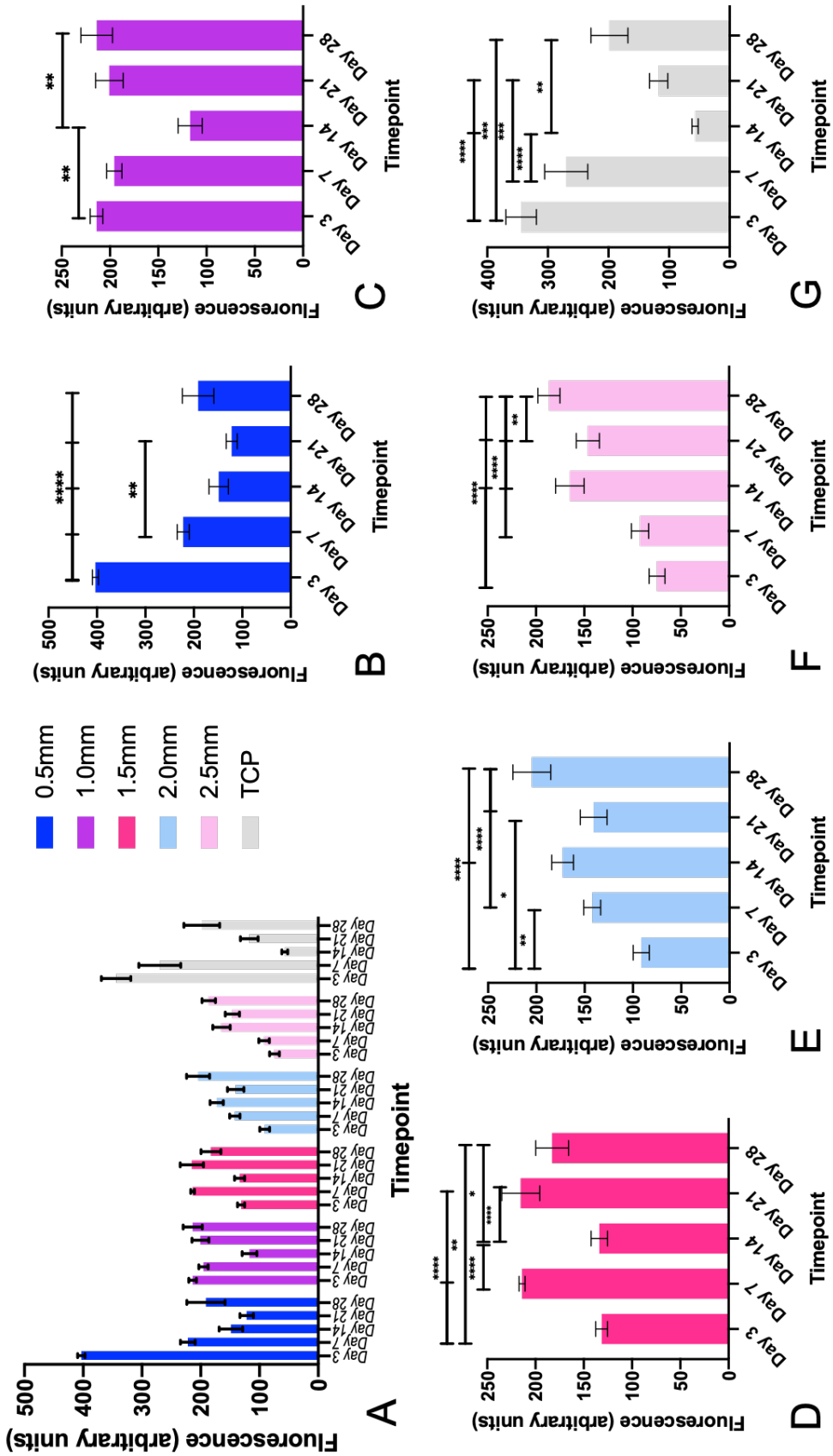

Figure 4.4:The metabolic activity of 3T3 cells on chitosan-gelatin hydrogel of increasing thickness over a 28-day time period, using an alamarBlue assay. A) An overview of the results from all sample thicknesses. B-G) The detailed results from each sample thickness represented in A. Note B-G depict the same data as seen in A. Where * p <0.0332, ** p <0.0021, *** p <0.0002, and **** p <0.0001 and n=12 with 2 repeats.

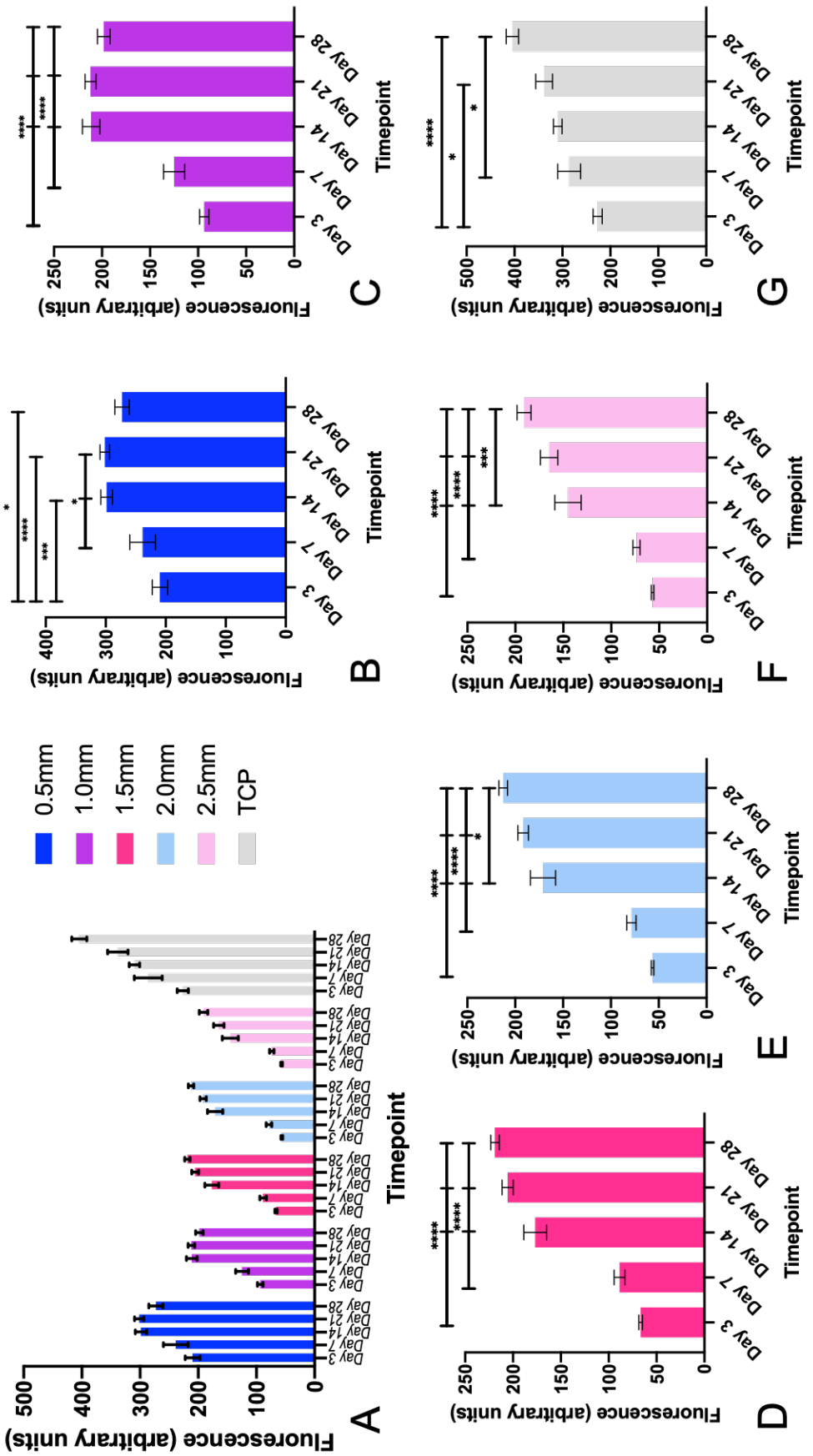

Figure 4.5: The metabolic activity of PFib cells grown on chitosan-gelatin hydrogel of increasing thickness over a 28-day period, using an alamarBlue assay. A) An overview of the results from all sample thicknesses. B-G) The detailed results from each sample thickness represented in A. Note B-G depict the same data as seen in A. Where * p <0.0332, ** p <0.0021, *** p <0.0002, and **** p <0 and n=12 with 2 repeats.

4.3.5. DNA Quantification

The DNA content in each of the 3T3 samples varied more than the PFib DNA content, as seen through the larger error bars in Figure 4.6. The 3T3 cells exhibited the highest mean DNA content on the 1.0mm thick sample at 0.03916 µg/ml. The PFib cells showed the highest DNA content on TCP at 0.04561 µg/ml. Of the hydrogel samples, the PFib cells resulted in the highest DNA content on the 2.0mm sample with 0.02556 µg/ml.

The 3T3 cells on the 1.0mm sample had significantly more DNA content than all other 3T3 samples, except the 2.0mm sample. Of the PFib samples, only the TCP sample was significantly different than all other samples.

There were several significant differences between the DNA content of the 3T3 and PFib cells across the hydrogel thicknesses. The 3T3 DNA content was significantly higher than the PFib DNA content on the 1.0mm, 1.5mm, and 2.0mm sample. However, the PFib DNA content was significantly higher than the 3T3 DNA content on the TCP sample. There was no significant difference found between the DNA content of the 3T3 and PFib cells at the 0.5mm and 2.5mm samples.

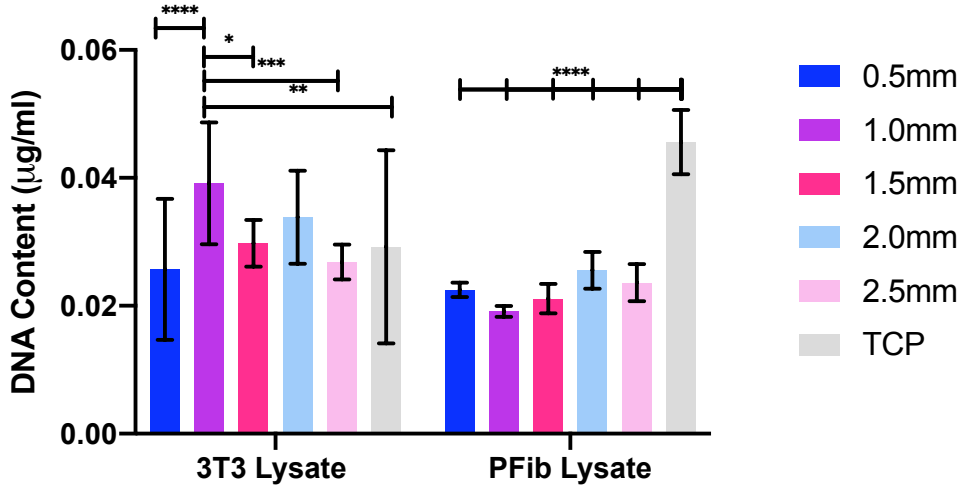

Figure 4.6: DNA quantification of 3T3 and PFib cell lysate after 28 days of cell culture on chitosan-gelatin hydrogel of increasing thickness, using the PicoGreen DNA kit. The error bars represent the standard error of mean. Where * p <0.0332, ** p <0.0021, *** p <0.0002, and **** p <0.0001 and n=12 with 2 repeats.

4.3.6. GAG Content

There was a bimodal trend seen in the GAG content from both the 3T3 and PFib lysate across the hydrogel samples where both the thinnest and thickest hydrogel samples had the highest content, as seen in Figure 4.7. The highest GAG content of the 3T3 cells was recorded from the lysate of the 2.5mm sample at 6.239µg/ml, and

the lysate from the TCP sample at 10.043µg/ml. The highest GAG content of the PFib cells was recorded from the lysate of the 2.5mm sample at 5.514µg/ml. There was no GAG content detected in the lysate of the 1.5mm sample with 3T3 cells.

The 3T3 TCP lysate had a significantly higher GAG content than the lysate of the 3T3 hydrogel samples. There was no significant difference found in the GAG content between the PFib lysate of the hydrogel and TCP samples. There was no significant difference in the GAG content found between the lysate of the 3T3 and PFib cells across the hydrogel samples, TCP excluded.

The GAG content of the collected medium exhibited a similar bimodal trend for both the 3T3 and PFib cells. The collected medium of the 3T3 cells on the 1.5mm sample showed GAG content, in contrast to the related cell lysate. The collected medium of both cell types showed a decreased amount of GAG content across the samples compared to the related cell lysate, except in the 0.5mm sample with 3T3 cells. The highest GAG content from the collected medium was found on the 0.5mm sample with 3T3 cells at 5.754µg/ml. The lysate of the 2.5mm sample of both cell types showed significantly higher GAG content than the related collected medium. The lysate of the 3T3 TCP sample showed significantly higher GAG content than the related collected medium.

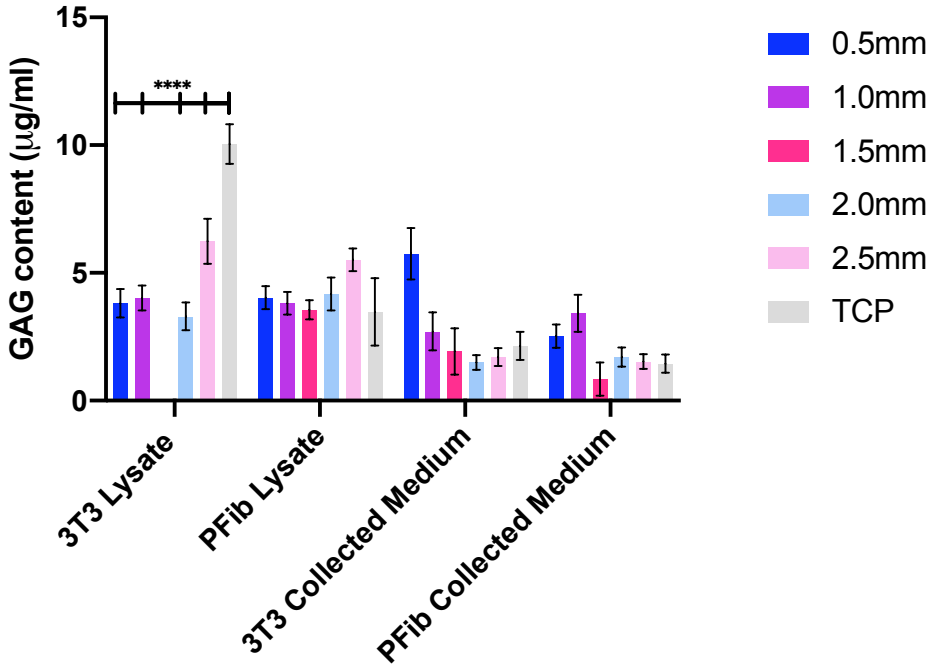

Figure 4.7: GAG content of the lysate and collected cell culture medium of the 3T3 and PFib cells after 28 days of growth on increasing thicknesses of chitosan-gelatin hydrogel, using a DMMB assay. The 3T3 lysate from the 1.5mm hydrogel sample did not show any GAG content, despite the related medium detecting GAG content. Error bars represent standard error of mean. Where * p <0.0332, ** p <0.0021, *** p <0.0002, and **** p <0.0001 and n=12 with 2 repeats.

The GAG/DNA ratio displayed a bimodal trend for the lysate of the 3T3 hydrogel samples and a slight positive trend for the lysate of the PFib hydrogel samples, as seen in Figure 4.8. The lysate from the 2.5mm hydrogel samples for both the 3T3 and PFib cells showed the highest GAG/DNA ratio, excluding TCP. The GAG/DNA ratio of the 3T3 cells on TCP showed a significantly higher ratio in the lysate than the related collected medium.

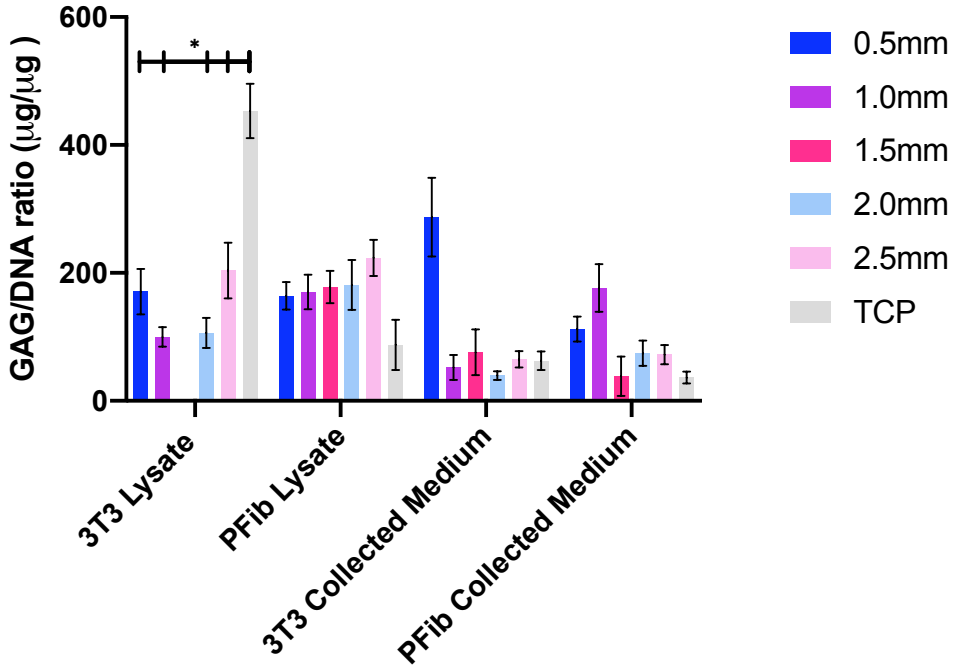

Figure 4.8: GAG/DNA ratio of the lysate and collected cell culture medium from the 3T3 and PFib cells on increasing thicknesses of chitosan-gelatin hydrogel after 28 days of cell culture. The error bars represent standard error of mean. Where * p <0.0332, ** p <0.0021, *** p <0.0002, and **** p <0.0001 and n=12 with 2 repeats.

4.3.7. ALP Activity

As alkaline phosphatase is an early marker for osteogenic differentiation, high levels of ALP activity were not expected from either fibroblast culture on this chitosan-gelatin hydrogel. Though some ALP activity from the 3T3 cells was seen on the 0.5mm and TCP samples. The PFib cells showed ALP activity on the 0.5mm, 1.5mm, 2.5mm, and TCP samples, Figure 4.9. However, only one sample from the PFib 1.5mm and 2.5mm samples showed ALP activity resulting in the lack of error bars.

There was no significant difference found between the 3T3 ALP activity on the 0.5mm and TCP samples. Similarly, there was no significant difference between the ALP activity of the PFib samples.

The MG63 cell line and primary osteoblast culture were used as reference to show the ALP activity of osteogenic cells, the dotted and dashed line in Figure 4.9 respectively. Both osteoblasts showed significantly higher ALP activity than the 3T3 and PFib cells on the 0.5mm and TCP samples.

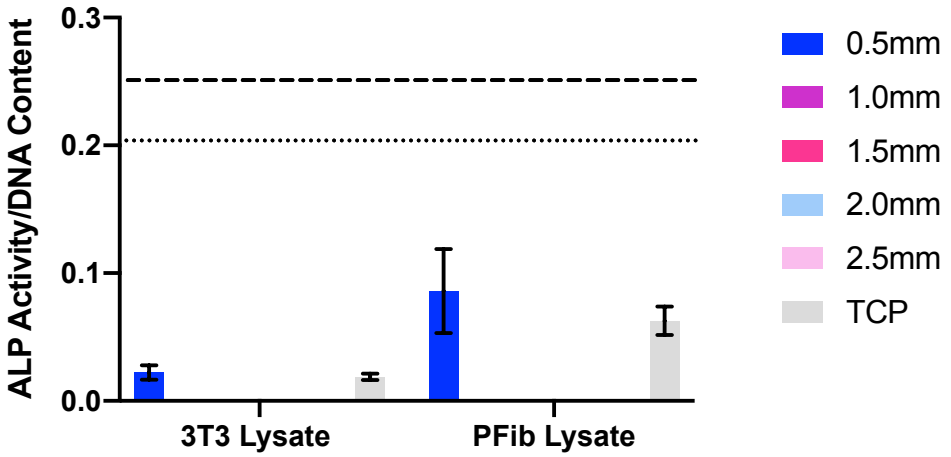

Figure 4.9: Normalized ALP activity of 3T3 lysate and PFib lysate on chitosan-gelatin hydrogel of increasing thickness after 28 days of culture, using the ALP Randox Kit. The dotted line represents a mean ALP activity of the MG63 cell line and the dashed line represents a mean ALP activity of a primary mouse osteoblast culture as reference of ALP activity of osteoblast cultures. The error bars represent standard error of mean. Where n=12 with 2 repeats.

4.4. Discussion

4.4.1. Chitosan-Gelatin Hydrogel Cytocompatibility

The scaffold is a central element in tissue engineering as it must provide structural support without inhibiting cellular ingrowth and ECM production [17, 210]. Research has turned towards hydrogels for soft tissue applications for their extensive composition possibilities, malleability, adaptable mechanical properties, and their cytocompatibility [314, 315]. The chitosan-gelatin hydrogel used in this study was demonstrated to be cytocompatible in line with previous research using similar hydrogel assemblies [277, 293, 370]. All hydrogel samples showed 3T3 and PFib fibroblast growth and some degree of ECM production over the 28-day period of cell culture.

The 3T3 cell line has been a model cell line used extensively across many applications and is known to reach confluency in a relatively short period, followed by cell death and a period of latency, resulting in a regrowth of cells [374]. The stages of cell death and regrowth can be identified in the cell metabolic graphic, Figure 4.4, by the sharp declines and surges at the sequential timepoints. This uncontrolled proliferation can be attributed to the lack of cell contact inhibition of proliferation of

the 3T3 cells [375, 376]. The change in mean area of the cells was also an indicator of the proliferation, death, and regrowth cycle of the 3T3 cells, Figure 4.1. The increase in metabolic activity was attributed to cell confluency and a decrease of the mean cell area. Immediately following the sharp decline in metabolic activity signifying cell death, the mean cell area was seen to increase as more space was available to allow proliferation and spreading of the 3T3 cells.

In contrast, the PFib cells exhibited a slower proliferation rate and did not experience significant periods of cell death compared to the 3T3 cell line. As a primary culture, the PFib cells possess cell contact inhibition characteristics and therefore did not display signs of overcrowding leading to cell death [376]. Additionally, the change in mean cell area of the PFib cells was more variable and potentially indicated periods where there was some degree of cell death to allow for continued proliferation.

4.4.2. The Effect of Hydrogel Thickness on Cell Proliferation, ECM Production, and Differentiation

The stiffness of a material is a key property of a scaffold in tissue engineering, as the cell behaviour can be directly influenced by the substrate stiffness [377-381]. The stiffness of the material has shown to have a direct influence on the ECM organisation as the cell exerts large forces onto the substrate for focal adhesions and stress fibre organisation [382, 383]. Stiff substrates are able to reciprocate these cellular forces whereas a soft substrate is unable to do so leading to lesser developed focal adhesions and fewer stress fibres [384].

A study by Encerrado et al. investigating the mechanical properties of a similar chitosan-gelatin hydrogel confirmed that the tensile modulus of the hydrogel does not change by altering its thickness but rather by modifying the OPC and crosslinking concentration [373]. Additionally, they concluded that the differing morphology of cells found on the varying thicknesses of hydrogel was a result of how the cell perceived the stiffness of the substrate. In this research, it can be presumed that the sample thickness is inversely correlated to its perceived stiffness, as hydrogels are an innately soft material [311, 385]. As such, the perceived stiffness of the hydrogel decreases as the thickness increases. There may have been some contribution to the perceived stiffness of the thinner hydrogels from the underlying TCP as the hydrogel was tightly adhered to the well plate, contributing to the similar results seen on the TCP and 0.5mm samples. Consequently, the sample thickness played a substantial role

on the metabolic activity of the cells, and thus, the proliferation, spread, and GAG production of the cells.

It is well known that most adherent cells, such as fibroblasts and osteoblasts, proliferate and spread more on stiff substrates, especially glass and TCP, leading to the increase in research of hydrogels with varying stiffness [311, 381, 385, 386]. Following this trend, both the 3T3 cells and PFib cells showed highest metabolic activity on the 0.5mm and 1.0mm hydrogel samples, as well as TCP. The metabolic activity was lower on the increasing thicknesses of samples, suggesting that the proliferation was slower. These trends support the reasoning that the cells perceived the 0.5mm and 1.0mm samples as stiffer than the 1.5mm, 2.0mm, and 2.5mm samples.

The mean area of both cell types on the sample thicknesses further supports the trend of fibroblasts spreading on perceived stiffer substrates, based on the understanding that fibroblasts spread when the substrate can reciprocate the cytoskeletal forces leading to reorganisation of the cytoskeleton [378, 379]. In this way, the perceived stiffness of the substrate has an effect on the internal structure of the cell, which governs the morphology and composition of the cell [377, 379]. The PFib mean cell area, in Figure 4.1, demonstrates this as the cells spread to the largest mean area on TCP.

With this in mind, it is interesting to see the lack of significant difference in metabolic activity across sample thicknesses at Day 28 for both the 3T3 and PFib cells. This may indicate that although both cell types initially perceived the thicker samples as softer, the cells became acclimatized to the substrate and the proliferation rate increased [387]. The DNA content displayed a similar result as there was no significant difference in DNA concentration found at Day 28. This is accepted as the metabolic activity and DNA content are indicators of cells numbers.

Fibroblasts, mesenchymal in derivation, have a wide, scoping role in wound healing and therefore the fate and function of the fibroblast is based largely on its environment [388]. The perceived stiffness of the substrate has the potential to govern the outcome of the maturation, or production of ECM, of the fibroblast [335, 389].

Previous studies have shown an increase in the GAG/DNA ratio of ligament and tendon scaffolds at the enthesis region [157, 390, 391]. The close relation of GAG at the entheses of ligaments and tendons and to the stiffness of articular cartilage within joints led to the hypothesis that the GAG content would be highest on the perceived stiffer substrates [392]. This was supported by the significantly higher GAG

content results of the 3T3 cells on TCP compared to the hydrogel samples. The PFib GAG content results did not support this as there was no significant difference across the hydrogel and TCP samples. The lysate of the PFib cells had an overall higher mean GAG/DNA ratio across the hydrogel thicknesses, except 0.5mm, than the 3T3 cell lysate, however this difference was not significant. Of the hydrogel samples, the lysate from the 2.5mm samples of both cell types showed the highest GAG/DNA ratio, further disproving that the perceived stiffest samples would prompt the highest GAG production. The GAG/DNA ratio of the 3T3 and PFib cells suggest that environmental cues for differentiation into a fibrochrondrogenic phenotype were present [377].

The medium was also collected for quantification of GAG content. The collected medium indicates that the thinnest samples had a higher release rate of GAG [393]. The kinetics of GAG release were not evaluated in this research, although there may be a correlation between the cell proliferation and the released GAG [393]. The released GAG in the collected medium may serve as an additional tool to measure the production of GAG on the increasing thicknesses of hydrogel, however this would require further investigation.

ALP activity was not expected from either of these fibroblasts on this chitosan-gelatin hydrogel; however, it was interesting to see some levels of ALP activity on the 0.5mm and TCP samples for both the 3T3 and PFib cells. These results suggest an osteoblastic differentiation due to the environmental signals [388]. As stated previously, the metabolic activity of both cell types suggests that the 0.5mm hydrogel sample and the TCP sample are perceived as the stiffest. The modulus of the polystyrene plastic is roughly 10^6 kPa most closely resembling bone at 20^6 kPa, whereas cartilage and muscle are in the range of 42 kPa and 12 kPa, respectively [394, 395]. The ALP activity of the 3T3 and PFib cells suggest the perceived stiffness of the 0.5mm and TCP samples resembles an osteogenic environment. Although some 1.5mm and 2.5mm samples showed some ALP activity from PFib cells this was not observed in the majority of samples and was therefore discounted [396].

4.4.3. Modelling with a Cell Line vs. a Primary Culture

There are many benefits to using a cell line in an early tissue engineering study, such as the ease and speed of use, immortality, cost, and preapproved ethics [376, 397, 398]. However, cell lines do not always give an accurate representation of how true cell cultures will react and behave [397]. Tissue engineering strives to achieve a

biochemical content and biomechanical structure that is similar to that of the native tissue and a cell line may not always be a representative model of tissue growth.

Many studies have recorded the DNA, GAG, and total collagen content from ovine and rabbit cruciate ligaments, patellar tendon, and Achilles' tendon [66, 390]. The fibroblasts from cruciate ligaments are highly differentiated and specialized to form such a biomechanically and anatomically unique ligament [66, 133]. The intrinsic properties show that the DNA and GAG content is much higher in the cruciate ligaments compared to the patellar and Achilles' tendon, while the collagen content is roughly similar, Table 4.1 [66, 390]. It is worth noting that the biochemical concentrations found in Table 4.1 are calculated from native tissue that has been dehydrated prior to analysis. In this research, the cell monolayer was unable to be dissociated, dried, and then weighed and can be assumed to be ~1μg per sample solubilized in 1 ml of liquid, either papain solution or SDW.

The DNA and GAG content of the 3T3 and PFib cells was lower than those listed from previous studies in Table 4.1 [24, 66, 390]. The 3T3 cell line has a higher metabolic activity across the samples but its lack of contact inhibition may have hindered the production of ECM components, such as GAG. The PFib cells showed a higher GAG content than the 3T3 cells, despite lower metabolic activity results and DNA content. Based on the GAG content, signifying the production of ligament-like ECM components, the PFib cells may be a more accurate representation for ligament engineering research [66, 150, 158].

Table 4.1: Concentrations of DNA, GAG, and collagen found in the cruciate ligaments, patellar tendon, and Achilles' tendon. Adapted from Amiel et al. and Rumian et al. [66, 390].

	DNA Content (ug/g dry mass)	**GAG Content (ug/mg)**	**Collagen Content (mg/g)**
Cruciate Ligaments	2.73 ± 0.05	7.4 ± 1.3	802.6 ± 9.8
Patellar Tendon	1.40 ± 0.05	2.3 ± 0.3	867.2 ± 8.9
Achilles' Tendon	1.74 ± 0.04	2.75 ± 0.2	868.2 ± 10.2

Additionally, the intrinsic qualities of the PFib cells may decrease the ligamentization period that has been seen in tenocytes of tendon autografts used for ACL reconstruction [69, 94, 103, 133]. However, it is noted that the highly differentiated cells from a cruciate ligament proliferate and produce an ECM at a much slower rate than mesenchymal stem cells and dermal fibroblasts [133].

Further, the ALP activity results prove that the PFib culture has retained the inherent ability of fibroblasts to differentiate into osteoblast like cells [156]. However, these results are inconsistent due to the large error bars and few samples with recorded activity. A more comprehensive analysis is needed to conclusively prove if the PFib cells maintain the ability to differentiate into an osteoblastic lineage. Additionally, further analysis of the surface chemistry of the chitosan-gelatin hydrogel may reveal if the PFib cells respond to the chitosan-gelatin hydrogel better than the 3T3 cells.

4.5. Conclusion

The chitosan-gelatin hydrogel is a suitable biomaterial for cell culture. The variation in thickness of the hydrogel showed a similar trend in response from both the 3T3 and PFib cells in terms of metabolic activity, DNA concentration, and GAG production.

Of the five thicknesses, the 1.0mm thickness showed a realistic and repeatable response from both cell types. Additionally, the 1.0mm thickness was consistent in production. Therefore, the 1.0mm thickness will be the preferred sample thickness moving forward.

The GAG content and ALP activity results show that the PFib cells began to produce ECM components and appear to differentiate into an osteoblastic lineage upon reaching confluency, whereas the 3T3 cell line did not respond to such environmental cues and continued to proliferate. The PFib culture does not lack contact inhibition and will begin the sequence of maturation once the cell monolayer has reached confluency. The lack of significant difference of metabolic activity at Day 28 may be due to the PFib cells having a longer adjustment period on perceived softer substrates. Additionally, the PFib cells showed some ECM production across all sample types, with similar GAG/DNA ratios.

The PFib cell culture is the preferred cell model on this chitosan-gelatin hydrogel scaffold but the 3T3 cell line proves an invaluable preliminary model to test cytotoxicity before the rigors of producing a primary cell culture are undertaken. The fast proliferating 3T3 cell line is a quick marker to determine if the substrate can proceed to further tests and to understand the potential behaviour of cells. As with other cell lines, a precaution is taken in understanding the modifications to the cells and the loss of their inherent characteristics.

5. Production of Detached Hydrogel using an Intermediate Layer

5.1. Introduction

This chapter discusses the development of an intermediate layer to create a chitosan-gelatin hydrogel that does not adhere to the TCP of the well plate or bioreactor chamber. As chitosan-gelatin hydrogel is adherent to TCP, a method to produce a detached scaffold is necessary to assemble the hydrogel scaffold within the tensile loading bioreactor and to enable the stress dispersion through the scaffold [399]. Additionally, a detached scaffold is required to replicate the contraction seen in previous tissue engineered ligament studies [218, 400, 401]. The intermediate layer must not compromise the cytocompatibility of the hydrogel through the addition of further material to the cell culture system.

There has been success fabricating freestanding hydrogel membranes using layer-by-layer and surface-initiated polymerization technologies, however these methods typically are more suited to films and membranes in the nano-meter scale of thickness, employ multiple components, and often use toxic crosslinkers such as glutaraldehyde [402-405]. A similar layer method has been utilized in studies that have cast fibrin hydrogel onto SYLGARD coated plates with cell culture medium to 'release' the fibrin sinew scaffold producing a scaffold of appropriate thickness without the addition of toxic crosslinkers [218, 401, 406, 407].

The advancement of the fibrin hydrogels was adapted in this research by developing several methods to act as a releasing agent of the chitosan-gelatin hydrogel from the TCP. This involved the production and use of a polyurethane (PU) coating, a polytetrafluorethylene (PTFE) membrane, and an intermediate layer of either cell culture medium or PBS. The intermediate layer method had the added benefit of maintaining the cost-effective philosophy of this tissue engineered ligament system.

The resultant novel detached chitosan-gelatin hydrogel was assessed for cytocompatibility using the alamarBlue assay and characterized using X-ray photoelectron spectroscopy (XPS), near ambient X-ray photoelectron spectroscopy (NAP-XPS), and ESEM. The physical properties of the detached hydrogel were also analysed by measuring the density, swelling, degradation, and tensile behaviour. As

contraction of detached fibrin hydrogels has been recorded, the detached chitosan-gelatin hydrogels were also monitored for contraction [218, 401, 407].

5.2. Methodology

5.2.1. Polyurethane Coating

The PU coating was created by dissolving PU pellets (Chonoflex AL 80A, Advansource, CA) in tetrahydrofuran (THF) on a magnetic stirrer at 50°C. The beaker was kept covered to reduce evaporation of the THF during mixing. Once the pellets were fully dissolved, the PU solution was quickly poured into the wells of a 6-well plate to create a coating within the well. The coated well plates were left to air-dry in the fume cupboard with a loose covering of aluminium foil for a minimum of 48 hours. The wells were washed with IMS and detergent before use.

Chitosan-gelatin hydrogel was made with the same protocol as given in section 3.5 (page 50). After washing the PU coated well plates, the hydrogel was cast into the wells at 1mm thickness and allowed to gel. The hydrogel was then sterilized as described previously.

5.2.2. Polytetrafluoroethylene Membrane

A premade PTFE membrane from Goodfellow (Cambridge, UK) was purchased to place into the wells. The membrane came in two thicknesses, 0.5mm and 1.0mm, in sheets of approximately 15cm x 15cm. The membranes were cut to size for placement in 6-well plates. The membrane pieces were thoroughly washed with detergent and IMS before use.

The hydrogel was made and cast onto the PTFE membrane discs within the well plate at 1mm thickness. The hydrogel was sterilized as described previously.

5.2.3. Intermediate Layer

Cell culture medium and PBS were investigated to create the intermediate layer as these materials are regularly used in cell culture. To create the intermediate layer, cell culture medium or PBS was frozen into a 2mm thick layer in a 6-well cell culture plate. Chitosan-gelatin hydrogel was then made using the protocol described previously. Once the intermediate layer was frozen, the hydrogel was swiftly cast into the wells to create a circular shape of 1mm thickness. The hydrogel was also cast into well plates without an intermediate layer.

The frozen cell culture medium or PBS was allowed to melt at room temperature as gelation of the hydrogel occurred. Complete gelation occurred within 15 minutes. Once fully melted, roughly 45 minutes, the liquid was removed leaving

behind a detached hydrogel disc. The thawed liquid covered the surface of the hydrogel discs. Hydrogels cast onto the cell culture medium were coded sample 'MH.' Hydrogels cast onto the PBS were coded sample 'PH.' Hydrogels cast into the well plate without an intermediate layer were coded 'NH.'

The MH and PH detached hydrogel discs and NH were then sterilized as outlined previously. The 10% NaOH solution was gently pipetted into the wells to cover the entire detached hydrogel sample.

5.2.4. Cross-Section Detached Hydrogel Measurement

To ensure that the casting of the detached hydrogel produced the desired thickness, the MH and PH samples were cut in a cross section and measured. The detached hydrogel was removed from the well plate using a spatula and gently placed on a dry paper towel. The detached hydrogel was then cut through the midline using the spatula. The cut piece of hydrogel was then measured against a ruler.

5.2.5. Density Measurement

The density of the hydrogel was calculated to determine whether the hydrogel discs, MH and PH, would remain fully submerged in the cell culture medium during cell culture. Density was calculated by measuring the mass of 500 µl of hydrogel in 5 replicates using the equation: $d=m/v$. Where d is the density, m is the mass, and v is the volume. The density of the cell culture medium and PBS was calculated in the same manner.

5.2.6. Hydrogel Swelling and Degradation

The swelling of MH and PH was monitored using a protocol similar to Bryant and Anseth and the ASTM F2900-11 standard [408, 409]. MH and PH were created and sterilized. After sterilization, the samples were incubated in PBS for 24 hours and then the wet mass was measured. The samples were then dried in an oven at 50ºC for 2 hours and then the dry mass was measured.

The swelling ratio, Q, of the hydrogel was calculated using Equation 1, where Ds is the mass of the swollen hydrogel and Dw is the mass of the dried hydrogel [408].

Equation 1: Swelling Ratio

$$Q = \frac{Ds - Dw}{Dw}$$

The degradation of MH and PH was measured by creating and sterilizing the samples and then incubating the samples in either cell culture medium, PBS, or SDW. Each sample was kept in triplicate in each treatment and kept completely submerged in the designated liquid during incubation. Fresh medium, PBS, and SDW was replaced every 7 days. The wet mass of the hydrogel was measured prior to casting, Day 0, and then the wet mass of each sample was measured after sterilization, Day 1, and then after 21 days.

5.2.7. MicroTensile Testing

A stress/strain curve was calculated using a Deben in-situ MicroTest tensile-compression stage MTEST200VT unit for FEI Quanta 650 ESEM with a Peltier Cooling Stage. The Peltier Cooling stage was used to stabilize the mid-section of the hydrogel, the temperature control function was not utilized.

In order to calculate a stress/strain curve for the hydrogel, adaptations to the casting method were needed to suit the testing unit. The dimensions of the detached hydrogel were required to be a minimum of 10mm x 50mm. To account for this, the hydrogel was cast in a large glass petri dish with a 2mm thick intermediate layer of either the cell culture medium or PBS. An outline of 10mm x 85mm was drawn on the bottom of the petri dish to guide casting, with the excess length allowing for easier mounting into the testing unit. These samples were sterilized followed the same methods described previously. It was recommended that the hydrogel samples be cast in a ‘dumbbell’ shape to reduce breakage at the clamps but this shape could not be cast and uniform strips were used [409].

The detached hydrogel samples were transferred into the testing unit using forceps and a spatula. To secure the ends of the hydrogel within the clamps, two pieces of painter’s tape were attached to the top and bottom of the inside of the metal clamp. The pieces of tape were replaced once the adhesive became oversaturated and detached from the metal. The detached hydrogel strip was loaded at the stationary clamp first. At the mobile end, the hydrogel was held as taught as possible to reduce any sag while the clamp was secured. The complete set-up of the MicroTest unit and hydrogel can be seen in Figure 5.1.

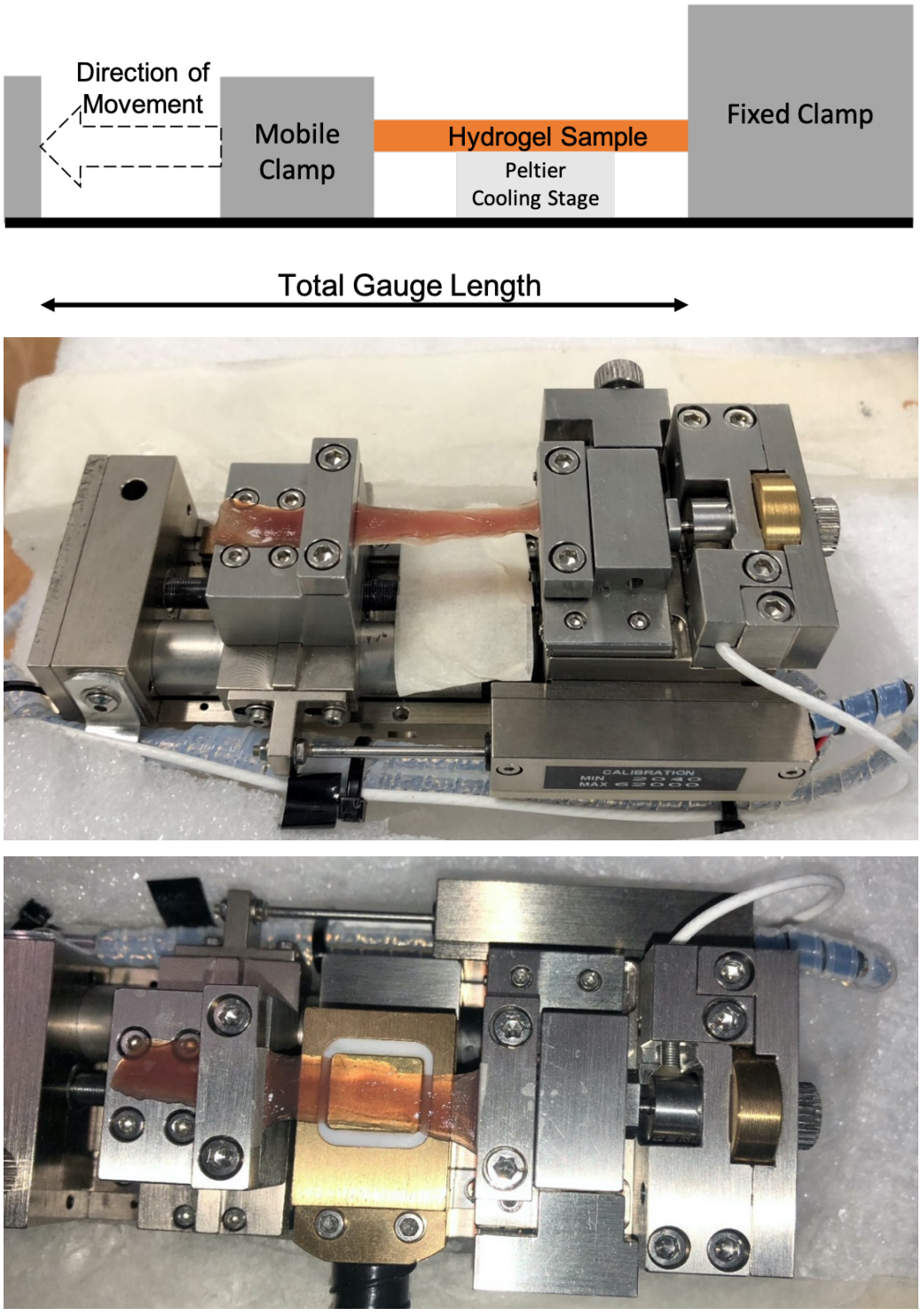

Figure 5.1: (Top) A schematic of the MicroTest unit with direction of movement. The schematic shows the mobile and fixed clamps of the rig with the hydrogel sample attached to both. The Peltier Cooling stage can be seen underneath the middle portion of the hydrogel sample. (Middle) An oblique view of the testing unit using a MH sample without a Peltier Cooling Stage at mid extension. The stationary clamp can be seen on the right and the mobile clamp on the left, with excess hydrogel protruding out. A piece of tape covers the rotating motor rod to reduce any remnant liquid from the sample dripping onto the rod. Data from tests without the Peltier Cooling stage was not used. (Bottom) A superior view of the MicroTest unit using a MH sample with a Peltier Cooling stage at the resting position. The stationary clamp is on the right and the mobile clamp on the left, again with excess hydrogel protruding. The Peltier stage reduces sagging of hydrogel between the clamps.

5.2.8. XPS

The surface chemistry of the hydrogels was analysed using XPS. In order to analyse the samples, the hydrogel had to be fully dehydrated. The MH, PH, and NH samples were cast and sterilized as described previously at 1mm thickness. After sterilizing, excess liquid was removed and all samples placed into a drying oven at 45°C for 24 hours, all in 6 well plates. After complete drying, all three samples resembled a brown film and were removed from the well plates in 5mm sections. There were no structural deformities, such as a tear or rupture, in any of the samples. As the dehydrated hydrogels had adhered to the culture plastic, the hydrogels were scraped off of the culture plastic and both the lower surface (plate side) and surface exposed to air during hydrogel casting were analysed. The surfaces of the samples were analysed using a LiPPS, Kratos Axis Ultra Instrument (Kratos Analytical, Kyoto, Japan). The charge was corrected so the peak of C 1s was read at 285 eV. Samples were secured using double sided tape. Three areas per sample were used for wide scans and high-resolution spectra. CasaXPS software was used to analyse the data.

5.2.9. NAP-XPS

The surface chemistry of the hydrogels was also examined with NAP-XPS using a SPECS Devi-sim NAP-XPS instrument with a Peltier stage (SPECS, Berlin, Germany). The MH and PH samples were cast at 1mm thickness, sterilized, and stored in a well plate with excess medium until reading. Excess cell culture medium was allowed to run off before loading the sample onto the stage. The surface of the detached hydrogel exposed to air during casting was analysed. However, as the intermediate layer thawed, the liquid encapsulated the hydrogel disc and both surfaces of the hydrogel disc were expected to be similar. The NAP-XPS was cooled to 5ºC, kept at 100% relative humidity, and the pressure at 8 mbar. SpecsLab Prodigy software version 4.12 was used to analyse the data.

5.2.10. Cell Culture

MH, PH, and NH were cast and sterilized at 1mm thickness. NH was cast in a 12-well plate. After sterilization, the conditioning medium was removed and the MH and PH hydrogel discs were transferred to 12-well plates that were coated with poly(2-hydroxyethyl methacrylate) (poly-HEMA) (Sigma, UK) to reduce cell adhesion to the well plate. 3T3 cells were then seeded at a density of 80,000 cells/cm^2 at a volume of 500 µl. In order to maximize the adhesion of cells to the hydrogel disc rather than the

well plate, the cell solution was pipetted dropwise onto the disc, ensuring the cell solution covered the entire hydrogel disc. The cells were incubated for 1 hour before additional medium was added. During medium changes, extra care was taken to not disturb the hydrogel disc. There was one biological replicate and 6 technical replicates, repeated three times.

An alamarBlue metabolic assay was carried out at Day 3 and Day 7 as described in section 3.4.1 (page 46). As before, there was care taken during the washing steps to not disturb the hydrogel disc.

Following alamarBlue, the samples chosen for ESEM were fixed following the same protocol as described previously in section 3.5.5 (page 51), with care during fixation and PBS washes.

An additional NH sample was cast with a glass coverslip underneath and sterilized for ESEM. This sample was seeded with 3T3 cells at a density of 5,000 cells/cm^2 at a volume of 500 µl and cultured for 5 days before imaging to analyse the morphology of the 3T3 cells.

5.3. Results

5.3.1. PU Coating and PTFE Membrane

There was concern regarding the emission of toxic particles from the PU and THF but these two materials have been proven to be non-cytotoxic [255, 410]. Similarly, leaching from the PTFE was questioned for future use within cell culture. However, the hydrogel adhesion to the PU coating and PTFE membrane was similar to that of the TCP in well plates. No further investigation took place using either of these methods.

5.3.2. Intermediate Layer

The hydrogel of the MH samples remained detached from the well plate and intact throughout sterilization, cell culture, assays, and imaging. The PH samples were inconsistent in production where not all samples remained intact during sterilization. The PH samples that disintegrated during sterilization were not used and further samples were created. This led to no more than three PH samples cast at the same time to better monitor the quality of the samples. Additionally, it was observed that upon removal of the liquid of the intermediate layers, the volume of liquid had decreased from the initial volume used, indicating the potential uptake of the intermediate layer by the hydrogel.

The development of the cell culture medium and PBS intermediate layers produced a convex lens-like hydrogel scaffold that could be repositioned or transferred to a separate container, as seen in Figure 5.2. Due to the convexity, the centre of the hydrogel discs remained 1mm in thickness as the edges became thinner.

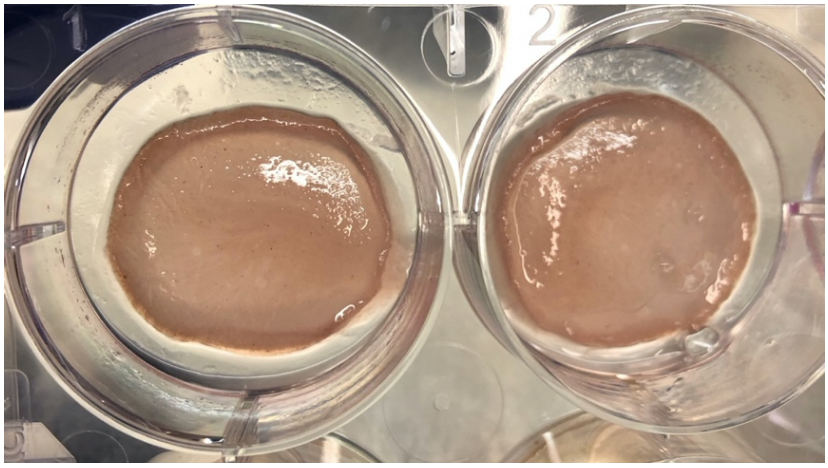

Figure 5.2: An image of two MH samples after sterilization in a 6-well plate. Note the size of the scaffolds are significantly smaller than the well itself.

The cross-section of the detached hydrogel confirmed that the casting method produced the desired thickness, Figure 5.3. The cross-section also confirmed that the detached hydrogel samples had a convex shape, similar to a convex lens, as the centre of the sample remained 1mm in thickness and the edges became thinner. The 1mm PH samples, Figure 5.4, appeared to have a lesser degree of convexity than the MH samples.

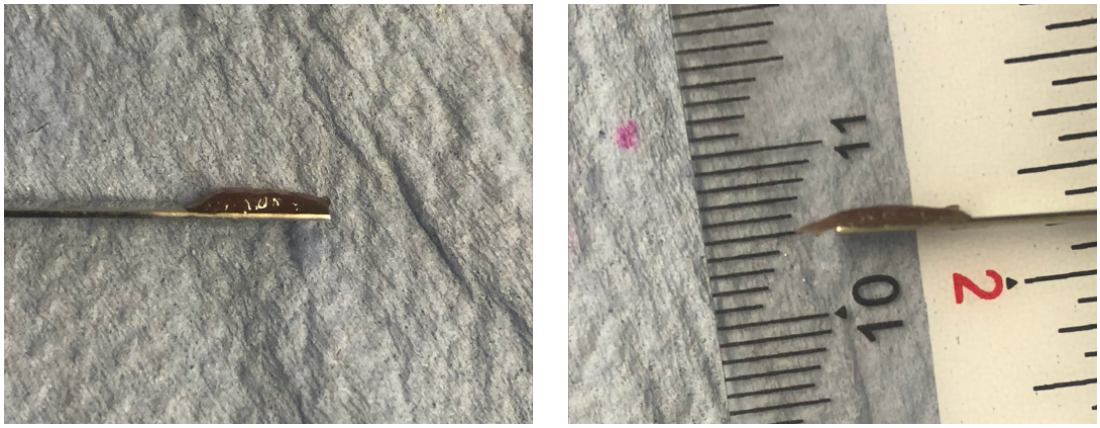

Figure 5.3: The cross-section of a MH sample of 1mm thickness. Left) The portion of the MH sample held against the paper towel to observe the slice. Right) The portion of the MH held against a ruler to measure the thickness.

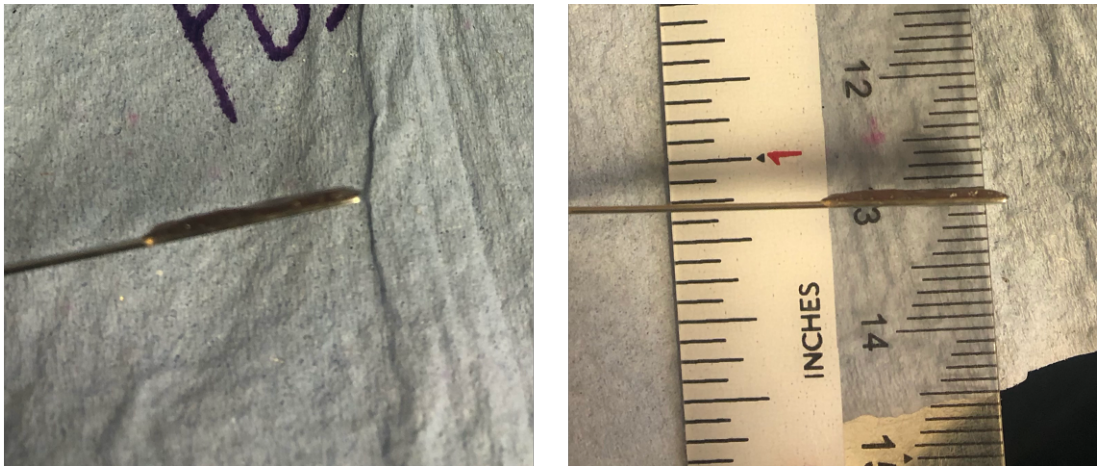

Figure 5.4: The cross-section of a PH sample of 1mm thickness. Left) The portion of the PH sample held against the paper towel to observe the slice. Right) The portion of the PH sample held against a ruler to measure the thickness.

5.3.3. Characterisation of the Detached Hydrogel

5.3.3.1. Density

The density of the hydrogel was 0.8 g/cm^3. The density of the cell culture medium was 0.949 g/cm^3 and PBS was 0.977 g/cm^3. Despite the hydrogel being less dense than the cell culture medium, the hydrogel discs remained submerged in the cell culture medium during incubation and cell culture.

5.3.3.2. Swelling Ratio

The degree of swelling for MH was calculated to be 17.68 while the degree of swelling for PH was 10.78. This resulted in the MH sample having a 61% higher swelling ratio. The frozen cell culture medium appeared to undergo some phase separation during freezing and had a concentrated layer of medium constituents on the surface that may have affected the water uptake of the cast hydrogel. The frozen PBS did not appear to have this same concentrated layer. The decreased protein and salt content of the PBS may have increased the amount of water available for hydrogel absorption during casting. As the phase separation of the cell culture medium appeared to occur after prolonged storage in the freezer, effort was taken to reduce storage time to minimize this effect.

5.3.3.3. Degradation

The degradation profile of the MH sample can be seen in Figure 5.5. The decrease in wet mass at Day 1 was not significant after incubation in any of the three liquids. The decrease in wet mass was significant at Day 21 after incubation in the three liquids. At Day 21, the MH incubated in medium had a significantly higher wet

mass than in PBS and SDW. Similarly, the MH incubated in PBS had a significantly higher wet mass than in SDW at Day 21.

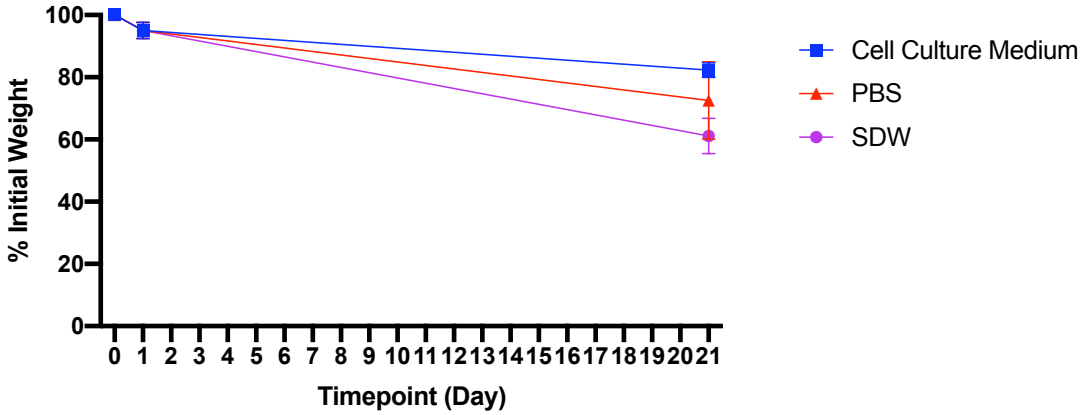

Figure 5.5: The degradation profile of MH in medium, PBS, and SDW after 21 days of incubation expressed as % initial weight. Day 0 indicates the hydrogel before casting. Day 1 indicates the day the hydrogel discs have been sterilized. The error bars represent standard error of mean. Where n=3.

The degradation profile of the PH sample can be seen in Figure 5.6. The decrease in wet mass at Day 1 and at Day 21, compared to Day 0, was significant after incubation in the three liquids. At Day 21, the wet mass of PH incubated in medium was significantly higher than in SDW. At Day 21, the difference of wet mass between PH incubated in medium and incubated in PBS was not significant, as well as between PBS and SDW.

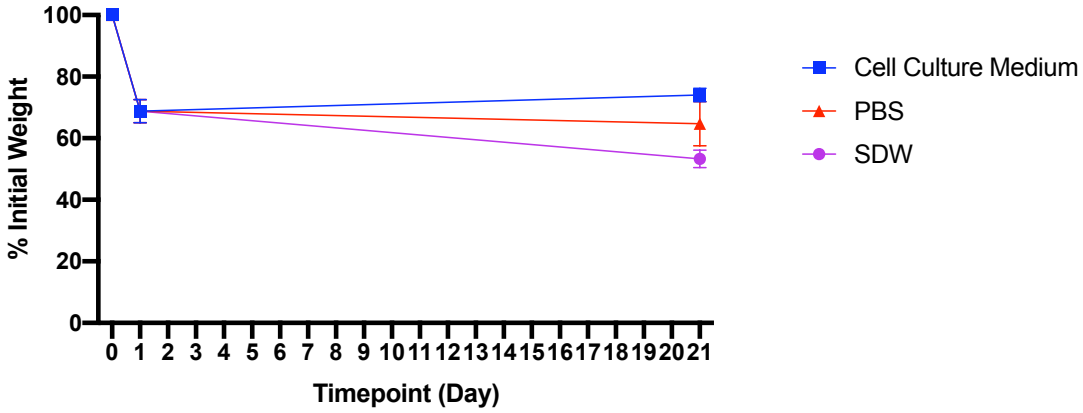

Figure 5.6: The degradation profile of PH in medium, PBS, and SDW after 21 days of incubation expressed as % initial weight. Day 0 indicates the hydrogel before casting. Day 1 indicates the day the hydrogel discs have been sterilized. The error bars represent standard error of mean. Where n=3.

The wet mass of MH was significantly higher than PH after sterilization across incubation in all three liquids. The difference in mass between MH and PH was not significant at Day 21 across all three liquids. Overall, the MH samples experienced a less significant change in mass loss after sterilization compared to PH. The PH sample

incubated in cell culture medium showed an increase in wet mass at Day 21 from Day 1, however this was not significant.

5.3.3.4. XPS

The XPS results showed a significantly higher weight percentage for Na and Cl in the MH and PH samples compared to NH, listed in Table 5.1. Both MH and PH had similar weight percentage results of all elements found on the surface and no significant difference was found between the two sample surfaces. Additionally, the weight percentage of C and O was significantly higher on the NH surface than the MH and PH.

The wide scan, Figure 5.7, revealed a small peak at Na 1s for NH. The O 1s peaks for MH and PH were shifted to the Auger feature of Na KLL. This could be due to the increased amount of Na present in these samples. The C 1s peaks for all three samples occurred at 284 eV, indicating C-N, C-O, and C-Cl bonds. The N 1s peak for all three samples occurred at 400 eV. The O 1s peak occurred at 532 eV for the NH sample indicating the presence of hydroxides and phosphates. The Na 1s peak for all three samples occurred at 1072 eV indicating presence of NaCl and sodium phosphates, however the peak for NH had a much lower intensity. The peak for Cl 2p occurred at 198 eV for NH and 199 eV for MH and PH indicating the presence of alkali chlorides.

Table 5.1: Weight percentage values of the MH, PH, and NH samples estimated from the wide scan of XPS. Si was not detected in either MH or PH samples, resulting in a '0' weight percentage. The total of each row is equal to 100.

	C 1s (%)	Cl 2p (%)	N 1s (%)	Na 1s (%)	O 1s (%)	Si 2p (%)
MH	35.64	40.07	1.89	16.27	6.13	0
PH	34.81	44.31	1.48	15.12	4.28	0
NH	72.64	1.16	8.75	0.40	15.20	1.83

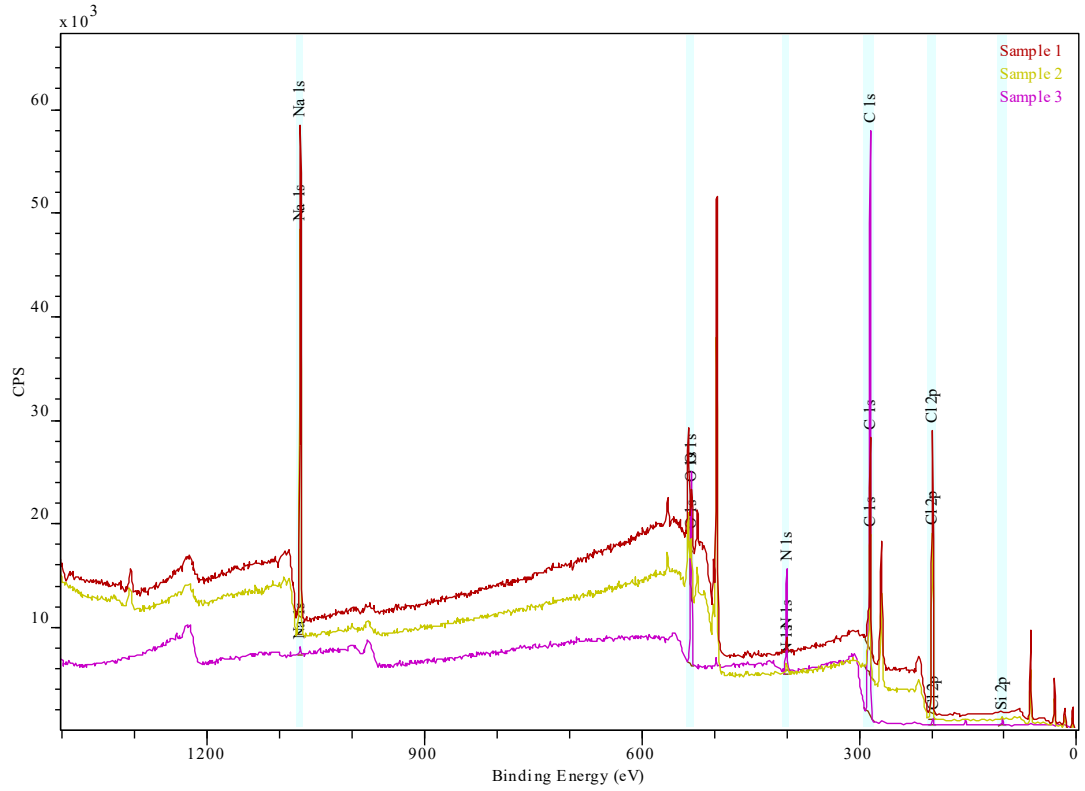

Figure 5.7: The wide survey scan of MH (Sample 1), PH (Sample 2), and NH (Sample 3). Note the much smaller peak for Na 1s from NH (Sample 3). The O 1s peak for Sample 1 and 2 sits on the Auger feature produced by Na KLL. Graph courtesy of Mrs. Emily Smith.

5.3.3.5. NAP-XPS

The NAP-XPS results revealed no residue of salt deposits from the intermediate layer of cell culture medium or PBS. The survey scan detected N, O, C, and Na but Cl could not be detected, as seen in Figure 5.8. The detailed spectra showed peaks for N 1s, O 1s, and C 1s that were similar for both MH and PH. As Na was not detected in the survey scan, a peak for Na was absent for both MH and PH in the detailed spectra. The peak for N 1s occurred around 400.00eV for both MH and PH, representing NH_2 stretching. The peak for O 1s occurred around 532.00eV for both MH and PH, representing O-H or N-O stretching. The peak for C 1s occurred around 285.00eV for both MH and PH, representing C-C, C-N, or C-O-C stretching. The varying intensity was due to the change in proximity of the detector to the sample, as the location of the detector was unable to be monitored due to the low reflectivity of the sample.

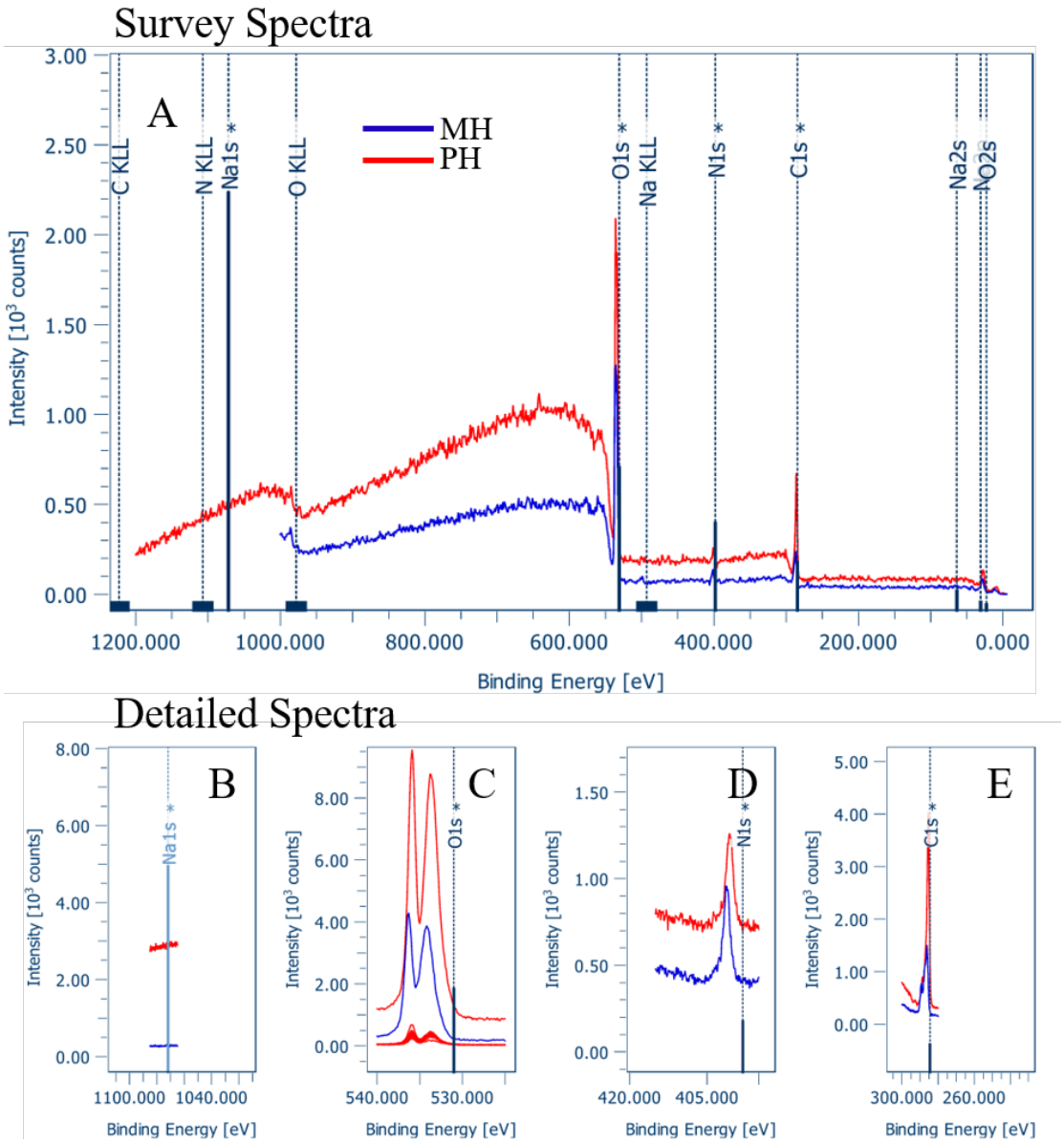

Figure 5.8: NAP-XPS survey (A) and detailed (B-E) spectra of MH, blue, and PH, red. In the detailed spectra, (B) shows the area where the peak for Na would be seen, (C) where the peak for O is seen, (D) where the peak for N is seen, and (E) where the peak for C can be seen. Note that there are no peaks found for Na. The peaks seen in C, D, and E for both MH and PH are similar. The difference in intensity is due to the distance the sample is from the detector.

5.3.3.6. Surface Imagery

The ESEM images of MH, PH, and NH prior to cell culture showed similar surface textures, as seen in Figure 5.9. All three samples appeared to have a smooth surface with no outstanding micro-features. The MH and PH samples showed undulations throughout the sample, which were considered to be due to the sample loading as there was no underlying constraint such as the glass coverslip of NH.

After prolonged imaging, some specks were visible on the MH and PH samples. This is believed to be caused from the ESEM imaging process where the

sample was dehydrated from the decreasing temperature and pressure. These specks were homogenous and not believed to be salt depositions as a result from the intermediate layer.

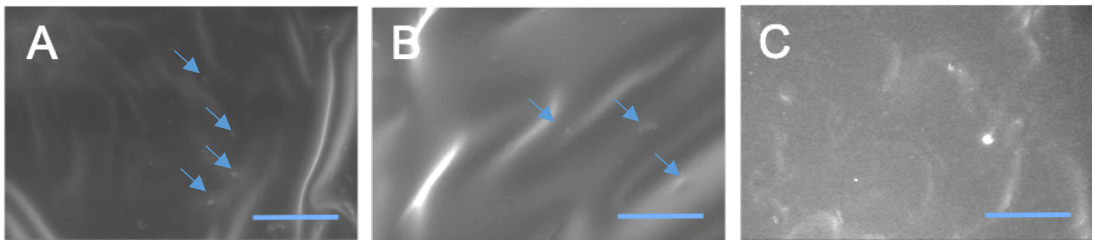

Figure 5.9: ESEM images of MH (A), PH (B), and NH (C) prior to cell culture. All samples were sterilized before imaging. The smooth surfaces of all three samples can be seen while several undulations are visible on the MH and PH sample. The NH sample does not have any visible significant surface features. The blue arrows indicate specks that became visible on the surface of the MH and PH samples. The blue bar indicates 100 μm.

5.3.3.7. Microtensile Testing

MH and PH were tested with 100% rupture rate. The ruptures occurred near or at the mobile clamp. The results are reported as mean with standard error of mean, as seen in Figure 5.10. The elongation at failure for MH and PH was 32.3% ± 0.006 and 29.3% ± 0.031, respectively, resulting in no significant difference between the two samples.

There was no visible slippage at the clamps. As tension was applied, both MH and PH adopted a slight ‘dog bone’ shape and became thinner in width between the clamps and the Peltier Stage while maintaining the original width near the clamps. MH was stiffer in tension with a tensile modulus of 3757.4 Pa while PH had a modulus of 782.7 Pa, resulting in a 79.17% difference between the two samples.

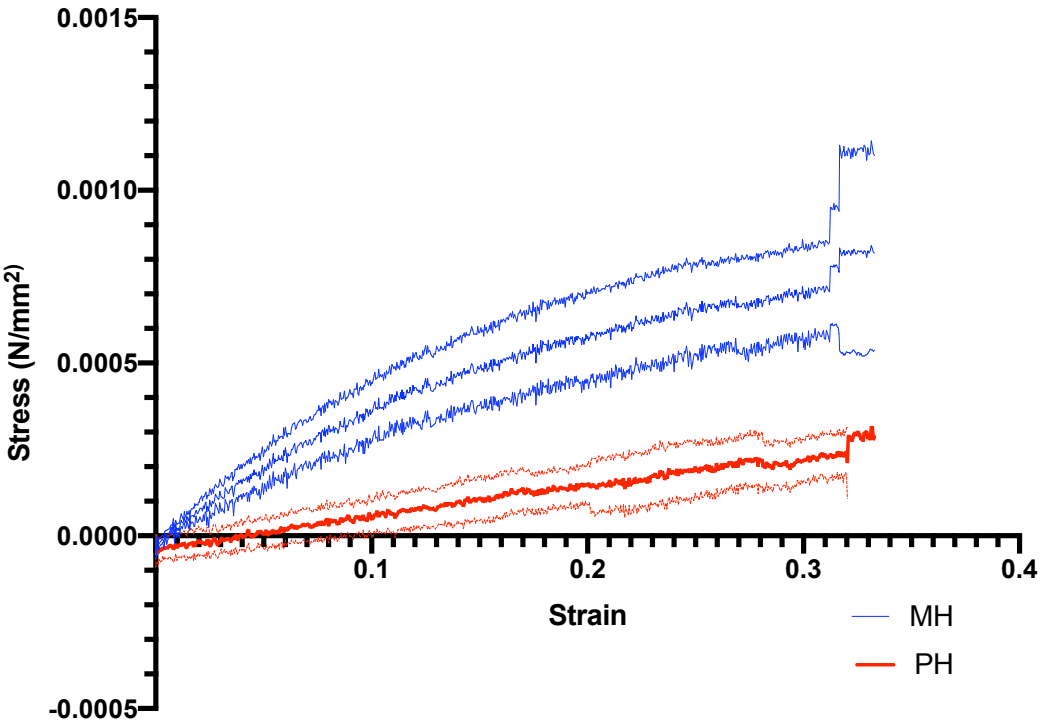

Figure 5.10: Stress/strain curve based on the data from the MicroTest unit. MH is indicated by the blue line and PH by the red line. The outer, thinner lines represent the standard error of mean. n=4 for both samples.

5.3.4. Cytocompatibility

5.3.4.1. Metabolic Quantification

The alamarBlue results confirmed that the intermediate layer does not affect the cytocompatibility of the hydrogel, as seen in Figure 5.11. The TCP, as expected, had significantly higher metabolic activity than all three hydrogel samples at both time points. However, there was no significant difference between the MH and PH samples and NH at either timepoint. An interesting result of the metabolic activity from this short experiment, is the decrease in significant difference between the TCP and hydrogel samples from Day 3 to Day 7. At Day 7, the level of significance between MH and TCP decreases from p <0.0002 to p <0.0021. The level of significance between PH and TCP decreases in a similar fashion from p <0.0001 to p <0.0002. There is no change in level of significance between the NH sample and TCP at Day 7.

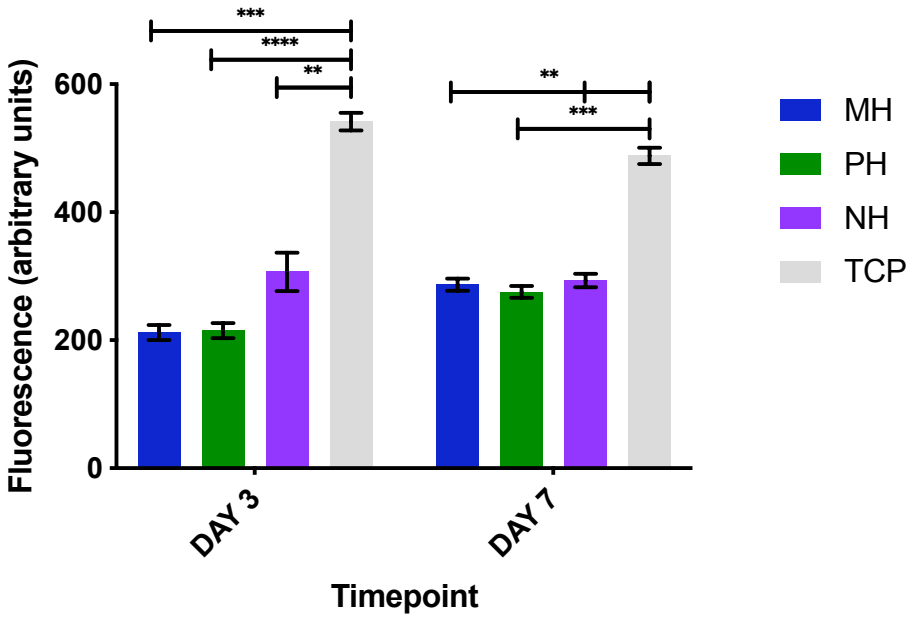

Figure 5.11: Metabolic activity of 3T3 cells at Day 3 and Day 7 using alamarBlue on MH, PH, NH, and TCP. Where * p <0.0332, ** p <0.0021, *** p <0.0002, **** p <0.0001. The error bars represent standard error of mean and n=6 with 3 repeats.

5.3.4.2. Cell Morphology

After 7 days of cell culture, the cell morphology varied between the sample types and appeared to be dependent upon the location within one sample type, Figure 5.12.

At the centre of the MH and PH samples, the 3T3 cells had a rounded morphology. At 250 μm from the edge of MH and PH, there were several cells that had an elongated morphology and there were clusters of cells growing near and on top of each other. The PH sample showed a higher number of cells that had an elongated morphology at this area. At the very edge of the MH and PH sample, roughly 50-100 μm from the edge, there were large clusters of elongated cells that appeared to be growing on top of other cells. Within these clusters, there were still a large number of spherical cells seen however, the majority of the cells were elongated.

The cells formed a complete monolayer on the NH sample which could be seen in the central and edge images. The morphology of individual cells could not be seen. To view the morphology of individual cells on the NH sample, 3T3 cells were seeded at a low seeding density of 5,000 cells/cm^2 and imaged at Day 5. While there were still some rounded cells seen, a majority of these cells showed an elongated morphology throughout the sample.

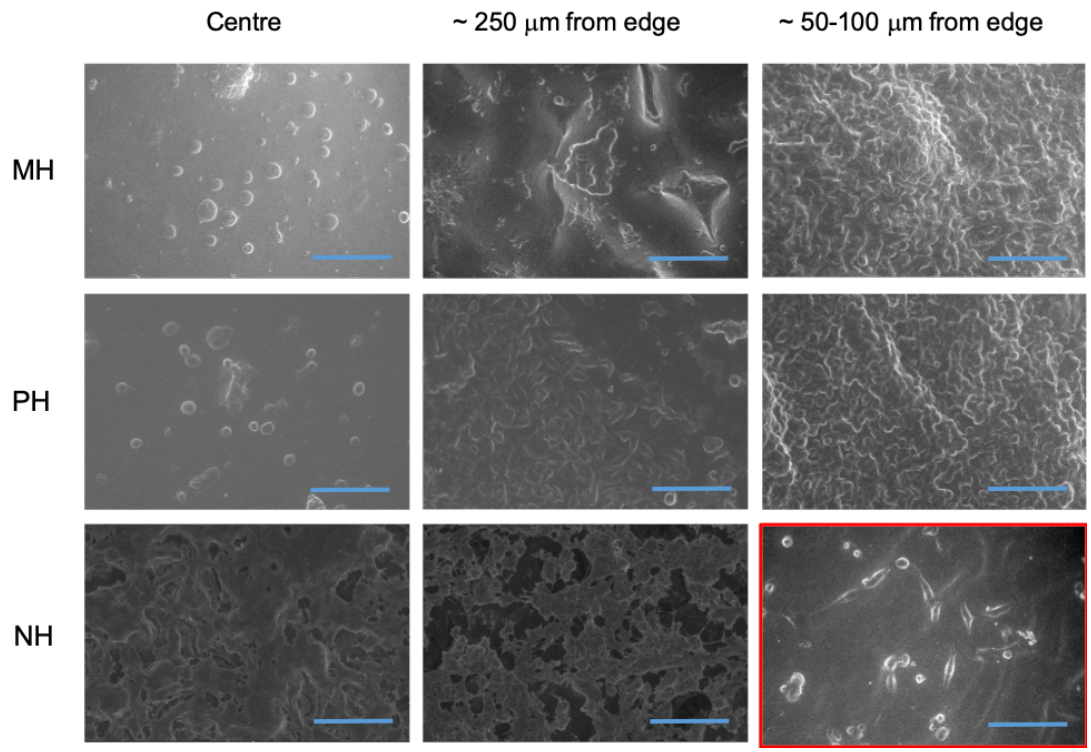

Figure 5.12: ESEM imagery of 3T3 fibroblasts after 7 days of culture on MH, PH, and NH. Images were taken at the centre of the sample, approximately 250 µm from the sample edge, and approximately 50-100 µm from the sample edge. The image with the red border indicates the centre of NH after 5 days of culture using a low seeding density of 5,000 cells/cm^2 to highlight the elongated morphology of the cells. The blue bar indicates 100 µm.

5.3.4.3. Contraction

At the beginning of this experiment, the contraction of the hydrogel to form a sinew structure was investigated as fibroblasts possess a unique contractile characteristic necessary for wound healing [401, 411]. The contraction of the hydrogel was deemed necessary to create the desired sinew shape of the tissue engineered ligament [218]. In order to facilitate the contraction, detached hydrogel scaffolds were needed as the adhesion of the hydrogel to the TCP of well plates would restrict this movement. However, it was found that the detached chitosan-gelatin hydrogel did not contract in this study.

5.4. Discussion

5.4.1. Physical Properties of the Detached Hydrogel

The translation of *in vitro* studies to *in vivo* studies and then into further clinical practice has been difficult within tissue engineering. The challenge arises in creating a 2-dimensional *in vitro* study and translating it into a 3-dimensional *in vivo* environment of the natural tissue [412]. To further understand and model the *in vivo* cell interactions, the complexities of the cell response to biomaterials must be

investigated extensively at an *in vitro* level [125]. In response to this process, the *in vitro* model of ligament tissue engineering has been considerably adapted to better replicate the ligament *in vivo* [125, 130, 227].

The final objective of this research is to utilize a tensile bioreactor to more accurately apply mechanical stimulation in an attempt to replicate an *in vivo* environment. In order to use the chitosan-gelatin hydrogel in the bioreactor, a method to release the adherent hydrogel from the well plate was needed. The intermediate layer resulted in a functional detached hydrogel scaffold that was able to be handled and transferred, producing a representative biomaterial for *in vitro* studies. The detached hydrogel scaffolds maintained their structural integrity throughout all cell culture assays and characterisation tests. Despite the difference in densities, the hydrogel discs remained fully submerged in cell culture medium at all times. This is necessary to preserve a homogenous hydrated state throughout the hydrogel and to maintain cell viability as the cells must be kept in cell culture medium.

The biodegradation of the scaffold and ingrowth of cells is crucial in recreating a ligament or tendon with characteristics similar to native tissue [130, 315]. The biodegradation of the scaffold causes chemical and mechanical changes to occur that may affect the cell response [413]. Typically, the degradation of a hydrogel leads to the loss of its mechanical strength, unless the ingrowth of cells is adequate enough to replace the waning hydrogel [315, 413, 414]. The balance of degradation to cell ingrowth is imperative to the tissue development.

As there were no available enzymes present within this experiment that are able to degrade the chitosan-gelatin hydrogel, namely lysozyme, it became apparent that of the degradation mechanisms seen in hydrogels, this chitosan-gelatin hydrogel degrades by a combination of dissolution and hydrolysis rather than enzymatic cleavage [293, 315, 370, 399, 415, 416]. The high degree of deacetylation and crystallinity of the chitosan contribute to the rate of degradation of the hydrogel as it is shown that the higher degree of deacetylation causes higher crystallinity which decreases the degradation rate of chitosan [415, 417]. As the constituents of this chitosan-gelatin hydrogel are all cytocompatible, it is presumed that this hydrogel would experience a similar degradation rate *in vivo* as lysozyme is not typically found within the joint capsule or synovial fluid of the knee unless there is an inflammatory reaction [418, 419].

Although the degradation profile of the chitosan-gelatin detached hydrogels was performed without cells or mechanical stimulation, degradation is affected by the composition of the scaffold rather than the environment [315]. Therefore, it is expected that the hydrogel discs would be able to sustain cell culture and mechanical stimulation without accelerated dissolution.

During the swelling studies, it was shown that the period in which the hydrogel was fully swollen was prior to sterilization. The bulk of mass loss occurred during sterilization, most likely from the UV process as the swelling behaviour decreases with increased absorbed energy, such as through UV radiation [420]. The chitosan-gelatin hydrogel exhibited a high swelling degree that is comparable to previous studies using a similar hydrogel composition, which is necessary to maintain the high water content of the hydrogel [293, 372, 421]. Additionally, a high swelling degree proves advantageous for homogenous GAG perfusion throughout the scaffold [408]. The study by Han et al. has shown that the degree of swelling of a chitosan-gelatin hydrogel is directly proportional to the level of crosslinking [421]. Further, the stable swelling and degradation of the chitosan-gelatin hydrogel can be attributed to the compatible crosslinking interaction of gelatin and chitosan [293, 399, 422]. The swelling degree results of this research has shown that the crosslinking of the chitosan-gelatin hydrogel is beneficial to maintain the high water content of the hydrogel.

The XPS results revealed an increased concentration of Cl and Na on the surface of MH and PH, indicating that the intermediate layers deposited salt residue on the hydrogel surface. The weight percentage of C and N were similar to a chitosan-gelatin hydrogel membrane produced by Mao et al. [423]. Increased salt concentrations have may have an unwanted effect on the cell-material interaction, such as hyperosmolarity or a change in the ECM production [424, 425]. It has also been shown that an increase in NaCl has a negative effect on the modulus of the hydrogel substrate [414]. However, the dehydration of the hydrogel samples for XPS caused the surface to become dissimilar to the surface environment that cells would experience. This leads to the conclusion that the XPS data may not give a true surface composition analysis of the detached hydrogels in accordance with cell interactions.

The NAP-XPS gave a more realistic representation of the surface chemistry based on the hydrated environment the cells would experience both *in vitro* and *in vivo*. The NAP-XPS results did not show Cl or Na residue on the surface of either MH or PH, contrary to the XPS results. Although, some levels of Cl and Na are expected

to be available at the surface of the chitosan-gelatin hydrogel due to its constituents. It is possible that when the hydrogel is in a hydrated state, these underlying components are masked and do not affect the cell-material interaction and response. The NAP-XPS results reported here match previous studies of the surface chemistry of chitosan-gelatin hydrogel crosslinked with OPC [293, 422]. The decreased liquid volume of the intermediate layer immediately after hydrogel casting suggested trace amounts of fluid uptake by the hydrogel but the NAP-XPS results did not show salt residues from the cell culture medium or PBS.

A previous study by Nagahama et al. reports the elasticity and flexibility of chitosan-gelatin hydrogels are best when the ratio of gelatin to chitosan is 0.50, as it is in this experiment [399]. Previous studies have also confirmed the addition of OPC further strengthens chitosan-gelatin hydrogel [293, 373]. The microtensile results showed that MH and PH can withstand small forces performed in a relatively slow manner. Although difficult to image, MH and PH appeared to act similarly to ligamentous tissue in that the tensile strain was transmitted radially and formed a ‘dog bone’ shape between the grip and Peltier stage [426].

The elongation before failure of the MH and PH samples was similar to that of a natural ACL, near 33%, and higher than that of several commercially available synthetic grafts such as Gore-Tex and Dacron, 9% and 18.7% respectively [7, 135]. However, MH and PH had significantly lower ultimate tensile strengths than the natural ACL and synthetic grafts. The tensile moduli of MH and PH were significantly lower than previous studies investigating braided PLGA (100-400 MPa) and PLLA scaffolds (55.0 MPa), collagen fibres (359.6 MPa), and chitosan/hyaluronan fibres 217.6 MPa) [213, 225, 227, 228]. The tensile moduli of the MH scaffolds was most similar to stromal tissue, with a modulus around 3000 Pa, while the PH scaffolds were most similar to breast tissue, with a modulus around 900 Pa [427]. Additionally, the tensile modulus of both MH and PH were significantly lower than the modulus of a 2% OPC chitosan-gelatin hydrogel (127.4 kPa) calculated from compressive testing in a study by Encerrado et al., indicating that the intermediate layer may have a negative effect on the strength of the scaffold [373]. This may be due to water uptake during casting or a potential phase separation of the hydrogel once it is cast on the frozen layer. The large difference between the modulus of MH and PH suggested that the PBS intermediate layer may have a more significant effect on the structural integrity of the hydrogel compared to the cell culture medium intermediate layer. It

can be reasoned that the chitosan-gelatin hydrogel mixed at 37°C experienced a large decrease in temperature upon casting on a frozen substrate, potentially producing some phase separation, although this was not visible. In a study by Goycoolea et al., a correlation between the temperature and shear and storage modulus of a chitosan hydrogel was reported, with a significant decrease in both moduli at ~21°C [428]. This further suggests that the structure of the hydrogel was altered due to casting on the frozen intermediate layer.

Chitosan-gelatin hydrogel is typically adherent to TCP and has a smooth surface [399]. The NH sample was relatively featureless as the hydrogel was constrained through its complete adhesion to the well plate. In contrast, randomly oriented undulations were seen in MH and PH. It is presumed that the undulations were a result of the lack of an underlying constraint and loose mounting for ESEM imaging. As these hydrogels have been created with intention of use in a tensile bioreactor, it is expected that undulations would not be present while mounted in the bioreactor and the surface of MH and PH would become similar to NH.

The contraction of the hydrogel scaffold was assumed to be a natural occurrence once seeded with cells, as outlined previously. However, it was noted that contraction was seen on scaffolds composed of only collagen or had the addition of fibrin [218, 400, 429, 430]. Fibrin is a known protein associated with wound contraction and healing, which has accelerated its use in tissue engineering research [217]. As collagen and fibrin are the main hydrogel components in the previous studies, the lack of contraction seen in this research may be a result of the composition or crosslinking of the chitosan-gelatin hydrogel.

5.4.2. Cell Response to Detached Hydrogels

The metabolic activity of the 3T3 cells demonstrated that the intermediate layer did not negatively affect the cytocompatibility of the chitosan-gelatin hydrogel. Both MH and PH had similar metabolic activity as NH by Day 7, suggesting that the adhesion and acclimation period of the fibroblasts may be longer on the detached hydrogels than the constrained NH hydrogels, potentially due to the perceived stiffness of the substrate. Hadjipanayi has reported a similar lag period when using fibroblasts to investigate substrates with gradient stiffness [387]. A lag period of fibroblast proliferation has also been recorded during contraction of collagen-GAG scaffolds [431, 432]. There is potential that increasing the cell seeding density on MH and PH would decrease the lag period and result in similar metabolic activity and proliferation

rates to NH at earlier timepoints. The decreased significance at Day 7 between TCP and hydrogel samples may be due to a combination of proliferation on the hydrogel samples and a declined 3T3 cell population due to overcrowding on the TCP sample.

The surface topography and roughness are important factors in the cell interaction with the scaffold. Some studies report that a smooth surface topography is ideal for fibroblast attachment, proliferation, and spreading [433, 434], whereas there is also evidence that fibroblasts may prefer a rougher surface [435]. Several studies have reported the spread and organised actin filament network of fibroblasts on smooth surfaces [399, 433]. In this study, a smooth topography with extensive fibroblast proliferation and spreading is evident in the ESEM images of NH, further confirming that the chitosan-gelatin hydrogel is a satisfactory biomaterial for fibroblast growth.

The surface chemistry of a substrate also plays an important role in cell adhesion as the functional groups available on the surface dictate the type of attachment from cells through the adsorbed protein layer and selective integrin binding [143, 436, 437]. As the adsorbed protein layer on biomaterials forms quicker than cell adhesion, this protein layer plays a large role on the type of cell adhesion that occurs [434]. The NAP-XPS results indicated the presence of amine and COOH functional groups on the surface of the detached hydrogels which are beneficial for adsorption of adhesive proteins leading to increased fibroblast attachment, proliferation, spreading, and enhanced ECM formation [434, 438]. Despite NH not analysed using NAP-XPS, it is reasonable to believe that the surface chemistry of NH has similar functional groups available as there was no indication that the intermediate layer caused surface modification.

The correlation between cell morphology and location on the MH and PH sample suggests that the perceived stiffness of the hydrogel plays a large role in fibroblast proliferation and spreading. As discussed in Chapter 4, the perceived stiffness of a material can affect the growth, spread, organisation, ECM production, and differentiation of fibroblasts [377, 379, 389]. The ESEM results indicate that the fibroblasts perceived the thinning edges of the MH and PH samples stiffer than the centre of the discs through the increased cell numbers and some elongation of cells.

Still, if the 1mm constrained NH samples are compared to the 1mm centre of MH and PH, the cell morphology is considerably different. At all timepoints on NH, the fibroblasts were significantly more numerous and elongated. At the centre of MH

and PH, the fibroblasts remained rounded and sparse in number at Day 7. This suggests that the internal rigidity of MH and PH affected the cell morphology, and therefore the cell proliferation.

The internal rigidity, or pliability and compliance, of a substrate has an impact on the cell-cell and cell-substrate interactions [394, 439]. Several studies have shown that focal adhesions and cytoskeletal structure are directly affected by the rigidity of a sample, such as depicted in Figure 5.13 [125, 378, 379, 440]. A compliant substrate is unable to reciprocate the cell mediated forces and can lead to a decrease in cell proliferation, ECM production, and differentiation [441]. Without the reciprocal forces, cell migration is also limited by the rigidity of a substrate [356]. In this way, the low internal rigidity of the MH and PH samples influenced the adhesion, morphology, and proliferation of the 3T3 cells. Hadjipanayi et al. have shown that the internal rigidity of a substrate can be increased by being 'anchored', such as the adherence of the NH sample to the well plate in this research [387]. The higher internal rigidity of the NH sample led to a higher proportion of elongated cells as seen through the ESEM images.

It is shown that soft, compliant substrates with low internal rigidity can trigger fibroblasts into a quiescent state [440]. This quiescent state arrests the cells in the G_0 phase, causing a slowed rate of proliferation, growth, and maturation [442]. While in the quiescent state, fibroblasts stop any DNA production and direct their metabolic activity towards self-preservation [443]. The rounded fibroblasts at the centre of MH and PH may have entered a quiescent state as the low internal rigidity was unfavourable for growth and spreading [444]. As this detached hydrogel is being developed for use in a tensile bioreactor, it is expected that the implementation in the bioreactor would increase the internal rigidity of the hydrogel and decrease the likeliness of the fibroblasts entering a quiescent state.

Additionally, the internal rigidity of the hydrogel may also influence its contraction as Freyman et al. have shown that total stiffness of the substrate does not affect the contractile ability of fibroblasts and is rather force-limited, Figure 5.14 [431]. Therefore, a substrate that is unable to compensate and reciprocate the cell mediated forces required for cell spreading, ECM production, and remodelling is less likely to show contraction. The limiting factor to the contraction of the detached MH and PH samples may be the lack of strong focal adhesions of the 3T3 cells and lack of a reciprocal force by the substrate. In this way, the chitosan-gelatin composition of the

hydrogel and the low internal rigidity of the detached samples may influence the exerted cell forces and therefore limit the contraction. This further suggests that the crosslinking percentage and interaction between chitosan, gelatin, and OPC do not prohibit contraction of the hydrogel, as previously hypothesised.

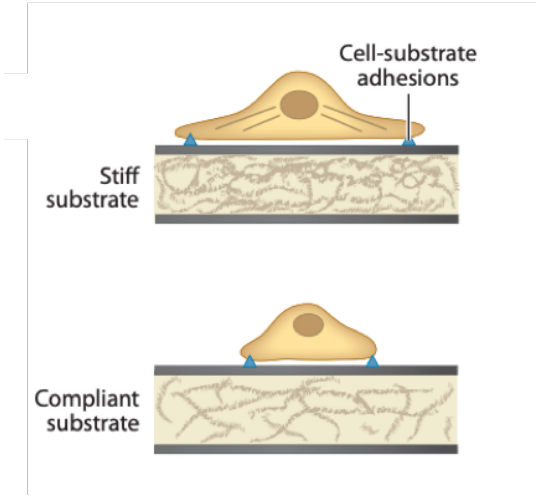

Figure 5.13: A graphical description of how the stiffness and rigidity, or compliance, of a substrate can affect the cell morphology. In this depiction, the cell is spread and has developed organised actin fibres on the stiff substrate. While the cell on the soft, compliant substrate maintains a more rounded morphology and has not been triggered to develop actin fibres. Image adapted from Underhill et al. [125].

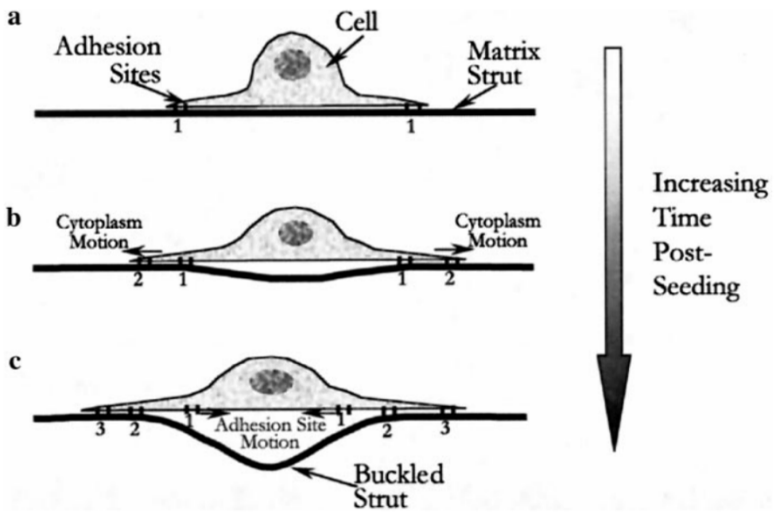

Figure 5.14: A depiction of the force mediated contraction of a cell on a substrate. At (a) the cell has formed adhesion sites along the leading edge (1). At (b) new adhesion sites are beginning to form (2) as the cell continues to elongate and a slight buckling of the substrate is seen. At (c) further adhesion sites are formed (3) and a noticeable strut, or substrate contraction, has formed. This motion is dependent upon the force exerted by the cell. Image adapted from Freyman et al. [431].

5.5. Conclusion

The intermediate layer allowed the progression of a hydrogel biomaterial that is dependent upon the vessel it is cast in to a versatile and functional scaffold. The resultant hydrogel disc was robust during handling which is a positive indication that

it can be reproduced in a tissue engineering setting or worked with clinically. This fabrication method has shown to allow the adaptability of casting dimensions, as seen in the MicroTest casting.

By removing the anchorage of the hydrogel to the well plate, the internal rigidity of MH and PH was decreased resulting in a rounded morphology of the 3T3 cells due to the weaker focal adhesions of the cells to the hydrogel. The lack of contraction seen in the MH and PH samples was more likely a result of the weak focal adhesions of the cells to the substrate rather than the physicochemical interactions between chitosan, gelatin, and OPC.

The cell metabolic activity was comparable for the MH and PH samples, suggesting that neither intermediate layer had a detrimental effect on the cytocompatibility which was confirmed by the alamarBlue results. The detached hydrogel scaffolds had a similar elongation at failure and tensile modulus, indicating that the cell culture medium and PBS had a similar structural effect on the detached hydrogel. The NAP-XPS results confirmed that there was no salt residue on the surface of the hydrogel scaffolds as a result of the intermediate layers. However, the consistency in creating the MH samples was preferred in comparison to PH. For further experiments requiring detached hydrogel, the cell culture medium intermediate layer will be used for its slightly higher metabolic activity, resultant modulus of the detached hydrogel, and the consistency in production.

6. Modified Chitosan-Gelatin Hydrogel to Promote an Osteogenic Response

6.1. Introduction

The bony anchors are an essential design element of a tissue engineered ligament that can increase the likelihood of enthesis success [445]. Failure at the enthesis has been a common occurrence in ACL tendon grafts due to several factors such as lack of tissue integration and mismatched biomechanical behaviours [446, 447]. The development of the enthesis is a critical challenge in ligament tissue engineering due to the complex biomechanical loading of the region and the intricate graded mineralization from soft ligament midsubstance to hard bony tissue.

Recently, several studies have investigated the decellularization of the bony insertion of an animal tendon to maintain the optimal biomechanics of the enthesis region [173, 448, 449]. These decellularized scaffolds showed success in maintaining their biomechanical strength and infiltration of cells into the scaffold. However, this research is in its early stages and requires further investigation into the implementation, such as the attachment of decellularized midsubstance to native tendon or transformation into a ligament prosthesis requiring an additional enthesis region.

Previous methods of developing an artificial enthesis for tissue engineering have involved the creation of bony insertions using hydroxyapatite or brushite [184, 401]. The manufacture of the enthesis from hydroxyapatite and brushite increases the availability of calcium phosphates and influences an osteoblastic response to this region of the scaffold [171, 192]. The crystallinity of these calcium phosphates also helps to regulate the degradation rate of the biomaterial [450]. While hydroxyapatite and brushite have shown an increase in biomaterial strength of the enthesis scaffold and an osteogenic cell response, further development is required to replicate the functional, biological attachment of the enthesis of a ligament or tendon.

This chapter aims to build on the recent success in enthesis biomaterials through the addition of calcium carbonate and calcium phosphate to the chitosan-gelatin hydrogel, creating a composite hydrogel. The response of 3T3 cells and PFib cells to increasing thicknesses of this composite hydrogel will be analysed through their morphology, metabolic activity, DNA content, GAG content, and ALP activity.

As the main goal of this research is to develop a tissue engineered ligament in a tensile bioreactor system, anchorage points are required to secure the detached hydrogel scaffold (discussed in Chapter 5) to the bioreactor and to transmit tensile strain to the hydrogel scaffold. Several designs of anchors will be assessed for suitability within the bioreactor, including a design made entirely of the composite hydrogel and a design using an acetal rod as a reinforcing core with a coating of the composite hydrogel. These designs aim to incorporate the composite hydrogel as an enthesis biomaterial while providing the functionality of the anchor within the bioreactor. The anchor designs will be characterized through degradation studies, ESEM, and compressive analysis.

6.2. Methodology

6.2.1. Composite Hydrogel Synthesis

Chitosan-gelatin hydrogel was created as outlined previously in section 3.5 (page 50). A combination of calcium carbonate ($CaCO_3$) and dibasic calcium phosphate ($CaHPO_4$) was then added to the chitosan-gelatin hydrogel to create a 30% w/w composite hydrogel. The amounts of $CaCO_3$ and $CaHPO_4$ were calculated to maintain a theoretical Ca:P molar ratio of 1.5, similar to previous protocols [16, 401]. This ratio is representative of ß-tricalcium phosphate [191]. The $CaCO_3$ and $CaHPO_4$ were used to increase the availability of calcium and phosphate without introducing the brittle nature of brushite and hydroxyapatite [192, 194]. Alternative dry weight percentages (10%, 20%, 40% w/w) of the $CaCO_3$ and $CaHPO_4$ in the chitosan-gelatin hydrogel were also explored.

The $CaCO_3$ and $CaHPO_4$ was mixed into the hydrogel directly before casting. A small spatula was used to gently stir the composite hydrogel mixture to avoid creating air bubbles. Once fully mixed, the beaker of composite hydrogel was tapped against the work surface to bring any air bubbles to the surface.

6.2.2. Cell Culture on Composite Hydrogel

The composite hydrogel was cast into well plates with increasing thickness from 0.5mm to 2.5mm in 0.5mm increments and sterilized using the same protocol as outlined previously. Separately, the 3T3 and PFib cells were seeded onto the composite hydrogel in a volume of 500 µl at a density of 10,000 cells/cm^2 with an alamarBlue assay carried out at Day 3, 7, 14, 21, and 28. The cell culture medium was changed every 2-3 days. At Day 28, the cell culture medium was collected for assays,

which included the medium from the final 3 days of culture. There was one biological replicate and 12 technical replicates, repeated twice.

After the final alamarBlue assay, the samples were lysed by the freeze/thaw method and prepared for DNA, GAG, and ALP activity assays. These assays were carried out as described previously in section 3.5.4 (page 51). The collected medium was prepared in a similar manner for GAG quantification. In all assays, a composite hydrogel sample without cells was used as a blank to normalize the results.

The composite hydrogel was also cast at increasing thicknesses into a well plate with glass coverslips, allowing for fixation and removal for ESEM imaging. Separately, the 3T3 and PFib cells were seeded onto the composite hydrogel at 10,000 cells/cm^2 at a volume of 500 µl. At Day 28, the composite hydrogels were fixed for ESEM. These samples were not used for any further assays.

The mean ALP activity results from the MG63 cell line and a primary osteoblast culture from neonatal mouse calvaria were used as a reference for osteoblastic levels of ALP activity. The MG63 and primary osteoblasts were cultured on TCP at a similar initial cell density to the same timepoint. These osteoblast cultures were not used for any other assays.

6.2.3. Degradation of the Composite Hydrogel

To measure the degradation of the composite hydrogel, detached composite hydrogel discs were made to the same protocol as outlined in section 5.2.3 (page 71) creating a composite MH and composite PH. The detached composite hydrogel discs were sterilized and then incubated in an excess of cell culture medium. The wet mass was measured before casting at Day 0, after sterilization at Day 1, at Day 7, and at Day 14. The cell culture medium was replaced after Day 7.

6.2.4. Anchor Design

Two designs for anchors were assessed:

1) Anchors made entirely of the composite hydrogel. These anchors were dried at 4°C (MA4C) or freeze-dried (MAFD).
2) Anchors with a reinforced acetal core coated with composite hydrogel (CA). These anchors were dried at room temperature.

Acetal (Plastics Direct, UK) was used to create the moulding for the MA4C and MAFD anchors and as the reinforced core of the CA anchors. Acetal was chosen for its low coefficient of friction and ease of machining [451, 452].

6.2.4.1. Entirely Composite Hydrogel Anchor Model

The first design consisted of an anchor made entirely of the composite hydrogel. This was done by creating a three-piece acetal mould that produced anchors 12mm in length with a tapered diameter from 5mm to 4mm using the SolidWorks software package (Dassault Systèmes, France), as seen in Figure 6.1 [453]. The tapered design was fashioned for the attachment of the anchors to the bioreactor. Acetal moulds of 12mm and 22mm length and 4mm diameter that attached directly to the bioreactor plates were modelled and machined. The composite hydrogel anchor would be inserted into the moulds and the taper of the design would cause it to be lodged within the mould.

Six bolts held the two acetal mould pieces together firmly while spring-loaded clips secured an additional piece of acetal to the bottom of the mould, as seen in Figure 6.2. The composite hydrogel was injected into each well and gently tapped to remove any air bubbles. The surface of the mould was not covered during drying time. The composite hydrogel anchors were dried at 4°C for 16 hours (MA4C) or freeze dried for 48 hours (MAFD).

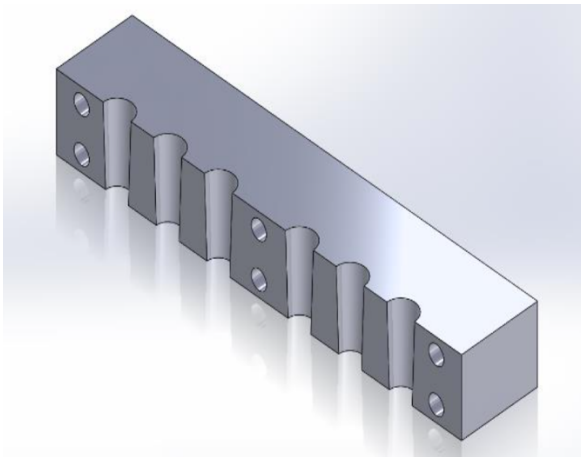

Figure 6.1: The SolidWorks design of one half of the composite hydrogel anchor mould. The top of each anchor well measures 5mm and the bottom measures 4mm. Courtesy of Dominic Wylie [453].

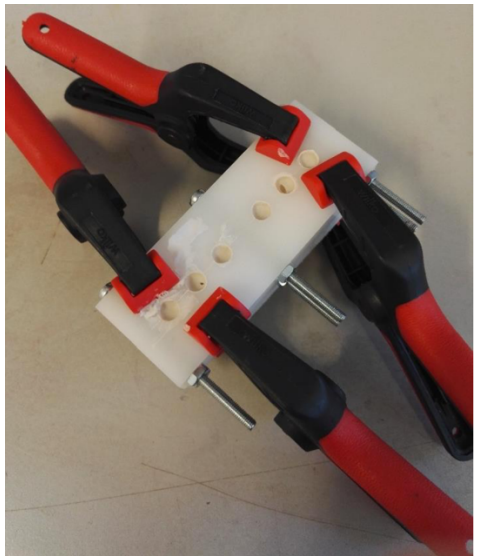

Figure 6.2: The complete framework of the acetal mould for composite hydrogel anchors, MA4C and MAFD, with spring-loaded clamps securing the acetal base. The composite hydrogel has been injected into each well.

6.2.4.2. Reinforced Anchor Model

A second design was based on an acetal rod that would act as the core of the anchor with a coating of composite hydrogel (CA). The acetal rod had a diameter of 8mm ± 0.1mm and was cut into lengths of 18mm ± 0.5mm and 28mm ± 0.5mm. As these rods will eventually be fastened to the bioreactor, a hole for a screw was fashioned at the superior end of the acetal rods for attachment to the bioreactor plates.

The acetal rods were sandblasted using a Formula 1200 Sand Blaster with white saftigrit alumina (Guyson International Ltd, UK) to increase the surface roughness and allow for better adhesion of the composite hydrogel to the acetal. The rods were sandblasted for approximately 60 seconds with constant rotation. The rods were then cleaned by sonication followed by detergent and IMS.

After cleaning, the inferior ends of the rods were then coated with the composite hydrogel that was made up directly before coating. The coating was allowed to gel for approximately 5 minutes before a second coating was applied. The coated acetal anchors were allowed to dry at room temperature before further testing.

6.2.5. Compression Testing of Anchors

Compression testing was performed on the anchors from both manufacturing methods. The MAFD and CA anchors were tested alongside uncoated acetal rods. An Instron Dual Column Universal Testing system was used at a crosshead speed of 1.00mm/min. The tensile modulus and compressive strength were calculated for each sample.

6.2.6. Degradation of Anchors

The mass of the composite hydrogel anchors was measured directly after production. After 24 hours of incubation in cell culture medium, the mass was measured again.

6.3. Results

6.3.1. Composite Hydrogel

The addition of the $CaCO_3$ and $CaHPO_4$ created a homogenous composite chitosan-gelatin hydrogel. The homogeneity of the composite hydrogel can be seen in Figure 6.11. The consistency of the composite hydrogel was incompatible with pipettes and a syringe was more appropriate for casting. The composite hydrogel gelled in a similar time as the chitosan-gelatin hydrogel, indicating that the addition of the $CaCO_3$ and $CaHPO_4$ did not affect the gelling time. Some separation was seen when the composite hydrogel was left on low heat (35°C) without agitation for a period longer than three hours, therefore the composite hydrogel was made up immediately prior to use.

The ratio and mixture of both compounds in hydrogel has been seen in previous literature without a negative effect during the gelation stage [16, 401]. However, the solubility of both the $CaCO_3$ and $CaHPO_4$ in the chitosan-gelatin hydrogel was not investigated in this study.

6.3.1. Adjustment of Calcium Salts to Composite Hydrogel

The viscosity of the composite hydrogel was altered by adjusting the dry weight percentage of the $CaCO_3$ and $CaHPO_4$. The 10% and 20% w/w composite hydrogels had a thin consistency and were not stable during sterilization. The 40% w/w composite hydrogel resembled a paste and was unable to be consistently cast into well plates.

6.3.2. Cell Assays on Composite Hydrogel

6.3.2.1. Metabolic Activity

The 3T3 metabolic activity showed an inverse correlation to the thickness of the composite hydrogel; as the thickness increased, the metabolic activity decreased, as seen in Figure 6.3. All samples experienced a significant decline in metabolic activity; however, this decline was seen at later timepoints for the thicker samples. The cycle of proliferation, overpopulation, death, and regrowth of the 3T3 cells was seen on the composite hydrogels where the metabolic activity exhibited significant declines, or population death, followed by an increase in metabolic activity, or

regrowth. The pattern of continued proliferation leading to cell death and regrowth of the 3T3 cells was most prominent in the 0.5mm, 1.0mm, and TCP samples.

The metabolic activity of the PFib cells on the composite hydrogel showed a steady increase in activity from Day 3 to Day 28 across all sample types, as seen in Figure 6.4. There were no significant declines in metabolic activity on any sample, though a decrease in activity on the 0.5mm and 1.0mm samples was visible. A plateau was seen on the 1.5mm, 2.0mm, and 2.5mm samples at Day 28 as there was no significant increase of metabolic activity beyond Day 21. The PFib cells did not show as strong an inverse correlation of metabolic activity to hydrogel thickness as the 3T3 cells did. At Day 28, there was no significant difference of metabolic activity values of the PFib cells between the composite hydrogel samples of increasing thickness.

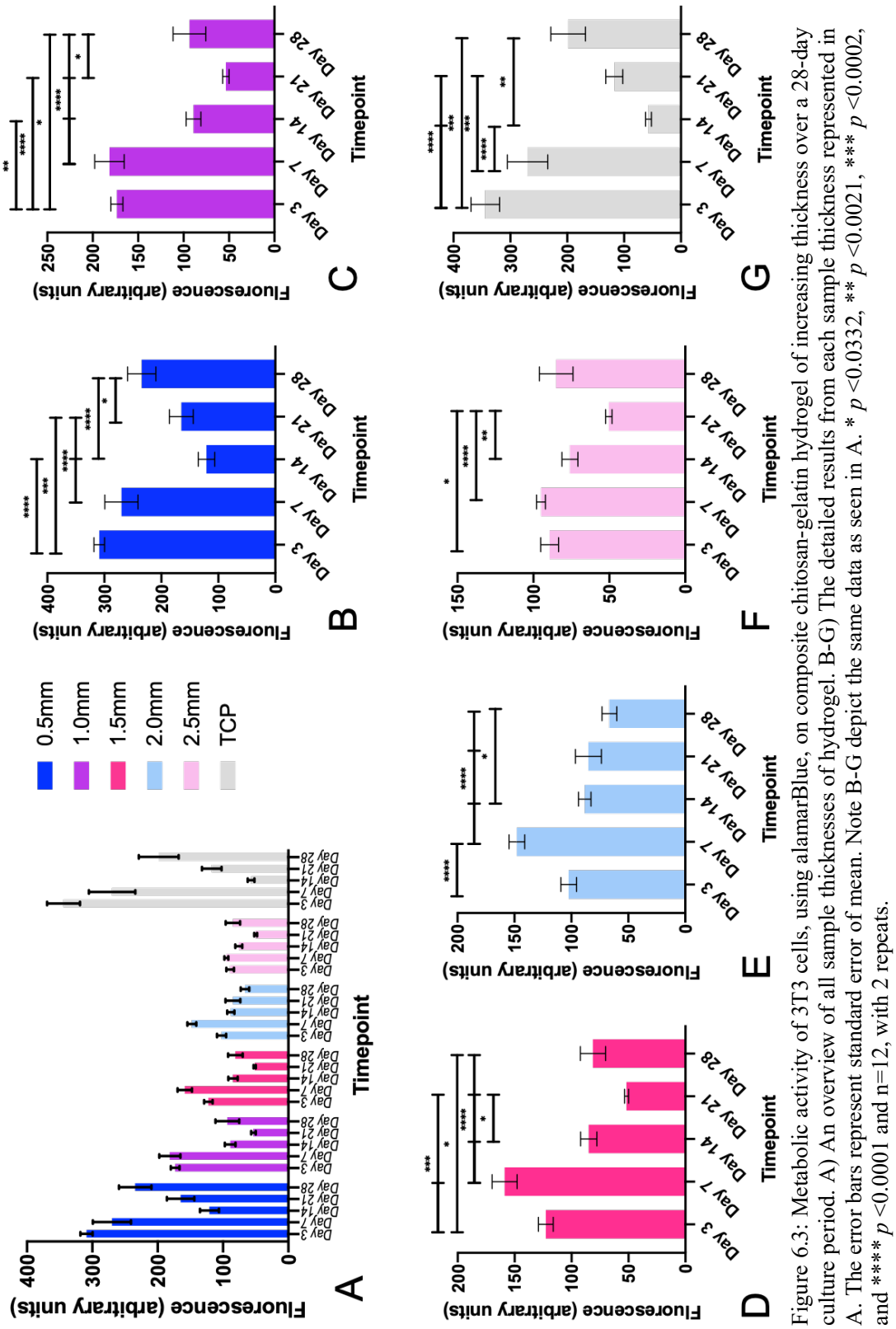

Figure 6.3: Metabolic activity of 3T3 cells, using alamarBlue, on composite chitosan-gelatin hydrogel of increasing thickness over a 28-day culture period. A) An overview of all sample thicknesses of hydrogel. B-G) The detailed results from each sample thickness represented in A. The error bars represent standard error of mean. Note B-G depict the same data as seen in A. * p <0.0332, ** p <0.0021, *** p <0.0002, and **** p <0.0001 and n=12, with 2 repeats.

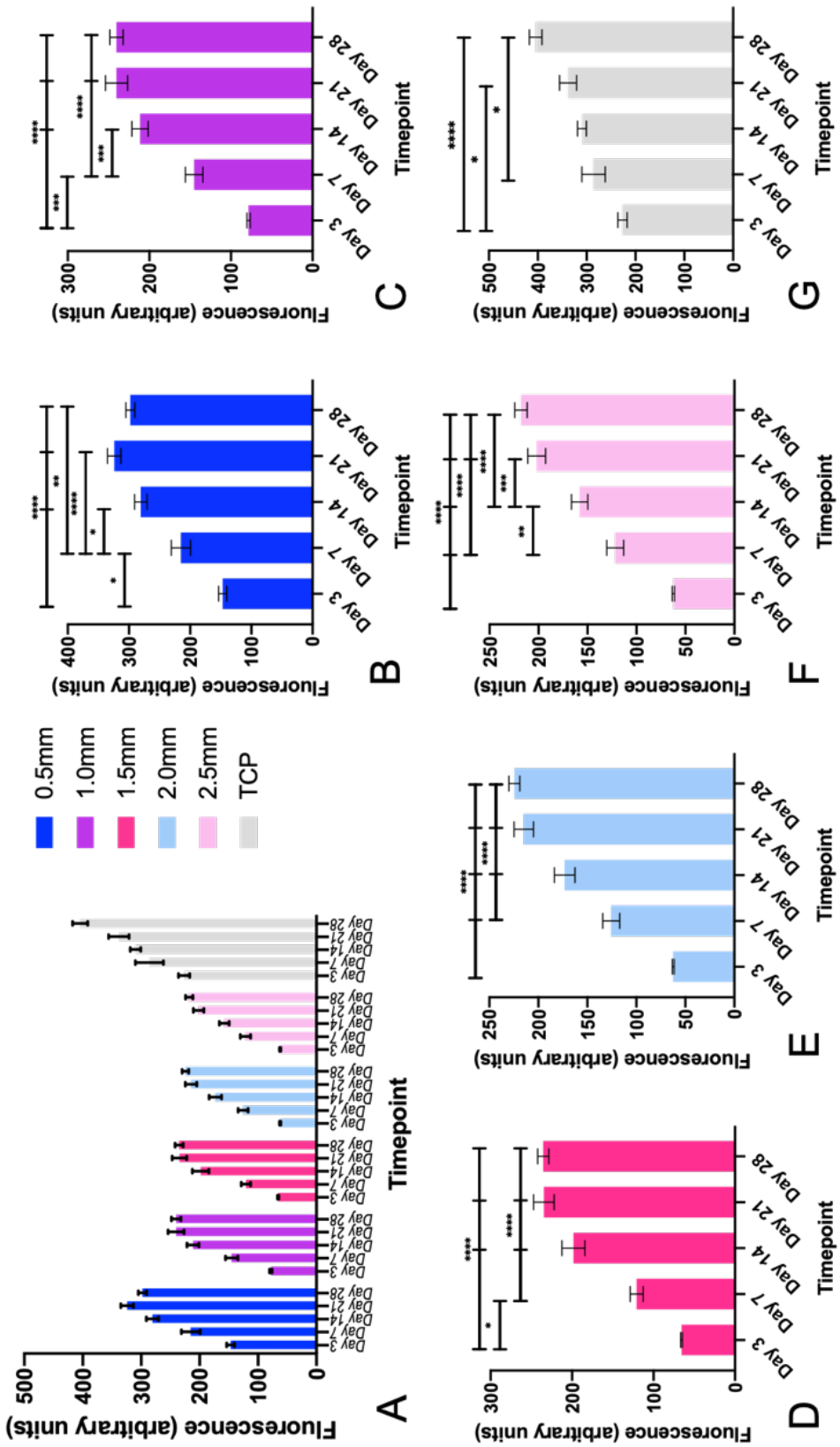

Figure 6.4: Metabolic activity of PFib cells, using alamarBlue, on composite chitosan-gelatin hydrogel of increasing thickness over a 28-day culture period. A) An overview of all sample thicknesses of hydrogel. B-G) The detailed results from each individual thickness represented in A. The error bars represent standard error of mean. Note B-G depict the same data as seen in A. * p <0.0332, ** p <0.0021, *** p <0.0002, and **** p <0.0001 and n=12, with 2 repeats.

6.3.2.2. DNA Quantification

Interestingly, the 3T3 and PFib DNA concentration appeared to increase with increasing thickness of composite hydrogel, as seen in Figure 6.5. This differs from the metabolic activity results, as the thickest samples showed the lowest metabolic activity from both the 3T3 and PFib cells.

The highest mean concentration of DNA in the composite hydrogel samples was on the 2.5mm sample for both the 3T3 and PFib cells, 0.02579 µg/ml and 0.02764 µg/ml respectively. The lowest mean concentration of DNA was on the 1.0mm sample for the 3T3 cells, 0.01827 µg/ml, and on the 0.5mm sample for the PFib cells, 0.01951 µg/ml. The TCP sample had the highest mean concentration of DNA for both the 3T3 and PFib cells across all samples.

The 3T3 cells had significantly different DNA content across several samples. The TCP sample had significantly higher DNA content than the 1.0mm and 1.5mm samples. The 1.0mm sample had significantly lower DNA content than all other samples. The 2.0mm sample had significantly higher content than the 1.5 sample. The 2.5mm sample had significantly higher DNA content than the 1.5mm, and 2.0mm samples.

Of the PFib samples, the TCP sample had a significantly higher DNA content than all of the composite hydrogel samples. The 0.5mm sample had significantly lower DNA content than all other hydrogel samples except the 1.0mm samples. The 2.5mm sample had significantly higher DNA content than the composite hydrogels of decreasing thickness. The DNA content of the 2.0mm sample followed a similar trend as the 2.5mm sample.

The 3T3 cells showed significantly higher DNA content on the 0.5mm sample compared to the PFib cells. The PFib cells had significantly higher DNA content on the 1.0mm, 2.0mm, 2.5mm, and TCP samples compared to the 3T3 cells. There was no significant difference in DNA content between the 3T3 and PFib cell cultures on the 1.5mm sample.

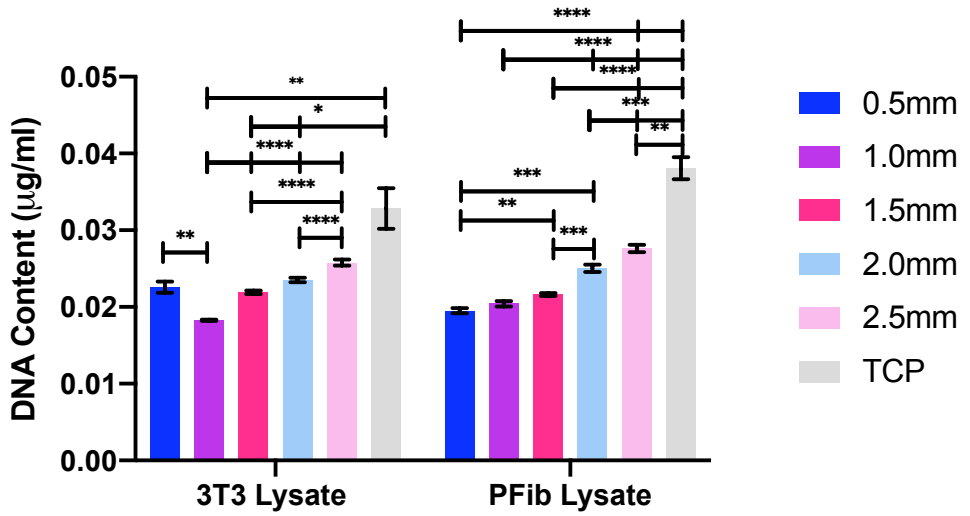

Figure 6.5: DNA concentration of 3T3 and PFib cells on composite hydrogel of increasing thickness after 28 days of cell culture, using the PicoGreen DNA kit. The error bars represent standard error of mean. All composite hydrogel samples were blanked against composite hydrogel without cells. * p <0.0332, ** p <0.0021, *** p <0.0002, and **** p <0.0001 and n=12, with 2 repeats.

6.3.2.3. GAG Content

The 3T3 cells demonstrated sporadic GAG content on the composite hydrogel, as seen in Figure 6.6. The 0.5mm and 1.0mm lysate samples were significantly higher than the 2.0mm lysate sample. Although GAG content was undetected in the 1.5mm and 2.5mm sample lysate, it was detected in the related cell culture medium. The GAG content was lower in the collected medium than the digested lysate samples, however this difference was significant only in the 1.0mm related sample. There was no significant difference found in the GAG content between the collected medium from the increasing thickness of composite hydrogel samples.

The GAG content of the PFib TCP lysate was significantly higher than the lysate from the composite hydrogel samples, except the 1.5mm sample. There was no significant difference of the GAG content between the lysate of the composite hydrogel samples. The collected medium from the PFib TCP sample had significantly lower GAG content than the collected medium from the composite hydrogel samples and the related TCP lysate. The PFib cell lysate had higher GAG content than the 3T3 cell lysate on the 1.5mm, 2.0mm, 2.5mm, and TCP samples, however this difference was not significant.

The GAG/DNA ratio showed a similar trend as the GAG content, Figure 6.7. The PFib cells exhibited higher GAG/DNA ratios than the 3T3 cells, except the 1.0mm lysate, however this difference was not significant. The only significant difference in

the GAG:DNA ratio arose from the 3T3 lysate of the 1.0mm sample compared to the collected medium from the 1.0mm sample.

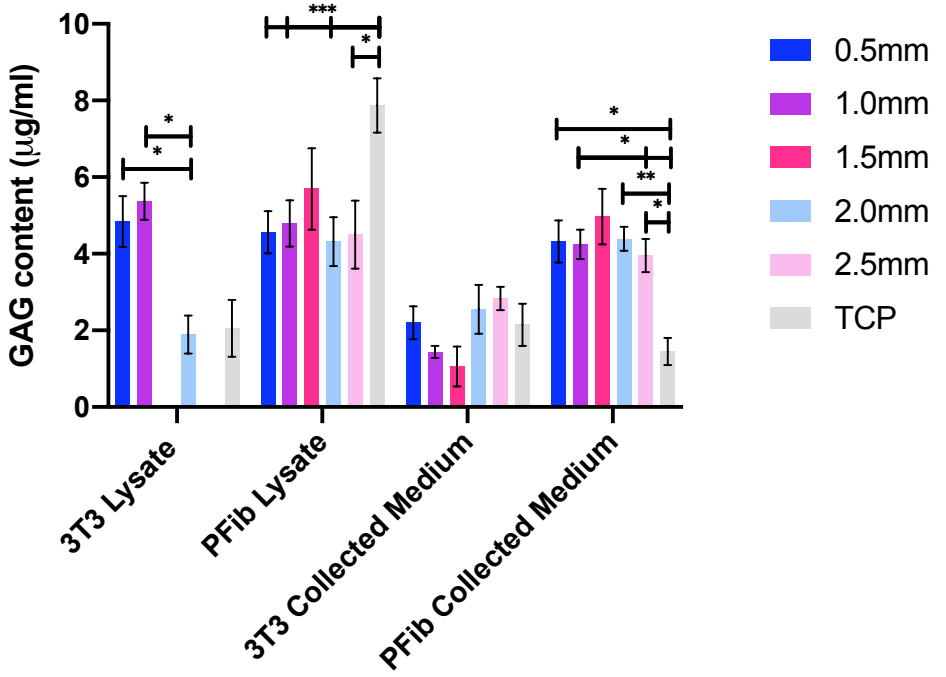

Figure 6.6: GAG content measured through the DMMB assay of the 3T3 and PFib fibroblasts on composite hydrogel samples of increasing thickness, including the medium collected from these samples. The error bars represent the standard error of mean. All samples were blanked against composite hydrogel without cells. The collected medium was blanked against the medium collected from the blank composite hydrogel. * p <0.0332, ** p <0.0021, *** p <0.0002, and **** p <0.0001 and n=12.

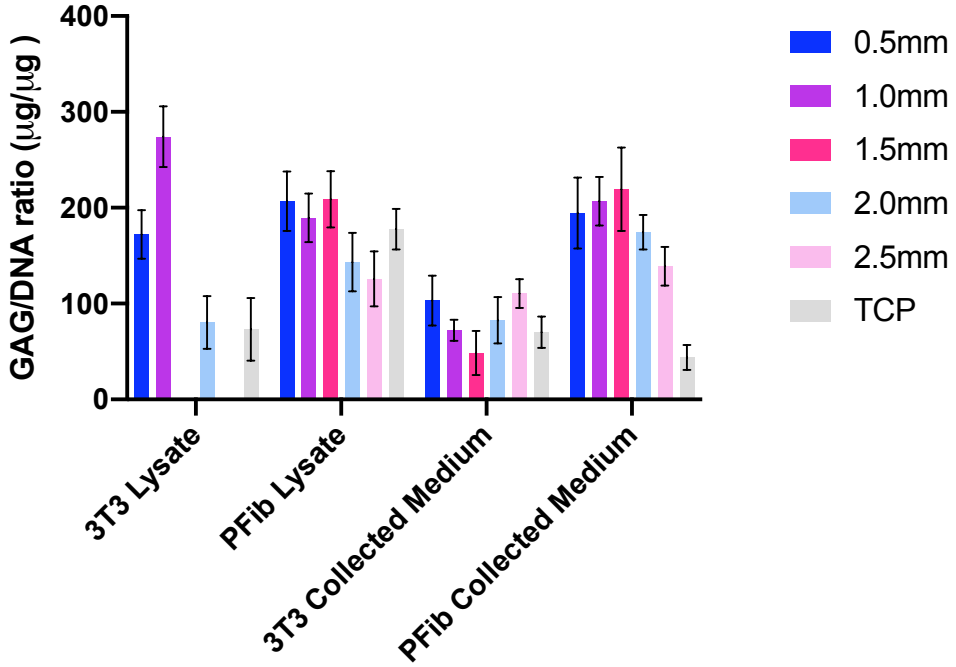

Figure 6.7: GAG/DNA ratio of 3T3 and PFib fibroblasts on composite hydrogel samples of increasing thickness after 28 days of cell culture. The collected medium was collected after the 28 days of culture. The error bars represent standard error of mean. n=12.

6.3.2.4. ALP Activity

ALP activity is an early marker for osteogenesis and, therefore, high levels of activity were not expected from either fibroblast cell type. The 3T3 cells showed low levels of ALP activity on the 0.5mm and 1.5mm samples, as seen in Figure 6.8. As only one 1.5mm replicate showed ALP activity, this can be disregarded as an outlier. The 3T3 ALP activity exhibited higher results on the composite hydrogel compared to the chitosan-gelatin hydrogel of Chapter 4 in section 4.3.7 (page 63).

The PFib fibroblasts showed significantly higher ALP activity on TCP than all composite hydrogel samples. No significant difference was found between the composite hydrogel samples. The PFibs on the composite hydrogel showed more consistent ALP activity when compared to the chitosan-gelatin hydrogel.

The mean ALP activity of the MG63 cell line and a primary osteoblast culture were used as reference to show the ALP activity of osteogenic cells, the dotted and dashed line in Figure 6.8 respectively. Both osteoblasts had ALP activity results that were significantly higher than the 3T3 and PFib results across samples, as expected.

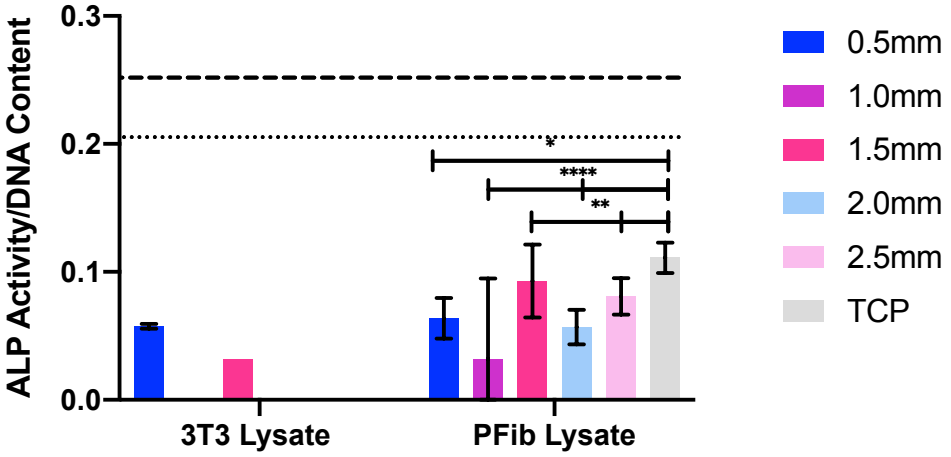

Figure 6.8: Normalized ALP activity against DNA content of lysate of the 3T3 and PFib cells on composite hydrogel of increasing thickness after 28 days of cell culture, using the ALP Randox kit. The dotted line represents an osteoblastic MG63 cell line and the dashed line represents a primary mouse osteoblast culture. Error bars represent standard error of mean. Where there are no error bars, there was not enough data to accurately represent a standard error of mean and this result should be disregarded as a chance happening. All samples were blanked against composite hydrogel without cells. * p <0.0332, ** p <0.0021, *** p <0.0002, and **** p <0.0001 and n=12 with 2 repeats.

6.3.2.5. ESEM Images

The composite hydrogel was difficult to image during ESEM compared to the chitosan-gelatin hydrogel due to the reduced amount of time before the composite hydrogel began to dehydrate and fracture. There was no issue of a residual water layer

on the surface, as seen during the ESEM imaging of the chitosan-gelatin hydrogel. In all images of the composite hydrogel, large mineral crystals could be seen which often obscured the identification of cells.

The 3T3 cells grew on the entirety of the composite hydrogel surface of the 1.0mm thickness sample, as seen in Figure 6.9. The 3T3 cells were numerous across the sample, with a rounded morphology and some extensions. The cells did not appear to adhere or grow directly on the large mineral crystals found throughout the sample. Minimal amounts of 3T3 cells had remained intact while spanning a fissure, a consequence of the dehydration and fracturing.

The PFib cells were seen across the sample but appeared to be less numerous and larger than the 3T3 cells. The individual cells had a mostly rounded morphology with some extensions. Similar large mineral crystals could be seen in the sample, especially where the sample had fractured. Similar to the 3T3s, the PFibs did not appear to adhere to the mineral crystals. Where there were fractures caused by the dehydration, a handful of PFib cells remained intact traversing the fissures, as seen in the bottom right corner of Figure 6.9.

The 1.0mm thickness was representative for the morphology of the 3T3 and PFib cells on the remaining composite hydrogel thicknesses. The morphology of the 3T3 and PFib cells remained rounded on all sample thicknesses. The number of cells and cell extensions appeared to decrease with increasing sample thickness.

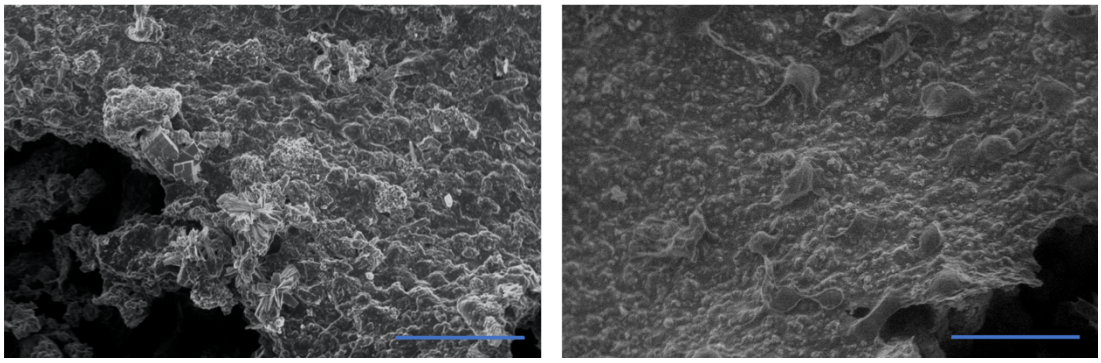

Figure 6.9: ESEM image of 3T3 fibroblasts (left) and PFib fibroblasts (right) grown on composite chitosan-gelatin hydrogel of 1.0mm thickness after 28 days of culture. Mineral crystals can be seen in both images. (Left) The 3T3 cells can be seen across the sample but not growing on the composite crystals. A large fracture of the composite hydrogel can be seen towards the left of the image. (Right) The PFib cells can be seen across the sample. Individual PFib cells can be clearly identified in the image. A fracture can be seen in the bottom right corner of the image with a PFib cell spanning the two edges of composite hydrogel. The blue bar indicates 50 µm.

6.3.3. Degradation of the Detached Composite Hydrogel

The degradation profile of the detached composite hydrogel can be seen in Figure 6.10. The wet mass loss at Day 1 was found to be significant for the composite PH and not significant for the composite MH. Both composite PH and composite MH experienced significant wet mass loss between Day 1 and Day 7. The wet mass loss at Day 14 was not significant for either composite MH or PH compared to Day 7. However, the overall mass loss from Day 0 to Day 14 was found to be significant for both composite MH and PH. This resulted in a 16.67% mass loss for the composite MH and a 24.12% mass loss for the composite PH.

In comparison to the detached MH and PH of Chapter 5 section 5.3.3.3 (page 78), there was a significantly larger mass loss for both composite MH and PH after sterilization. The composite MH and PH had a similar weight loss percentage as the chitosan-gelatin MH and PH, respectively, when incubated in cell culture medium.

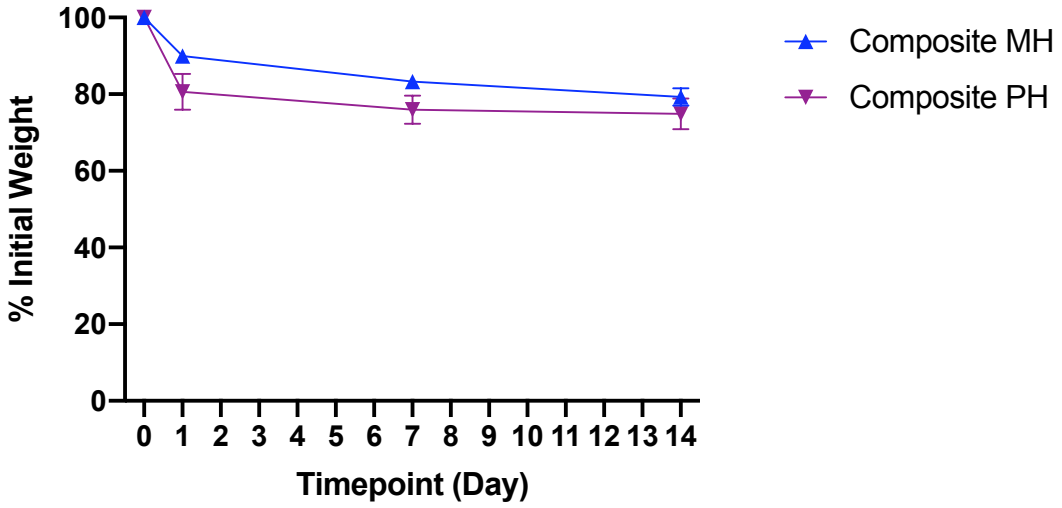

Figure 6.10: Degradation profile of detached composite hydrogel discs MH and PH in cell culture medium expressed as % initial weight. Day 0 is the wet mass prior to casting and Day 1 is the wet mass after sterilization. Error bars represent standard error of mean. n=3.

6.3.4. Anchor Modelling

The MA4C design did not produce consistent anchors. The middle portion of the composite hydrogel in the mould did not have a similar drying effect as the exposed surface, as seen in Figure 6.11. These samples did not maintain integrity upon transferring and often sheared upon removal from the mould. When the MA4C anchors were successfully removed from the mould, a rapid disintegration was seen upon incubation. Full disintegration was seen in as quickly as 2 hours. For this reason,

MA4C anchors were not used in degradation testing, compression testing, or future experiments.

The freeze-drying technique of the MAFD design produced anchors that had uniform size and comparable drying effects throughout the anchor, as seen in Figure 6.12. The anchors maintained their structural integrity throughout handling and were used in the degradation testing and compression testing.

The composite hydrogel coating of CA was uniform and was not dislodged or damaged during transfer or incubation. A coating of the chitosan-gelatin hydrogel on acetal rods can be seen in Figure 6.13. The chitosan-gelatin hydrogel was used for the image as the colour of the composite hydrogel was not distinguishable from the acetal rod.

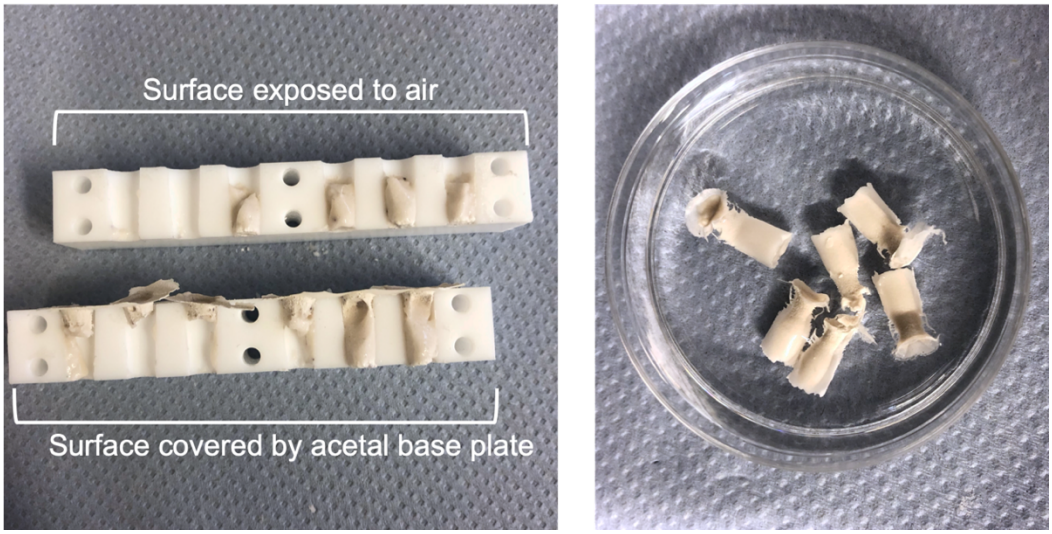

Figure 6.11: MA4C anchors after 16 hours of drying at room temperature. In both images, the surface exposed to air has a considerably different consistency than the surface covered by the acetal base plate. (Left) The separated acetal mould, shearing the MA4C anchors at the zone where the different drying effects were evident. (Right) Six MA4C anchors that were successfully extracted from the acetal mould but possessed an uneven structure due to the exposure to air at one end. In both images, the homogeneity of the composite hydrogel can be seen. There are no areas of high concentration of either the chitosan-gelatin hydrogel or the $CaCO_3$ and $CaHPO_4$.

Figure 6.12: The result of freeze-drying the composite hydrogel in an acetal mould, producing MAFD. The image was taken directly after freeze drying. The anchors have uniform size and drying effect throughout the sample.

Figure 6.13: Acetal rods of varying lengths coated in chitosan-gelatin hydrogel to allow imaging of the coating. The colour of the composite hydrogel was not distinguishable from the white of the acetal rod in images. These rods were not used in any further tests.

6.3.5. Anchor Compression Testing

The compression results for the MAFD anchors and the CA anchors can be found in Table 6.1. The testing set-up can be seen in Figure 6.14. The uncoated acetal rod and CA anchor withstood a significantly higher load than the MAFD anchors.

The MAFD anchors withstood loads of over 24 N, with a mean load of 35.15 N. The highest maximum load withstood by the MAFD anchors was 43.90 N. The compressive strength of the MAFD anchors ranged from 1.55 MPa to 2.76 MPa, with a mean of 2.21 MPa.

The CA anchors withstood loads between 8611 N to 9406 N, with a mean load of 8885.72 N. The compressive strength ranged from 203 MPa to 231 MPa, with a mean load of 220.14 MPa. The uncoated acetal rod withstood a higher maximum load but had a lower compressive strength than the CA anchor.

Table 6.1: Compressive testing results, showing mean figures, of the MAFD anchors, the CA anchors, and the uncoated acetal rod.

	Maximum Load (N)	Compressive Strength (MPa)
MAFD Anchor	35.15	2.21
CA Anchor	8663.84	227.61
Uncoated Acetal Rod	8959.68	217.65

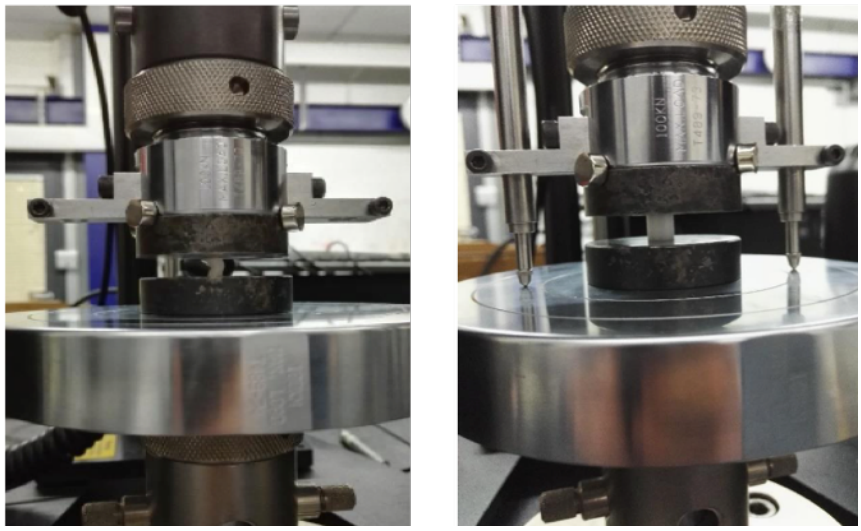

Figure 6.14: The compression testing of a MAFD anchor, left, and a CA anchor, right, using an Instron Dual Column Universal Testing system.

6.3.6. Degradation of the Composite Hydrogel Anchors

After 24 hours of incubation in cell culture medium, the MA4C anchors had entirely disintegrated. The wet mass was unable to be measured after incubation. This disintegration was seen from all MA4C samples.

The MAFD anchors had an average wet mass of 0.079 g before incubation in cell culture medium and had an average wet mass of 0.042 g after 24 hours of incubation. This resulted in a 46.84% mass loss. The degradation rate of the MAFD anchors was significantly faster than that of the detached composite MH and PH.

6.4. Discussion

In ligament and tendon tissue engineering, the enthesis is of great importance due to its interface of two distinctly different tissue types and its biomechanical role in stress dispersal [139, 184, 445]. The native enthesis of the ACL is a direct insertion of the ligament into the periosteum of the trabecular bone consisting of a ligamentous region, an unmineralized fibrocartilaginous region, a mineralized fibrocartilaginous region, and a bony region [164, 169, 454]. The intricate graded mineralized tissue disperses great stresses during joint movement by reducing the modulus disparity between the bone and ligament tissues [18, 176]. After injury, the natural healing of the enthesis does not regenerate the organised graded mineral content and often results in disorganised fibrovascular scar tissue with weaker mechanical properties than the physiological enthesis [164]. Due to the poor healing of this complex interface, research has focused on the cellular interactions to regenerate the structural

organisation of the graded mineralized regions leading to a more functional modulus match between the soft and hard tissues of the ligament and bone [159, 169, 455].

The cell response to the composite hydrogel is a key factor to understanding if this biomaterial is suitable for enthesis engineering. The anchor is a paramount component of the bioreactor system as the detached hydrogel scaffold requires a point of attachment to the bioreactor for stress dispersal. The design of the anchors must provide attachment of the detached hydrogel scaffold (of Chapter 5) to the bioreactor and endure the tensile strain and culture environment within the bioreactor.

6.4.1. The Composite Hydrogel as an Enthesis Biomaterial

The enthesis is a complex interface where there are several cell types found within the graded mineralized areas such as osteoblasts at the bony region, fibrochrondrocytes in the fibrocartilaginous regions, and fibroblasts in the ligament region [52, 180]. Regenerating this complex mineralization has proven difficult within tissue engineering due to the complex cell responses required in each region.

The need for a varying cell response on a scaffold has prompted research into composite scaffolds, custom bioreactors, modified cell culture medium by introducing growth factors, and co-culturing of multiple cell types to produce the desired cell phenotype throughout the scaffold [456, 457]. Previous studies have shown success with composite scaffolds to provoke mesenchymal differentiation in osteochondral studies investigating the articular cartilage in joints [458, 459]. However, there has been little translation of the success of composite scaffolds in osteochondral studies into enthesis development. The scaffolds in this research aim to build on the progress of osteochondral composite scaffolds by modifying the midsubstance material through the addition of $CaCO_3$ and $CaHPO_4$ to produce a composite hydrogel for the enthesis region.

Although the metabolic activity of the 3T3 and PFib fibroblasts was slightly lower on the composite hydrogel compared to the chitosan-gelatin hydrogel of Chapter 4 (page 59), the metabolic activity results showed that the composite hydrogel is cytocompatible [396]. The metabolic activity results of both cell types followed a similar trend to that of the chitosan-gelatin hydrogel, with the highest metabolic activity seen on the thinnest samples and a decline in metabolic activity as the thickness increased. The significant declines of 3T3 cell metabolic activity at several timepoints on the composite hydrogel can be attributed to the continued proliferation of the cells leading to overpopulation and cell death [374, 375]. The PFib fibroblasts

showed a positive trend of increased metabolic activity at each subsequent timepoint across all thicknesses of the composite hydrogel with no significant declines in metabolic activity. The differences in the 3T3 and PFib metabolic activity between the thicknesses of the composite hydrogel became less significant as a function of time, consistent with fibroblasts grown on a collagen hydrogel scaffold [430]. The lack of significant difference of metabolic activity related to sample thicknesses at Day 28 may be attributed to the acclimation lag of the PFibs to the substrate [387]. A similar delay of cell colonization on a calcium phosphate modified substrate was seen in a study by Daculsi et al. investigating an injectable hydrogel with microporous biphasic calcium phosphate granules, 40% hydroxyapatite and 60% ß-tricalcium phosphate, as a bone filler [460].

The DNA concentration results showed a conflicting response to the hydrogel thickness compared to the metabolic activity, with the highest DNA concentration found on the thickest hydrogel samples for both the 3T3 and PFib cells. The DNA results suggest that there was a higher cell number on the thicker samples, for both the 3T3 and PFib cells, despite having a lower metabolic activity [461].

The morphology of the 3T3 fibroblasts on the composite hydrogel was unlike the morphology seen on the chitosan-gelatin hydrogel of section 4.3.3 (page 57). Where the 3T3 cells had formed a monolayer and individual cells were difficult to identify on the chitosan-gelatin hydrogel, the 3T3 cells were rounded and more distinctive individually on the composite hydrogel. The PFib cells on the composite hydrogel maintained a rounded morphology with extensions across all sample thicknesses, unlike the elongated morphology of the PFib cells on the chitosan-gelatin hydrogel.

The perceived stiffness of the substrate, discussed previously in section 4.4.2 (page 65), may also play a role in the 3T3 and PFib cell proliferation, morphology, and DNA content on the composite hydrogel [377, 462]. However, where the perceived stiffness of the chitosan-gelatin hydrogel of Chapter 4 appeared to decrease with the increasing hydrogel thickness, the perceived stiffness of the composite hydrogel did not appear to have the same pattern with increasing thickness. This is evidenced through the decreased level of significance of metabolic activity between the composite hydrogel thicknesses at Day 28, especially from the PFib cells, and the similar morphology of the 3T3 and PFib cells across the sample thicknesses. The positive correlation of DNA content to sample thickness suggests the perceived

stiffness may even increase with increasing hydrogel thickness. It is possible that the calcium phosphate salts increased the perceived stiffness of the composite hydrogel by decreasing the contribution to the perceived stiffness from the chitosan-gelatin hydrogel. While it has been shown that calcium salts increase the mechanical stiffness of a hydrogel substrate, the perceived stiffness of the hydrogel substrate after addition of calcium phosphate salts has not been previously reported [184, 463].

It is well known that bone contains a high percentage of inorganic mineral content, mainly in the form of hydroxyapatite [464-466]. This has led to the investigation of hydroxyapatite as a biomaterial for bone grafts. The osteoconductivity and resemblance to bone composition makes hydroxyapatite an attractive biomaterial, however it is very brittle, remains in the body for a prolonged period, and has little biological and mechanical similarity to bone [465, 467, 468]. These unfavourable qualities of hydroxyapatite have directed research towards other calcium phosphate salts, such as brushite and ß-tricalcium phosphate [469-471]. Brushite has shown success as a biomimetic bone scaffold, however its tendency to hydrolyse to form hydroxyapatite result in similar graft instability [16, 192, 472, 473]. ß-tricalcium phosphate has gained success as an orthopaedic biomaterial due to its ability to produce pyrophosphate ions while preventing hydrolysis into hydroxyapatite [192, 465]. The pyrophosphate ion is crucial in mediating the biomineralization of new bone formation [465]. In the presence of ALP, the pyrophosphatase ions are hydrolysed releasing a concentration of phosphate ions resulting in localized mineral deposition and bone formation [465, 474]. However, the main constituents required for tissue mineralization are a surplus of calcium and phosphate ions, which can be created through the addition of calcium phosphate salts [469, 474].

The composite hydrogel of this research intended to mimic the calcium and phosphate availability of ß-tricalcium phosphate through the addition of $CaCO_3$ and $CaHPO_4$. The ALP activity found in the PFib samples suggests that the composite hydrogel increased the availability of calcium and phosphate ions on the surface, initiating an osteogenic response. In a study by Zhang et al., an increase of ALP activity through the addition of calcium phosphates to a chitosan scaffold was reported [473]. Mutsuzaki et al. have also shown success of the incorporation of calcium phosphate salts into a tendinous graft that resulted in an osteogenic response and a bony interface that resembled a natural direct insertion [171]. A previous study by Zhao et al. has reported that the incorporation of hydroxyapatite nano-particles into a

chitosan-gelatin hydrogel created a biomimetic scaffold with similar density and porosity to bone that promoted biomineralization by rat osteoblasts after 3 weeks of cell culture [368]. It can be reasoned that the addition of calcium phosphate salts to the chitosan-gelatin hydrogel increased the availability of calcium and phosphate ions and thereby increased the osteogenic potential of the hydrogel.

As both fibroblasts and osteoblasts have a similar origin, it is no surprise that fibroblasts can differentiate into an osteoblastic phenotype [156, 475]. Both cell types have similar gene expression, with the exception that osteoblasts encode for production of osteocalcin and fibroblasts do not [476]. Several studies have reported that fibroblasts, namely from ligaments, have differentiated into osteoblasts and produced ECM similar to bone [477-479]. The differentiation of fibroblasts has been shown to be dependent on several factors, such as the type and maturity of fibroblast, the chemical signals, the substrate, and the surrounding ECM [156]. It has also been shown that tensile stress in bone fractures recruits neighbouring fibroblasts, eventually initiating an osteoblastic differentiation [480]. The ALP activity levels from the PFib cells reported here indicate that the calcium phosphate-rich environment of this hydrogel was favourable for an osteogenic differentiation.

GAG, mainly chondroitin sulfate, are found throughout the organic matrix of bone, alongside collagen, and play a key role in the mineralization of new bone [481-485]. The GAG content is inversely correlated to the mineral density of bone, therefore, newly ossified bone has a higher GAG content than mature bone of high mineral density [481, 486]. The GAG/DNA ratio of the 3T3 and PFib cells across the sample thicknesses suggest a chondrogenic response, which may be beneficial for the graded fibrocartilaginous regions of the enthesis where fibrochondrocytes are found [52, 164, 169, 487].

The ALP activity and GAG content results suggest that the composite hydrogel elicits an osteogenic and chondrogenic response from the PFib cells indicative of enthesis formation. The 3T3 cells indicate some GAG production, however the ALP results were not consistent enough to suggest an osteogenic response. These results further confirm that the PFib fibroblasts have maintained their innate ability to differentiate into an osteoblastic lineage [156, 475].

6.4.2. Mechanical Functionality of the Anchors

The structure of an enthesis is highly complex due to its role mechanical loading [54]. The bony anchor of an enthesis model should withstand the mechanical

forces during active and passive movement of the joint. An appropriate cellular response should also be seen on the bony anchor to generate the fibrocartilage digitations into the periosteum [162]. The mechanical properties of the anchor can influence the cell response leading to the successful stress management between the graded mineralization of the tissues [54, 445]. It has been shown that after injury, the healed enthesis has lower mechanical strength than before injury with an increased rate of tendon pull-out due to the inadequate regeneration of the fibrocartilaginous regions [173]. The mechanical strength and the influenced cell response are critical factors to enthesis engineering.

The main goal of the anchors within this tissue engineered ligament bioreactor system was to provide an attachment for the detached hydrogel scaffold that could disperse the tensile forces through to the hydrogel midsubstance while also permitting cell proliferation and differentiation. The anchors must be able to withstand shear forces while in the bioreactor and not degrade before adequate cell growth. Within this experiment, the MAFD and CA anchors were subjected to forces much higher than the projected 2.4% strain of the tensile loading bioreactor and fared well. However, the degradation rate of the MAFD anchors indicates that their inclusion in a cell culture environment over a period of several weeks may be detrimental to the MAFD structure and strength.

Based on previous papers incorporating calcium phosphate salts into chitosan hydrogel, it is expected that the $CaCO_3$ and $CaHPO_4$ weakly interacted with the chitosan-gelatin hydrogel, with the potential of some hydrogen bonding [473, 488]. This may explain why some settlement was seen when the composite hydrogel was not immediately used.

A study by Huang et al. has shown that chitosan-gelatin hydrogel does not have the required mechanical strength to act as the sole biomaterial for the anchors of a tissue engineered ligament [370]. However, several studies have shown that the addition of calcium increases the stiffness of chitosan-gelatin hydrogel [385, 463, 472, 489]. A similar study by Maji et al. incorporated a bioactive glass into a chitosan-gelatin scaffold through freeze-drying and found sufficient scaffold mechanical properties for an osteogenic application [267]. The addition of calcium phosphates to chitosan scaffolds has shown to increase the mechanical strength of the chitosan scaffold while decreasing the brittleness of the calcium phosphate [473, 488]. From

the results of previous studies, the addition of $CaCO_3$ and $CaHPO_4$ would enhance the mechanical strength of the chitosan-gelatin hydrogel used in this experiment.

Compared to the detached MH and PH hydrogel discs of section 5.3.3.3 (page 78), the wet mass loss after sterilization at Day 1 of the detached composite MH and PH was significantly larger, suggesting a decreased swelling behaviour [420]. The chitosan-gelatin PH and composite PH detached hydrogel samples showed a significant wet mass loss immediately after sterilization. The MH samples of both studies, chitosan-gelatin and composite hydrogels, did not show a significant decline in wet mass after sterilization. These results suggest that the addition of $CaCO_3$ and $CaHPO_4$ had a negative effect on the swelling behaviour of the chitosan-gelatin hydrogel. Although the crystallinity of the $CaCO_3$ and $CaHPO_4$ was not investigated, it was assumed that the addition of these increased the crystallinity of the chitosan-gelatin hydrogel, as discussed in section 5.4.1, and therefore decreased the swelling capacity and affected the degradation [450, 490, 491]. However, the intermediate layer most likely did not affect the swelling behaviour of the composite hydrogel.

The degradation rate of the MAFD was significantly faster than the detached composite hydrogel discs, suggesting that the freeze-drying process altered the physicochemical properties of the chitosan-gelatin hydrogel. This led to the rejection of MAFD design for the anchors to be used in the bioreactor. Paxton et al. and Zhao et al. have shown that anchors of a similar mineral composition were able to withstand the culture conditions for up to 3 weeks without significant degradation suggesting that the composition used in this research may be sufficient during cell culture [16, 368]. For a better understanding of the degradation profile of the anchor designs and composite hydrogel, further investigation using simulated body fluid is needed [472].

6.5. Conclusion

The composite hydrogel has shown to be a cytocompatible material for the proliferation and growth of the PFib and 3T3 cells. The positive ALP activity results indicated that the $CaCO_3$ and $CaHPO_4$ content of the composite hydrogel promoted an osteogenic response. The significantly higher levels of ALP activity found within the PFib samples suggests that this primary fibroblast culture is a more viable cell source for a tissue engineered ligament application rather than the 3T3 cell line. In order to confirm the suitability of the composite hydrogel as an enthesis material, further investigation into the cell response to the composite hydrogel and the availability of the calcium and phosphate ions on the surface is required.

It has been shown that the addition of $CaCO_3$ and $CaHPO_4$ are advantageous in increasing the mechanical strength of a chitosan-gelatin hydrogel [463, 489]. Although the mechanical strength of the composite hydrogel was not analysed, it can be expected that the addition of the $CaCO_3$ and $CaHPO_4$ would have a similar effect on the mechanical strength of the composite hydrogel as the previous studies. Both of the anchor designs, MAFD and CA, showed mechanical strength that indicate they would be able to endure the tensile and shear stresses applied by the bioreactor once implemented in the system. However, the degradation of the MAFD anchor indicates that it may not be able to withstand a long-term cell culture environment.

7. Bioreactor Design, Assembly, and Application

7.1. Introduction

Bioreactors have quickly become a staple in ligament and tendon tissue engineering research due to their controllable and reproducible changes of environmental factors, reduced risk of contamination, upscaling ability, and their ability to accurately apply mechanical loads [492, 493]. The necessity of applied tension to fibroblast seeded scaffolds to facilitate the organised ECM production similar to ligament tissue has driven the use of tensile loading bioreactors within ligament and tendon tissue engineering research [400, 494, 495]. There have been a range of bioreactors reported in the literature, ranging from commercial models to custom designs that have contributed to a deeper understanding of the ligament and tendon regeneration process (see Table 2.6) [8, 492, 496].

While it is known that mechanical loading of fibroblasts is required for ECM production similar to a ligament or tendon, the optimal amount and application of this loading is unknown [497, 498]. A number of studies have attempted to replicate the physiological loading of the natural ligament, however this has led to a range of strain rates from 2-10% [339, 343, 499, 500]. These studies reported an increase in many factors that indicate production of ECM similar to that of a ligament, such as collagen type I synthesis, cell density, elongated cell morphology with orientation along the axis of tension, as well as many genetic markers. The duration of applied stress and rest period is also less understood, as studies suggest that cells require some rest time to actively synthesize the ECM components—the optimal rest period is yet to be reported [345, 347, 498]. Despite the varying rates and duration periods, it has been widely accepted that a cyclic strain regime is beneficial for ligament tissue development [8, 19, 501]. While the majority of bioreactors for ligament tissue engineering apply uniaxial strain, Altman et al. created a biaxial tensile bioreactor to more accurately replicate the tensile and torque forces experienced by an ACL during movement and found that mesenchymal stem cells showed differentiation into ligament like fibroblasts [136]. Since the findings of Altman et al., several studies have further investigated a similar multi-dimensional bioreactor [502-505]. Multi-dimensional bioreactors may be more accurate in mimicking the physiological loading of the ACL, however uniaxial tensile systems remain the most common bioreactors for ligament tissue engineering.

This chapter outlines the design, application, and results of a custom tensile bioreactor as a model for ligament engineering research. The bioreactor incorporates the previously discussed detached hydrogel scaffolds (MH), the composite hydrogel coated acetal anchors (CA), and the PFib cells while applying a cyclic strain regime to upregulate cell proliferation and the production of ligament ECM components. A strain rate of 2.4% was chosen due to its similarity to the physiological loading of an ACL and the reported success of an increase in collagen synthesis and scaffold stiffness [62, 339, 342-344, 506].

To analyse the effect of the tensile strain on the hydrogel sinew and the PFib cell response, a static system was assembled as a control. After 3 weeks of culture within the cyclic bioreactor or static control, the hydrogel sinews were prepared for imaging and biochemical analysis. The imaging allowed the morphology, orientation, and number of cells to be analysed. The biochemical assays allowed for quantification of the metabolic activity, DNA content, and GAG production. As the bioreactors were fixed within the incubators during culture, NH (at 1mm thickness) and TCP samples were used to monitor the cell growth and risk of contamination.

7.2. Methodology

7.2.1. Bioreactor Design

The custom-made bioreactor design was uniquely tailored for the development of tissue engineered ligament constructs. The design allows for an arduous strain regime, beyond the strain parameters reported here. The design was based on previous bioreactors in elastic cell culture systems [255, 317, 507]. An elastic cell culture system employs scaffolds, bioreactors, or a combination of the two to create a more biomimetic cell environment [255, 508].

Creo software (PTC, MA, USA) was used in the design process to model and optimise each of the components and to specify the component dimensions for machining. The frame was constructed from an aluminium base plate and two aluminium vertical plates that attached firmly to the base plate. The frame housed the 6-well cell culture plate and the two acetal plates that held the anchors. A Creo rendering image and assembly of the bioreactor are shown in Figure 7.1.

A non-captive linear actuator with a resolution of 0.03mm/step (size 14) was purchased from Hayden-Kirk (CT, USA). The actuator was attached to the taller of the vertical plates of the frame. The actuator rod passed through the frame and attached to an aluminium block secured to the top, mobile acetal plate. A large bolt through the

shorter vertical plate, at the opposite end of the actuator, was used to secure the cell culture plate within the frame.

The mobile and static acetal plates were positioned within the frame on top of the 6-well plate. The static plate was housed directly atop the cell culture plate and held the ‘short’, fixed anchors. The mobile plate was directly atop the static plate and held the ‘long’, mobile anchors. Each anchor connection to the acetal plate was bevelled and inset to reduce any obstruction of movement by the mobile plate. Acetal was chosen for its mechanical strength, ease of machining, and low coefficient of friction [451, 509].

The original concept of the bioreactor was described here. There were several limitations to this design that were exposed during assembly. These limitations were modified prior to the assembly and activation with the hydrogel sinews and cell culture.

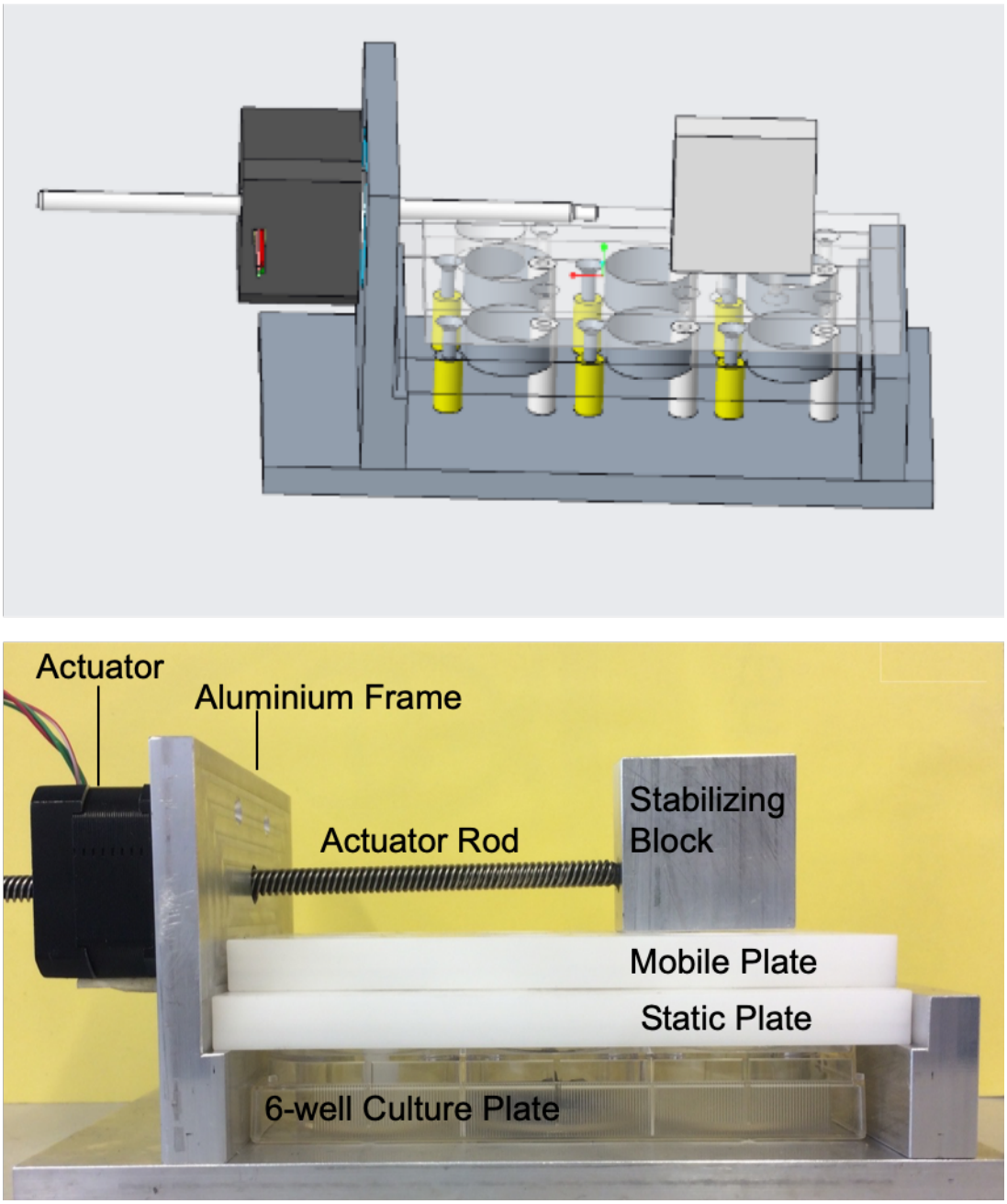

Figure 7.1: Top) A Creo rendering image of the bioreactor model, without a cell culture well plate. The yellow pillars represent the fixed anchors attached to the static plate. The white pillars are the mobile anchors attached to the mobile plate. The actuator rod is not attached to the stabilizing block of the mobile plate. Bottom) The assembled bioreactor with labelled components. The 6-well culture plate was placed in the bioreactor to display the relationship of the frame, the mobile and static plates, and the culture plate. The anchors are not attached to the mobile or static plates.

7.2.2. Experimental Design and Assembly

The assembly of the bioreactor and hydrogel scaffold was sequential and required great care at each step. The initial plan of using a poly-HEMA coating in the 6-well culture plate was unsuccessful due to the potential damage during the assembly process, such as from the freezing of the intermediate layer or sterilization of the

hydrogel. Therefore, non-treated tissue culture 6-well culture plates (Nunc™, ThermoFisher, UK) were used in place.

The day prior to assembly, the chitosan-gelatin hydrogel was made to the specifications outlined in section 3.5.1 (page 50) while cell culture medium was frozen into non-treated 6-well culture plates. All metal parts of the bioreactor were autoclaved at 121°C at 15psi for 30 minutes and allowed to cool overnight. This included the aluminium frame, the screws, the actuator rod, the bolt, and stabilizing block. The acetal anchor rods and plates were left overnight in IMS.

On the day of assembly, all bioreactor materials were placed into a Class II laminar flow hood. The actuator was attached to the frame and the rod inserted into the actuator but did not pass through into the frame. The anchor legs were attached to the mobile and static acetal plates, with caution to not over-tighten. The composite hydrogel was then made as described in section 6.2.1 (page 96). The anchors were each coated in composite hydrogel twice, creating the CA anchors, and allowed to dry. The culture plate with frozen medium was then placed into the frame and secured by the bolt. The static and mobile plates were then quickly aligned onto the culture plate and the actuator rod pushed through and fastened to the stabilizing block on the mobile plate.

Once the static and mobile plates were in place, 750 µl of hydrogel was rapidly cast around the anchors to create a sinew shape. The culture medium was allowed to thaw and was removed. The hydrogel was then sterilized as described previously, using great caution to not agitate the hydrogel sinew or the composite hydrogel anchors. Modifications were made by increasing the NaOH wash time to 2.5 hours and the UV radiation time to 3.0 hours. Because the whole bioreactor system was under the UV radiation, the actuator was covered with foil to prevent any damage. The sterilized bioreactor was carefully transferred into the incubator. Complete cell culture medium was then added to each well in excess to condition the hydrogel overnight.

A second set of hydrogel sinews was created using a static control system. In this system, identical acetal plates with CA anchors as the mobile bioreactor system were aligned atop a non-treated 6-well culture plate with frozen medium and secured with sterile tape. Hydrogel was cast and sterilized in the same manner as the mobile bioreactor. This static control was transferred to the same incubator as the bioreactor and medium conditioned overnight.

Due to the design of the mobile bioreactor and static control system, both systems were open within the incubator. To compensate for this, aluminium foil that was sprayed with IMS loosely covered each system when the mechanical stimulation was not taking place. This helped to minimize evaporation of cell culture medium and the potential spread of contaminants. Alongside the bioreactor and static control, NH of 1.0mm thickness in a 6-well plate and TCP of a 24-well plate were used as controls to monitor cell growth and ensure no contaminants had entered the incubator and spread to the bioreactor well plates. The NH was cast and sterilized as described previously.

7.2.3. Cell Culture

After the overnight conditioning, PFib cells at passage 1 were seeded at a density of 70,000 cells/cm^2 at a volume of 9950 µl in a focal manner directly onto the midsubstance of the hydrogel sinews in the bioreactor and static control systems and on the NH and TCP samples. Despite the focused seeding, the surface tension of the cell suspension caused the majority of the suspension to gravitate to the surface of the wells in the bioreactor and static control. The volume of cell suspension was subsequently modified to ensure that the hydrogel sinews of both systems were covered. After an hour, an excess of cell culture medium was added to the bioreactor and static control. The cells were incubated for 72 hours before the medium was changed and daily stimulation began. The availability of the PFib cells created a biological replicate of 3 and technical replicate of 1 for the bioreactor and static system. The biological replicate for the NH and TCP cells was 1 and the technical replicate was 6.

The cell culture medium in the bioreactor and static control was changed every other day taking care to not disturb the hydrogel sinews and anchors. No more than half of the medium was removed from each well to ensure the scaffolds remained submerged and undisturbed. The medium was replaced to the original volume. The cell culture medium in the NH and TCP samples was changed every third day as described in section 3.2 (page 42).

The PFib cells on the NH and TCP samples were monitored through phase contrast microscopy throughout the experiment.

7.2.4. Mechanical Stimulation

A code for 2.4% strain at 0.0167 Hz was created using the programming language C, courtesy of Alastair Campbell Ritchie. The code was programmed into an

Arduino microcontroller. The code for the mechanical stimulation can be found in the Appendix section 10.3 (page 180).

The mechanical stimulation of the mobile bioreactor began 72 hours after cell culture. The bioreactor was turned on for 1 hour per weekday, with the start time the same each day, or as close as possible. The weekends acted as rest days. This resulted in 1 hour of stimulation to 23 hours rest, with an additional 48 hours of rest after 5 days of stimulation. The cell culture medium was changed a minimum of 2 hours prior to the start of the stimulation on the days when the medium needed changing.

Images of the hydrogel sinews in the mobile bioreactor and static control were taken with a camera phone through sterilized clingfilm every day before and after mechanical stimulation. These images were used to monitor the shape and integrity of the hydrogel sinew.

7.2.5. Cell Culture Assays

After 21 days of culture, the PFib cells were analysed for their morphology, orientation, metabolic activity, ALP activity, and DNA and GAG content. The cell culture medium at Day 21 was collected to carry out selected assays, containing the medium from the final 2 days. The imaging and ALP, DNA, and GAG assays were carried out as described in Section 3.4 (page 45).

Due to damage of the NH samples, a 1.0mm NH sample seeded with PFib cells from a previous study was used for analysis of DNA, ALP, and GAG content, labelled NH*. The NH* sample results were normalized to an equivalent seeding density and culture period as the bioreactor, static control, and TCP samples of this experiment.

7.2.5.1. AlamarBlue

An alamarBlue assay was run after the 21 days of culture and stimulation. Earlier timepoints could not take place due to the bioreactor configuration. The assay was modified by increasing the amount of alamarBlue dye in the mobile bioreactor, static control, and NH samples from 1 ml to 2 ml and increasing the incubation time from 90 to 120 minutes. The TCP samples were in a 24-well plate and could only accommodate 1 ml of solution, so this was not changed. As the bioreactor samples could not be placed on the plate shaker after incubation, the alamarBlue dye was gently pipetted up and down several times to ensure thorough mixing of the dye in the wells before plating and reading the fluorescence. All samples were washed with PBS to remove excess dye before any further assays took place.

7.2.5.2. ESEM

One sample from the mobile bioreactor and static control were chosen for ESEM. Prior to dismantling the bioreactor and static control, the midsubstance of the hydrogel scaffolds was cut as close to the anchor as possible in an attempt to reduce any damage to the scaffold. The bioreactor and static control were disassembled and the samples for ESEM removed for fixation and imaging following the protocol in Section 3.4.7 (page 49). The ESEM samples were not used for further assays.

7.2.5.3. DNA, ALP, and GAG Assays

The remaining samples from each bioreactor were then prepared for further analysis. During the dismantling process, as much of the sinew was left in the well as possible resulting in the removal of the anchors from the scaffold leaving some damaged composite hydrogel alongside the hydrogel midsubstance. The cell samples, including the NH and TCP samples, were then lysed by 3 cycles of snap freezing & thawing in SDW.

The DNA content and ALP activity were assayed using the lysate. The remaining lysate and collected cell culture medium were digested using papain. The DMMB assay was used to calculate the GAG content of the lysate and the collected medium. A GAG/DNA ratio was then calculated. These assays followed the protocols outlined in section 3.4 (page 45).

7.3. Results

7.3.1. Bioreactor Design

As a consequence of several limitations of the bioreactor design that were discovered during dry trial assembly runs, such as inadequate room for hydrogel casting, inability to attach the stabilizing block and actuator rod to the mobile acetal plate, and misalignment of the mobile acetal plate during the mechanical stimulation periods, modifications to the bioreactor design were required.

The circular openings of the mobile and static acetal plates created an elliptical opening into the well plate in which to cast the hydrogel around the anchors within the well. This opening would not allow a pipette or syringe to properly cast the hydrogel around the anchors to create a sinew shape. To accommodate for the casting, the circular openings were widened around the anchor fixation, as seen in Figure 7.2. A bevelled edge was also fashioned to allow for increased reach of the pipette.

Additionally, it was found that the stabilizing block could not be fastened to the mobile acetal plate that would also allow for the actuator rod to be attached during

the sequential assembly process. To allow the attachment of the stabilizing block to the acetal plate, the stabilizing block was machined to create a superior 2/3 portion which attached to the actuator rod and an inferior 1/3 portion that attached directly to the mobile acetal plate with a hole for screw fixation. The inferior portion was attached directly to the mobile acetal plate during attachment of the anchors. The actuator rod was then attached to the superior portion of the stabilizing block and aligned on top of the inferior portion to allow a screw to fasten the two portions of the stabilizing block together.

Further, upon activation of the mechanical stimulation it was found that the mobile acetal plate did not remain aligned on the static acetal plate and moved diagonally to the left. To correct for this, two aluminium blocks were fashioned to create a guideway to ensure the alignment and movement of the mobile acetal plate. The aluminium blocks were fastened to the static acetal plate using Araldite Epoxy (Araldite, Switzerland). The epoxy was applied following manufacturer's instructions. Excess epoxy was removed after it was completely dried.

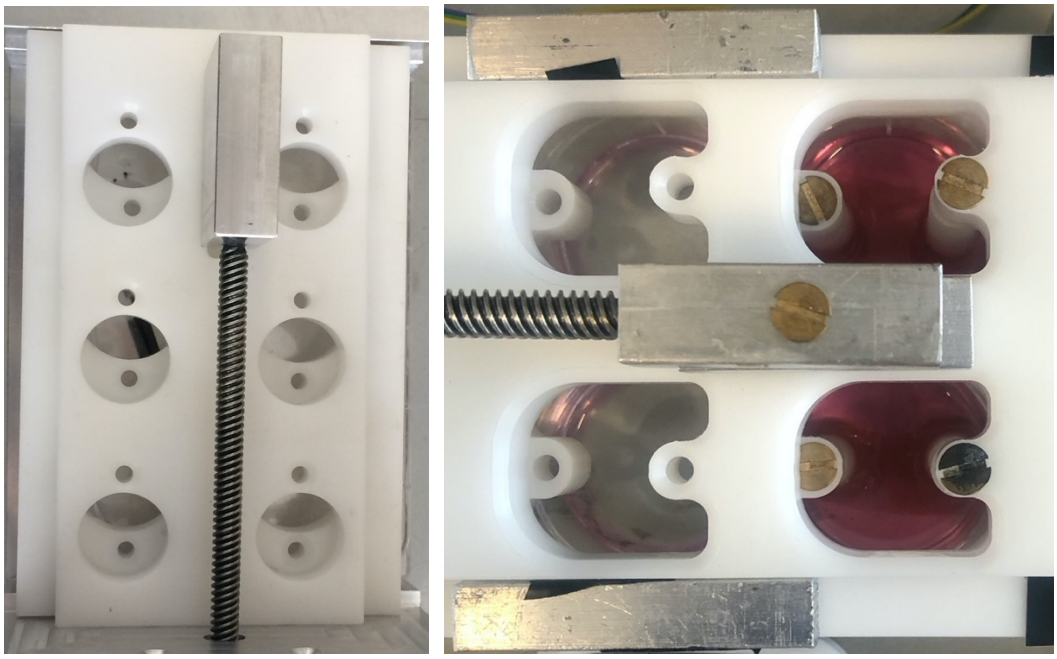

Figure 7.2: (Left) The original design of the acetal plate assembly and stabilizing block within the bioreactor. The circular openings of each plate created an elliptical opening into the well plate beneath. Anchors are not attached in this image. (Right) The modified openings of the acetal plates. The circular openings were widened around the anchor fixation points to allow a larger area with which to reach the well plate. The modified stabilizing block and actuator rod are attached in the image. The two aluminium guiding blocks can be seen on either side of the mobile acetal plate. Hydrogel sinews and cell culture medium can be seen in the two wells on the right.

7.3.2. Hydrogel Sinew

The chitosan-gelatin hydrogel formed a sinew around the CA anchors and endured the tensile strain from the bioreactor throughout the 21 days of culture, as seen in Figure 7.3. There was no separation at the midsubstance-anchor interface and there were no evident tears in the midsubstance, however, several small splits occurred during the dismantling of the bioreactor systems. The samples chosen for ESEM did not have any damage from dismantling. The tears would be presumed to not have an impact on the biochemical assays as the entire scaffold was lysed then digested.

Figure 7.3: (Left) An image of a hydrogel sinew within the mobile bioreactor taken before mechanical stimulation. (Right) An image of a hydrogel sinew within the static control. Each sinew is intact and there is no separation between the hydrogel midsubstance and the anchors.

7.3.3. Metabolic Activity

The TCP sample showed significantly higher metabolic activity than the NH, mobile bioreactor, and static control samples, as seen in Figure 7.4. The NH sample had significantly higher metabolic activity than the mobile bioreactor and static samples. There was no significant difference of metabolic activity between the mobile bioreactor and static control.

The variation in experimental setup justifies the significantly higher metabolic activity of the NH and TCP samples than the mobile bioreactor and static control. The increased area of the well plates used for the bioreactor, static control, and NH samples required additional alamarBlue solution and a longer incubation period. Additionally, the gravitation of the cell suspension towards the well plate of the bioreactor and control samples may have reduced the initial cell density, as the entire cell suspension could attach to the surface of NH and TCP

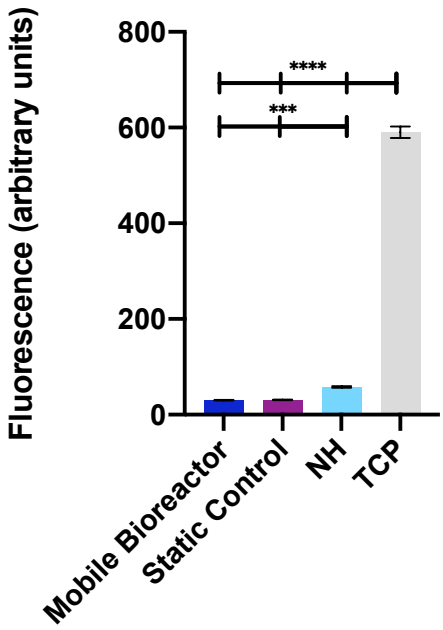

Figure 7.4: Metabolic activity of the PFib cells after 21 days of cell culture within the mobile bioreactor, static control, on NH, and on TCP, using an alamarBlue assay. Error bars represent standard error of mean. Where * p <0.0332, ** p <0.0021, *** p <0.0002, and **** p <0.0001 and n=3.

7.3.4. Cell Morphology

The PFib cells on the NH and TCP samples were able to be observed during culture through phase contrast microscopy. The cells on TCP were elongated and showed areas of high confluence. The NH samples showed elongated PFib cells in fewer numbers compared to the TCP samples. The PFib cells maintained an elongated morphology throughout the 21-day culture period on the NH and TCP samples.

The bioreactor and static control samples were imaged using ESEM to examine the cell morphology. Despite the low metabolic activity results, cells were visible on the bioreactor and static control samples. The PFib cells were sparse and rounded in morphology across the mobile bioreactor sample, as seen in Figure 7.5. There appeared to be some alignment of the PFib cells towards the axis of tension in the midsection of the hydrogel and near the mobile anchor. Cell debris was seen in the midsubstance of the sample. A higher number of cells were seen near the anchor interfaces than the midsubstance. Near the junction of the mobile anchor, grooves and patterning could be seen on the hydrogel. The hydrogel at the fixed anchor showed some signs of grooves but were not as evident.

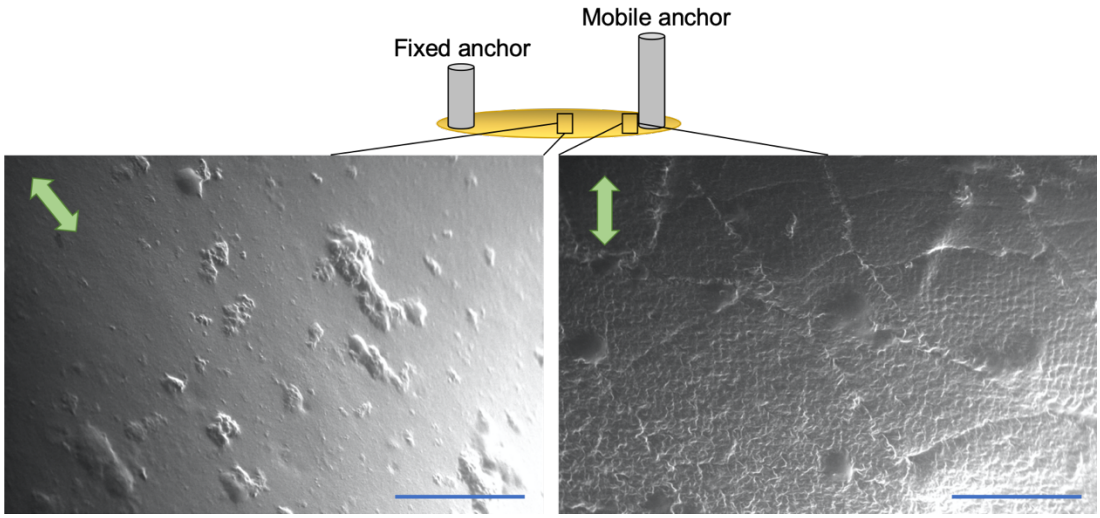

Figure 7.5: ESEM images of the PFib cells after 21 days of culture in the mobile bioreactor at the midsection, left, and near the mobile anchor junction, right. The green arrow indicates the direction of tension. Some alignment of the cells can be seen towards the axis of tension. Cell debris was present in the midsection of the scaffold. The hydrogel near the mobile anchor interface showed some patterning, a possible result of the tension. In both images, cells can be seen with rounded morphology and soft edges. The blue bar indicates 100 µm.

The PFib cells on the static control sample possessed a similar rounded morphology across the sample, as seen in Figure 7.6. The cells appeared randomly oriented and no evidence of patterning in the hydrogel was found. The cells were more numerous and grew in clusters near the anchor convergence, while the cells were more isolated in the midsection. Significantly more cell debris could be seen throughout the static control sample than the mobile bioreactor sample.

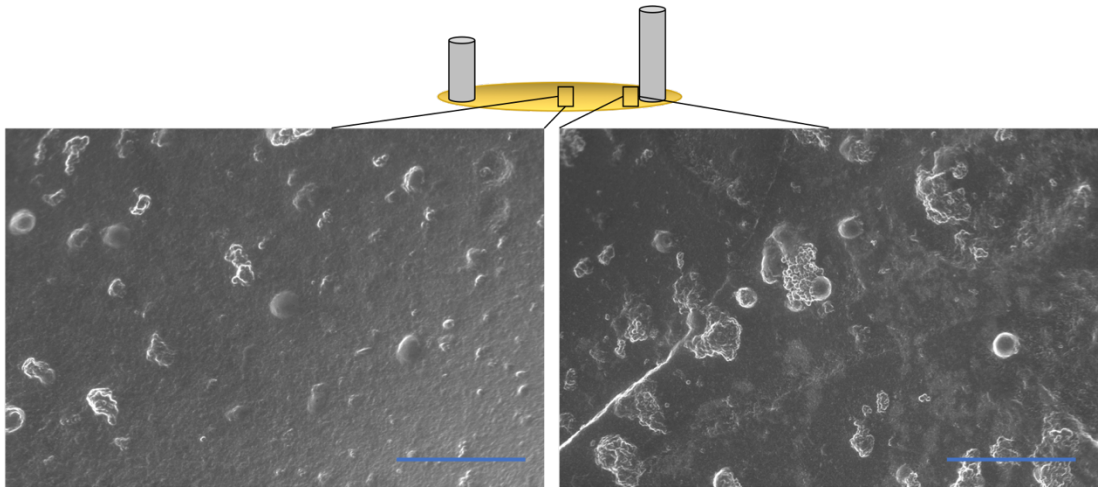

Figure 7.6: ESEM images of the PFib cells after 21 days of culture in the static control at the midsection, left, and near the anchor junction, right. The PFib cells possessed a rounded morphology at the midsection and near the anchor. Cell debris was present throughout the scaffold. Clusters of cells could be seen near the anchor, whereas the cells were more isolated in the midsection. The blue bar indicates 100 µm.

7.3.5. Cell Lysing and Digestion

The NH samples experienced significant damage during the lysing process and were unable to be used for further cell analysis. To compensate for this, the PFib results on 1.0mm NH samples from a previous study were normalized to the corresponding initial cell density and culture period used in this study (NH*).

7.3.6. DNA Content

There was no significant difference of DNA content found between the mobile bioreactor and static control, Figure 7.7. The NH* and TCP samples had significantly higher DNA content than both the mobile bioreactor and static control. The DNA content of the TCP sample was significantly higher than the NH* samples. These results were expected following the alamarBlue results.

The variation in experimental setup justifies the difference in results of the bioreactor and static system compared to the TCP samples, similar to the alamarBlue results.

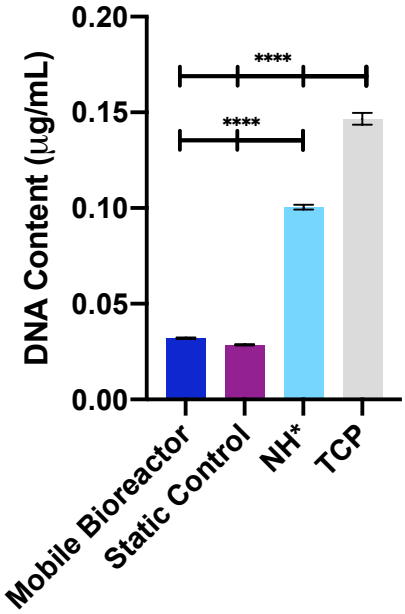

Figure 7.7: DNA content (µg/ml) of the PFib cells from the mobile bioreactor, static control, and TCP samples, using the PicoGreen DNA kit. As NH was significantly damaged during lysing, the included NH* was normalized from a previous PFib culture on 1.0mm NH in accordance to the seeding density and culture period. Where * p <0.0332, ** p <0.0021, *** p <0.0002, and **** p <0.0001 and n=2.

7.3.7. ALP Activity

ALP activity was not detected in either of the mobile bioreactor or static control systems. It was hypothesized that the ALP activity would be concentrated around the convergence of the chitosan-gelatin hydrogel and composite hydrogel, but

measurement of the separate midsubstance and anchor areas was not feasible. The scaffold was unable to be separated prior to lysing leading to the entire scaffold subjected to the same lysing treatment. This resulted in a single cell lysate from the midsubstance and at the anchor regions of the sinew.

7.3.8. GAG Production

There was no significant difference of GAG content found between the mobile bioreactor and static control, for the lysate and the collected medium, as seen in Figure 7.8. The lysate of NH* had significantly higher GAG content than the lysate of the mobile bioreactor and static control samples. There was no significant difference of GAG content between the lysate of TCP and the mobile bioreactor and static control. There was no significant difference found for the collected medium between all samples.

The collected medium of the mobile bioreactor had significantly higher GAG content than the cell lysate from the mobile bioreactor. The collected medium of the static control followed this trend. There was no significant difference of GAG content between the lysate and collected medium for both NH* and TCP.

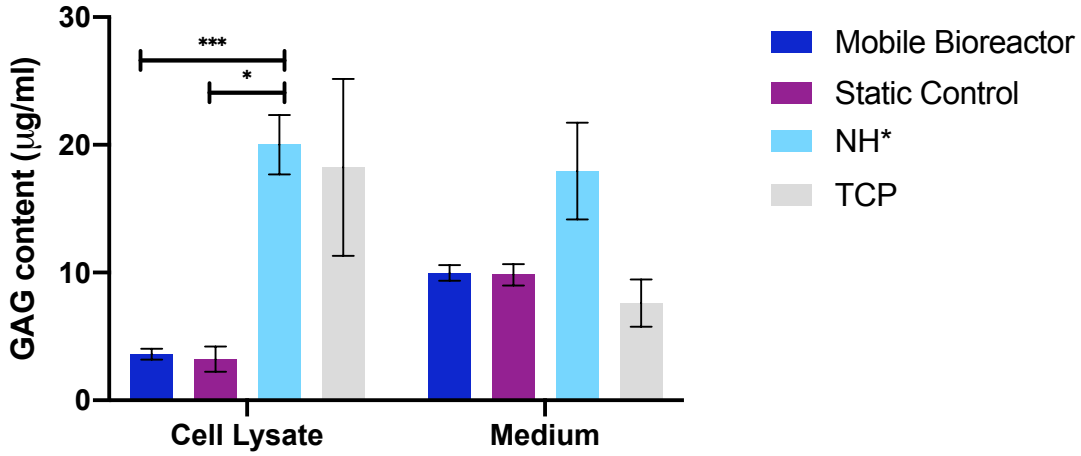

Figure 7.8: GAG content (µg/ml) of the cell lysate and collected medium of the PFib cells on the mobile bioreactor, static control, NH*, and TCP samples, using a DMMB assay. The error bars represent standard error of mean. Where * p <0.0332, ** p <0.0021, *** p <0.0002, and **** p <0.0001 and n=2 for cell lysate, n=3 for medium.

There was no significant difference of GAG/DNA ratio from the cell lysate across the bioreactor, control, NH*, and TCP, as seen in Figure 7.9. However, the GAG/DNA ratio of the collected medium of the mobile bioreactor was significantly higher than the ratio of NH* and TCP. The collected medium from the static control followed a similar trend and was significantly higher than that of NH* and TCP.

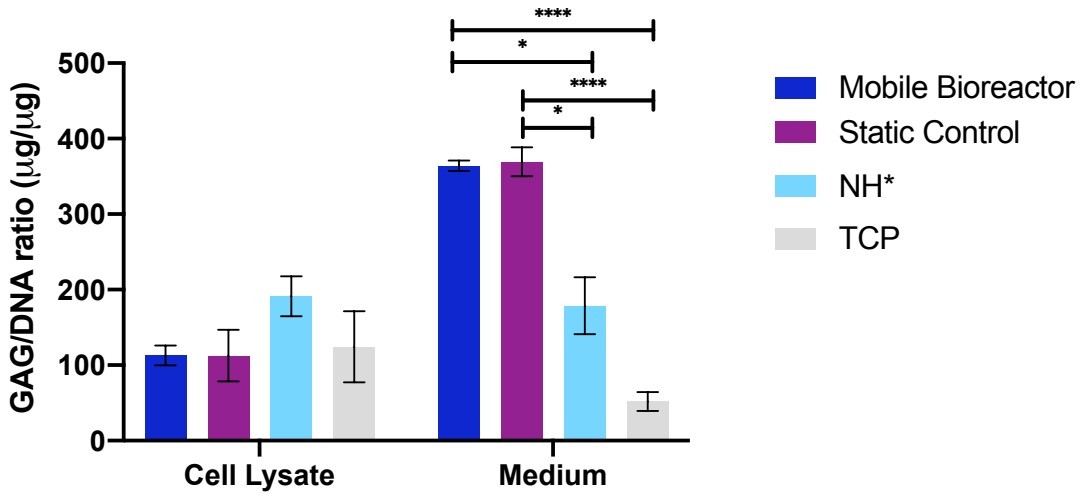

Figure 7.9: GAG/DNA ratio of the lysate and collected medium of the PFib cells on the mobile bioreactor, static control, NH*, and TCP. The error bars represent standard error of mean. Where * p <0.0332, ** p <0.0021, *** p <0.0002, and **** p <0.0001 and n=2 for cell lysate, n=3 for medium.

7.4. Discussion

Tissue engineering research typically begins with the study of cell response on a biomaterial surface for ease of experimentation and fast production of results. This simple model is then expanded to include additional variables that may impact the cell response. Eventually, a 3D environment that resembles the physiological environment is produced that includes the mechanical, chemical, and other environmental signals required for successful tissue regeneration [510].

In order to recreate a natural environment, bioreactors have been utilized within ligament tissue engineering to mechanically stimulate cells in a more realistic and controlled manner [140]. Bioreactors may also control other environmental aspects, such as chambers for co-culture of cells or perfusion of cell culture medium [8, 329].

In this research, a custom bioreactor was developed as a model for ligament and tendon tissue engineering. The bioreactor was designed to allow a wide range of strain rates, from 0.01-10%, however a 2.4% strain rate was used in this study to replicate the physiological loading of the ACL [62, 511]. The combination of the detached hydrogel scaffold and the composite hydrogel coated anchors produced a novel chitosan-gelatin hydrogel sinew that could be implemented in a tensile loading bioreactor and evaluated for application within ligament tissue engineering research. The incorporation of the PFib fibroblasts onto the hydrogel scaffold allowed for the evaluation of the cell morphology and orientation and the biochemical content after the application of the tensile strain, that could act as an indicator of ECM synthesis.

7.4.1. Bioreactor Design and Application

The design of this bioreactor was a preliminary model for ligament and tendon tissue engineering research. As each component of the bioreactor was assembled, there were ideas of improvement to better facilitate the assembly and transmission of tension to the hydrogel scaffold. Fundamentally, the development and use of bioreactors is iterative in nature and continually improving as technology and information advances and expands [140].

Previous studies on bioreactors for tissue engineered ligament applications have identified four key components of a bioreactor: the cell culture medium circulation, the culture compartment, the environmental control system, and mechanical stimulation system [8, 135, 329, 330]. The desired outcome of the tissue engineered scaffold commands control on each of the above factors [512]. Within this bioreactor design, the focus was on the durability of the hydrogel scaffold and the response of the attached PFib cells while cultured with cyclic tensile strain, therefore the three other factors were kept as simple as possible.

The chitosan-gelatin hydrogel sinew remained intact during assembly and throughout the culture period with mechanical stimulation. There was no separation at the interface between the chitosan-gelatin hydrogel of the midsubstance and the composite hydrogel of the CA anchor. This suggests that the chitosan-gelatin hydrogel and composite hydrogel successfully integrated. Additionally, there was no separation of the composite hydrogel from the acetal rod further indicating that this anchor design was satisfactory for a ligament engineering model.

There was no evidence of contamination found within the samples after culture, indicating the design was successful in mitigating risk of contaminants. The PFib cells were found across the bioreactor and control samples, despite the low numbers, suggesting that the cell seeding method allowed attachment of cells, although optimization of this method is required to promote an increased cell density on the scaffold.

7.4.2. Cell Response on the Hydrogel Sinew

The chitosan-gelatin hydrogel was successfully cast into a sinew structure around the CA anchors that endured tensile strain over a 21-day period of cell culture. As discussed previously, there was no contraction seen in the chitosan-gelatin hydrogel sinews that has been seen in previous fibrin and collagen scaffolds [218, 317, 401, 513, 514]. The lack of contraction or change of scaffold shape may be due to the

crosslinking within the chitosan-gelatin hydrogel, as there have been no previous signs of possible contraction in prior chitosan-gelatin hydrogel studies [372, 515]. There has been evidence of contraction in collagen-chitosan hydrogels with fibroblast culture, however the chitosan content has shown to increase the hydrogel resistance to contraction [251, 516]. Additionally, the force generated by the cells may be a limiting factor in the contraction, as discussed in section 5.4.2 (page 90) [431]. Based on these previous studies, the lack of contraction of the chitosan-gelatin hydrogel used in this research was accepted leading to a sinew shape formed through the casting of the hydrogel. Further, there was no indication of deformation of the hydrogel sinew while cultured in the mobile bioreactor; any change would have been infinitesimal and imperceptible by the methods of monitoring used here.

Despite the low alamarBlue results from the mobile bioreactor and static control, the ESEM images of both of these samples indicated that cells were dispersed across the scaffold. As discussed in section 5.4.2 (page 90), the rounded morphology of fibroblasts may indicate a period of self-preservation, or a quiescent state, as they await more favourable conditions for growth and proliferation [443, 444]. The low DNA and GAG results can be attributed to the latent phase that the fibroblasts remained in on the hydrogel surface.

Further, the results of the DNA and GAG content do not align with previous studies using fibroblasts in a tensile bioreactor for tendon and ligament repair [215, 341]. Interestingly, the GAG/DNA ratio from the collected medium of the bioreactor and control samples was comparable to the composite hydrogel scaffolds, section 6.3.2.3 (page 105). This suggests that the cells that had adhered to the hydrogel at the midsubstance or anchor regions had begun to mature, despite the rounded morphology.

The lack of detected ALP activity would suggest that the composite hydrogel of the anchors did not promote an osteogenic response from the PFib cells that had adhered in this area. However, it is possible that any ALP activity from the PFib cells near the composite anchors was so diluted during the lysing process that the activity fell well under the sensitivity range of the plate reader. It is also possible that there was not a substantial amount of composite hydrogel exposed that could influence the proliferation and differentiation of the PFib cells to produce a detectable amount of ALP activity.

It was hypothesized that the mechanical stimulation from the bioreactor would promote the activation of the rounded PFib cells, however the results suggest that the conditions were not favourable for production of ECM components on the midsubstance and differentiation near the anchors, despite these cells showing positive responses to the chitosan-gelatin hydrogel and composite hydrogel separately. It is probable that the small population of adhered cells to the sinew were metabolically active, synthesised GAG, and expressed ALP activity but the results were diluted in the excess solution of the assay or lysate producing inaccurate results.

It is possible that a higher initial seeding density may have increased the number of adhered PFib cells to the sinew which may have influenced the proliferation, GAG production, and differentiation of the cells. Several studies that investigated the effect of cell seeding density found an increased initial seeding density had a positive effect on the cell adhesion, proliferation and ECM production [83, 133, 343, 517]. There are reports suggesting that the initial seeding density has no impact on the cell density after several days or weeks of culture, dependant on the scaffold, however a significant increase in ECM constituents was reported in the samples with higher initial cell seeding density [517, 518]. Further, it is possible that during seeding the fibroblasts attempted to adhere to the well plate rather than the hydrogel. Holy et al. found that only 25% of the seeded cells adhere to a freestanding scaffold within a well, suggesting the adherence of the PFib cells to the hydrogel was significantly lower than the seeding density used [518]. Measures were taken to prevent this, such as the non-treated tissue culture well plate and the directed pipetting of the cell suspension, but the fluid nature of the medium may have carried a majority of the cells towards the well plate rather than the hydrogel scaffold. Additionally, the PFib cells were grown to confluence in culture flasks to maximize seeding numbers and could not fulfil a higher seeding density than used here.

It is well known that connective tissues, including ligaments and tendons, require mechanical forces such as tension, compression, shear, and torsion to regulate homeostasis [519]. As fibroblasts are the main cell type in many connective tissues, there has been extensive research into the fibroblast response to various mechanical stimuli [520-522]. Tensile strain causes fibroblasts to produce a more organised ECM appropriate for ligament or tendon application, including an increase in cell density and collagen content [8, 331, 498].Thus, the application of tensile strain in ligament tissue engineering research has been implemented on various scaffolds to investigate

the fibroblast response and suitability for ligament regeneration [136, 345, 523, 524]. The mobile bioreactor metabolic activity and biochemical assay results did not show a similar increase of cell proliferation and ligament ECM markers as previous studies when compared to the control [334, 501]. This potentially indicates that the tensile strain was not dispersed throughout the scaffold and did not influence the cell response. However, some alignment of the PFib cells on the bioreactor sample was seen in the ESEM images suggesting that the tensile strain may have been incompletely dispersed to the scaffold, only impacting the mobile anchor and the portion of hydrogel midsubstance near it.

The stiffness and rigidity properties of the hydrogel scaffold that were discussed as a result of the method to create a detached hydrogel in section 5.4.2 (page 90) are also probable causes for the PFib cell response seen on the sinew in the bioreactor. From this reasoning, the cells that were able to adhere to the sinew may have been influenced by the perceived stiffness of the hydrogel and consequently migrated from the softer region of the midsubstance to the edges of the scaffold where the substrate would have been perceived as stiffer, similar to the detached hydrogel of MH and PH [377, 379, 386]. The rigidity of the midsubstance of the sinews may have influenced the cell response within the bioreactor, as a substrate with low rigidity has been shown to negatively influence ECM production and organisation compared to a substrate with a higher rigidity [378, 379, 439, 440]. It was expected that the low rigidity seen in the detached MH and PH hydrogel samples would have increased from attachment in the tensile bioreactor due to the anchorage system. Hadjipanayi et al. reported the increase in rigidity of a collagen scaffold by its attachment to a well plate [387]. Although the detached chitosan-gelatin hydrogel has low perceived stiffness and rigidity, these properties were expected to increase by putting the scaffold under tension while attached in the bioreactor. The morphological and biochemical results did not suggest that these properties were altered once the hydrogel was cast in a sinew shape in the bioreactor.

7.4.3. Scaffold Modification & Reinforcement

Although the elongation before failure of the chitosan-gelatin hydrogel was similar to the ACL, its tensile strength would not support its use a tissue engineered ligament without modification [234]. The application of mechanical loading to the PFib seeded hydrogel scaffold was hypothesised to increase the strength of the scaffold as Saber et al. have reported an increased mechanical strength of an acellular

tendon graft seeded with tenocytes after cyclic strain [19]. Several studies have reported an increased collagen I content after cyclic strain on various constructs for ligament repair [149, 215, 341, 345]. The cyclic loading of the cells promotes the production of an ECM similar to a ligament, including organised collagen I synthesis which can lead to increased strength of the construct [135]. The chitosan-gelatin hydrogel used in this research has shown to promote ECM production of the PFib cells through GAG synthesis and it would be reasonable to believe that after optimization of cell adherence to the scaffold, the tensile loading of the bioreactor would upregulate collagen synthesis which may lead to increased strength of the construct.

At several points of this research, the addition of a reinforcement into the midsubstance of the hydrogel scaffold was deliberated. Wang et al. investigated the addition of a titanium spring into a hydrogel scaffold, resulting in a mechanically stronger scaffold for ligament repair without adverse cell response [317]. Huguet et al. utilized a synthetic fibre prosthesis with a collagen gel coating in ovine models for 6 months without failure but the histological analysis showed insignificant osseous ingrowth at the anchor and an absence of growth between the fibres of the prosthesis [525]. Several other studies have researched the development of synthetic fibres without a hydrogel or collagen coating with excellent short-term compatibility but the long-term results showed failure at the site of implantation [526, 527]. The malleable nature of the chitosan-gelatin hydrogel would support a scaffold reinforcement, such as a spring, fibres, or mesh, while still possessing the biocompatibility of the chitosan-gelatin hydrogel. There is potential to improve the mechanical strength, such as the tensile modulus, of the chitosan-gelatin hydrogel through the addition of a reinforcement.

7.5. Conclusion

The bioreactor enabled an environment where tensile strain could be applied to the hydrogel sinew while contained within the incubator. The hydrogel sinew maintained its structural integrity throughout the mechanical loading during cell culture and no evidence of ruptures or tears were found. The anchor interface between the composite hydrogel of the CA anchors and the hydrogel midsubstance endured the tensile strain with no evidence of separation. Cells were successfully seeded on the hydrogel sinews and there were no signs of contamination at the end of the culture period. These results suggest that this custom bioreactor design is an adequate model to be used for ligament tissue engineering research. Additionally, the design of this

bioreactor could accommodate a range of scaffold biomaterials, such as other hydrogels or fibre-based constructs.

At the conclusion of the culture with mechanical stimulation, there was a lack of mature PFib cells found at the midsubstance of the sinew and differentiated PFib cells at the enthesis regions on both the bioreactor and control samples, as evident through the cell morphology, low DNA and GAG content, and ALP activity. The cell morphology and biochemical assay results suggest inefficient cell adhesion and proliferation on the sinews. However due to the bioreactor design, the adhesion of the PFib cells after seeding and their proliferation during the culture period were unable to be separately monitored and analysed.

Although the analysis of cell response did not show a significant increase in proliferation of PFib cells and upregulation of GAG production in the bioreactor sample compared to the static control, the results indicated that the cells survived the culture period with mechanical loading. As this was the first trial of the mobile bioreactor, this can be seen as a success that the design allowed intricate casting of the hydrogel and seeding of the PFib cells. The design of the bioreactor and hydrogel sinew allows for improvements that could increase the synthesis of ligament ECM markers. Such improvements could include the acetal plate design to allow for more efficient hydrogel casting and cell seeding.

There is potential for this tensile bioreactor model to become a component for regenerative therapy for ligament and tendon repair, such as for ACL reconstruction. In order to accomplish this, results indicating a significant upregulation and organisation of ligament ECM components would need to be produced. The complete and accurate transmission of the tensile strain to the hydrogel scaffold and attached cells would need to be confirmed.

8. General Conclusions and Future Work

This research has investigated the development of a chitosan-gelatin based hydrogel scaffold that could be implemented into a tensile loading bioreactor for a tissue engineered ligament application. This required the innovation of an intermediate layer that produced a practical detached hydrogel scaffold, an essential element of application in the tensile loading bioreactor. Several factors were assessed to ensure the adequate cytocompatibility, biodegradability, and mechanical durability of the detached hydrogel scaffold. The hydrogel was further modified with the addition of $CaCO_3$ and $CaHPO_4$ to investigate the cell response at the enthesis region. The suitability of two fibroblast cultures were assessed for use in a ligament engineering application. Finally, the detached hydrogel scaffold and composite hydrogel were incorporated into a tensile loading bioreactor and seeded with fibroblasts to determine the effectiveness of the tissue engineered sinew construct during a tensile loading regime.

8.1. Chitosan-Gelatin Hydrogel Optimization

The chitosan-gelatin hydrogel was demonstrated to be cytocompatible, aligning with previous studies using a similar hydrogel composition [399, 422, 528]. The cytocompatibility was maintained across the increasing thicknesses of the cast hydrogel, however a decreased rate of proliferation of both the 3T3 and PFib cells was seen with increasing thickness.

The increasing hydrogel thickness of this study has shown the effect of perceived stiffness on the cell growth and ECM production. The metabolic activity results of the 3T3 cells and PFib cells showed a decline in activity with increasing hydrogel thickness. Both cell cultures exhibited spread morphology with elongation on the thinner hydrogels, indicating a higher perceived stiffness [378]. The morphology of both cell cultures became more rounded with less extensions as the hydrogel thickness increased, indicating a lower perceived stiffness. The 3T3 and PFib morphology and metabolic activity results on the increasing thickness of hydrogel indicated that the perceived stiffness of the hydrogel decreased with increasing thickness, as fibroblasts tend to spread and proliferate more on stiffer substrates [382, 389]. However, the GAG content results suggest that the thinnest hydrogels, 0.5mm, were not suitable for deposition of ECM by the 3T3 or PFib cells. This aligns with

previous studies that have found that fibroblasts prefer substrates with a modulus similar to the physiological tissue for production of ECM [394, 439, 529].

This study has demonstrated the effect that the hydrogel thickness has on the perceived stiffness of the hydrogel by the cells. This is an important factor in influencing the cell response to the desired application. The 1.0mm thickness was found most suitable for future work due to its consistency in cell response for both cell types and accuracy of casting.

8.2. Detached Hydrogel Disc Produced by an Intermediate Layer

The fabrication of a detached hydrogel scaffold was a key factor in implementing the hydrogel into the tensile bioreactor. As chitosan-gelatin hydrogel is typically adhesive to TCP, a method of detaching the hydrogel from the underlying well plate without compromising the cytocompatibility of the hydrogel was necessary [399]. Aligning with the cost-effective approach, cell culture medium and PBS were investigated as an intermediate layer to release the hydrogel from the well plate.

This study proved that the intermediate layer, of either cell culture medium or PBS, did not adversely affect the cytocompatibility of the hydrogel. The surface chemistry results indicated that there were no excess salt residues on the hydrogel surface as a result of the intermediate layer [293]. However, the cell morphology and metabolic activity results indicated that the cells perceived the detached hydrogel scaffolds as softer than the hydrogel of similar thickness constrained in well plates [387]. It was believed that the low rigidity of the detached hydrogel decreased the perceived stiffness by the cells [394, 439].

The mechanical properties of tissue engineered constructs for ligament repair are important in maintaining the strength and stability of the joint once implanted [130]. The tensile testing of both detached hydrogel types, MH and PH, resulted in a similar elongation at failure as the native ACL [234]. However, the resulting tensile strength of the detached chitosan-gelatin hydrogel requires modification to more accurately replicate the biomechanical properties of the native ACL [132].

The cell culture medium intermediate layer produced a more consistent detached hydrogel scaffold than the PBS intermediate layer. The PBS intermediate layer did not reliably produce hydrogel scaffolds that withstood the handling during transfer and sterilization. Therefore, the cell culture medium intermediate layer was utilized in further experiments. The method of fabricating detached chitosan-gelatin

hydrogel scaffolds proves to be an interesting research tool to modify biomaterials that are dependent upon an external structure for support.

8.3. Composite Hydrogel

The enthesis has proven to be a challenging area within tissue engineering due to the graded mineralization, organisation of collagen, and its role in stress dispersal [162, 446, 530]. Previous studies have investigated hydroxyapatite, brushite, and calcium phosphate to replicate the bony interface and regenerate the graded mineralization [184, 186, 189]. This study demonstrated that the addition of $CaCO_3$ and $CaHPO_4$ prompted the production of early osteogenic markers by the PFib cells, possibly indicating the differentiation towards an osteoblastic lineage. The cytocompatibility of the hydrogel was not compromised by the integration of the calcium phosphate salts, aligning with previous studies that have incorporated calcium phosphate into chitosan and gelatin scaffolds [463, 472].

As previously discussed, the substrate stiffness has a profound impact on the cell response. To create a more biomimetic environment for osteogenic differentiation, several studies have incorporated calcium phosphate salts into chitosan-gelatin hydrogel to increase the stiffness [368, 385, 489]. The morphology and metabolic activity of the 3T3 and PFib cells indicated that the perceived stiffness of the composite hydrogel was less variable with increasing thickness than the chitosan-gelatin hydrogel. This was believed to be a result of the decreased contribution to the perceived stiffness from the chitosan-gelatin hydrogel through the integration of the calcium phosphate salts. The results showed a similar rounded morphology of both fibroblasts across all composite hydrogel thicknesses and a decrease in significant difference of metabolic activity between the sample thicknesses at respective timepoints compared to the chitosan-gelatin hydrogel metabolic activity results.

The GAG/DNA ratio results reveal a more consistent GAG production by the PFib cells than the 3T3 cells. These results may indicate a chondrogenic potential from the PFib cells, which is beneficial for the fibrocartilaginous regions of the enthesis. These results in combination with the ALP results, provide evidence that the composite hydrogel promotes a response from the PFib cells that is indicative of the cells found at the enthesis. However, histological analysis and additional assays for ECM components should be considered to confirm the production of these matrix components.

8.4. Primary Ovine Fibroblast Culture

In tissue engineering applications that require a multitude of cell lineages, the cell source is a key factor in the appropriate phenotype on the distinct areas of the scaffold [4]. The scaffold in this research necessitates two separate cell phenotypes—a fibroblastic phenotype in the midsubstance of the scaffold and an osteoblastic phenotype at the anchors on either end.

Upon investigating the growth and GAG production of the 3T3 and PFib cells on the chitosan-gelatin hydrogel and composite hydrogel, the PFib cells proved to be a more viable option for preliminary models of ligament tissue engineering research. The 3T3 cell line is a convenient model for cell culture, in part due to its rapid growth rate and accessibility [375]. However, the 3T3 cell line may not always be an accurate representation of a fibroblastic response due to the loss of some characteristics, such as cell contact inhibition. The experiments in this research have shown that the 3T3 cell line has a decreased capacity to differentiate into an osteoblastic phenotype.

Previous studies have explored the suitability of primary ACL fibroblasts as models for ligament engineering research for ACL reconstruction and have found upregulated production of ECM components, such as collagen type I & II and decorin [148, 150, 215]. The results from these studies demonstrate that the PFib culture is an adequate model for ligament engineering applications due to its potential for osteoblastic differentiation and innate capability to produce the physiological ECM. Collagen synthesis of the PFib cells was not analysed but can be predicted to be similar to the primary ACL cultures used in published studies [211, 279]. Further phenotyping would be beneficial to confirm the technique of tissue digestion for cell isolation resulted in the single fibroblast cell type and did not incorporate cells from the synovial sheath or surrounding tissues.

8.5. Bioreactor Design & Application

In order to implement the detached hydrogel into the bioreactor, an anchorage system was required that would allow for attachment of the detached hydrogel to the bioreactor and would allow for stress dispersal through to the hydrogel and attached cells. Of the three designs investigated, the acetal rod with a composite hydrogel coating (CA) proved to be the most suitable anchor design for cell culture within the bioreactor. The degradation of the MAFD anchors in cell culture medium and the low structural integrity of the MA4C anchors during handling rendered these two designs inadequate for use within the bioreactor.

The design and application of the tensile bioreactor system was the final aspect of this research. Several faults of the bioreactor design were identified during early assembly trials and modifications to the affected components were completed to facilitate assembly. The final configuration of the bioreactor allowed for both the complete casting of the chitosan-gelatin hydrogel around the CA anchors, creating the hydrogel sinew, and for the seeding of the PFib cells. The hydrogel sinew endured the tensile strain and the anchor-midsubstance interface remained intact throughout the culture. After the culture period, the PFib cells were found adhered across the sample. There was no evidence of contamination throughout the culture period. The successful assembly of the bioreactor indicates that the design of this tensile loading bioreactor may be a suitable model for ligament tissue engineering research.

Based on previous tendon and ligament tissue engineering studies, a significant increase in DNA and GAG content was expected after culture within the tensile loading bioreactor compared to the static control [8, 19, 345]. There was disparity between the initial results from this work and the results observed in previous ligament tissue engineering research. However, some cell alignment towards the axis of tension was seen in the bioreactor sample indicating the anchors transmitted the strain to the hydrogel and adhered cells. Additionally, there was some detection of GAG production from the lysate and collected cell culture medium of both the bioreactor and static control systems, indicating some production of ligament-like ECM of the PFib cells on the sinews. It is difficult to pinpoint the exact cause behind the similarity of the metabolic activity, DNA content, and GAG content results of the bioreactor and static control samples, thus demanding additional trial runs to confirm results.

The results from the application of the tensile loading bioreactor suggest that the sequential process of assembly was not detrimental to the hydrogel sinew or the PFib cells. However, the cell seeding could be optimised to increase the initial number of adhered cells to the sinew. Further, histology and mechanical testing of the sinews following culture within the bioreactor should be analysed to understand the effect of tensile strain on the spatial relationship of the cells and ECM production and the overall strength of the sinew.

8.6. Future Work

This chitosan-gelatin hydrogel has proven to be an exciting biomaterial with malleable physicochemical properties to direct the fibroblast response. In this study, we have shown the proliferation, GAG production, and differentiation of a primary

ovine fibroblast culture for use in a ligament tissue engineering application. However, to further justify our results the histology and additional ECM components, such as collagen and elastin, should be analysed. A total collagen quantification would be a useful measure of collagen content, which can be done by a SirCol Assay or a hydroxyproline assay. A more detailed account of the types of collagen produced would allow a deeper understanding of the newly generated tissue, which would require specific ELISA assays or PCR. Further genetic markers of ligamentous ECM could also be analysed through PCR, such as tenascin C, decorin, and fibronectin. While histological analysis could reveal the spatial relationship of the cells and ECM production and the organisation of matrix components, such as collagen fibrils.

As the tensile strength of the detached chitosan-gelatin hydrogel scaffolds was not similar to the tensile strength of the native ACL, improving the strength of the scaffold through increased crosslinking or the addition of a reinforcement should be explored. A potential future study of this chitosan-gelatin hydrogel could examine the effect of varying the OPC percentage on the tensile modulus of the detached hydrogel. Previous work has investigated the incorporation of springs and fibres with success in increasing the tensile modulus of the hydrogel construct [226, 317]. The development of this hydrogel allows for flexibility in the composition of the scaffold in which a central reinforcement, such as a spring or fibres, could be applied.

Continued improvements to the osseous anchors would be beneficial in creating a more natural enthesis. The anchor was originally designed to be composed entirely of composite hydrogel, which was hypothesized to create the graded fibrocartilage junction and decrease the risk of delamination between the chitosan-gelatin hydrogel and composite hydrogel at the interface [52]. Though, the progression of this research favoured a reinforced anchor with increased mechanical strength. While this research utilized acetal as the material for the osseous anchors, other calcium phosphate ceramics and bioglasses, magnesium and its alloys, and titanium and its alloys could be investigated due to their use in other orthopaedic applications [531, 532]. The anchors composed of only composite hydrogel showed some promise, however the fabrication of these anchors would need to be considerably improved before further cell culture and bioreactor experiments could take place. Further, the interface between the composite hydrogel and chitosan-gelatin hydrogel should be investigated before and after mechanical stimulation to better understand the mechanical limitations of this tissue engineering construct.

In the literature, there are few studies that have developed an entire sinew construct, consisting of a ligamentous midsubstance and two entheses. Further, investigation of the mechanical properties of the sinew construct prior to and after mechanical stimulation is limited. Due to the fabrication of the hydrogel sinews and limited PFib numbers, the measurement of the tensile modulus and elongation at failure of the hydrogel sinew following mechanical stimulation was unable to be measured. The tensile properties of the sinew before and after mechanical stimulation should be investigated in further research of this hydrogel sinew.

Overall, the chitosan-gelatin hydrogel has proven to be a malleable material that has the potential to be used in a wide variety of applications. As a detached scaffold, the tensile modulus suggests that it is most suitable for light load bearing applications, such as neural, kidney, or endothelial tissue engineering. Further modifications and alterations to this hydrogel composition can expand its use. The tensile loading bioreactor can be a useful model for ligament tissue engineering and has the capacity to accommodate a range of scaffold materials.

9. References

1. Batty, L.M., et al., *Synthetic devices for reconstructive surgery of the cruciate ligaments: a systematic review.* Arthroscopy: The Journal of Arthroscopic & Related Surgery, 2015. **31**(5): p. 957-968.
2. Ghalayini, S., et al., *Arthroscopic anterior cruciate ligament surgery: Results of autogenous patellar tendon graft versus the Leeds-Keio synthetic graft: Five year follow-up of a prospective randomised controlled trial.* The Knee, 2010. **17**(5): p. 334-339.
3. Dheerendra, S.K., et al., *Suppl 2: Anterior Cruciate Ligament Graft Choices: A Review of Current Concepts.* The open orthopaedics journal, 2012. **6**: p. 281.
4. Petrigliano, F.A., D.R. McAllister, and B.M. Wu, *Tissue engineering for anterior cruciate ligament reconstruction: a review of current strategies.* Arthroscopy: The Journal of Arthroscopic & Related Surgery, 2006. **22**(4): p. 441-451.
5. Legnani, C., et al., *Anterior cruciate ligament reconstruction with synthetic grafts. A review of literature.* International orthopaedics, 2010. **34**(4): p. 465-471.
6. Kdolsky, R., et al., *Measurement of stress-strain relationship and stress relaxation in various synthetic ligaments.* Knee Surgery, Sports Traumatology, Arthroscopy, 1994. **2**(1): p. 47-49.
7. Ge, Z., et al., *Biomaterials and scaffolds for ligament tissue engineering.* Journal of Biomedical Materials Research Part A: An Official Journal of The Society for Biomaterials, The Japanese Society for Biomaterials, and The Australian Society for Biomaterials and the Korean Society for Biomaterials, 2006. **77**(3): p. 639-652.
8. Wang, T., et al., *Bioreactor design for tendon/ligament engineering.* Tissue Engineering Part B: Reviews, 2012. **19**(2): p. 133-146.
9. Alshomer, F., C. Chaves, and D.M. Kalaskar, *Advances in tendon and ligament tissue engineering: materials perspective.* Journal of Materials, 2018. **2018**.
10. Butler, D.L., N. Juncosa, and M.R. Dressler, *Functional efficacy of tendon repair processes.* Annu. Rev. Biomed. Eng., 2004. **6**: p. 303-329.
11. Leiter, J.R., et al., *Long-term follow-up of ACL reconstruction with hamstring autograft.* Knee Surgery, Sports Traumatology, Arthroscopy, 2014. **22**(5): p. 1061-1069.
12. Arnoczky, S.P., *Anatomy of the anterior cruciate ligament.* Clinical orthopaedics and related research, 1983(172): p. 19-25.
13. Odensten, M. and J. Gillquist, *Functional anatomy of the anterior cruciate ligament and a rationale for reconstruction.* The Journal of bone and joint surgery. American volume, 1985. **67**(2): p. 257-262.
14. Yang, G., B.B. Rothrauff, and R.S. Tuan, *Tendon and ligament regeneration and repair: clinical relevance and developmental paradigm.* Birth defects research part C: embryo today: reviews, 2013. **99**(3): p. 203-222.
15. Woo, S.L., et al., *Tissue engineering of ligament and tendon healing.* Clinical Orthopaedics and Related Research®, 1999. **367**: p. S312-S323.

16. Paxton, J.Z., et al., *Factors affecting the longevity and strength in an in vitro model of the bone–ligament interface.* Annals of biomedical engineering, 2010. **38**(6): p. 2155-2166.
17. Laurencin, C.T., et al., *Tissue engineering: orthopedic applications.* Annual review of biomedical engineering, 1999. **1**(1): p. 19-46.
18. Schwartz, A.G., et al., *Mineral distributions at the developing tendon enthesis.* PloS one, 2012. **7**(11).
19. Saber, S., et al., *Flexor tendon tissue engineering: bioreactor cyclic strain increases construct strength.* Tissue Engineering Part A, 2010. **16**(6): p. 2085-2090.
20. Franchi, M., et al., *Collagen structure of tendon relates to function.* TheScientificWorldJOURNAL, 2007. **7**.
21. Kjær, M., et al., *From mechanical loading to collagen synthesis, structural changes and function in human tendon.* Scandinavian journal of medicine & science in sports, 2009. **19**(4): p. 500-510.
22. Kaynak, M., et al., *Genetic variants and anterior cruciate ligament rupture: a systematic review.* Sports Medicine, 2017. **47**(8): p. 1637-1650.
23. Ma, J., et al., *Cyclic stretch induced gene expression of extracellular matrix and adhesion molecules in human periodontal ligament cells.* Archives of oral biology, 2015. **60**(3): p. 447-455.
24. Amiel, D., et al., *Tendons and ligaments: a morphological and biochemical comparison.* Journal of Orthopaedic Research, 1983. **1**(3): p. 257-265.
25. Parmar, K., *Tendon and ligament: basic science, injury and repair.* Orthopaedics and Trauma, 2018. **32**(4): p. 241-244.
26. Goodship, A.E., H.L. Birch, and A.M. Wilson, *The pathobiology and repair of tendon and ligament injury.* Veterinary Clinics of North America: Equine Practice, 1994. **10**(2): p. 323-349.
27. September, A.V., M.P. Schwellnus, and M. Collins, *Tendon and ligament injuries: the genetic component.* British journal of sports medicine, 2007. **41**(4): p. 241-246.
28. Sharma, P. and N. Maffulli, *Basic biology of tendon injury and healing.* The surgeon, 2005. **3**(5): p. 309-316.
29. Murray, M.M., P. Vavken, and B.C. Fleming, *The ACL handbook.* NY: Springer, 2013.
30. Girgis, F.G., J.L. Marshall, and A. Monajem, *The cruciate ligaments of the knee joint. Anatomical, functional and experimental analysis.* Clinical orthopaedics and related research, 1975(106): p. 216-231.
31. Boden, B.P., et al., *Mechanisms of anterior cruciate ligament injury.* Orthopedics, 2000. **23**(6): p. 573-578.
32. Mengsteab, P.Y., et al., *Regenerative Engineering of the Anterior Cruciate Ligament*, in *Regenerative Strategies for the Treatment of Knee Joint Disabilities*. 2017, Springer. p. 391-410.
33. Øiestad, B.E., et al., *Winner of the 2008 systematic review competition: knee osteoarthritis after anterior cruciate ligament injury.* The American journal of sports medicine, 2009. **37**(7): p. 1434-1443.
34. Clatworthy, M. and A. Amendola, *The anterior cruciate ligament and arthritis.* Clinics in sports medicine, 1999. **18**(1): p. 173-198.
35. Blackburn, T.A. and E. Craig, *Knee anatomy: a brief review.* Physical therapy, 1980. **60**(12): p. 1556-1560.

36. Goldblatt, J.P. and J.C. Richmond, *Anatomy and biomechanics of the knee.* Operative Techniques in Sports Medicine, 2003. **11**(3): p. 172-186.
37. Kaplan, E.B., *Some aspects of functional anatomy of the human knee joint.* Clinical Orthopaedics and Related Research®, 1962. **23**: p. 18-29.
38. Flandry, F. and G. Hommel, *Normal anatomy and biomechanics of the knee.* Sports medicine and arthroscopy review, 2011. **19**(2): p. 82-92.
39. Moore, K.L., A.M. Agur, and A.F. Dalley, *Essential clinical anatomy*. 2015: Wolters Kluwer Health.
40. Hall-Craggs, E.C., *Anatomy as a basis for clinical medicine*. 1990: Urban & Schwarzenberg.
41. Toy, B.J., et al., *Arterial supply to the human anterior cruciate ligament.* Journal of athletic training, 1995. **30**(2): p. 149.
42. Petersen, W. and B. Tillmann, *Anatomy and function of the anterior cruciate ligament.* Der Orthopade, 2002. **31**(8): p. 710-718.
43. Lee, S.H., et al., *Extrasynovial spaces of the cruciate ligaments: anatomy, MR imaging, and diagnostic implications.* AJR. American journal of roentgenology, 1996. **166**(6): p. 1433-1437.
44. Amiel, D., et al., *Synovial fluid nutrient delivery in the diathrial joint: an analysis of rabbit knee ligaments.* Journal of Orthopaedic research, 1986. **4**(1): p. 90-95.
45. Magnussen, R.A., et al., *A CT-based classification of prior ACL femoral tunnel location for planning revision ACL surgery.* Knee Surgery, Sports Traumatology, Arthroscopy, 2012. **20**(7): p. 1298-1306.
46. Jackson, D.W. and S.I. Gasser, *Tibial tunnel placement in ACL reconstruction.* Arthroscopy, 1994. **10**(2): p. 124-131.
47. Burkart, A., et al., *Precision of ACL tunnel placement using traditional and robotic techniques.* Computer Aided Surgery, 2001. **6**(5): p. 270-278.
48. Kaseta, M.K., et al., *Reconstruction technique affects femoral tunnel placement in ACL reconstruction.* Clinical orthopaedics and related research, 2008. **466**(6): p. 1467-1474.
49. Petersen, W., et al., *Technique of anatomical footprint reconstruction of the ACL with oval tunnels and medial portal aimers.* Archives of orthopaedic and trauma surgery, 2013. **133**(6): p. 827-833.
50. Rosenberg, T.D., *Method for acl reconstruction*. 1992, Google Patents.
51. Benjamin, M., et al., *The "enthesis organ" concept: why enthesopathies may not present as focal insertional disorders.* Arthritis & Rheumatism: Official Journal of the American College of Rheumatology, 2004. **50**(10): p. 3306-3313.
52. Apostolakos, J., et al., *The enthesis: a review of the tendon-to-bone insertion.* Muscles, ligaments and tendons journal, 2014. **4**(3): p. 333.
53. Zhao, L., A. Thambyah, and N.D. Broom, *A multi-scale structural study of the porcine anterior cruciate ligament tibial enthesis.* Journal of anatomy, 2014. **224**(6): p. 624-633.
54. Shaw, H. and M. Benjamin, *Structure–function relationships of entheses in relation to mechanical load and exercise.* Scandinavian journal of medicine & science in sports, 2007. **17**(4): p. 303-315.
55. Arliani, G.G., et al., *Three dimensional anatomy of the anterior cruciate ligament: a new approach in anatomical orthopedic studies and a literature review.* Open access journal of sports medicine, 2012. **3**: p. 183-188.

56. Borbon, C.A., G. Mouzopoulos, and R. Siebold, *Why perform an ACL augmentation?* Knee surgery, sports traumatology, arthroscopy, 2012. **20**(2): p. 245-251.
57. Adachi, N., et al., *Mechanoreceptors in the anterior cruciate ligament contribute to the joint position sense.* Acta Orthopaedica Scandinavica, 2002. **73**(3): p. 330-334.
58. Nyland, J., et al., *Permanent knee sensorimotor system changes following ACL injury and surgery.* Knee Surgery, Sports Traumatology, Arthroscopy, 2017. **25**(5): p. 1461-1474.
59. Pandy, M.G. and K.B. Shelburne, *Dependence of cruciate-ligament loading on muscle forces and external load.* Journal of biomechanics, 1997. **30**(10): p. 1015-1024.
60. Yagi, M., et al., *Biomechanical analysis of an anatomic anterior cruciate ligament reconstruction.* The American journal of sports medicine, 2002. **30**(5): p. 660-666.
61. Markatos, K., et al., *The anatomy of the ACL and its importance in ACL reconstruction.* European Journal of Orthopaedic Surgery & Traumatology, 2013. **23**(7): p. 747-752.
62. Beynnon, B.D. and B.C. Fleming, *Anterior cruciate ligament strain in-vivo: a review of previous work.* Journal of biomechanics, 1998. **31**(6): p. 519-525.
63. Gao, J., et al., *The morphology of ligament insertions after failure at low strain velocity: an evaluation of ligament entheses in the rabbit knee.* Journal of anatomy, 1996. **189**(Pt 1): p. 127.
64. Siebold, R. and F.H. Fu, *Assessment and augmentation of symptomatic anteromedial or posterolateral bundle tears of the anterior cruciate ligament.* Arthroscopy: The Journal of Arthroscopic & Related Surgery, 2008. **24**(11): p. 1289-1298.
65. Liu, S.H., et al., *Collagen in tendon, ligament, and bone healing: a current review.* Clinical Orthopaedics and Related Research®, 1995. **318**: p. 265-278.
66. Amiel, D., et al., *Intrinsic properties of ACL and MCL cells and their responses to growth factors.* Medicine and science in sports and exercise, 1995. **27**(6): p. 844-851.
67. Riley, G., *Tendon and ligament biochemistry and pathology.* Soft tissue rheumatology, 2004. **2053**: p. 3-39.
68. Kharaz, Y.A., et al., *Variations in internal structure, composition and protein distribution between intra-and extra-articular knee ligaments and tendons.* Journal of anatomy, 2018. **232**(6): p. 943-955.
69. Marumo, K., et al., *The "ligamentization" process in human anterior cruciate ligament reconstruction with autogenous patellar and hamstring tendons: a biochemical study.* The American journal of sports medicine, 2005. **33**(8): p. 1166-1173.
70. Fujii, K., et al., *Biochemical properties of collagen from ligaments and periarticular tendons of the human knee.* Knee Surgery, Sports Traumatology, Arthroscopy, 1994. **2**(4): p. 229-233.
71. Min, B.-H., et al., *The origin of cells that repopulate patellar tendons used for reconstructing anterior cruciate ligaments in man.* The Journal of bone and joint surgery. British volume, 2003. **85**(5): p. 753-757.
72. Ristaniemi, A., et al., *Comparison of water, hydroxyproline, uronic acid and elastin contents of bovine knee ligaments and patellar tendon and their*

relationships with biomechanical properties. Journal of the Mechanical Behavior of Biomedical Materials, 2020. **104**: p. 103639.
73. Cheng, W., et al., *The content and ratio of type I and III collagen in skin differ with age and injury.* African Journal of Biotechnology, 2011. **10**(13): p. 2524-2529.
74. Juneja, S.C., *Defects in Tendon, Ligament, and Enthesis in Response to Genetic Alterations in Key Proteoglycans and Glycoproteins.* 2019.
75. Yoon, J.H. and J. Halper, *Tendon proteoglycans: biochemistry and function.* J Musculoskelet Neuronal Interact, 2005. **5**(1): p. 22-34.
76. Sopakayang, R. and G.A. Holzapfel, *A Constitutive Model of Ligaments and Tendons Accounting for Fiber-Matrix Interaction.* International Journal of Biomedical and Biological Engineering, 2017. **11**(5): p. 245-249.
77. Liu, W., et al., *Spontaneous and experimental osteoarthritis in dog: similarities and differences in proteoglycan levels.* Journal of orthopaedic research, 2003. **21**(4): p. 730-737.
78. Mannion, S., et al., *Genes encoding proteoglycans are associated with the risk of anterior cruciate ligament ruptures.* British journal of sports medicine, 2014. **48**(22): p. 1640-1646.
79. Ilic, M.Z., et al., *Proteoglycans and catabolic products of proteoglycans present in ligament.* Biochemical Journal, 2005. **385**(2): p. 381-388.
80. Qu, D., et al., *Compositional mapping of the mature anterior cruciate ligament-to-bone insertion.* Journal of Orthopaedic Research, 2017. **35**(11): p. 2513-2523.
81. Vogel, K.G., et al., *Proteoglycans in the compressed region of human tibialis posterior tendon and in ligaments.* Journal of orthopaedic research, 1993. **11**(1): p. 68-77.
82. Vogel, K.G. and S.P. Evanko, *Proteoglycans of fetal bovine tendon.* Journal of Biological Chemistry, 1987. **262**(28): p. 13607-13613.
83. Ross, S.M., R. Joshi, and C.B. Frank, *Establishment and comparison of fibroblast cell lines from the medial collateral and anterior cruciate ligaments of the rabbit.* In vitro cellular & developmental biology, 1990. **26**(6): p. 579-584.
84. Cięszczyk, P., et al., *Are genes encoding proteoglycans really associated with the risk of anterior cruciate ligament rupture?* Biology of sport, 2017. **34**(2): p. 97.
85. Young, K., et al., *Extracellular matrix content of ruptured anterior cruciate ligament tissue.* The Knee, 2011. **18**(4): p. 242-246.
86. Weiss, M., F.N. Unterhauser, and A. Weiler, *Crimp frequency is strongly correlated to myofibroblast density in the human anterior cruciate ligament and its autologous tendon grafts.* Knee Surgery, Sports Traumatology, Arthroscopy, 2012. **20**(5): p. 889-895.
87. Franchi, M., et al., *Crimp morphology in relaxed and stretched rat Achilles tendon.* Journal of anatomy, 2007. **210**(1): p. 1-7.
88. Surrao, D.C., et al., *A crimp-like microarchitecture improves tissue production in fibrous ligament scaffolds in response to mechanical stimuli.* Acta biomaterialia, 2012. **8**(10): p. 3704-3713.
89. Freeman, J.W. and A.L. Kwansa, *Recent advancements in ligament tissue engineering: the use of various techniques and materials for ACL repair.* Recent Patents on Biomedical Engineering, 2008. **1**(1): p. 18-23.

90. Woo, S.-Y., G. Johnson, and B. Smith, *Mathematical modeling of ligaments and tendons.* 1993.
91. Järvinen, T.A., et al., *Collagen fibres of the spontaneously ruptured human tendons display decreased thickness and crimp angle.* Journal of orthopaedic research, 2004. **22**(6): p. 1303-1309.
92. Stouffer, D., D. Butler, and D. Hosny, *The relationship between crimp pattern and mechanical response of human patellar tendon-bone units.* 1985.
93. Lane, J., et al., *The ligamentization process: a 4 year case study following ACL reconstruction with a semitendinosis graft.* Arthroscopy: The Journal of Arthroscopic & Related Surgery, 1993. **9**(2): p. 149-153.
94. Scheffler, S., F. Unterhauser, and A. Weiler, *Graft remodeling and ligamentization after cruciate ligament reconstruction.* Knee surgery, sports traumatology, arthroscopy, 2008. **16**(9): p. 834-842.
95. Molloy, T., Y. Wang, and G.A. Murrell, *The roles of growth factors in tendon and ligament healing.* Sports medicine, 2003. **33**(5): p. 381-394.
96. Chamberlain, C.S., E. Crowley, and R. Vanderby, *The spatio-temporal dynamics of ligament healing.* Wound repair and regeneration, 2009. **17**(2): p. 206-215.
97. Woo, S.L.-Y., et al., *Biomechanics of knee ligaments: injury, healing, and repair.* Journal of biomechanics, 2006. **39**(1): p. 1-20.
98. Herrington, L., et al., *Anterior cruciate ligament reconstruction, hamstring versus bone–patella tendon–bone grafts: a systematic literature review of outcome from surgery.* The Knee, 2005. **12**(1): p. 41-50.
99. Chen, L., V. Cooley, and T. Rosenberg, *ACL reconstruction with hamstring tendon.* The Orthopedic clinics of North America, 2003. **34**(1): p. 9-18.
100. Chang, S.K., et al., *Anterior cruciate ligament reconstruction: allograft versus autograft.* Arthroscopy: The journal of Arthroscopic & Related Surgery, 2003. **19**(5): p. 453-462.
101. Adachi, N., et al., *Harvesting hamstring tendons for ACL reconstruction influences postoperative hamstring muscle performance.* Archives of orthopaedic and trauma surgery, 2003. **123**(9): p. 460-465.
102. Edgar, C.M., et al., *Prospective comparison of auto and allograft hamstring tendon constructs for ACL reconstruction.* Clinical orthopaedics and related research, 2008. **466**(9): p. 2238-2246.
103. Amiel, D., et al., *The phenomenon of "ligamentization": anterior cruciate ligament reconstruction with autogenous patellar tendon.* Journal of orthopaedic research, 1986. **4**(2): p. 162-172.
104. Janssen, R.P. and S.U. Scheffler, *Intra-articular remodelling of hamstring tendon grafts after anterior cruciate ligament reconstruction.* Knee surgery, sports traumatology, arthroscopy, 2014. **22**(9): p. 2102-2108.
105. Freedman, K.B., et al., *Arthroscopic anterior cruciate ligament reconstruction: a metaanalysis comparing patellar tendon and hamstring tendon autografts.* The American journal of sports medicine, 2003. **31**(1): p. 2-11.
106. Bach, B.R., et al., *Arthroscopically assisted anterior cruciate ligament reconstruction using patellar tendon autograft.* The American journal of sports medicine, 1998. **26**(1): p. 20-29.
107. Sachs, R.A., et al., *Patellofemoral problems after anterior cruciate ligament reconstruction.* The American journal of sports medicine, 1989. **17**(6): p. 760-765.

108. Bellier, G., et al., *Double-stranded hamstring graft for anterior cruciate ligament reconstruction.* Arthroscopy: The Journal of Arthroscopic & Related Surgery, 2004. **20**(8): p. 890-894.
109. Nikolaou, V.S., N. Efstathopoulos, and T. Wredmark, *Hamstring tendons regeneration after ACL reconstruction: an overview.* Knee Surgery, Sports Traumatology, Arthroscopy, 2007. **15**(2): p. 153-160.
110. Zaffagnini, S., et al., *Single-bundle patellar tendon versus non-anatomical double-bundle hamstrings ACL reconstruction: a prospective randomized study at 8-year minimum follow-up.* Knee Surgery, Sports Traumatology, Arthroscopy, 2011. **19**(3): p. 390-397.
111. Siebold, R., C. Dehler, and T. Ellert, *Prospective randomized comparison of double-bundle versus single-bundle anterior cruciate ligament reconstruction.* Arthroscopy: The Journal of Arthroscopic & Related Surgery, 2008. **24**(2): p. 137-145.
112. Siebold, R., et al., *Primary ACL reconstruction with fresh-frozen patellar versus Achilles tendon allografts.* Archives of orthopaedic and trauma surgery, 2003. **123**(4): p. 180-185.
113. Whitlock, P.W., et al., *A naturally derived, cytocompatible, and architecturally optimized scaffold for tendon and ligament regeneration.* Biomaterials, 2007. **28**(29): p. 4321-4329.
114. Milthorpe, B.K., *Xenografts for tendon and ligament repair.* Biomaterials, 1994. **15**(10): p. 745-752.
115. Rihn, J.A., et al., *Does irradiation affect the clinical outcome of patellar tendon allograft ACL reconstruction?* Knee Surgery, Sports Traumatology, Arthroscopy, 2006. **14**(9): p. 885-896.
116. Cohen, S.B. and J.K. Sekiya, *Allograft safety in anterior cruciate ligament reconstruction.* Clinics in sports medicine, 2007. **26**(4): p. 597-605.
117. Baer, G.S. and C.D. Harner, *Clinical outcomes of allograft versus autograft in anterior cruciate ligament reconstruction.* Clinics in sports medicine, 2007. **26**(4): p. 661-681.
118. Leong, N.L., F.A. Petrigliano, and D.R. McAllister, *Current tissue engineering strategies in anterior cruciate ligament reconstruction.* Journal of biomedical materials research Part A, 2014. **102**(5): p. 1614-1624.
119. Romanini, E., et al., *Graft selection in arthroscopic anterior cruciate ligament reconstruction.* Journal of orthopaedics and traumatology, 2010. **11**(4): p. 211-219.
120. Ventura, A., et al., *Synthetic grafts for anterior cruciate ligament rupture: 19-year outcome study.* The Knee, 2010. **17**(2): p. 108-113.
121. Shaerf, D.A., et al., *Anterior cruciate ligament reconstruction best practice: a review of graft choice.* World journal of orthopedics, 2014. **5**(1): p. 23.
122. Machotka, Z., et al., *Anterior cruciate ligament repair with LARS (ligament advanced reinforcement system): a systematic review.* BMC Sports Science, Medicine and Rehabilitation, 2010. **2**(1): p. 29.
123. Parchi, P.D., et al., *Anterior cruciate ligament reconstruction with LARS™ artificial ligament results at a mean follow-up of eight years.* International orthopaedics, 2013. **37**(8): p. 1567-1574.
124. Hsu, S.-L., R. Liang, and S.L. Woo, *Functional tissue engineering of ligament healing.* BMC Sports Science, Medicine and Rehabilitation, 2010. **2**(1): p. 12.

125. Underhill, G.H., et al., *Bioengineering methods for analysis of cells in vitro.* Annual review of cell and developmental biology, 2012. **28**: p. 385-410.
126. Yates, E., et al., *Ligament tissue engineering and its potential role in anterior cruciate ligament reconstruction.* Stem cells international, 2011. **2012**.
127. Petrigliano, F.A., et al., *In vivo evaluation of electrospun polycaprolactone graft for anterior cruciate ligament engineering.* Tissue Engineering Part A, 2015. **21**(7-8): p. 1228-1236.
128. Nau, T. and A. Teuschl, *Regeneration of the anterior cruciate ligament: Current strategies in tissue engineering.* World journal of orthopedics, 2015. **6**(1): p. 127.
129. Lannutti, J., et al., *Electrospinning for tissue engineering scaffolds.* Materials Science and Engineering: C, 2007. **27**(3): p. 504-509.
130. Laurencin, C.T. and J.W. Freeman, *Ligament tissue engineering: an evolutionary materials science approach.* Biomaterials, 2005. **26**(36): p. 7530-7536.
131. Sahoo, S., et al., *Characterization of a novel polymeric scaffold for potential application in tendon/ligament tissue engineering.* Tissue engineering, 2006. **12**(1): p. 91-99.
132. Ge, Z., J.C.H. Goh, and E.H. Lee, *Selection of cell source for ligament tissue engineering.* Cell transplantation, 2005. **14**(8): p. 573-583.
133. Van Eijk, F., et al., *Tissue engineering of ligaments: a comparison of bone marrow stromal cells, anterior cruciate ligament, and skin fibroblasts as cell source.* Tissue engineering, 2004. **10**(5-6): p. 893-903.
134. Hoffmann, A. and G. Gross, *Tendon and ligament engineering in the adult organism: mesenchymal stem cells and gene-therapeutic approaches.* International orthopaedics, 2007. **31**(6): p. 791-797.
135. Vunjak-Novakovic, G., et al., *Tissue engineering of ligaments.* Annu. Rev. Biomed. Eng., 2004. **6**: p. 131-156.
136. Altman, G.H., et al., *Advanced bioreactor with controlled application of multi-dimensional strain for tissue engineering.* J. Biomech. Eng., 2002. **124**(6): p. 742-749.
137. Tellado, S.F., E.R. Balmayor, and M. Van Griensven, *Strategies to engineer tendon/ligament-to-bone interface: Biomaterials, cells and growth factors.* Advanced drug delivery reviews, 2015. **94**: p. 126-140.
138. Kuo, C.K., J.E. Marturano, and R.S. Tuan, *Novel strategies in tendon and ligament tissue engineering: advanced biomaterials and regeneration motifs.* BMC sports science, medicine and rehabilitation, 2010. **2**(1): p. 20.
139. Hogan, M.V., et al., *Tissue engineering of ligaments for reconstructive surgery.* Arthroscopy: The Journal of Arthroscopic & Related Surgery, 2015. **31**(5): p. 971-979.
140. Chaudhuri, J.B., *Design of Bioreactor Systems for Tissue Engineering*. 2015, Multidisciplinary Digital Publishing Institute.
141. Edwards, S., et al., *Design of nonwoven scaffold structures for tissue engineering of the anterior cruciate ligament.* AUTEX Research Journal, 2004. **4**(2): p. 86-94.
142. Yilgor, C., P. Yilgor Huri, and G. Huri, *Tissue engineering strategies in ligament regeneration.* Stem cells international, 2012. **2012**.
143. Ponsonnet, L., et al., *Effect of surface topography and chemistry on adhesion, orientation and growth of fibroblasts on nickel–titanium substrates.* Materials Science and Engineering: C, 2002. **21**(1-2): p. 157-165.

144. Fan, H., et al., *Anterior cruciate ligament regeneration using mesenchymal stem cells and silk scaffold in large animal model.* Biomaterials, 2009. **30**(28): p. 4967-4977.
145. Arthur, A., A. Zannettino, and S. Gronthos, *The therapeutic applications of multipotential mesenchymal/stromal stem cells in skeletal tissue repair.* Journal of cellular physiology, 2009. **218**(2): p. 237-245.
146. Wei, X., et al., *Local administration of TGFβ-1/VEGF165 gene-transduced bone mesenchymal stem cells for Achilles allograft replacement of the anterior cruciate ligament in rabbits.* Biochemical and biophysical research communications, 2011. **406**(2): p. 204-210.
147. Sahoo, S., S.L. Toh, and J.C. Goh, *A bFGF-releasing silk/PLGA-based biohybrid scaffold for ligament/tendon tissue engineering using mesenchymal progenitor cells.* Biomaterials, 2010. **31**(11): p. 2990-2998.
148. Cooper Jr, J.A., et al., *Evaluation of the anterior cruciate ligament, medial collateral ligament, achilles tendon and patellar tendon as cell sources for tissue-engineered ligament.* Biomaterials, 2006. **27**(13): p. 2747-2754.
149. Kim, S.-G., et al., *Gene expression of type I and type III collagen by mechanical stretch in anterior cruciate ligament cells.* Cell structure and function, 2002. **27**(3): p. 139-144.
150. Brune, T., et al., *In vitro comparison of human fibroblasts from intact and ruptured ACL for use in tissue engineering.* Eur Cell Mater, 2007. **14**(0): p. 78-91.
151. Vavken, P., S.M. Joshi, and M.M. Murray, *Fibrin concentration affects ACL fibroblast proliferation and collagen synthesis.* The Knee, 2011. **18**(1): p. 42-46.
152. Bellincampi, L.D., et al., *Viability of fibroblast-seeded ligament analogs after autogenous implantation.* Journal of Orthopaedic Research, 1998. **16**(4): p. 414-420.
153. Spindler, K., et al., *Expression of collagen and matrix metalloproteinases in ruptured human anterior cruciate ligament: an in situ hybridization study.* Journal of orthopaedic research, 1996. **14**(6): p. 857-861.
154. Murray, M.M., S. Martin, and M. Spector, *Migration of cells from human anterior cruciate ligament explants into collagen-glycosaminoglycan scaffolds.* Journal of Orthopaedic Research, 2000. **18**(4): p. 557-564.
155. Murray, M.M. and M. Spector, *The migration of cells from the ruptured human anterior cruciate ligament into collagen-glycosaminoglycan regeneration templates in vitro.* Biomaterials, 2001. **22**(17): p. 2393-2402.
156. Alberts, B., et al., *Fibroblasts and their transformations: the connective-tissue cell family*, in *Molecular Biology of the Cell. 4th edition*. 2002, Garland Science.
157. Gantenbein, B., et al., *Mesenchymal stem cells and collagen patches for anterior cruciate ligament repair.* World journal of stem cells, 2015. **7**(2): p. 521.
158. Stalling, S.S. and S.B. Nicoll, *Fetal ACL fibroblasts exhibit enhanced cellular properties compared with adults.* Clinical orthopaedics and related research, 2008. **466**(12): p. 3130-3137.
159. Calejo, I., R. Costa-Almeida, and M.E. Gomes, *Cellular complexity at the interface: Challenges in enthesis tissue engineering.* Cell Biology and Translational Medicine, Volume 5: Stem Cells: Translational Science to Therapy, 2019: p. 71-90.

160. Thomopoulos, S., et al., *Variation of biomechanical, structural, and compositional properties along the tendon to bone insertion site.* Journal of orthopaedic research, 2003. **21**(3): p. 413-419.
161. Benjamin, M., et al., *The skeletal attachment of tendons—tendon 'entheses'.* Comparative Biochemistry and Physiology Part A: Molecular & Integrative Physiology, 2002. **133**(4): p. 931-945.
162. Benjamin, M., et al., *Where tendons and ligaments meet bone: attachment sites ('entheses') in relation to exercise and/or mechanical load.* Journal of anatomy, 2006. **208**(4): p. 471-490.
163. Kuntz, L.A., et al., *Biomarkers for tissue engineering of the tendon-bone interface.* PloS one, 2018. **13**(1).
164. Lu, H.H. and S. Thomopoulos, *Functional attachment of soft tissues to bone: development, healing, and tissue engineering.* Annual review of biomedical engineering, 2013. **15**: p. 201-226.
165. Spalazzi, J., et al., *Characterization of the mechanical properties, structure, and composition of the anterior cruciate ligament-bone insertion site.* Ligament, 2004. **1**(2.98): p. 0.57.
166. Qu, D., et al., *Engineering complex orthopaedic tissues via strategic biomimicry.* Annals of biomedical engineering, 2015. **43**(3): p. 697-717.
167. Smith, L., et al., *Tissue-engineering strategies for the tendon/ligament-to-bone insertion.* Connective tissue research, 2012. **53**(2): p. 95-105.
168. Wilson, C.G., J.F. Nishimuta, and M.E. Levenston, *Chondrocytes and meniscal fibrochondrocytes differentially process aggrecan during de novo extracellular matrix assembly.* Tissue Engineering Part A, 2009. **15**(7): p. 1513-1522.
169. Moffat, K.L., et al., *Orthopedic interface tissue engineering for the biological fixation of soft tissue grafts.* Clinics in sports medicine, 2009. **28**(1): p. 157-176.
170. Beaulieu, M.L., et al., *On the heterogeneity of the femoral enthesis of the human ACL: microscopic anatomy and clinical implications.* Journal of experimental orthopaedics, 2016. **3**(1): p. 14.
171. Mutsuzaki, H., et al., *Calcium-phosphate-hybridized tendon directly promotes regeneration of tendon-bone insertion.* Journal of Biomedical Materials Research Part A, 2004. **70**(2): p. 319-327.
172. Nukavarapu, S., J. Freeman, and C. Laurencin, *Regenerative engineering of musculoskeletal tissues and interfaces*. 2015: Woodhead Publishing.
173. Xu, K., et al., *Efficient decellularization for tissue engineering of the tendon-bone interface with preservation of biomechanics.* PloS one, 2017. **12**(2).
174. Locke, R.C., A.C. Abraham, and M.L. Killian, *Orthopedic Interface Repair Strategies Based on Native Structural and Mechanical Features of the Multiscale Enthesis.* ACS Biomaterials Science & Engineering, 2017. **3**(11): p. 2633-2643.
175. Ma, J., et al., *Three-dimensional engineered bone–ligament–bone constructs for anterior cruciate ligament replacement.* Tissue engineering part A, 2012. **18**(1-2): p. 103-116.
176. Schlecht, S.H., *Understanding entheses: bridging the gap between clinical and anthropological perspectives.* The Anatomical Record: Advances in Integrative Anatomy and Evolutionary Biology, 2012. **295**(8): p. 1239-1251.

177. Beaulieu, M.L., et al., *Quantitative comparison of the microscopic anatomy of the human ACL femoral and tibial entheses.* Journal of Orthopaedic Research, 2015. **33**(12): p. 1811-1817.
178. Schwartz, A.G., F. Long, and S. Thomopoulos, *Enthesis fibrocartilage cells originate from a population of Hedgehog-responsive cells modulated by the loading environment.* Development, 2015. **142**(1): p. 196-206.
179. Sun, W., K. Moffat, and H. Lu, *Characterization of fibrochondrocytes derived from the ligament-bone insertion.* Transactions of the Orthopaedic Research Society, 2007. **32**.
180. Spalazzi, J.P., et al., *Mechanoactive scaffold induces tendon remodeling and expression of fibrocartilage markers.* Clinical orthopaedics and related research, 2008. **466**(8): p. 1938-1948.
181. Dyment, N.A., et al., *Gdf5 progenitors give rise to fibrocartilage cells that mineralize via hedgehog signaling to form the zonal enthesis.* Developmental biology, 2015. **405**(1): p. 96-107.
182. Vanderploeg, E.J., et al., *Oscillatory tension differentially modulates matrix metabolism and cytoskeletal organization in chondrocytes and fibrochondrocytes.* Journal of Biomechanics, 2004. **37**(12): p. 1941-1952.
183. Han, X., et al., *Contribution of PTHrP to mechanical strain-induced fibrochondrogenic differentiation in entheses of Achilles tendon of miniature pigs.* Journal of biomechanics, 2014. **47**(10): p. 2406-2414.
184. Paxton, J.Z., et al., *Engineering the bone–ligament interface using polyethylene glycol diacrylate incorporated with hydroxyapatite.* Tissue Engineering Part A, 2008. **15**(6): p. 1201-1209.
185. Tien, Y.-C., et al., *Augmentation of tendon-bone healing by the use of calcium-phosphate cement.* The Journal of bone and joint surgery. British volume, 2004. **86**(7): p. 1072-1076.
186. Wen, C.Y., et al., *The use of brushite calcium phosphate cement for enhancement of bone-tendon integration in an anterior cruciate ligament reconstruction rabbit model.* Journal of Biomedical Materials Research Part B: Applied Biomaterials: An Official Journal of The Society for Biomaterials, The Japanese Society for Biomaterials, and The Australian Society for Biomaterials and the Korean Society for Biomaterials, 2009. **89**(2): p. 466-474.
187. He, P., et al., *Enhanced osteoinductivity and osteoconductivity through hydroxyapatite coating of silk-based tissue-engineered ligament scaffold.* Journal of biomedical materials research part A, 2013. **101**(2): p. 555-566.
188. Pendegrass, C., et al., *A histomorphological study of tendon reconstruction to a hydroxyapatite-coated implant: Regeneration of a neo-enthesis in vivo.* Journal of orthopaedic research, 2004. **22**(6): p. 1316-1324.
189. Perla, V., M. Sato, and T.J. Webster, *Increased skeletal muscle cell and osteoblast numbers on hydrothermally-treated nano-hydroxyapatite/collagen type I composites for entheses applications.* Journal of Biomedical Nanotechnology, 2005. **1**(3): p. 297-305.
190. Wu, G., et al., *Enhanced biological properties of biomimetic apatite fabricated polycaprolactone/chitosan nanofibrous bio-composite for tendon and ligament regeneration.* Journal of Photochemistry and Photobiology B: Biology, 2018. **178**: p. 27-32.
191. Barralet, J., et al., *Cements from nanocrystalline hydroxyapatite.* Journal of Materials Science: Materials in Medicine, 2004. **15**(4): p. 407-411.

192. Grover, L.M., et al., *Biologically mediated resorption of brushite cement in vitro.* Biomaterials, 2006. **27**(10): p. 2178-2185.
193. Huangfu, X. and J. Zhao, *Tendon-bone healing enhancement using injectable tricalcium phosphate in a dog anterior cruciate ligament reconstruction model.* Arthroscopy: The Journal of Arthroscopic & Related Surgery, 2007. **23**(5): p. 455-462.
194. Barber, F.A. and S.A. Hrnack, *Poly L-lactide co-glycolide/β-tricalcium phosphate interference screw fixation for bone-patellar tendon bone anterior cruciate ligament reconstruction.* The journal of knee surgery, 2013. **26**(06): p. 423-428.
195. Li, X., et al., *Nanofiber scaffolds with gradations in mineral content for mimicking the tendon-to-bone insertion site.* Nano letters, 2009. **9**(7): p. 2763-2768.
196. Erisken, C., D.M. Kalyon, and H. Wang, *Functionally graded electrospun polycaprolactone and β-tricalcium phosphate nanocomposites for tissue engineering applications.* Biomaterials, 2008. **29**(30): p. 4065-4073.
197. Barber, F.A. and W.D. Dockery, *Long-term absorption of β–tricalcium phosphate poly-l-lactic acid interference screws.* Arthroscopy: The Journal of Arthroscopic & Related Surgery, 2008. **24**(4): p. 441-447.
198. Mutsuzaki, H., et al., *Effect of calcium phosphate–hybridized tendon graft on biomechanical behavior in anterior cruciate ligament reconstruction in a goat model: novel technique for improving tendon-bone healing.* The american journal of sports medicine, 2011. **39**(5): p. 1059-1066.
199. Mutsuzaki, H., et al., *Calcium phosphate-hybridised tendon graft to reduce bone-tunnel enlargement after ACL reconstruction in goats.* The Knee, 2012. **19**(4): p. 455-460.
200. Mutsuzaki, H., et al., *Firm anchoring between a calcium phosphate-hybridized tendon and bone for anterior cruciate ligament reconstruction in a goat model.* Biomedical Materials, 2009. **4**(4): p. 045013.
201. Farnebo, S., et al., *Reconstruction of the Tendon–Bone Insertion With Decellularized Tendon–Bone Composite Grafts: Comparison With Conventional Repair.* The Journal of hand surgery, 2014. **39**(1): p. 65-74.
202. Bronstein, J.A., et al., *Physicochemical decellularization of composite flexor tendon–bone interface grafts.* Plastic and reconstructive surgery, 2013. **132**(1): p. 94-102.
203. Fox, P.M., et al., *Decellularized Human Tendon–Bone Grafts for Composite Flexor Tendon Reconstruction: A Cadaveric Model of Initial Mechanical Properties.* The Journal of hand surgery, 2013. **38**(12): p. 2323-2328.
204. Bonnevie, E.D. and R.L. Mauck, *Physiology and engineering of the graded interfaces of musculoskeletal junctions.* Annual review of biomedical engineering, 2018. **20**: p. 403-429.
205. Vavken, P., S. Joshi, and M.M. Murray, *TRITON-X is most effective among three decellularization agents for ACL tissue engineering.* Journal of orthopaedic research: official publication of the Orthopaedic Research Society, 2009. **27**(12): p. 1612.
206. Altman, G.H., et al., *The use of long-term bioresorbable scaffolds for anterior cruciate ligament repair.* JAAOS-Journal of the American Academy of Orthopaedic Surgeons, 2008. **16**(4): p. 177-187.

207. No, Y.J., et al., *Role of Biomaterials and Controlled Architecture on Tendon/Ligament Repair and Regeneration.* Advanced Materials, 2019: p. 1904511.
208. Badylak, S.F., D.O. Freytes, and T.W. Gilbert, *Extracellular matrix as a biological scaffold material: structure and function.* Acta biomaterialia, 2009. **5**(1): p. 1-13.
209. Park, C.H., et al., *Tissue engineering bone-ligament complexes using fiber-guiding scaffolds.* Biomaterials, 2012. **33**(1): p. 137-145.
210. Chung, S. and M.W. King, *Design concepts and strategies for tissue engineering scaffolds.* Biotechnology and applied biochemistry, 2011. **58**(6): p. 423-438.
211. Dunn, M.G., et al., *Development of fibroblast-seeded ligament analogs for ACL reconstruction.* Journal of biomedical materials research, 1995. **29**(11): p. 1363-1371.
212. Gentleman, E., et al., *Development of ligament-like structural organization and properties in cell-seeded collagen scaffolds in vitro.* Annals of biomedical engineering, 2006. **34**(5): p. 726-736.
213. Funakoshi, T., et al., *Novel chitosan-based hyaluronan hybrid polymer fibers as a scaffold in ligament tissue engineering.* Journal of Biomedical Materials Research Part A: An Official Journal of The Society for Biomaterials, The Japanese Society for Biomaterials, and The Australian Society for Biomaterials and the Korean Society for Biomaterials, 2005. **74**(3): p. 338-346.
214. Majima, T., et al., *Alginate and chitosan polyion complex hybrid fibers for scaffolds in ligament and tendon tissue engineering.* Journal of Orthopaedic Science, 2005. **10**(3): p. 302-307.
215. Kreja, L., et al., *Effects of mechanical strain on human mesenchymal stem cells and ligament fibroblasts in a textured poly (L-lactide) scaffold for ligament tissue engineering.* Journal of Materials Science: Materials in Medicine, 2012. **23**(10): p. 2575-2582.
216. Wang, H.-J., et al., *Applications and degradation of proteins used as tissue engineering materials.* Materials, 2009. **2**(2): p. 613-635.
217. Ahmed, T.A., E.V. Dare, and M. Hincke, *Fibrin: a versatile scaffold for tissue engineering applications.* Tissue Engineering Part B: Reviews, 2008. **14**(2): p. 199-215.
218. Paxton, J.Z., et al., *Monitoring sinew contraction during formation of tissue-engineered fibrin-based ligament constructs.* Tissue Engineering Part A, 2012. **18**(15-16): p. 1596-1607.
219. Hankemeier, S., et al., *Tissue engineering of tendons and ligaments by human bone marrow stromal cells in a liquid fibrin matrix in immunodeficient rats: results of a histologic study.* Archives of orthopaedic and trauma surgery, 2007. **127**(9): p. 815-821.
220. Breidenbach, A.P., et al., *Fibrin gels exhibit improved biological, structural, and mechanical properties compared with collagen gels in cell-based tendon tissue-engineered constructs.* Tissue engineering Part A, 2015. **21**(3-4): p. 438-450.
221. Jockenhoevel, S., et al., *Fibrin gel–advantages of a new scaffold in cardiovascular tissue engineering.* European journal of cardio-thoracic surgery, 2001. **19**(4): p. 424-430.

222. Shaikh, F.M., et al., *Fibrin: a natural biodegradable scaffold in vascular tissue engineering.* Cells Tissues Organs, 2008. **188**(4): p. 333-346.
223. Lin, V.S., et al., *Ligament tissue engineering using synthetic biodegradable fiber scaffolds.* Tissue engineering, 1999. **5**(5): p. 443-451.
224. Liu, H., et al., *Modification of sericin-free silk fibers for ligament tissue engineering application.* Journal of Biomedical Materials Research Part B: Applied Biomaterials, 2007. **82**(1): p. 129-138.
225. Gentleman, E., et al., *Mechanical characterization of collagen fibers and scaffolds for tissue engineering.* Biomaterials, 2003. **24**(21): p. 3805-3813.
226. Altman, G.H., et al., *Silk matrix for tissue engineered anterior cruciate ligaments.* Biomaterials, 2002. **23**(20): p. 4131-4141.
227. Cooper, J.A., et al., *Fiber-based tissue-engineered scaffold for ligament replacement: design considerations and in vitro evaluation.* Biomaterials, 2005. **26**(13): p. 1523-1532.
228. Barber, J.G., et al., *Braided nanofibrous scaffold for tendon and ligament tissue engineering.* Tissue Engineering Part A, 2013. **19**(11-12): p. 1265-1274.
229. Freeman, J.W., M.D. Woods, and C.T. Laurencin, *Tissue engineering of the anterior cruciate ligament using a braid–twist scaffold design.* Journal of biomechanics, 2007. **40**(9): p. 2029-2036.
230. Sahoo, S., et al., *Bioactive nanofibers for fibroblastic differentiation of mesenchymal precursor cells for ligament/tendon tissue engineering applications.* Differentiation, 2010. **79**(2): p. 102-110.
231. Rothrauff, B.B., et al., *Braided and stacked electrospun nanofibrous scaffolds for tendon and ligament tissue engineering.* Tissue Engineering Part A, 2017. **23**(9-10): p. 378-389.
232. Laurent, C.P., et al., *A multilayer braided scaffold for Anterior Cruciate Ligament: Mechanical modeling at the fiber scale.* Journal of the mechanical behavior of biomedical materials, 2012. **12**: p. 184-196.
233. Moffat, K.L., et al., *Novel nanofiber-based scaffold for rotator cuff repair and augmentation.* Tissue Engineering Part A, 2009. **15**(1): p. 115-126.
234. Woo, S.L.-Y., et al., *Tensile properties of the human femur-anterior cruciate ligament-tibia complex: the effects of specimen age and orientation.* The American journal of sports medicine, 1991. **19**(3): p. 217-225.
235. Rittmeister, M., et al., *The effect of strand configuration on the tensile properties of quadrupled tendon grafts.* Arthroscopy: The Journal of Arthroscopic & Related Surgery, 2002. **18**(2): p. 194-200.
236. Cen, L., et al., *Collagen tissue engineering: development of novel biomaterials and applications.* Pediatric research, 2008. **63**(5): p. 492-496.
237. Parenteau-Bareil, R., R. Gauvin, and F. Berthod, *Collagen-based biomaterials for tissue engineering applications.* Materials, 2010. **3**(3): p. 1863-1887.
238. Glowacki, J. and S. Mizuno, *Collagen scaffolds for tissue engineering.* Biopolymers: Original Research on Biomolecules, 2008. **89**(5): p. 338-344.
239. Ning, L.J., et al., *Preparation and characterization of decellularized tendon slices for tendon tissue engineering.* Journal of biomedical materials research Part A, 2012. **100**(6): p. 1448-1456.
240. Youngstrom, D.W., et al., *Functional characterization of detergent-decellularized equine tendon extracellular matrix for tissue engineering applications.* PloS one, 2013. **8**(5).

241. Tischer, T., et al., *Tissue engineering of the anterior cruciate ligament: a new method using acellularized tendon allografts and autologous fibroblasts.* Archives of orthopaedic and trauma surgery, 2007. **127**(9): p. 735-741.
242. Deeken, C., et al., *Method of preparing a decellularized porcine tendon using tributyl phosphate.* Journal of Biomedical Materials Research Part B: Applied Biomaterials, 2011. **96**(2): p. 199-206.
243. Freeman, J.W., *Tissue engineering options for ligament healing.* Bone and Tissue Regeneration Insights, 2009. **2**: p. BTRI. S2826.
244. Dong, C. and Y. Lv, *Application of collagen scaffold in tissue engineering: recent advances and new perspectives.* Polymers, 2016. **8**(2): p. 42.
245. Matthews, J.A., et al., *Electrospinning of collagen nanofibers.* Biomacromolecules, 2002. **3**(2): p. 232-238.
246. Shields, K.J., et al., *Mechanical properties and cellular proliferation of electrospun collagen type II.* Tissue engineering, 2004. **10**(9-10): p. 1510-1517.
247. Cardwell, R.D., L.A. Dahlgren, and A.S. Goldstein, *Electrospun fibre diameter, not alignment, affects mesenchymal stem cell differentiation into the tendon/ligament lineage.* Journal of tissue engineering and regenerative medicine, 2014. **8**(12): p. 937-945.
248. Sachlos, E., et al., *Novel collagen scaffolds with predefined internal morphology made by solid freeform fabrication.* Biomaterials, 2003. **24**(8): p. 1487-1497.
249. Gigante, A., et al., *Purified collagen I oriented membrane for tendon repair: an ex vivo morphological study.* Journal of Orthopaedic Research, 2013. **31**(5): p. 738-745.
250. Robayo, L.M., et al., *New ligament healing model based on tissue-engineered collagen scaffolds.* Wound Repair and Regeneration, 2011. **19**(1): p. 38-48.
251. Peng, L., et al., *Preparation and evaluation of porous chitosan/collagen scaffolds for periodontal tissue engineering.* Journal of bioactive and compatible polymers, 2006. **21**(3): p. 207-220.
252. Wang, W., et al., *Physical crosslinkings of edible collagen casing.* International journal of biological macromolecules, 2015. **81**: p. 920-925.
253. Takitoh, T., et al., *Gamma-cross-linked nonfibrillar collagen gel as a scaffold for osteogenic differentiation of mesenchymal stem cells.* Journal of bioscience and bioengineering, 2015. **119**(2): p. 217-225.
254. Yoshioka, S.A. and G. Goissis, *Thermal and spectrophotometric studies of new crosslinking method for collagen matrix with glutaraldehyde acetals.* Journal of Materials Science: Materials in Medicine, 2008. **19**(3): p. 1215-1223.
255. Moles, M.D., C.A. Scotchford, and A.C. Ritchie, *Development of an elastic cell culture substrate for a novel uniaxial tensile strain bioreactor.* Journal of Biomedical Materials Research Part A, 2014. **102**(7): p. 2356-2364.
256. Ma, L., et al., *Collagen/chitosan porous scaffolds with improved biostability for skin tissue engineering.* Biomaterials, 2003. **24**(26): p. 4833-4841.
257. Mozdzen, L.C., et al., *Increasing the strength and bioactivity of collagen scaffolds using customizable arrays of 3D-printed polymer fibers.* Acta biomaterialia, 2016. **33**: p. 25-33.
258. Mizutani, N., et al., *The behavior of ligament cells cultured on elastin and collagen scaffolds.* Journal of Artificial Organs, 2014. **17**(1): p. 50-59.

259. Mozafari, M., et al., *Synthesis and characterisation of highly interconnected porous poly (ε-caprolactone)-collagen scaffolds: a therapeutic design to facilitate tendon regeneration.* Materials technology, 2018. **33**(1): p. 29-37.
260. Zhang, Q., et al., *Characterization of polycaprolactone/collagen fibrous scaffolds by electrospinning and their bioactivity.* International journal of biological macromolecules, 2015. **76**: p. 94-101.
261. Hardy, J.G., P. Lin, and C.E. Schmidt, *Biodegradable hydrogels composed of oxime crosslinked poly (ethylene glycol), hyaluronic acid and collagen: a tunable platform for soft tissue engineering.* Journal of Biomaterials Science, Polymer Edition, 2015. **26**(3): p. 143-161.
262. Zhang, Y., et al., *Crosslinking of the electrospun gelatin nanofibers.* Polymer, 2006. **47**(8): p. 2911-2917.
263. Duconseille, A., et al., *Gelatin structure and composition linked to hard capsule dissolution: A review.* Food Hydrocolloids, 2015. **43**: p. 360-376.
264. Fan, H., et al., *Development of a silk cable-reinforced gelatin/silk fibroin hybrid scaffold for ligament tissue engineering.* Cell transplantation, 2008. **17**(12): p. 1389-1401.
265. Yang, G., et al., *Multilayered polycaprolactone/gelatin fiber-hydrogel composite for tendon tissue engineering.* Acta biomaterialia, 2016. **35**: p. 68-76.
266. Li, M., et al., *Electrospinning polyaniline-contained gelatin nanofibers for tissue engineering applications.* Biomaterials, 2006. **27**(13): p. 2705-2715.
267. Maji, K., et al., *Preparation and evaluation of gelatin-chitosan-nanobioglass 3D porous scaffold for bone tissue engineering.* International journal of biomaterials, 2016. **2016**.
268. Liu, X., et al., *Biomimetic nanofibrous gelatin/apatite composite scaffolds for bone tissue engineering.* Biomaterials, 2009. **30**(12): p. 2252-2258.
269. Andres, Y., et al., *Antibacterial effects of chitosan powder: mechanisms of action.* Environmental technology, 2007. **28**(12): p. 1357-1363.
270. Rinaudo, M., *Chitin and chitosan: properties and applications.* Progress in polymer science, 2006. **31**(7): p. 603-632.
271. Rodríguez-Vázquez, M., et al., *Chitosan and its potential use as a scaffold for tissue engineering in regenerative medicine.* BioMed research international, 2015. **2015**.
272. Ho, M.-H., et al., *Preparation of porous scaffolds by using freeze-extraction and freeze-gelation methods.* Biomaterials, 2004. **25**(1): p. 129-138.
273. Croisier, F. and C. Jérôme, *Chitosan-based biomaterials for tissue engineering.* European Polymer Journal, 2013. **49**(4): p. 780-792.
274. Elieh-Ali-Komi, D. and M.R. Hamblin, *Chitin and chitosan: production and application of versatile biomedical nanomaterials.* International journal of advanced research, 2016. **4**(3): p. 411.
275. Racine, L., I. Texier, and R. Auzély-Velty, *Chitosan-based hydrogels: recent design concepts to tailor properties and functions.* Polymer International, 2017. **66**(7): p. 981-998.
276. Madihally, S.V. and H.W. Matthew, *Porous chitosan scaffolds for tissue engineering.* Biomaterials, 1999. **20**(12): p. 1133-1142.
277. Xia, W., et al., *Tissue engineering of cartilage with the use of chitosan-gelatin complex scaffolds.* Journal of Biomedical Materials Research Part B: Applied Biomaterials: An Official Journal of The Society for Biomaterials, The Japanese Society for Biomaterials, and The Australian Society for

Biomaterials and the Korean Society for Biomaterials, 2004. **71**(2): p. 373-380.
278. Tamura, H., Y. Tsuruta, and S. Tokura, *Preparation of chitosan-coated alginate filament.* Materials Science and Engineering: C, 2002. **20**(1-2): p. 143-147.
279. Sarukawa, J., et al., *Effects of chitosan-coated fibers as a scaffold for three-dimensional cultures of rabbit fibroblasts for ligament tissue engineering.* Journal of Biomaterials Science, Polymer Edition, 2011. **22**(4-6): p. 717-732.
280. Kim, I.-Y., et al., *Chitosan and its derivatives for tissue engineering applications.* Biotechnology advances, 2008. **26**(1): p. 1-21.
281. Berger, J., et al., *Structure and interactions in covalently and ionically crosslinked chitosan hydrogels for biomedical applications.* European Journal of Pharmaceutics and Biopharmaceutics, 2004. **57**(1): p. 19-34.
282. Zhang, Y., et al., *Preparation, characterization, and evaluation of genipin crosslinked chitosan/gelatin three-dimensional scaffolds for liver tissue engineering applications.* Journal of Biomedical Materials Research Part A, 2016. **104**(8): p. 1863-1870.
283. Chiono, V., et al., *Genipin-crosslinked chitosan/gelatin blends for biomedical applications.* Journal of Materials Science: Materials in Medicine, 2008. **19**(2): p. 889-898.
284. Muzzarelli, R.A., *Genipin-crosslinked chitosan hydrogels as biomedical and pharmaceutical aids.* Carbohydrate Polymers, 2009. **77**(1): p. 1-9.
285. Monteiro Jr, O.A. and C. Airoldi, *Some studies of crosslinking chitosan–glutaraldehyde interaction in a homogeneous system.* International Journal of Biological Macromolecules, 1999. **26**(2-3): p. 119-128.
286. Ge, S., et al., *Bone repair by periodontal ligament stem cellseeded nanohydroxyapatite-chitosan scaffold.* International Journal of Nanomedicine, 2012. **7**: p. 5405.
287. Yan, X.Z., et al., *Enzymatic control of chitosan gelation for delivery of periodontal ligament cells.* Macromolecular bioscience, 2014. **14**(7): p. 1004-1014.
288. Koo, H.-J., et al., *Antiinflammatory effects of genipin, an active principle of gardenia.* European journal of pharmacology, 2004. **495**(2-3): p. 201-208.
289. Muzzarelli, R.A., et al., *Genipin-crosslinked chitosan gels and scaffolds for tissue engineering and regeneration of cartilage and bone.* Marine drugs, 2015. **13**(12): p. 7314-7338.
290. Mekhail, M., K. Jahan, and M. Tabrizian, *Genipin-crosslinked chitosan/poly-l-lysine gels promote fibroblast adhesion and proliferation.* Carbohydrate polymers, 2014. **108**: p. 91-98.
291. Gao, L., et al., *Effects of genipin cross-linking of chitosan hydrogels on cellular adhesion and viability.* Colloids and Surfaces B: Biointerfaces, 2014. **117**: p. 398-405.
292. Han, B., et al., *Proanthocyanidin: a natural crosslinking reagent for stabilizing collagen matrices.* Journal of Biomedical Materials Research Part A: An Official Journal of The Society for Biomaterials, The Japanese Society for Biomaterials, and The Australian Society for Biomaterials and the Korean Society for Biomaterials, 2003. **65**(1): p. 118-124.
293. Kim, S., et al., *Chitosan/gelatin–based films crosslinked by proanthocyanidin.* Journal of Biomedical Materials Research Part B: Applied Biomaterials: An Official Journal of The Society for Biomaterials, The

Japanese Society for Biomaterials, and The Australian Society for Biomaterials and the Korean Society for Biomaterials, 2005. **75**(2): p. 442-450.
294. Jing, Y., J. Huang, and X. Yu, *Preparation, characterization, and functional evaluation of proanthocyanidin-chitosan conjugate.* Carbohydrate polymers, 2018. **194**: p. 139-145.
295. Alfaro-Viquez, E., et al., *Cranberry proanthocyanidin-chitosan hybrid nanoparticles as a potential inhibitor of extra-intestinal pathogenic Escherichia coli invasion of gut epithelial cells.* International journal of biological macromolecules, 2018. **111**: p. 415-420.
296. Ye, X., et al., *The cytotoxic effects of a novel IH636 grape seed proanthocyanidin extract on cultured human cancer cells*, in *Stress Adaptation, Prophylaxis and Treatment*. 1999, Springer. p. 99-108.
297. Scalbert, A., et al., *Proanthocyanidins and human health: systemic effects and local effects in the gut.* Biofactors, 2000. **13**(1-4): p. 115-120.
298. Liu, B.S., *Fabrication and evaluation of a biodegradable proanthocyanidin-crosslinked gelatin conduit in peripheral nerve repair.* Journal of Biomedical Materials Research Part A: An Official Journal of The Society for Biomaterials, The Japanese Society for Biomaterials, and The Australian Society for Biomaterials and the Korean Society for Biomaterials, 2008. **87**(4): p. 1092-1102.
299. Zhang, J., et al., *HPLC detection of loss rate and cell migration of HUVECs in a proanthocyanidin cross-linked recombinant human collagen-peptide (RHC)–chitosan scaffold.* Materials Science and Engineering: C, 2015. **56**: p. 555-563.
300. Longo, U.G., et al., *Scaffolds in tendon tissue engineering.* Stem cells international, 2012. **2012**.
301. Choi, Y., H.-J. Kim, and K.-S. Min, *Effects of proanthocyanidin, a crosslinking agent, on physical and biological properties of collagen hydrogel scaffold.* Restorative dentistry & endodontics, 2016. **41**(4): p. 296-303.
302. Tsai, C.C., et al., *In vitro evaluation of the genotoxicity of a naturally occurring crosslinking agent (genipin) for biologic tissue fixation.* Journal of biomedical materials research, 2000. **52**(1): p. 58-65.
303. Nair, L.S. and C.T. Laurencin, *Biodegradable polymers as biomaterials.* Progress in polymer science, 2007. **32**(8-9): p. 762-798.
304. Lu, H.H., et al., *Anterior cruciate ligament regeneration using braided biodegradable scaffolds: in vitro optimization studies.* Biomaterials, 2005. **26**(23): p. 4805-4816.
305. Ge, Z., et al., *Characterization of knitted polymeric scaffolds for potential use in ligament tissue engineering.* Journal of Biomaterials Science, Polymer Edition, 2005. **16**(9): p. 1179-1192.
306. Wu, H.Y., et al., *Wet-spun silk fibroin scaffold with hierarchical structure for ligament tissue engineering.* Materials Letters, 2014. **135**: p. 63-66.
307. Chvapil, M., et al., *Collagen fibers as a temporary scaffold for replacement of ACL in goats.* Journal of biomedical materials research, 1993. **27**(3): p. 313-325.
308. Chen, G., et al., *Application of PLGA-collagen hybrid mesh for three-dimensional culture of canine anterior cruciate ligament cells.* Materials Science and Engineering: C, 2004. **24**(6-8): p. 861-866.

309. Surrao, D.C., S.D. Waldman, and B.G. Amsden, *Biomimetic poly (lactide) based fibrous scaffolds for ligament tissue engineering.* Acta Biomaterialia, 2012. **8**(11): p. 3997-4006.
310. Chung, E.J., et al., *A biodegradable tri-component graft for anterior cruciate ligament reconstruction.* Journal of tissue engineering and regenerative medicine, 2017. **11**(3): p. 704-712.
311. Caliari, S.R. and J.A. Burdick, *A practical guide to hydrogels for cell culture.* Nature methods, 2016. **13**(5): p. 405.
312. Park, H. and K. Park, *Hydrogels in bioapplications*. 1996.
313. Zhu, J. and R.E. Marchant, *Design properties of hydrogel tissue-engineering scaffolds.* Expert review of medical devices, 2011. **8**(5): p. 607-626.
314. Lee, K.Y. and D.J. Mooney, *Hydrogels for tissue engineering.* Chemical reviews, 2001. **101**(7): p. 1869-1880.
315. Drury, J.L. and D.J. Mooney, *Hydrogels for tissue engineering: scaffold design variables and applications.* Biomaterials, 2003. **24**(24): p. 4337-4351.
316. Hoffman, A.S., *Hydrogels for biomedical applications.* Advanced drug delivery reviews, 2012. **64**: p. 18-23.
317. Wang, A., et al., *Development of tissue engineered ligaments with titanium spring reinforcement.* RSC Advances, 2016. **6**(100): p. 98536-98544.
318. Freeman, J.W., et al., *Evaluation of a hydrogel–fiber composite for ACL tissue engineering.* Journal of biomechanics, 2011. **44**(4): p. 694-699.
319. Kim, J.H., et al., *A cell-laden hybrid fiber/hydrogel composite for ligament regeneration with improved cell delivery and infiltration.* Biomedical Materials, 2017. **12**(5): p. 055010.
320. Coburn, J., et al., *Biomimetics of the extracellular matrix: an integrated three-dimensional fiber-hydrogel composite for cartilage tissue engineering.* Smart structures and systems, 2011. **7**(3): p. 213.
321. Hong, Y., et al., *Mechanical properties and in vivo behavior of a biodegradable synthetic polymer microfiber–extracellular matrix hydrogel biohybrid scaffold.* Biomaterials, 2011. **32**(13): p. 3387-3394.
322. Thayer, P.S., et al., *Cellularized cylindrical fiber/hydrogel composites for ligament tissue engineering.* Biomacromolecules, 2014. **15**(1): p. 75-83.
323. Deepthi, S., et al., *Chitosan–hyaluronic acid hydrogel coated poly (caprolactone) multiscale bilayer scaffold for ligament regeneration.* Chemical Engineering Journal, 2015. **260**: p. 478-485.
324. Hayami, J.W., et al., *Design and characterization of a biodegradable composite scaffold for ligament tissue engineering.* Journal of Biomedical Materials Research Part A, 2010. **92**(4): p. 1407-1420.
325. Murray, M.M., et al., *Collagen-platelet rich plasma hydrogel enhances primary repair of the porcine anterior cruciate ligament.* Journal of Orthopaedic Research, 2007. **25**(1): p. 81-91.
326. Janmey, P.A., J.P. Winer, and J.W. Weisel, *Fibrin gels and their clinical and bioengineering applications.* Journal of the Royal Society Interface, 2009. **6**(30): p. 1-10.
327. Moreau, D., et al., *In vivo evaluation of the bone integration of coated poly (vinyl-alcohol) hydrogel fiber implants.* Journal of Materials Science: Materials in Medicine, 2017. **28**(8): p. 114.
328. Bach, J.S., et al., *Hydrogel fibers for ACL prosthesis: design and mechanical evaluation of PVA and PVA/UHMWPE fiber constructs.* Journal of biomechanics, 2013. **46**(8): p. 1463-1470.

329. Pörtner, R., et al., *Bioreactor design for tissue engineering.* Journal of bioscience and bioengineering, 2005. **100**(3): p. 235-245.
330. Martin, I., D. Wendt, and M. Heberer, *The role of bioreactors in tissue engineering.* TRENDS in Biotechnology, 2004. **22**(2): p. 80-86.
331. Benhardt, H.A. and E.M. Cosgriff-Hernandez, *The role of mechanical loading in ligament tissue engineering.* Tissue Engineering Part B: Reviews, 2009. **15**(4): p. 467-475.
332. Bilodeau, K. and D. Mantovani, *Bioreactors for tissue engineering: focus on mechanical constraints. A comparative review.* Tissue engineering, 2006. **12**(8): p. 2367-2383.
333. Buckwalter, J.A., *Effects of early motion on healing of musculoskeletal tissues.* Hand clinics, 1996. **12**(1): p. 13-24.
334. Zeichen, J., M. van Griensven, and U. Bosch, *The proliferative response of isolated human tendon fibroblasts to cyclic biaxial mechanical strain.* The American journal of sports medicine, 2000. **28**(6): p. 888-892.
335. Ingber, D.E., et al., *Cellular tensegrity: exploring how mechanical changes in the cytoskeleton regulate cell growth, migration, and tissue pattern during morphogenesis*, in *International review of cytology*. 1994, Elsevier. p. 173-224.
336. Connelly, J., et al. *Cyclic tensile loading influences differentiation of bovine bone marrow stromal cells in a TGF-beta dependent manner*. in *Abstract presented at the Orthopaedic Research Society Meeting, Washington, DC*. 2005.
337. Nöth, U., et al., *Anterior cruciate ligament constructs fabricated from human mesenchymal stem cells in a collagen type I hydrogel.* Cytotherapy, 2005. **7**(5): p. 447-455.
338. ALTMAN, G., et al., *Cell differentiation by mechanical stress.* The FASEB Journal, 2002. **16**(2): p. 270-272.
339. Juncosa-Melvin, N., et al., *Effects of mechanical stimulation on the biomechanics and histology of stem cell–collagen sponge constructs for rabbit patellar tendon repair.* Tissue engineering, 2006. **12**(8): p. 2291-2300.
340. Kang, S.M., L. Zou, and S.L. Woo, *THE CYCLIC INTERMITTENT STRETCH IS NOT DETRIMENTAL TO CELL PROLIFERATION IN SIS.* The Deltoid and Teres Minor Compensate for Loss of Infraspinatus and Supraspinatus Function: p. 23.
341. Paxton, J.Z., et al., *Optimizing an intermittent stretch paradigm using ERK1/2 phosphorylation results in increased collagen synthesis in engineered ligaments.* Tissue Engineering Part A, 2011. **18**(3-4): p. 277-284.
342. Abousleiman, R.I., et al., *Tendon tissue engineering using cell-seeded umbilical veins cultured in a mechanical stimulator.* Tissue engineering part A, 2009. **15**(4): p. 787-795.
343. Issa, R.I., et al., *The effect of cell seeding density on the cellular and mechanical properties of a mechanostimulated tissue-engineered tendon.* Tissue Engineering Part A, 2011. **17**(11-12): p. 1479-1487.
344. Butler, D.L., et al., *Using functional tissue engineering and bioreactors to mechanically stimulate tissue-engineered constructs.* Tissue Engineering Part A, 2009. **15**(4): p. 741-749.
345. Riboh, J., et al., *Optimization of flexor tendon tissue engineering with a cyclic strain bioreactor.* The Journal of hand surgery, 2008. **33**(8): p. 1388-1396.

346. Laurent, C., et al., *Towards a Tissue-Engineered Ligament: Design and Preliminary Evaluation of a Dedicated Multi-Chamber Tension-Torsion Bioreactor.* Processes, 2014. **2**: p. 167-179.
347. Goodhart, J.M., et al., *Design and validation of a cyclic strain bioreactor to condition spatially-selective scaffolds in dual strain regimes.* Processes, 2014. **2**(2): p. 345-360.
348. Doroski, D.M., K.S. Brink, and J.S. Temenoff, *Techniques for biological characterization of tissue-engineered tendon and ligament.* Biomaterials, 2007. **28**(2): p. 187-202.
349. Hoyer, M., et al., *In vitro characterization of self-assembled anterior cruciate ligament cell spheroids for ligament tissue engineering.* Histochemistry and cell biology, 2015. **143**(3): p. 289-300.
350. Frank, C., et al., *Optimisation of the biology of soft tissue repair.* Journal of Science and Medicine in Sport, 1999. **2**(3): p. 190-210.
351. Steinert, A.F., et al., *In situ IGF-1 gene delivery to cells emerging from the injured anterior cruciate ligament.* Biomaterials, 2008. **29**(7): p. 904-916.
352. Provenzano, P.P. and R. Vanderby Jr, *Collagen fibril morphology and organization: implications for force transmission in ligament and tendon.* Matrix Biology, 2006. **25**(2): p. 71-84.
353. Chamberlain, C.S., et al., *Quantification of collagen organization and extracellular matrix factors within the healing ligament.* Microscopy and microanalysis, 2011. **17**(5): p. 779.
354. Burk, J., et al., *Gene expression of tendon markers in mesenchymal stromal cells derived from different sources.* BMC Research Notes, 2014. **7**(1): p. 826.
355. Wang, I.N.E., et al., *Role of osteoblast–fibroblast interactions in the formation of the ligament-to-bone interface.* Journal of Orthopaedic Research, 2007. **25**(12): p. 1609-1620.
356. Pelham, R.J. and Y.-l. Wang, *Cell locomotion and focal adhesions are regulated by substrate flexibility.* Proceedings of the National Academy of Sciences, 1997. **94**(25): p. 13661-13665.
357. Chen, Y.-J., et al., *Effects of cyclic mechanical stretching on the mRNA expression of tendon/ligament-related and osteoblast-specific genes in human mesenchymal stem cells.* Connective tissue research, 2008. **49**(1): p. 7-14.
358. Schweitzer, R., et al., *Analysis of the tendon cell fate using Scleraxis, a specific marker for tendons and ligaments.* Development, 2001. **128**(19): p. 3855-3866.
359. Cyster, L., et al., *Bioengineering Research Group Cell Culture Training and Protocols Manual*. 2011, University of Nottingham.
360. Proffen, B.L., et al., *A comparative anatomical study of the human knee and six animal species.* The Knee, 2012. **19**(4): p. 493-499.
361. Allen, M.J., et al., *The surgical anatomy of the stifle joint in sheep.* Veterinary Surgery, 1998. **27**(6): p. 596-605.
362. Shortkroff, S. and M. Spector, *Isolation and in vitro proliferation of chondrocytes, tenocytes, and ligament cells*, in *Tissue engineering methods and protocols*. 1999, Springer. p. 195-203.
363. Mastrogiacomo, M., A. Derubeis, and R. Cancedda, *Bone and cartilage formation by skeletal muscle derived cells.* Journal of cellular physiology, 2005. **204**(2): p. 594-603.

364. Farndale, R.W., C.A. Sayers, and A.J. Barrett, *A direct spectrophotometric microassay for sulfated glycosaminoglycans in cartilage cultures.* Connective tissue research, 1982. **9**(4): p. 247-248.
365. Zheng, C. and M. Levenston, *Fact versus artifact: avoiding erroneous estimates of sulfated glycosaminoglycan content using the dimethylmethylene blue colorimetric assay for tissue-engineered constructs.* European cells & materials, 2015. **29**: p. 224.
366. Coulson-Thomas, V.a.G., Tarsis Ferreira, *Dimethylmethylene Blue Assay (DMMB)*. 2014: Bio-protocol.
367. Mihov, D. and M. Spiess, *Glycosaminoglycans: Sorting determinants in intracellular protein traffic.* The international journal of biochemistry & cell biology, 2015. **68**: p. 87-91.
368. Zhao, F., et al., *Preparation and histological evaluation of biomimetic three-dimensional hydroxyapatite/chitosan-gelatin network composite scaffolds.* Biomaterials, 2002. **23**(15): p. 3227-3234.
369. Padmanabhan, A. and L.S. Nair, *Chitosan hydrogels for regenerative engineering*, in *Chitin and Chitosan for Regenerative Medicine*. 2016, Springer. p. 3-40.
370. Huang, Y., et al., *In vitro characterization of chitosan–gelatin scaffolds for tissue engineering.* Biomaterials, 2005. **26**(36): p. 7616-7627.
371. Sundaram, M.N., S. Deepthi, and R. Jayakumar, *Chitosan-Gelatin composite scaffolds in bone tissue engineering*, in *Chitin and Chitosan for Regenerative Medicine*. 2016, Springer. p. 99-121.
372. Franco, R.A., T.H. Nguyen, and B.-T. Lee, *Preparation and characterization of electrospun PCL/PLGA membranes and chitosan/gelatin hydrogels for skin bioengineering applications.* Journal of Materials Science: Materials in Medicine, 2011. **22**(10): p. 2207.
373. Encerrado, A., C. Scotchford, and A. Campbell Ritchie, *Fabrication of Cost Effective Proanthocyanidin Cross-linked Chitosan-Gelatin Hydrogel Scaffolds with Tuneable Mechanical Properties for Tissue Engineering*, in *United Kingdom Society for Biomaterials*. 2017: Loughborough University p. 10.
374. Green, H. and O. Kehinde, *Sublines of mouse 3T3 cells that accumulate lipid.* Cell, 1974. **1**(3): p. 113-116.
375. England, P.H. *ECACC General Cell Collection: 3T3 Swiss Albino*. Available from: https://www.phe-culturecollections.org.uk/products/celllines/generalcell/detail.jsp?refId=85022108&collection=ecacc_gc#medDoc.
376. Pavel, M., et al., *Contact inhibition controls cell survival and proliferation via YAP/TAZ-autophagy axis.* Nature communications, 2018. **9**(1): p. 2961.
377. Discher, D.E., P. Janmey, and Y.-l. Wang, *Tissue cells feel and respond to the stiffness of their substrate.* Science, 2005. **310**(5751): p. 1139-1143.
378. Yeung, T., et al., *Effects of substrate stiffness on cell morphology, cytoskeletal structure, and adhesion.* Cell motility and the cytoskeleton, 2005. **60**(1): p. 24-34.
379. Solon, J., et al., *Fibroblast adaptation and stiffness matching to soft elastic substrates.* Biophysical journal, 2007. **93**(12): p. 4453-4461.
380. Handorf, A.M., et al., *Tissue stiffness dictates development, homeostasis, and disease progression.* Organogenesis, 2015. **11**(1): p. 1-15.

381. Sunyer, R., et al., *Fabrication of hydrogels with steep stiffness gradients for studying cell mechanical response.* PloS one, 2012. **7**(10): p. e46107.
382. Breuls, R.G., T.U. Jiya, and T.H. Smit, *Scaffold stiffness influences cell behavior: opportunities for skeletal tissue engineering.* The open orthopaedics journal, 2008. **2**: p. 103.
383. Ingber, D.E., *Cellular mechanotransduction: putting all the pieces together again.* The FASEB journal, 2006. **20**(7): p. 811-827.
384. Dado, D. and S. Levenberg. *Cell–scaffold mechanical interplay within engineered tissue*. in *Seminars in cell & developmental biology*. 2009. Elsevier.
385. Stowers, R.S., S.C. Allen, and L.J. Suggs, *Dynamic phototuning of 3D hydrogel stiffness.* Proceedings of the National Academy of Sciences, 2015. **112**(7): p. 1953-1958.
386. Ahearne, M., *Introduction to cell–hydrogel mechanosensing.* Interface focus, 2014. **4**(2): p. 20130038.
387. Hadjipanayi, E., V. Mudera, and R. Brown, *Close dependence of fibroblast proliferation on collagen scaffold matrix stiffness.* Journal of tissue engineering and regenerative medicine, 2009. **3**(2): p. 77-84.
388. Wong, T., J. McGrath, and H. Navsaria, *The role of fibroblasts in tissue engineering and regeneration.* British Journal of Dermatology, 2007. **156**(6): p. 1149-1155.
389. Hopp, I., et al., *The influence of substrate stiffness gradients on primary human dermal fibroblasts.* Biomaterials, 2013. **34**(21): p. 5070-5077.
390. Rumian, A.P., A.L. Wallace, and H.L. Birch, *Tendons and ligaments are anatomically distinct but overlap in molecular and morphological features—a comparative study in an ovine model.* Journal of orthopaedic research, 2007. **25**(4): p. 458-464.
391. Lee, J., et al., *Enhanced regeneration of the ligament–bone interface using a poly (l-lactide–co-ε-caprolactone) scaffold with local delivery of cells/BMP-2 using a heparin-based hydrogel.* Acta Biomaterialia, 2011. **7**(1): p. 244-257.
392. Nickmanesh, R., et al., *Contrast-enhanced computed tomography (CECT) attenuation is associated with stiffness of intact knee cartilage.* Journal of Orthopaedic Research®, 2018. **36**(10): p. 2641-2647.
393. Mouw, J., et al., *Variations in matrix composition and GAG fine structure among scaffolds for cartilage tissue engineering.* Osteoarthritis and Cartilage, 2005. **13**(9): p. 828-836.
394. Gilbert, P.M., et al., *Substrate elasticity regulates skeletal muscle stem cell self-renewal in culture.* Science, 2010. **329**(5995): p. 1078-1081.
395. Rho, J.Y., R.B. Ashman, and C.H. Turner, *Young's modulus of trabecular and cortical bone material: ultrasonic and microtensile measurements.* Journal of biomechanics, 1993. **26**(2): p. 111-119.
396. Institution, T.B.S., *EN ISO 10993-5:2018 Biological evaluation of medical devices*, in *Tests for in vitro cytotoxicity*. 2018.
397. Kaur, G. and J.M. Dufour, *Cell lines: Valuable tools or useless artifacts*. 2012, Taylor & Francis.
398. Pastor, D.M., et al., *Primary cell lines: false representation or model system? a comparison of four human colorectal tumors and their coordinately established cell lines.* International journal of clinical and experimental medicine, 2010. **3**(1): p. 69.

399. Nagahama, H., et al., *Preparation and characterization of novel chitosan/gelatin membranes using chitosan hydrogel.* Carbohydrate polymers, 2009. **76**(2): p. 255-260.
400. Kapacee, Z., et al., *Tension is required for fibripositor formation.* Matrix Biology, 2008. **27**(4): p. 371-375.
401. Paxton, J.Z., L.M. Grover, and K. Baar, *Engineering an in vitro model of a functional ligament from bone to bone.* Tissue Engineering Part A, 2010. **16**(11): p. 3515-3525.
402. Kang, C., et al., *Ultrathin, freestanding, stimuli-responsive, porous membranes from polymer hydrogel-brushes.* Nanoscale, 2015. **7**(30): p. 13017-13025.
403. Becker, A.L., et al., *Tuning the formation and degradation of layer-by-layer assembled polymer hydrogel microcapsules.* Langmuir, 2009. **25**(24): p. 14079-14085.
404. Mehrotra, S., et al., *Time controlled protein release from layer-by-layer assembled multilayer functionalized agarose hydrogels.* Advanced functional materials, 2010. **20**(2): p. 247-258.
405. Zhang, Y., Y. Guan, and S. Zhou, *Single component chitosan hydrogel microcapsule from a layer-by-layer approach.* Biomacromolecules, 2005. **6**(4): p. 2365-2369.
406. Wudebwe, U.N., et al., *Exploiting cell-mediated contraction and adhesion to structure tissues in vitro.* Phil. Trans. R. Soc. B, 2015. **370**(1661): p. 20140200.
407. Bayer, M.L., et al., *The initiation of embryonic-like collagen fibrillogenesis by adult human tendon fibroblasts when cultured under tension.* Biomaterials, 2010. **31**(18): p. 4889-4897.
408. Bryant, S.J. and K.S. Anseth, *Hydrogel properties influence ECM production by chondrocytes photoencapsulated in poly (ethylene glycol) hydrogels.* Journal of Biomedical Materials Research: An Official Journal of The Society for Biomaterials and The Japanese Society for Biomaterials, 2002. **59**(1): p. 63-72.
409. Materials, T.A.S.f.T.a., *Standard Guide for Characterization of Hydrogels used in Regenerative Medicine (Withdrawn 2020)*. 2011, ASTM International: West Conshohocken, PA.
410. Moles, M.D., C.A. Scotchford, and A.C. Ritchie, *Oxidation state of a polyurethane membrane after plasma etching. Conference Papers in Science, 2014. 347979/1-347979/11. ISSN 2356-6108.* 2014.
411. Ehrlich, H.P., *The modulation of contraction of fibroblast populated collagen lattices by types I, II, and III collagen.* Tissue and Cell, 1988. **20**(1): p. 47-50.
412. Griffith, L.G. and G. Naughton, *Tissue engineering--current challenges and expanding opportunities.* science, 2002. **295**(5557): p. 1009-1014.
413. Benoit, D.S., A.R. Durney, and K.S. Anseth, *Manipulations in hydrogel degradation behavior enhance osteoblast function and mineralized tissue formation.* Tissue engineering, 2006. **12**(6): p. 1663-1673.
414. LeRoux, M.A., F. Guilak, and L.A. Setton, *Compressive and shear properties of alginate gel: effects of sodium ions and alginate concentration.* Journal of Biomedical Materials Research: An Official Journal of The Society for Biomaterials, The Japanese Society for Biomaterials, and The Australian Society for Biomaterials and the Korean Society for Biomaterials, 1999. **47**(1): p. 46-53.

415. Hong, Y., et al., *Covalently crosslinked chitosan hydrogel: properties of in vitro degradation and chondrocyte encapsulation.* Acta biomaterialia, 2007. **3**(1): p. 23-31.
416. Azevedo, H.S. and R.L. Reis, *Understanding the enzymatic degradation of biodegradable polymers and strategies to control their degradation rate.* Biodegradable systems in tissue engineering and regenerative medicine, 2005: p. 177-201.
417. Ganji, F., M. Abdekhodaie, and A.R. SA, *Gelation time and degradation rate of chitosan-based injectable hydrogel.* Journal of sol-gel science and technology, 2007. **42**(1): p. 47-53.
418. Greenwald, R.A., et al., *Human cartilage lysozyme.* The Journal of clinical investigation, 1972. **51**(9): p. 2264-2270.
419. Redin, V. and I. Rebrikova, *Dynamics of lysozyme activity in the synovial fluid of patients with knee joint injuries.* Vestnik khirurgii imeni II Grekova, 1980. **124**(5): p. 86-88.
420. Felinto, M.C., et al., *The swelling behavior of chitosan hydrogels membranes obtained by UV-and γ-radiation.* Nuclear Instruments and Methods in Physics Research Section B: Beam Interactions with Materials and Atoms, 2007. **265**(1): p. 418-424.
421. Han, F., et al., *Photocrosslinked layered gelatin-chitosan hydrogel with graded compositions for osteochondral defect repair.* Journal of Materials Science: Materials in Medicine, 2015. **26**(4): p. 160.
422. Ng, W.L., W.Y. Yeong, and M.W. Naing, *Polyelectrolyte gelatin-chitosan hydrogel optimized for 3D bioprinting in skin tissue engineering.* International Journal of Bioprinting, 2016. **2**(1).
423. Mao, J.S., Y.J. Yin, and K. De Yao, *The properties of chitosan–gelatin membranes and scaffolds modified with hyaluronic acid by different methods.* Biomaterials, 2003. **24**(9): p. 1621-1629.
424. Bloomer, J.R., D.A. Brenner, and M.J. Mahoney, *Study of factors causing excess protoporphyrin accumulation in cultured skin fibroblasts from patients with protoporphyria.* The Journal of clinical investigation, 1977. **60**(6): p. 1354-1361.
425. Petronini, P.G., et al., *Adaptive response of cultured fibroblasts to hyperosmolarity.* Experimental cell research, 1986. **165**(1): p. 180-190.
426. Hansen, K.A., J.A. Weiss, and J.K. Barton, *Recruitment of tendon crimp with applied tensile strain.* J. Biomech. Eng., 2002. **124**(1): p. 72-77.
427. Cox, T.R. and J.T. Erler, *Remodeling and homeostasis of the extracellular matrix: implications for fibrotic diseases and cancer.* Disease models & mechanisms, 2011. **4**(2): p. 165-178.
428. Goycoolea, F., et al., *Temperature and pH-sensitive chitosan hydrogels: DSC, rheological and swelling evidence of a volume phase transition.* Polymer Bulletin, 2007. **58**(1): p. 225-234.
429. Ngo, P., et al., *Collagen gel contraction assay*, in *Cell-Cell Interactions*. 2006, Springer. p. 103-109.
430. Bell, E., B. Ivarsson, and C. Merrill, *Production of a tissue-like structure by contraction of collagen lattices by human fibroblasts of different proliferative potential in vitro.* Proceedings of the National Academy of Sciences, 1979. **76**(3): p. 1274-1278.

431. Freyman, T., et al., *Fibroblast contractile force is independent of the stiffness which resists the contraction.* Experimental cell research, 2002. **272**(2): p. 153-162.
432. Torres, D.S., et al., *Tendon cell contraction of collagen–GAG matrices in vitro: effect of cross-linking.* Biomaterials, 2000. **21**(15): p. 1607-1619.
433. Kunzler, T.P., et al., *Systematic study of osteoblast and fibroblast response to roughness by means of surface-morphology gradients.* Biomaterials, 2007. **28**(13): p. 2175-2182.
434. Schweikl, H., et al., *Proliferation of osteoblasts and fibroblasts on model surfaces of varying roughness and surface chemistry.* Journal of Materials Science: Materials in Medicine, 2007. **18**(10): p. 1895-1905.
435. Ribeiro, C., et al., *Surface roughness dependent osteoblast and fibroblast response on poly (l-lactide) films and electrospun membranes.* Journal of Biomedical Materials Research Part A, 2015. **103**(7): p. 2260-2268.
436. Arima, Y. and H. Iwata, *Effect of wettability and surface functional groups on protein adsorption and cell adhesion using well-defined mixed self-assembled monolayers.* Biomaterials, 2007. **28**(20): p. 3074-3082.
437. Yang, D., et al., *The molecular mechanism of mediation of adsorbed serum proteins to endothelial cells adhesion and growth on biomaterials.* Biomaterials, 2013. **34**(23): p. 5747-5758.
438. Altankov, G., K. Richau, and T. Groth, *The role of surface zeta potential and substratum chemistry for regulation of dermal fibroblasts interaction.* Materialwissenschaft und Werkstofftechnik: Entwicklung, Fertigung, Prüfung, Eigenschaften und Anwendungen technischer Werkstoffe, 2003. **34**(12): p. 1120-1128.
439. Guo, W.-h., et al., *Substrate rigidity regulates the formation and maintenance of tissues.* Biophysical journal, 2006. **90**(6): p. 2213-2220.
440. Grinnell, F., *Fibroblast biology in three-dimensional collagen matrices.* Trends in cell biology, 2003. **13**(5): p. 264-269.
441. Butcher, D.T., T. Alliston, and V.M. Weaver, *A tense situation: forcing tumour progression.* Nature Reviews Cancer, 2009. **9**(2): p. 108.
442. Kono, T., et al., *Cell cycle analysis of human dermal fibroblasts cultured on or in hydrated type I collagen lattices.* Archives of dermatological research, 1990. **282**(4): p. 258-262.
443. Lemons, J.M., et al., *Quiescent fibroblasts exhibit high metabolic activity.* PLoS biology, 2010. **8**(10).
444. Mitra, M., L.D. Ho, and H.A. Coller, *An in vitro model of cellular quiescence in primary human dermal fibroblasts*, in *Cellular Quiescence*. 2018, Springer. p. 27-47.
445. Paxton, J., K. Baar, and L. Grover, *Current progress in enthesis repair: Strategies for interfacial tissue engineering.* Orthopedic Muscul Sys, 2012.
446. Muller, B., K.F. Bowman, and A. Bedi, *ACL graft healing and biologics.* Clinics in sports medicine, 2013. **32**(1): p. 93-109.
447. Cheng, P., et al., *High-purity magnesium interference screws promote fibrocartilaginous entheses regeneration in the anterior cruciate ligament reconstruction rabbit model via accumulation of BMP-2 and VEGF.* Biomaterials, 2016. **81**: p. 14-26.
448. McCorry, M.C., et al., *A model system for developing a tissue engineered meniscal enthesis.* Acta biomaterialia, 2017. **56**: p. 110-117.

449. Su, M., et al., *Preparation of Decellularized Triphasic Hierarchical Bone-Fibrocartilage-Tendon Composite Extracellular Matrix for Enthesis Regeneration.* Advanced healthcare materials, 2019. **8**(19): p. 1900831.
450. Undin, J., A. Finne-Wistrand, and A.-C. Albertsson, *Adjustable degradation properties and biocompatibility of amorphous and functional poly (ester-acrylate)-based materials.* Biomacromolecules, 2014. **15**(7): p. 2800-2807.
451. Mao, K., et al., *Friction and wear behaviour of acetal and nylon gears.* Wear, 2009. **267**(1-4): p. 639-645.
452. Ramanjaneyulu, S., et al., *Design and Development of Graphene reinforced Acetal copolymer plastic gears and its performance evaluation.* Materials Today: Proceedings, 2017. **4**(8): p. 8678-8687.
453. Wylie, D., K. Kret, and C. Scotchford, *Achor Development For In Vitro Tissue Engineering*, in *Mechanical Engineering*. 2019, University of Nottingham.
454. Benjamin, M. and D. McGonagle, *The enthesis organ concept and its relevance to the spondyloarthropathies*, in *Molecular mechanisms of spondyloarthropathies*. 2009, Springer. p. 57-70.
455. Spalazzi, J.P., et al., *In vivo evaluation of a multiphased scaffold designed for orthopaedic interface tissue engineering and soft tissue-to-bone integration.* Journal of Biomedical Materials Research Part A: An Official Journal of The Society for Biomaterials, The Japanese Society for Biomaterials, and The Australian Society for Biomaterials and the Korean Society for Biomaterials, 2008. **86**(1): p. 1-12.
456. Nukavarapu, S.P. and D.L. Dorcemus, *Osteochondral tissue engineering: current strategies and challenges.* Biotechnology advances, 2013. **31**(5): p. 706-721.
457. Mahmoudifar, N. and P.M. Doran, *Tissue engineering of human cartilage and osteochondral composites using recirculation bioreactors.* Biomaterials, 2005. **26**(34): p. 7012-7024.
458. Popov, A.A., *Development of a cell-seeded construct for osteochondral modelling and repair*. 2016, University of Nottingham.
459. Tampieri, A., et al., *Design of graded biomimetic osteochondral composite scaffolds.* Biomaterials, 2008. **29**(26): p. 3539-3546.
460. Daculsi, G., et al., *Developments in injectable multiphasic biomaterials. The performance of microporous biphasic calcium phosphate granules and hydrogels.* Journal of Materials Science: Materials in Medicine, 2010. **21**(3): p. 855-861.
461. Quent, V.M., et al., *Discrepancies between metabolic activity and DNA content as tool to assess cell proliferation in cancer research.* Journal of cellular and molecular medicine, 2010. **14**(4): p. 1003-1013.
462. da Cunha, C.B., et al., *Influence of the stiffness of three-dimensional alginate/collagen-I interpenetrating networks on fibroblast biology.* Biomaterials, 2014. **35**(32): p. 8927-8936.
463. Raz, M., et al., *Development of biomimetic gelatin–chitosan/hydroxyapatite nanocomposite via double diffusion method for biomedical applications.* International journal of materials research, 2014. **105**(5): p. 493-501.
464. Feng, X., *Chemical and biochemical basis of cell-bone matrix interaction in health and disease.* Current chemical biology, 2009. **3**(2): p. 189-196.

465. Grover, L.M., et al., *The effect of amorphous pyrophosphate on calcium phosphate cement resorption and bone generation.* Biomaterials, 2013. **34**(28): p. 6631-6637.
466. Owen, T.A., et al., *Progressive development of the rat osteoblast phenotype in vitro: reciprocal relationships in expression of genes associated with osteoblast proliferation and differentiation during formation of the bone extracellular matrix.* Journal of cellular physiology, 1990. **143**(3): p. 420-430.
467. Xie, Y., et al., *Clinical, radiological and histological study of the failure of cervical interbody fusions with bone substitutes.* European Spine Journal, 2006. **15**(8): p. 1196-1203.
468. Barralet, J., M. Akao, and H. Aoki, *Dissolution of dense carbonate apatite subcutaneously implanted in Wistar rats.* Journal of Biomedical Materials Research: An Official Journal of The Society for Biomaterials and The Japanese Society for Biomaterials, 2000. **49**(2): p. 176-182.
469. Samavedi, S., A.R. Whittington, and A.S. Goldstein, *Calcium phosphate ceramics in bone tissue engineering: a review of properties and their influence on cell behavior.* Acta biomaterialia, 2013. **9**(9): p. 8037-8045.
470. Bohner, M., et al., *Compositional changes of a dicalcium phosphate dihydrate cement after implantation in sheep.* Biomaterials, 2003. **24**(20): p. 3463-3474.
471. Wang, P., et al., *Bone tissue engineering via nanostructured calcium phosphate biomaterials and stem cells.* Bone research, 2014. **2**: p. 14017.
472. Azami, M., et al., *Preparation of a biomimetic nanocomposite scaffold for bone tissue engineering via mineralization of gelatin hydrogel and study of mineral transformation in simulated body fluid.* Journal of Biomedical Materials Research Part A, 2012. **100**(5): p. 1347-1355.
473. Zhang, Y., et al., *Calcium phosphate—chitosan composite scaffolds for bone tissue engineering.* Tissue engineering, 2003. **9**(2): p. 337-345.
474. Fleisch, H. and S. Bisaz, *Mechanism of calcification: inhibitory role of pyrophosphate.* Nature, 1962. **195**(4844): p. 911-911.
475. Ducy, P., T. Schinke, and G. Karsenty, *The osteoblast: a sophisticated fibroblast under central surveillance.* Science, 2000. **289**(5484): p. 1501-1504.
476. Ducy, P., et al., *Increased bone formation in osteocalcin-deficient mice.* Nature, 1996. **382**(6590): p. 448-452.
477. Lin, W.L., C.A. McCulloch, and M.I. Cho, *Differentiation of periodontal ligament fibroblasts into osteoblasts during socket healing after tooth extraction in the rat.* The Anatomical Record, 1994. **240**(4): p. 492-506.
478. Bonson, S., B. Jeansonne, and T. Lallier, *Root-end filling materials alter fibroblast differentiation.* Journal of dental research, 2004. **83**(5): p. 408-413.
479. Nojima, N., et al., *Fibroblastic cells derived from bovine periodontal ligaments have the phenotypes of osteoblasts.* Journal of periodontal research, 1990. **25**(3): p. 179-185.
480. Ikegame, M., et al., *Tensile stress induces bone morphogenetic protein 4 in preosteoblastic and fibroblastic cells, which later differentiate into osteoblasts leading to osteogenesis in the mouse calvariae in organ culture.* Journal of Bone and Mineral Research, 2001. **16**(1): p. 24-32.

481. Grynpas, M.D. and G.K. Hunter, *Bone mineral and glycosaminoglycans in newborn and mature rabbits.* Journal of Bone and Mineral Research, 1988. **3**(2): p. 159-164.
482. Herring, G., *Studies on the protein-bound chondroitin sulphate of bovine cortical bone.* Biochemical Journal, 1967. **104**(2): p. 19P.
483. Engfeldt, B. and A. Hjerpe, *Glycosaminoglycans and proteoglycans of human bone tissue at different stages of mineralization.* Acta Pathologica Microbiologica Scandinavica Section A Pathology, 1976. **84**(1): p. 95-106.
484. Mansouri, R., et al., *Correction: Osteoblastic heparan sulfate glycosaminoglycans control bone remodeling by regulating Wnt signaling and the crosstalk between bone surface and marrow cells.* Cell death & disease, 2018. **9**(8): p. 1-1.
485. Salbach, J., et al., *Regenerative potential of glycosaminoglycans for skin and bone.* Journal of molecular medicine, 2012. **90**(6): p. 625-635.
486. Bonar, L., et al., *X-ray diffraction studies of the crystallinity of bone mineral in newly synthesized and density fractionated bone.* Calcified tissue international, 1983. **35**(1): p. 202-209.
487. Huang, J.I., et al., *Chondrogenic potential of progenitor cells derived from human bone marrow and adipose tissue: A patient-matched comparison.* Journal of Orthopaedic Research, 2005. **23**(6): p. 1383-1389.
488. Matinfar, M., A.S. Mesgar, and Z. Mohammadi, *Evaluation of physicochemical, mechanical and biological properties of chitosan/carboxymethyl cellulose reinforced with multiphasic calcium phosphate whisker-like fibers for bone tissue engineering.* Materials Science and Engineering: C, 2019. **100**: p. 341-353.
489. Madhumathi, K., et al., *Wet chemical synthesis of chitosan hydrogel–hydroxyapatite composite membranes for tissue engineering applications.* International journal of biological macromolecules, 2009. **45**(1): p. 12-15.
490. Galea, L., et al., *Control of the size, shape and composition of highly uniform, non-agglomerated, sub-micrometer β-tricalcium phosphate and dicalcium phosphate platelets.* Biomaterials, 2013. **34**(27): p. 6388-6401.
491. Bitter, J., *Effect of crystallinity and swelling on the permeability and selectivity of polymer membranes.* Desalination, 1984. **51**(1): p. 19-35.
492. Youngstrom, D.W. and J.G. Barrett, *Engineering tendon: scaffolds, bioreactors, and models of regeneration.* Stem cells international, 2016. **2016**.
493. Mace, J., et al., *The role of bioreactors in ligament and tendon tissue engineering.* Current stem cell research & therapy, 2016. **11**(1): p. 35-40.
494. Gantenbein, B., et al., *Developing bioreactors to host joint-derived tissues that require mechanical stimulation.* Reference Module in Biomedical Sciences. Elsevier, 2019.
495. Gonçalves, A.I., et al., *Bioreactors for tendon tissue engineering: challenging mechanical demands towards tendon regeneration.* 2018.
496. Freed, L.E., et al., *Advanced tools for tissue engineering: scaffolds, bioreactors, and signaling.* Tissue engineering, 2006. **12**(12): p. 3285-3305.
497. Wang, T., et al., *Programmable mechanical stimulation influences tendon homeostasis in a bioreactor system.* Biotechnology and bioengineering, 2013. **110**(5): p. 1495-1507.

498. Joshi, S.D. and K. Webb, *Variation of cyclic strain parameters regulates development of elastic modulus in fibroblast/substrate constructs.* Journal of Orthopaedic Research, 2008. **26**(8): p. 1105-1113.
499. Doroski, D.M., M.E. Levenston, and J.S. Temenoff, *Cyclic tensile culture promotes fibroblastic differentiation of marrow stromal cells encapsulated in poly (ethylene glycol)-based hydrogels.* Tissue Engineering Part A, 2010. **16**(11): p. 3457-3466.
500. Androjna, C., R.K. Spragg, and K.A. Derwin, *Mechanical conditioning of cell-seeded small intestine submucosa: a potential tissue-engineering strategy for tendon repair.* Tissue engineering, 2007. **13**(2): p. 233-243.
501. Webb, K., et al., *Cyclic strain increases fibroblast proliferation, matrix accumulation, and elastic modulus of fibroblast-seeded polyurethane constructs.* Journal of biomechanics, 2006. **39**(6): p. 1136-1144.
502. Wu, X. and X. Wang. *Advanced bioreactor for ligament tissue engineering*. in *2010 IEEE International Conference on Mechatronics and Automation*. 2010. IEEE.
503. Hohlrieder, M., et al., *Bioreactor and scaffold design for the mechanical stimulation of anterior cruciate ligament grafts.* Bio-medical materials and engineering, 2013. **23**(3): p. 225-237.
504. Scaglione, S., et al., *A three-dimensional traction/torsion bioreactor system for tissue engineering.* The International journal of artificial organs, 2010. **33**(6): p. 362-369.
505. Wu, X.D. and X. Wang. *Design of Bioreactor Control System for Ligament Tissue Engineering*. in *Applied Mechanics and Materials*. 2012. Trans Tech Publ.
506. Nirmalanandhan, V.S., et al., *Improving linear stiffness of the cell-seeded collagen sponge constructs by varying the components of the mechanical stimulus.* Tissue Engineering Part A, 2008. **14**(11): p. 1883-1891.
507. Ritchie, A., et al., *Dependence of alignment direction on magnitude of strain in esophageal smooth muscle cells.* Biotechnology and bioengineering, 2009. **102**(6): p. 1703-1711.
508. Landry, N.M., S.G. Rattan, and I.M. Dixon, *An improved method of maintaining primary murine cardiac fibroblasts in two-dimensional cell culture.* Scientific reports, 2019. **9**(1): p. 1-13.
509. Linton, W. and H. Goodman, *Physical properties of high molecular weight acetal resins.* Journal of Applied Polymer Science, 1959. **1**(2): p. 179-184.
510. Mazzoleni, G., D. Di Lorenzo, and N. Steimberg, *Modelling tissues in 3D: the next future of pharmaco-toxicology and food research?* Genes & nutrition, 2009. **4**(1): p. 13.
511. Yasuda, K., et al., *Dynamic elongation behavior in the medical collateral and anterior cruciate ligaments during lateral impact loading.* Journal of orthopaedic research, 1993. **11**(2): p. 190-198.
512. Godara, P., C.D. McFarland, and R.E. Nordon, *Design of bioreactors for mesenchymal stem cell tissue engineering.* Journal of Chemical Technology & Biotechnology: International Research in Process, Environmental & Clean Technology, 2008. **83**(4): p. 408-420.
513. Lotz, C., et al., *Cross-linked collagen hydrogel matrix resisting contraction to facilitate full-thickness skin equivalents.* ACS applied materials & interfaces, 2017. **9**(24): p. 20417-20425.

514. Murray, M.M., et al., *The effect of thrombin on ACL fibroblast interactions with collagen hydrogels.* Journal of orthopaedic research, 2006. **24**(3): p. 508-515.
515. Mao, J., et al., *Study of novel chitosan-gelatin artificial skin in vitro.* Journal of Biomedical Materials Research Part A: An Official Journal of The Society for Biomaterials, The Japanese Society for Biomaterials, and The Australian Society for Biomaterials and the Korean Society for Biomaterials, 2003. **64**(2): p. 301-308.
516. Romanova, O., et al., *Chitosan as a modifying component of artificial scaffold for human skin tissue engineering.* Bulletin of experimental biology and medicine, 2015. **159**(4): p. 557-566.
517. Harrison, R.D. and P.F. Gratzer, *Effect of extraction protocols and epidermal growth factor on the cellular repopulation of decellularized anterior cruciate ligament allografts.* Journal of Biomedical Materials Research Part A: An Official Journal of The Society for Biomaterials, The Japanese Society for Biomaterials, and The Australian Society for Biomaterials and the Korean Society for Biomaterials, 2005. **75**(4): p. 841-854.
518. Holy, C.E., M.S. Shoichet, and J.E. Davies, *Engineering three-dimensional bone tissue in vitro using biodegradable scaffolds: Investigating initial cell-seeding density and culture period.* Journal of Biomedical Materials Research: An Official Journal of The Society for Biomaterials, The Japanese Society for Biomaterials, and The Australian Society for Biomaterials and the Korean Society for Biomaterials, 2000. **51**(3): p. 376-382.
519. Chiquet, M., et al., *How do fibroblasts translate mechanical signals into changes in extracellular matrix production?* Matrix biology, 2003. **22**(1): p. 73-80.
520. Eastwood, M., et al., *Effect of precise mechanical loading on fibroblast populated collagen lattices: morphological changes.* Cell motility and the cytoskeleton, 1998. **40**(1): p. 13-21.
521. Carver, W., et al., *Collagen expression in mechanically stimulated cardiac fibroblasts.* Circulation research, 1991. **69**(1): p. 116-122.
522. Junker, J.P., et al., *Mechanical tension stimulates the transdifferentiation of fibroblasts into myofibroblasts in human burn scars.* Burns, 2008. **34**(7): p. 942-946.
523. Li, X. and J.G. Snedeker, *Wired silk architectures provide a biomimetic ACL tissue engineering scaffold.* Journal of the mechanical behavior of biomedical materials, 2013. **22**: p. 30-40.
524. Hannafin, J.A., et al., *Effect of cyclic strain and plating matrix on cell proliferation and integrin expression by ligament fibroblasts.* Journal of Orthopaedic Research, 2006. **24**(2): p. 149-158.
525. Huguet, D., et al., *Ovine anterior cruciate ligament reconstruction using a synthetic prosthesis and a collagen inductor.* Journal of Materials Science: Materials in Medicine, 1997. **8**(2): p. 67-73.
526. Weiss, A.B., et al., *Ligament replacement with an absorbable copolymer carbon fiber scaffold--early clinical experience.* Clinical orthopaedics and related research, 1985(196): p. 77-85.
527. Jenkins, D., *The repair of cruciate ligaments with flexible carbon fibre. A longer term study of the induction of new ligaments and of the fate of the implanted carbon.* The Journal of bone and joint surgery. British volume, 1978. **60**(4): p. 520-522.

528. Peng, Z., Z. Peng, and Y. Shen, *Fabrication and properties of gelatin/chitosan composite hydrogel.* Polymer-Plastics Technology and Engineering, 2011. **50**(11): p. 1160-1164.
529. Bott, K., et al., *The effect of matrix characteristics on fibroblast proliferation in 3D gels.* Biomaterials, 2010. **31**(32): p. 8454-8464.
530. Hashimoto, Y., et al., *Generation of tendon-to-bone interface "enthesis" with use of recombinant BMP-2 in a rabbit model.* Journal of Orthopaedic Research, 2007. **25**(11): p. 1415-1424.
531. Tan, L., et al., *Biodegradable materials for bone repairs: a review.* Journal of Materials Science & Technology, 2013. **29**(6): p. 503-513.
532. García-Gareta, E., M.J. Coathup, and G.W. Blunn, *Osteoinduction of bone grafting materials for bone repair and regeneration.* Bone, 2015. **81**: p. 112-121.

10. Appendix

10.1. Concentrations for PicoGreen Assay

Table 10.1: The standard concentrations used for the PicoGreen assay.

Volume TE (µl)	Volume (µl) of 2 µg/ml DNA Stock	Volume of Reagent (µl)	Final DNA Concentration
0	100	100	1 µg/ml
10	90	100	0.9 µg/ml
20	80	100	0.8 µg/ml
50	50	100	0.5 µg/ml
80	20	100	0.2 µg/ml
90	10	100	0.1 µg/ml
99	1	100	0.01 µg/ml
100	0	100	0 (Blank)

10.2. Concentrations for DMMB Assay

Table 10.2: The standard concentrations used for the DMMB assay.

Volume H_2O (µl)	Volume (µl) of 500 µg/ml GAG Stock	Volume of DMMB (µl)	Final GAG Concentration
20	0	200	0 (Blank)
17.8	2.2	200	5 µg/ml
16.7	3.3	200	7.5 µg/ml
15.6	4.4	200	10 µg/ml
13.4	6.6	200	15 µg/ml
9	11	200	25 µg/ml
2.4	17.6	200	40 µg/ml
0	20	200	45.45 µg/ml

10.3. Mean Cell Area Additional Images

These are additional images that were used to calculate the mean cell area of the 3T3 and PFib cells grown on chitosan-gelatin hydrogel of increasing thickness.

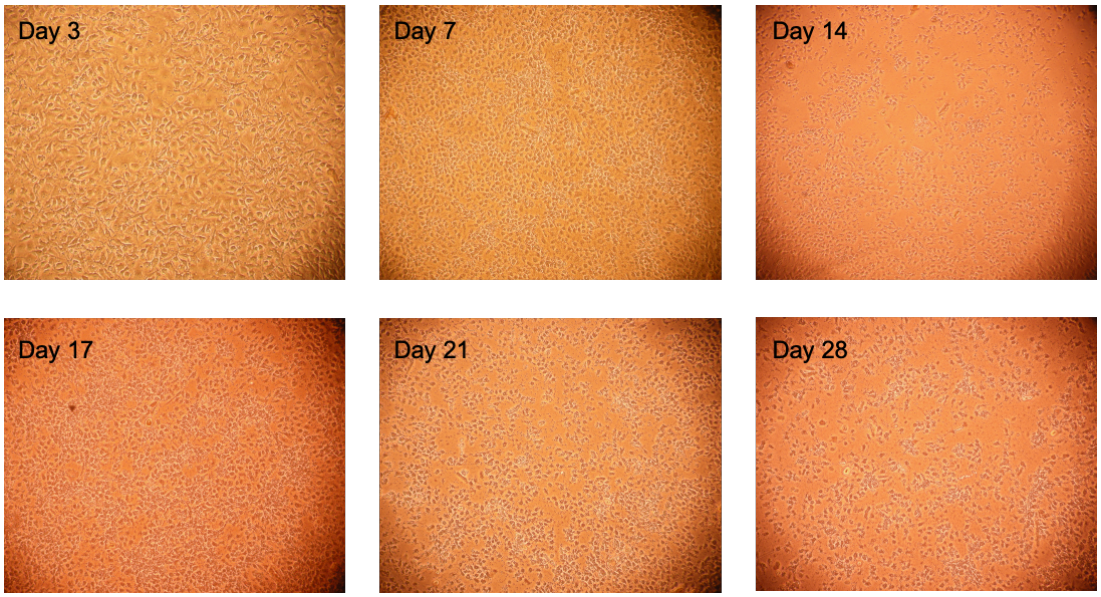

Figure 10.1: Images used for calculation of mean cell area of 3T3 cells on 0.5mm chitosan-gelatin hydrogel over a period of 28 days.

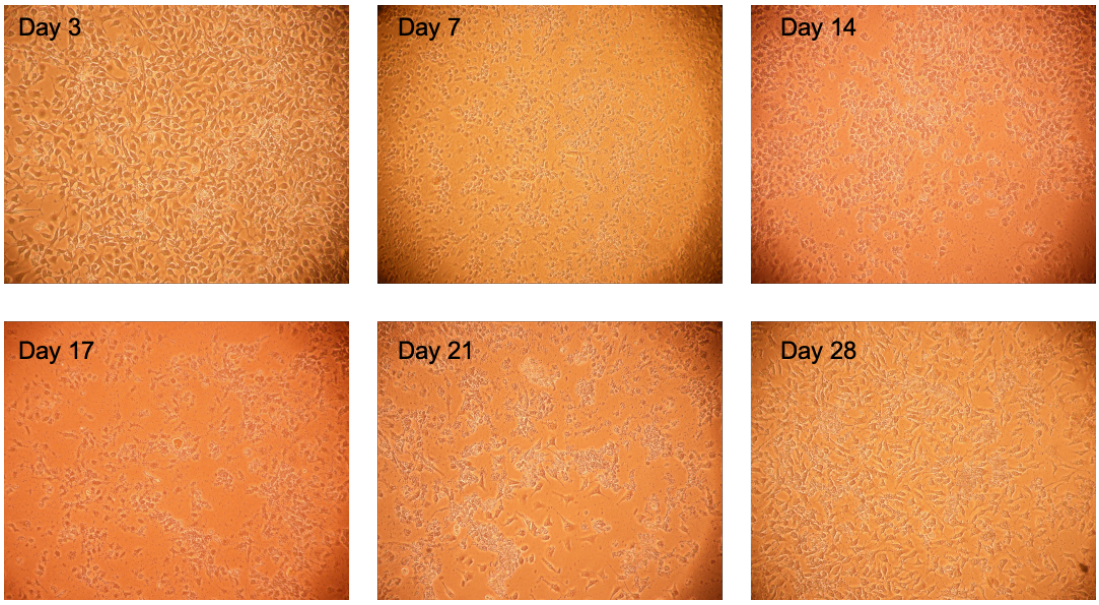

Figure 10.2: Images used for calculation of mean cell area of 3T3 cells on 1.0mm chitosan-gelatin hydrogel over a period of 28 days.

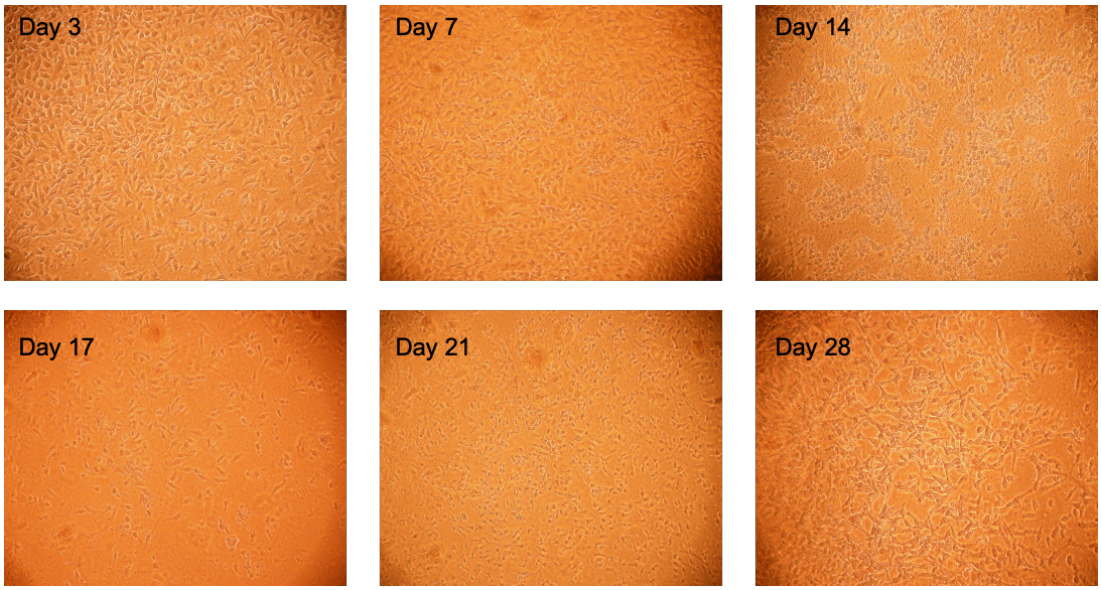

Figure 10.3: Images used for calculation of mean cell area of 3T3 cells on 1.5mm chitosan-gelatin hydrogel over a period of 28 days.

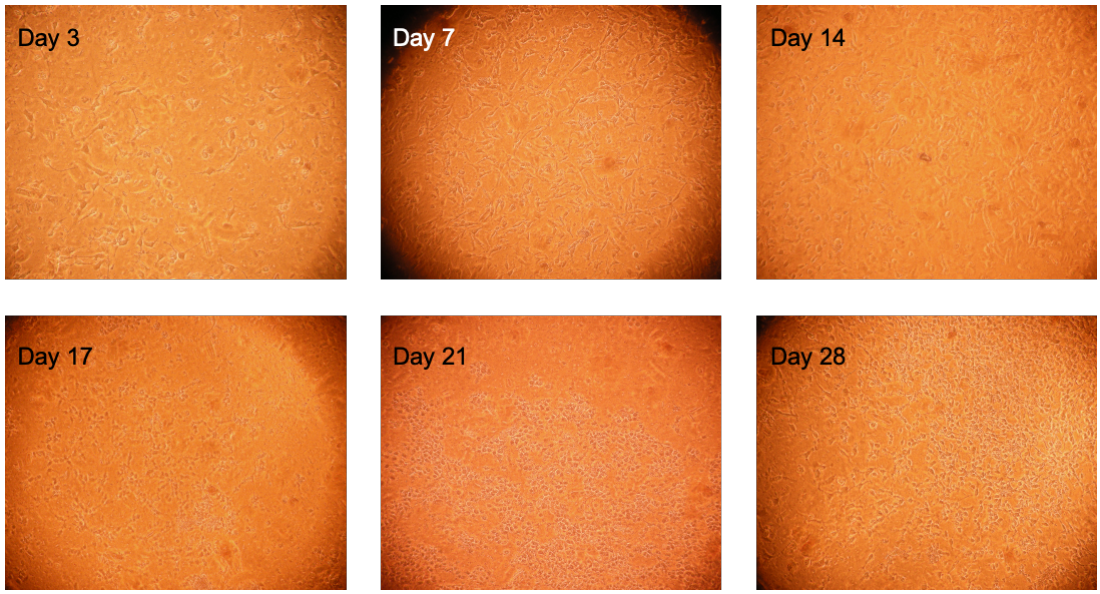

Figure 10.4: Images used for calculation of mean cell area of 3T3 cells on 2.0mm chitosan-gelatin hydrogel over a period of 28 days.

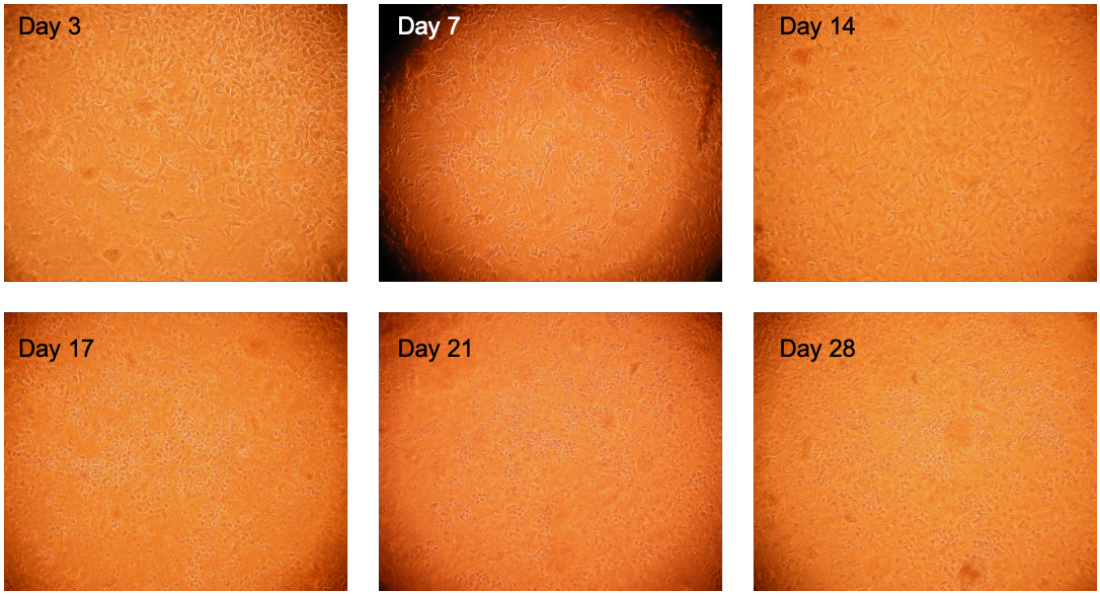

Figure 10.5: Images used for calculation of mean cell area of 3T3 cells on 2.5mm chitosan-gelatin hydrogel over a period of 28 days.

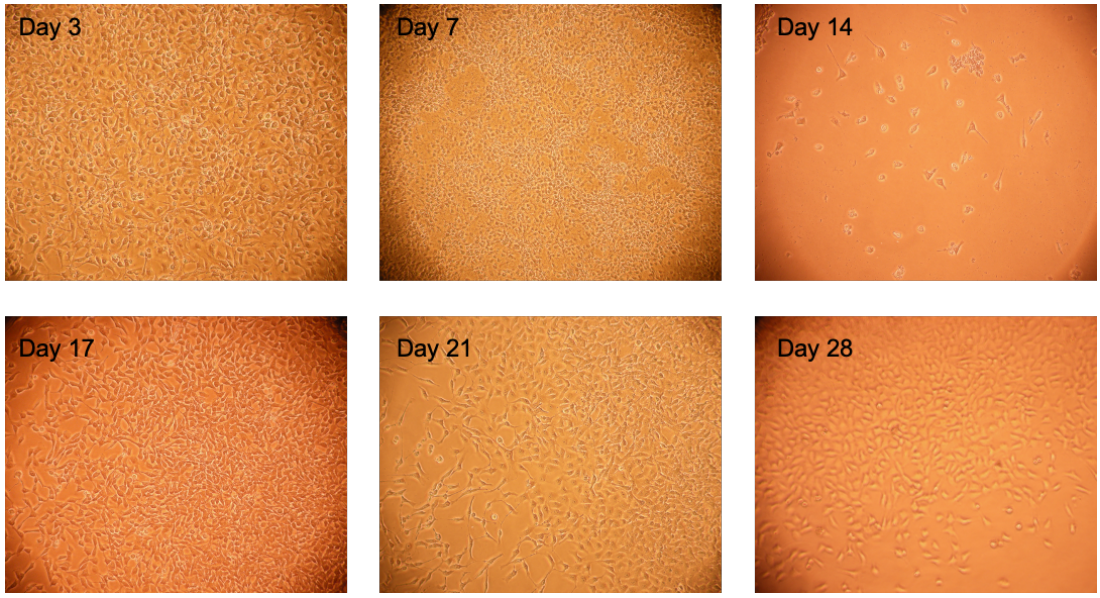

Figure 10.6: Images used for calculation of mean cell area of 3T3 cells on TCP over a period of 28 days.

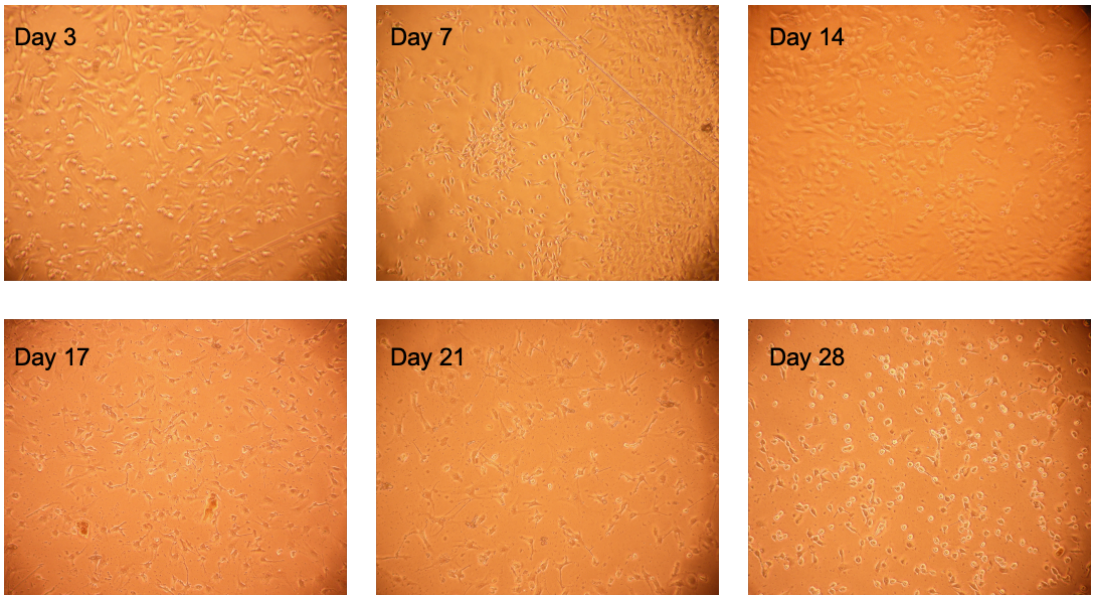

Figure 10.7: Images used for calculation of mean cell area of PFib cells on 0.5mm chitosan-gelatin hydrogel over a period of 28 days.

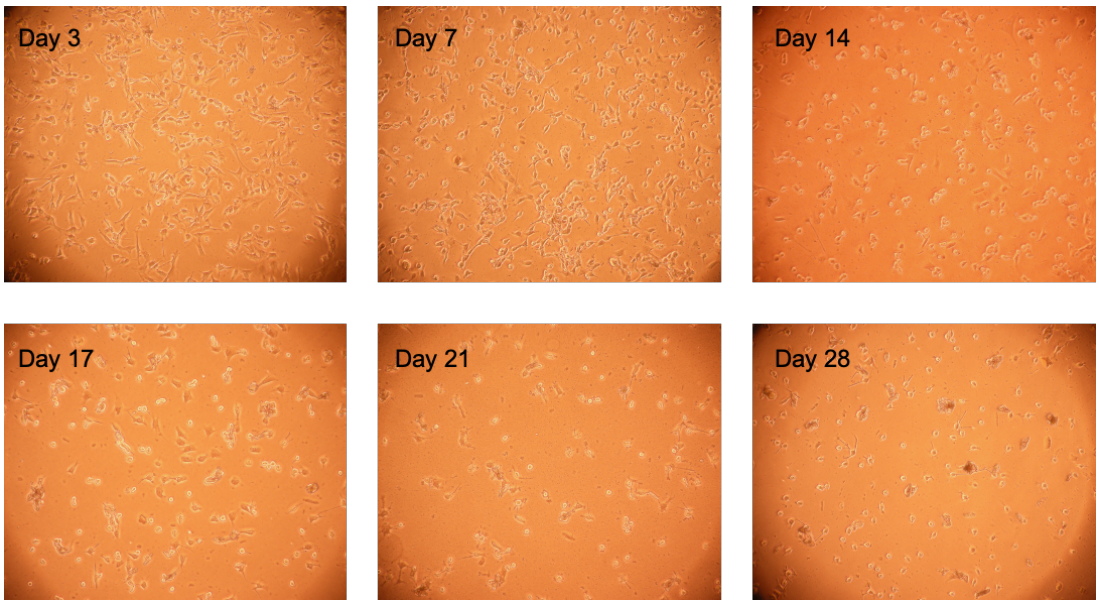

Figure 10.8: Images used for calculation of mean cell area of PFib cells on 1.0mm chitosan-gelatin hydrogel over a period of 28 days.

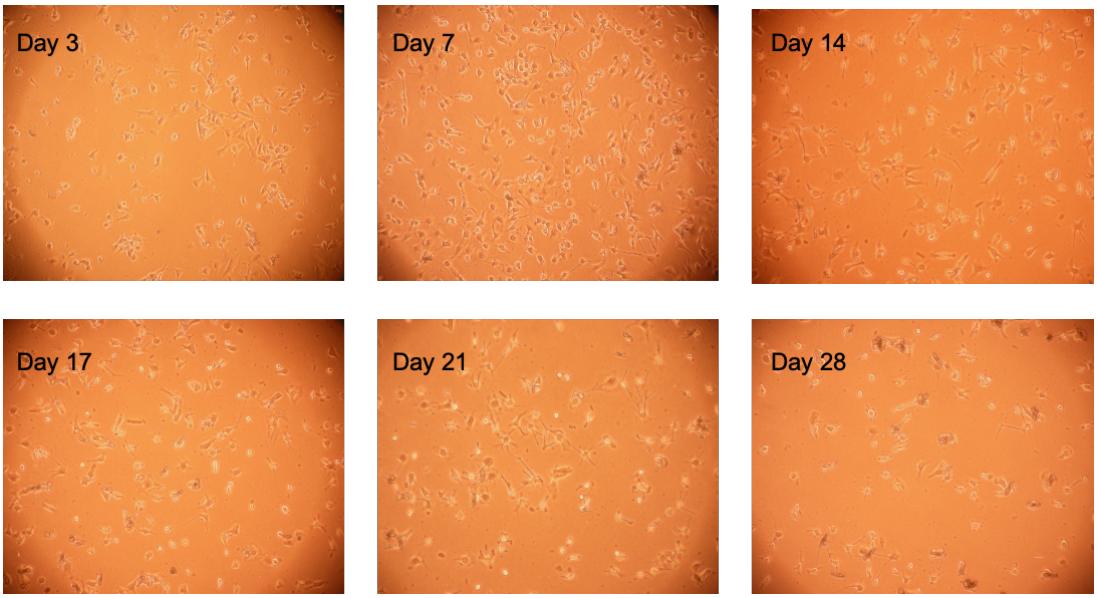

Figure 10.9: Images used for calculation of mean cell area of PFib cells on 1.5mm chitosan-gelatin hydrogel over a period of 28 days.

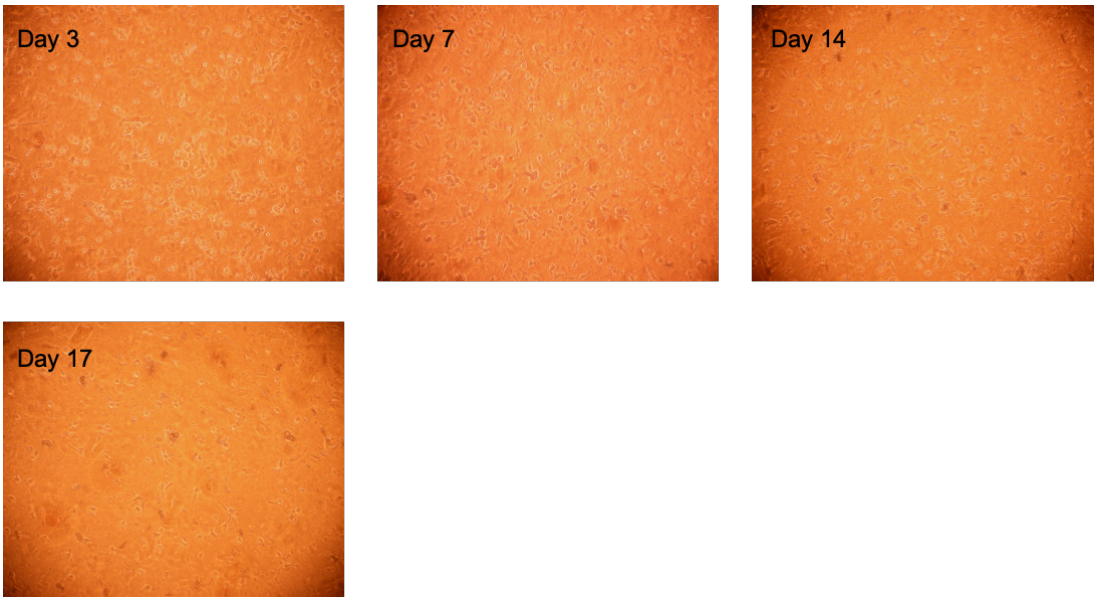

Figure 10.10: Images used for calculation of mean cell area of PFib cells on 2.0mm chitosan-gelatin hydrogel over a period of 28 days.

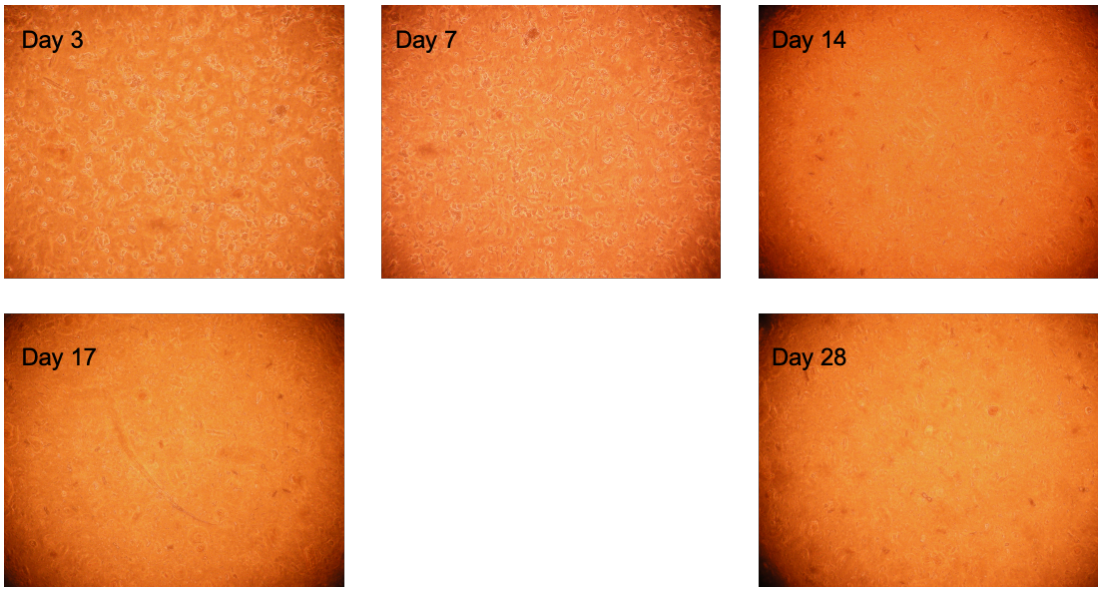

Figure 10.11: Images used for calculation of mean cell area of PFib cells on 2.5mm chitosan-gelatin hydrogel over a period of 28 days.

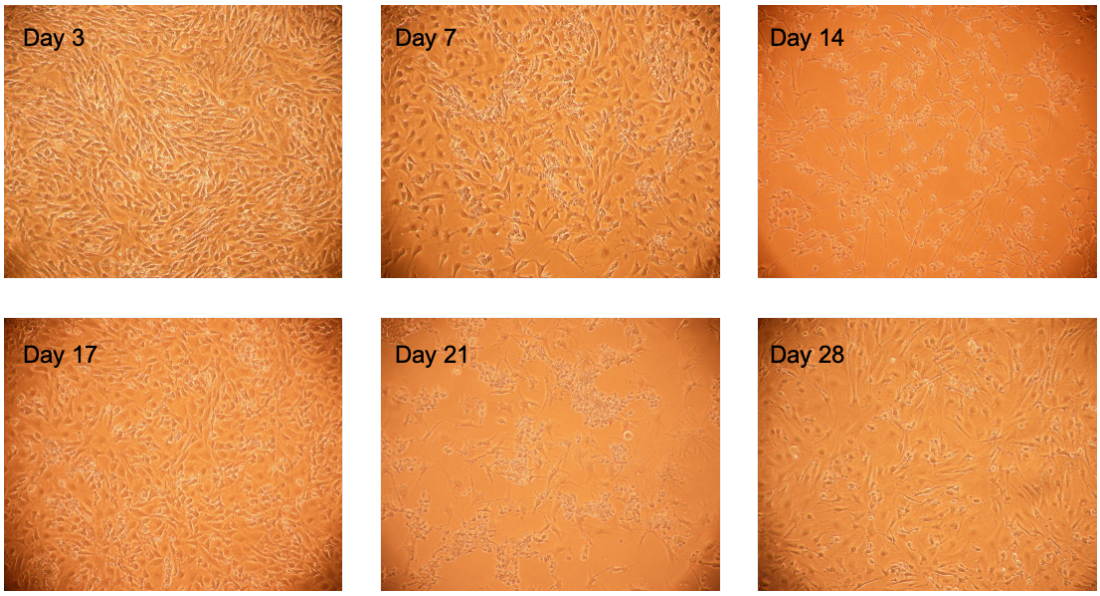

Figure 10.12: Images used for calculation of mean cell area of PFib cells on TCP over a period of 28 days.

10.4. Code for Mechanical Stimulation of Bioreactor

```
// This is setup code for finished Arduino microcontroller
// Declaration of pins
#define red_LED 10    // Write this pin HIGH to light RED led
#define yellow_LED 11 // Write this pin HIGH to light YELLOW led
#define green_LED 12  // Write this pin HIGH to light GREEN led
int start = A0; // Use AnalogRead - this is the "automation start pushbutton"  .. BROWN
int back = A1; // Use AnalogRead - this is the "jog backwards" pushbutton, enabled when the manual switch is thrown .. ORANGE (button cap red)
int forward = A2; // Use AnalogRead - this is the "jog forwards" pushbutton, enabled when the manual switch is thrown .. BLUE (button cap green)
```

```
int manual = A3; // Use AnalogRead - this is the "auto/manual" switch detection .. PURPLE
int startbuttonstate = 0; // This is the flag to note if the auto program start button has been pressed. Default to ZERO so the auto program won't commence uncommanded - it will drop straight into manual_operation() function
int M1inA1 = 1; // YLW - These are the 4 control inputs for motor 1
int M1inA2 = 0; // GRN - The apparent 0/1 mismatch is due to the numbering of the pins on the board.
int M1inB1 = 2; // BLU - These are the 4 control inputs for motor 1
int M1inB2 = 3; // PUR - These are the 4 control inputs for motor 1
int M2inA1 = 4; // BLK - These are the 4 control inputs for motor 2
int M2inA2 = 5; // WHT - These are the 4 control inputs for motor 2
int M2inB1 = 6; // RED - These are the 4 control inputs for motor 2
int M2inB2 = 7; // ORG - These are the 4 control inputs for motor 2

int M1_enable = 8; // WHITE/WHITE Motor enable logic. Write HIGH for motor ON, LOW for motor OFF - Needs both logic enable HIGH on L298N to operate motor
int M2_enable = 9; // PINK / PINK Motor enable logic. Write HIGH for motor ON, LOW for motor OFF - Needs both logic enable HIGH on L298N to operate motor

//int stepDelay = 20; // Delay between steps in milliseconds
float stepDelay = 1.5; // Delay between steps in milliseconds
int current_position = 1000;  //This keeps track of the overall position of the actuator

/*Defining Experimental parameters*/

#define PI 3.141592654
#define frequency 0.0167 //(frequency is in Hz)
#define magnitude 12 //(magnitude is in steps)
#define phase_difference 1 //difference in threads between actuators, if any
#define duration 3600 //duration of stimulation, in seconds

void setup() {
  Serial.begin(9600);

  // Here, the pin assignments are declared as inputs or outputs.
  // The 4 switches are inputs, everything else is output.


  pinMode (red_LED, OUTPUT);
  pinMode (yellow_LED, OUTPUT);
  pinMode (green_LED, OUTPUT);

  pinMode (start, INPUT);
  pinMode (back, INPUT);
  pinMode (forward, INPUT);
  pinMode (manual, INPUT);

  pinMode (M1_enable, OUTPUT);
```

```
  pinMode (M2_enable, OUTPUT);

  pinMode(M1inA1, OUTPUT);
  pinMode(M1inA2, OUTPUT);
  pinMode(M1inB1, OUTPUT);
  pinMode(M1inB2, OUTPUT);

  pinMode(M2inA1, OUTPUT);
  pinMode(M2inA2, OUTPUT);
  pinMode(M2inB1, OUTPUT);
  pinMode(M2inB2, OUTPUT);

  digitalWrite(M2_enable, LOW);
  digitalWrite(M1_enable, LOW);

}

// ************define the stepper "steps" for each motor

void M1step1() {

  digitalWrite(M1inA1, LOW);
  digitalWrite(M1inA2, HIGH);
  digitalWrite(M1inB1, HIGH);
  digitalWrite(M1inB2, LOW);
  delay(stepDelay);

}
void M1step2() {

  digitalWrite(M1inA1, LOW);
  digitalWrite(M1inA2, HIGH);
  digitalWrite(M1inB1, LOW);
  digitalWrite(M1inB2, HIGH);
  delay(stepDelay);

}
void M1step3() {

  digitalWrite(M1inA1, HIGH);
  digitalWrite(M1inA2, LOW);
  digitalWrite(M1inB1, LOW);
  digitalWrite(M1inB2, HIGH);
  delay(stepDelay);

}
void M1step4() {

  digitalWrite(M1inA1, HIGH);
  digitalWrite(M1inA2, LOW);
```

```
  digitalWrite(M1inB1, HIGH);
  digitalWrite(M1inB2, LOW);
  delay(stepDelay);

}
void M1stopMotor() {

  digitalWrite(M1inA1, LOW);
  digitalWrite(M1inA2, LOW);
  digitalWrite(M1inB1, LOW);
  digitalWrite(M1inB2, LOW);
}

void M2step1() {

  digitalWrite(M2inA1, LOW);
  digitalWrite(M2inA2, HIGH);
  digitalWrite(M2inB1, HIGH);
  digitalWrite(M2inB2, LOW);
  delay(stepDelay);

}
void M2step2() {

  digitalWrite(M2inA1, LOW);
  digitalWrite(M2inA2, HIGH);
  digitalWrite(M2inB1, LOW);
  digitalWrite(M2inB2, HIGH);
  delay(stepDelay);
}
void M2step3() {

  digitalWrite(M2inA1, HIGH);
  digitalWrite(M2inA2, LOW);
  digitalWrite(M2inB1, LOW);
  digitalWrite(M2inB2, HIGH);
  delay(stepDelay);
}
void M2step4() {

  digitalWrite(M2inA1, HIGH);
  digitalWrite(M2inA2, LOW);
  digitalWrite(M2inB1, HIGH);
  digitalWrite(M2inB2, LOW);
  delay(stepDelay);
}
void M2stopMotor() {

  digitalWrite(M2inA1, LOW);
  digitalWrite(M2inA2, LOW);
```

```
  digitalWrite(M2inB1, LOW);
  digitalWrite(M2inB2, LOW);
}

//**********************Stepper motor "steps" definition ends

//**********************Aggregate the stepper steps into a simple "forwards" "backwards" command set for the 2 motors

void M1forward()
{
  digitalWrite(M1_enable, HIGH);
  M1step1();
  M1step2();
  M1step3();
  M1step4();
  digitalWrite(M1_enable, LOW);
}

void M1backward()
{
  digitalWrite(M1_enable, HIGH);
  M1step3();
  M1step2();
  M1step1();
  M1step4();
  digitalWrite(M1_enable, LOW);
}


void M2forward()
{
  digitalWrite(M2_enable, HIGH);
  M2step1();
  M2step2();
  M2step3();
  M2step4();
  digitalWrite(M2_enable, LOW);
}

void M2backward()
{
  digitalWrite(M2_enable, HIGH);
  M2step3();
  M2step2();
  M2step1();
  M2step4();
  digitalWrite(M2_enable, LOW);
}
```

```
//**********************Aggregate the stepper steps into a simple "forwards" "backwards" command set for the 2 motors ends

//*************** Define manual operation function

int manual_operation(int bposition)
{
 int int_position;
 startbuttonstate = 0; //As soon as manual control is enabled, set the startbuttonstate to zero. Code lines at the top of void loop will detect the state change and allow the preset program to run.


 digitalWrite(yellow_LED, LOW);
 digitalWrite(M1_enable, HIGH);
 digitalWrite(M2_enable, HIGH);

 while (analogRead(manual) > 500)
 {
  digitalWrite(red_LED, HIGH);
  digitalWrite(green_LED, LOW);
  if (analogRead(forward) < 500)
  {
   bposition++;
  }

  if (analogRead(back) < 500)
  {
   bposition--;
  }
  digitalWrite(M1_enable, HIGH);
  digitalWrite(M2_enable, HIGH);
  digitalWrite(yellow_LED, HIGH);
  int_position = ((bposition) % 4);
  set_position(int_position);
  digitalWrite(yellow_LED, LOW);
  digitalWrite(M1_enable, LOW);
  digitalWrite(M2_enable, LOW);
  delay(100);
  Serial.print("Bposition = ");
  Serial.println(bposition);
  return bposition;
 }
 //*****************************Ends definition of manual operation

}  //Void setup ends

// This is the loop routine that runs over and over again forever:
void loop() {
 unsigned long timeistarted;
```

```
  unsigned long timenow;
  float aposition;
  int i = 0; //local looping variable
  int n; //local variable
  int int_position = 0;
  int start_position;

  int dutycycle = 200; //proportion of 1 second (in milliseconds) that motors are actuated
  if ((analogRead(manual) < 500) && (startbuttonstate == 0))
  {
    digitalWrite(red_LED, HIGH);
    digitalWrite(yellow_LED, HIGH);
    digitalWrite(green_LED, HIGH);  //Set indicator lights for the condition where manual/auto is set back to auto but the start light is not pressed - all LEDs on.
    Serial.print("StepD ");
    }
    Serial.print("StepA ");
  if ((analogRead(start) < 500) && (analogRead(manual) < 500))
  {
    startbuttonstate = 1; //Set the start button pressed flag to 1 if auto enable button is pressed AND auto/manual selector is at AUTO

    timeistarted = millis();
       Serial.print("StepE ");
  }
    Serial.print("StepB ");
  //Motor control by sinusoidal stimulation
  //This uses the sinusoidal waveform to move forward and backward: controlling parameters are
  //frequency, magnitude, and stimulation time
  if (startbuttonstate == 1)
  {
       Serial.print("StepC ");
    digitalWrite(red_LED, LOW);
    digitalWrite(yellow_LED, HIGH);
    digitalWrite(green_LED, HIGH); // Set indicator lights for automatic operation - green on only.
    //*******************Move actuator towards origin by magnitude*0.5 to de-tension the gel
    i = int(magnitude * 0.5 + 1);
    while (i > 0)
    {
      int_position = (current_position % 4);
      set_position(int_position);
      delay(500); //makes up delay to move gradually to start point
      current_position--;
      Serial.print("Current position = ");
      Serial.println(current_position);
      Serial.println(i);
```

```
      i--;
      timeistarted = millis();
    }
    //**********************************Set motor position by current time
    timenow = millis() - timeistarted;
    start_position = current_position;
    while (timenow < (1000 * duration))
    {

      if ((millis() % 1000) < dutycycle) //check system clock to set duty cycle for
motors
      {
        digitalWrite(M1_enable, HIGH);
        digitalWrite(M2_enable, HIGH);
      }
      else
      {
        digitalWrite(M1_enable, LOW);
        digitalWrite(M2_enable, LOW);
      }
      aposition = (magnitude * 0.5) - (0.5 * magnitude * cos(PI * frequency * timenow
/ 500));
      current_position = start_position + aposition;
      Serial.print("Current position = ");
      Serial.println(current_position);
      int_position = ((int(current_position)) % 4);

      set_position(int_position);
      timenow = millis() - timeistarted;
    }//end of while loop;
    // This next part of the code returns the actuator to the rest position
    i = 0;
    n = int((magnitude * 0.5) + 1);
    while (i < n)
    {
      int_position = (current_position % 4);
      set_position(int_position);
      delay(2000 / (magnitude * frequency) - 500); //makes up delay to move gradually
to start point
      current_position++;
      i++;
    }

    startbuttonstate = 0; //resets start button state
  }// < end of overarching "if startbuttonstate". This is the "default to manual on start"
catcher.


    while (analogRead(manual) > 500)
    {
```

```
      current_position = manual_operation(current_position);
    } // < End of "while" loop for auto/manual

      Serial.print("Current position ");
      Serial.println(current_position);

} //End of loop

void set_position(int i) {
  switch (i)
  {
    case 0:
      M1step1();
      M2step1();
      delay(100);
      break;
    case 1:
      M1step2();
      M2step2();
      delay(100);
      break;
    case 2:
      M1step3();
      M2step3();
      delay(100);
      break;
    default: //default is case 3!
      M1step4();
      M2step4();
      delay(100);
      break; //end of switch-case structure
  }
  M1stopMotor();
  M2stopMotor();
  Serial.println(i);
}
```